RECOMMENDED PRACTICE
DNV-RP-C205

ENVIRONMENTAL CONDITIONS AND ENVIRONMENTAL LOADS

OCTOBER 2010

DET NORSKE VERITAS

FOREWORD

DET NORSKE VERITAS (DNV) is an autonomous and independent foundation with the objectives of safeguarding life, property and the environment, at sea and onshore. DNV undertakes classification, certification, and other verification and consultancy services relating to quality of ships, offshore units and installations, and onshore industries worldwide, and carries out research in relation to these functions.

DNV service documents consist of amongst other the following types of documents:

— *Service Specifications.* Procedual requirements.
— *Standards.* Technical requirements.
— *Recommended Practices.* Guidance.

The Standards and Recommended Practices are offered within the following areas:

A) Qualification, Quality and Safety Methodology
B) Materials Technology
C) Structures
D) Systems
E) Special Facilities
F) Pipelines and Risers
G) Asset Operation
H) Marine Operations
J) Cleaner Energy
O) Subsea Systems

CHANGES

- **General**

As of October 2010 all DNV service documents are primarily published electronically.

In order to ensure a practical transition from the "print" scheme to the "electronic" scheme, all documents having incorporated amendments and corrections more recent than the date of the latest printed issue, have been given the date October 2010.

An overview of DNV service documents, their update status and historical "amendments and corrections" may be found through http://www.dnv.com/resources/rules_standards/.

- **Main changes**

Since the previous edition (April 2007), this document has been amended, most recently in April 2010. All changes have been incorporated and a new date (October 2010) has been given as explained under "General".

CONTENTS

1. General

1.1 Introduction

This new Recommended Practice (RP) gives guidance for modelling, analysis and prediction of environmental conditions as well guidance for calculating environmental loads acting on structures. The loads are limited to those due to wind, wave and current. The RP is based on state of the art within modelling and analysis of environmental conditions and loads and technical developments in recent R&D projects, as well as design experience from recent and ongoing projects.

The basic principles applied in this RP are in agreement with the most recognized rules and reflect industry practice and latest research.

Guidance on environmental conditions is given in Ch.2, 3 and 4, while guidance on the calculation of environmental loads is given in Ch.5, 6, 7, 8 and 9. Hydrodynamic model testing is covered in Ch.10.

1.2 Objective

The objective of this RP is to provide rational design criteria and guidance for assessment of loads on marine structures subjected to wind, wave and current loading.

1.3 Scope and application

1.3.1 Environmental conditions

1.3.1.1 Environmental conditions cover natural phenomena, which may contribute to structural damage, operation disturbances or navigation failures. The most important phenomena for marine structures are:

— wind
— waves
— current
— tides.

These phenomena are covered in this RP.

1.3.1.2 Phenomena, which may be important in specific cases, but not covered by this RP include:

— ice
— earthquake
— soil conditions
— temperature
— fouling
— visibility.

1.3.1.3 The environmental phenomena are usually described by physical variables of statistical nature. The statistical description should reveal the extreme conditions as well as the long- and short-term variations. If a reliable simultaneous database exists, the environmental phenomena can be described by joint probabilities.

1.3.1.4 The environmental design data should be representative for the geographical areas where the structure will be situated, or where the operation will take place. For ships and other mobile units which operate world-wide, environmental data for particularly hostile areas, such as the North Atlantic Ocean, may be considered.

1.3.1.5 Empirical, statistical data used as a basis for evaluation of operation and design must cover a sufficiently long time period. For operations of a limited duration, seasonal variations must be taken into account. For meteorological and oceanographical data 20 years of recordings should be available. If the data record is shorter the climatic uncertainty should be included in the analysis.

1.3.2 Environmental loads

1.3.2.1 Environmental loads are loads caused by environmental phenomena.

1.3.2.2 Environmental loads to be used for design shall be based on environmental data for the specific location and operation in question, and are to be determined by use of relevant methods applicable for the location/operation taking into account type of structure, size, shape and response characteristics.

1.4 Relationship to other codes

This RP provides the basic background for environmental conditions and environmental loads applied in DNV's Offshore Codes and is considered to be a supplement to relevant national (i.e. NORSOK) and international (i.e. ISO) rules and regulations.

Other DNV Recommended Practices give specific information on environmental loading for specific marine structures. Such codes include:

— DNV-RP-C102 "Structural Design of Offshore Ships"
— Recommended Practice DNV-RP-C103 "Column Stabilized Units"
— DNV-RP-C206 "Fatigue Methodology of Offshore Ships"
— DNV-RP-F105 "Free Spanning Pipelines"
— DNV-RP-F204 "Riser Fatigue"
— DNV-RP-F205 "Global Performance Analysis of Deepwater Floating Structures".

1.5 References

References are given at the end of each of Ch.2 to Ch.10. These are referred to in the text.

1.6 Abbreviations

ALS	Accidental Limit State
BEM	Boundary Element Method
CF	Cross Flow
CMA	Conditional Modelling Approach
CQC	Complete Quadratic Combination
DVM	Discrete Vortex Method
FD	Finite Difference
FEM	Finite Element Method
FLS	Fatigue Limit State
FPSO	Floating Production and Storage and Offloading
FV	Finite Volume
GBS	Gravity Based Structure
HAT	Highest Astronomical Tide
HF	High Frequency
IL	In-line
LAT	Lowest Astronomical Tide
LF	Low Frequency
LNG	Liquified natural Gas
LS	Least Squares
LTF	Linear Transfer Function
MHWN	Mean High Water Neaps
MHWS	Mean High Water Springs
MLE	Maximum Likelihood Estimation
MLM	Maximum Likelihood Model
MLWN	Mean Low Water Neaps
MLWS	Mean Low Water Springs
MOM	Method Of Moments
PM	Pierson-Moskowitz
POT	Peak Over Threshold
QTF	Quadratic Transfer Function
RAO	Response Amplitude Operator
SRSS	Square Root of Sum of Squares
SWL	Still Water Level
TLP	Tension Leg Platform
ULS	Ultimate Limit State
VIC	Vortex In Cell
VIM	Vortex Induced Motion
VIV	Vortex Induced Vibrations
WF	Wave Frequency

1.7 Symbols

1.7.1 Latin symbols

a_0	Still water air gap
a	Instantaneous air gap
A	Dynamic amplification factor
A	Cross-sectional area
$A(z)$	Moonpool cross-sectional area
A_1	V/L, reference cross-sectional area for riser with buoyancy elements
A_C	Charnock's constant
A_C	Wave crest height
A_{CF}	Cross flow VIV amplitude
A_{kj}	Added mass matrix elements
a_r	Relative acceleration
A_R	Reference area for 2D added mass coefficient
A_T	Wave trough depth
B	Bowen ratio
B_1	Linear damping coefficient
B_{kj}	Wave damping matrix elements
B_{xx}, B_{xy}	Wave drift damping coefficients
c	Wetted length during slamming
c	Wave phase velocity
C	Wind force shape coefficient
C_A	Added mass coefficient
C_{A0}	Added mass coefficient for $K_C = 0$
C_D	Drag coefficient
C_d	Hydrodynamic damping coefficient
C_{Dn}	Normal drag coefficient for inclined structural member
C_{DS}	Drag coefficient for steady flow
C_{Dt}	Axial drag coefficient for inclined structural member
C_e	Wind force effective shape coefficient
c_g	Wave group velocity
C_h	Horizontal wave-in-deck force coefficient
C_{kj}	Hydrostatic restoring elements
C_L	Lift coefficient
C_M	Mass coefficient
$Coh(r,f)$	Coherence spectrum
C_p	Wind pressure coefficient
C_p	Pressure coefficient
C_{pa}	Space average slamming pressure coefficient
C_v	Vertical wave-in-deck force coefficient
d	Water depth
D	Diameter or typical cross-sectional dimension
$D(\omega)$	Directionality function
$d(z/r)$	Instantaneous cross-sectional horizontal length during slamming
$D(\theta,\omega)$	Directionality function
$D[\ ]$	Standard deviation
D_b	Diameter of buoyancy element
D_C	Diameter of clean cylinder (without marine growth)
D_i	Diameter of element i in group of cylinders
D_p	Width of cluster of cylinder
E	Wave energy density
e	Gap ratio (= H/D)
E	Modulus of elasticity
$E^{(-)}$	Quadratic free surface transfer function
$E^{(+)}$	Quadratic free surface transfer function
$E[\ ]$	Mean value
EI	Bending stiffness
f	Wave frequency
F_c	Current induced drag force
$F_d(\omega)$	Mean drift force
f_{drag}	Sectional drag force on slender member

F_{dx}, F_{dy}	Wave drift damping forces	m_e	Effective mass
F_h	Horizontal wave-in-deck force	M_{eq}	Equivalent moonpool mass
$F_H(h)$	Cumulative probability function	M_{kj}	Global mass matrix elements
$F_{HT}(H,T)$	Joint probability distribution	m_n, M_n	Spectral moments
f_{lift}	Sectional lift force on slender member	m_t	Torsional moment on slender structural member
f_N	Sectional normal drag force on slender member	n	Number of propeller revolutions per unit time
f_n	Natural frequency	n	Exponent for wave spreading
F_s	Slamming force	n_x,n_y,n_z	Components of normal vector
f_s	Sectional slamming force	P	Wave energy flux
f_T	Sectional axial drag force on slender member	p	Pressure
F_v	Vertical wave-in-deck force	p_s	Space average slamming pressure
g	Acceleration of gravity	q	Basic wind pressure
g	Wind response peak factor	$q_{WA}^{(2+)}$	Sum frequency wave induced force
GM	Metacentric height	$q_{WA}^{(2-)}$	Difference frequency wave induced force
H	Wind reference height	R	Richardson number
H	Clearance between structure and fixed boundary	R	Reflection coefficient
H	Wave height	r	Ratio between modal frequencies
$H^{(1)}$	First order force transfer function	r	Displacement of structural member
$H^{(2-)}$	Second order difference frequency force transfer function	r_{44}	Roll radius of gyration
$H^{(2+)}$	Second order sum frequency force transfer function	r_{55}	Pitch radius of gyration
$h(z/r)$	Vertical reference height during slamming	R_e	Reynolds number = uD/ν
H_b	Breaking wave height	S	Projected area of structural member normal to the direction of force
H_{m0}	Significant wave height	S	Wave steepness
H_s	Significant wave height	s	Exponent for wave spreading
I	Interaction factor for buoyancy elements	S	Distance between buoyancy elements
I_{kj}	Mass moments of inertia	S	Waterplane area
J_n	Bessel function	$S(f)$, $S(\omega)$	Wave spectrum
k	Wave number	S_1	Average wave steepness
k	Roughness height	S_i, $i = 1,2$	First moments of water plane area
k_a	Von Karman's constant	S_{ij}	Second moments of water plane area
K_C	Keulegan-Carpenter number = $v_m T/D$ ($K_C = \pi H/D$ in wave zone)	S_{m02}	Estimate of significant wave steepness
K_{kj}	Mooring stiffness elements	S_{max}	Maximum wave steepness
K_n	Modified Bessel function of order ν	S_p	Average wave steepness
K_s	Shoaling coefficient	$S_R(\omega)$	Response spectrum
K_S	Stability parameter (Scrouton number)	S_s	Significant wave steepness
l	Length of buoyancy element	St	Strouhal number
$L(\omega)$	Linear structural operator	$S_U(f)$	Wind speed spectrum
l_c	Correlation length	T	Wave period
L_{MO}	Monin-Obukhov length	T	Transmission coefficient
L_u	Integral length scale in wind spectrum	t	Thickness of marine growth
m	Beach slope	T_0	Propeller thrust at zero speed
M	Mass of structure	T_0	One-hour wind reference period
m^*	Mass ratio	T_1	Mean wave period
m_{66}	Added moment of inertia for cross-section	T_{10}	10-minute wind reference period
M_a	3D added mass	T_c	Mean crest period
m_a	2D added mass (per unit length)	T_{m01}	Spectral estimate of mean wave period
m_a^T	Tangential added mass	T_{m02}	Spectral estimate of zero-up-crossing period
M_c	Current induced moment due to drag	T_{m24}	Spectral estimate of mean crest period
$M_d(\omega)$	Mean drift moment	T_n	Natural period
M_{dz}	Wave drift yaw moment	T_p	Peak period
		T_R	Return period
		T_z	Zero-up-crossing period

U	Forward speed of structure/vessel	β	Viscous frequency parameter $= R_e/K_C = D^2/vT$
$u^{(1)}$	First order horizontal velocity	β_H, β_c	Shape parameters in Weibull distribution
$u^{(2-)}$	Second-order difference-frequency horizontal velocity	δ	Logarithmic decrement ($= 2\pi\zeta$)
$u^{(2+)}$	Second-order sum-frequency horizontal velocity	δ	Spectral band width
u*	Friction velocity	Δ	Nondimensional roughness $= k/D$
u,v,w	Wave velocity components in x,y,z-direction	ΔS_S	Spatial extent of slamming pressure
U_0	One hour mean wind speed	ε	Local wave slope
U_{10}	10-minute mean wind speed	ε	Shallow water non-linearity parameter
U_G, A_G	Parameters of Gumbel distribution	ε	Spectral band width
U_R, U_r	Ursell numbers for regular wave	ε_k	Random phase
U_{rs}	Ursell number for irregular wave	ϕ	Velocity potential
$U_{T,z}$	Wind velocity averaged over a time interval T at a height z meter	ϕ	Solidity ratio
V	Volume displacement	$\phi(\omega)$	Depth function in TMA spectrum
v_c	Current velocity	γ	Peak shape parameter (Jonswap)
V_c	Volume of air cushion	γ	Length scale of wind speed process
$v_c(\infty)$	Far field current	γ	Location parameter in 3-parameter Weibull distribution
$v_{c,circ}$	Circulational current velocity	γ	Gas constant for air $= 1.4$
$v_{c,tide}$	Tidal current velocity	$\Gamma(\ )$	Gamma function
$v_{c,wind}$	Wind induced current velocity	η	Free surface elevation
v_d	Wake deficit velocity	η	Shielding factor
v_m	Maximum wave orbital particle velocity	h	Height of moonpool
v_n	Normal component of velocity	η_1	Linear (first order) free surface elevation
v_r	Relative velocity	η_2	Second order free surface elevation
V_R	Reduced velocity $= vT/D$ or $v/(fD)$	η_m	Local crest height
V_R	Reference area for 3D added mass coefficient	$\eta_{R,D}$	Radiation and diffraction free surface elevation
v_s	Significant velocity	κ	Surface friction coefficient
v_t	Normal component of velocity	κ	Finite length reduction factor
W	Projected diameter of split tube chord	κ	Moonpool geometry factor
$z(x,y,t)$	Vertical displacement of the structure	λ	Wave length
z_B	Vertical position of centre of buoyancy	μ	Shallow water parameter
z_G	Vertical position of centre of gravity	ν	Spectral band width
z_s	Stretched z-coordinate	ν	Kinematic viscosity coefficient
$\dot{r}$	Velocity of structural member	ν_a	Kinematic viscosity coefficient for air
$\ddot{r}$	Acceleration of structural member	ν_{ij}	Irregular wave numbers
		ρ	Mass density of water

1.7.2 Greek symbols

		ρ	Autocorrelation for wind speed field
α	Spacing ratio	ρ_a	Mass density of air
α	Angle between the direction of the wind and the axis of the exposed member or surface	ρ_{nm}	Cross-modal coefficients
α	Asymmetry factor	$\sigma(f)$	Standard deviation of dynamic structural response
α	Angle between wave ray and normal to the sea bed depth contour	σ_a, σ_b	Spectral width parameters (Jonswap)
α	Exponent in power law current profile	σ_b	Stress due to net buoyancy force
α	Wave attenuation coefficient	σ_{slam}	Stress in element due to slam load
α	Spectral band width	σ_U	Standard deviation of wind speed
α_c	Current flow velocity ratio $= v_c/(v_c+v_m)$	σ_w	Stress due to vertical wave forces
α_H, α_c	Scale parameters in Weibull distribution	ω	Wave angular frequency
β	Breaking wave parameter	ω_e	Wave angular frequency of encounter
β	Wave direction of propagation	ω_p	Angular spectral peak frequency
β	Deadrise angle during slamming	$\xi_i(\omega)$	Response transfer function
β	Aerodynamic solidity ratio	ξ_j	Rigid body motion in degree of freedom j
		ζ	Damping ratio
		δ	Aspect ratio $= b/l$
		Θ	Phase function

θ_p	Main wave direction
ψ	Stability function for wind profiles
ψ	Wave amplification factor
$\Phi(\ )$	Standard Gaussian cumulative distribution function
$\dot{\Omega}$	Angular acceleration of cross-section.

2. Wind Conditions

2.1 Introduction to wind climate

2.1.1 General

Wind speed varies with time. It also varies with the height above the ground or the height above the sea surface. For these reasons, the averaging time for wind speeds and the reference height must always be specified.

A commonly used reference height is $H = 10$ m. Commonly used averaging times are 1 minute, 10 minutes and 1 hour.

Wind speed averaged over 1 minute is often referred to as *sustained* wind speed.

2.1.2 Wind parameters

2.1.2.1 The wind climate can be represented by the 10-minute mean wind speed U_{10} at height 10 m and the standard deviation σ_U of the wind speed at height 10 m. In the short term, i.e. over a 10-minute period, stationary wind conditions with constant U_{10} and constant σ_U can often be assumed to prevail. This wind climate representation is not intended to cover wind conditions experienced in tropical storms such as hurricanes, cyclones and typhoons. It is neither intended to cover wind conditions experienced during small-scale events such as fast propagating arctic low pressures of limited extension. The assumption of stationary conditions over 10-minute periods is not always valid. For example, front passages and unstable conditions can lead to extreme wind conditions like wind gusts, which are transient in speed and direction, and for which the assumption of stationarity does not hold. Examples of such nonstationary extreme wind conditions, which may be critical for design, are given in DNV-OS-J101 and IEC61400-1.

2.1.2.2 The 10-minute mean wind speed U_{10} is a measure of the intensity of the wind. The standard deviation σ_U is a measure of the variability of the wind speed about the mean. When special conditions are present, such as when hurricanes, cyclones and typhoons occur, a representation of the wind climate in terms of U_{10} and σ_U may be insufficient. The instantaneous wind speed at an arbitrary point in time during 10-minute stationary conditions follows a probability distribution with mean value U_{10} and standard deviation σ_U.

2.1.2.3 The turbulence intensity is defined as the ratio σ_U/U_{10}.

2.1.2.4 The short term 10-minute stationary wind climate may be represented by a wind spectrum, i.e. the power spectral density of the wind speed process, $S_U(f)$. $S_U(f)$ is a function of U_{10} and σ_U and expresses how the energy of the wind speed in a specific point in space is distributed between various frequencies.

2.2 Wind data

2.2.1 Wind speed statistics

2.2.1.1 Wind speed statistics are to be used as a basis for representation of the long-term and short-term wind conditions. Long-term wind conditions typically refer to 10 years or more, short-term conditions to 10 minutes. The 10-minute mean wind speed at 10 m height above the ground or the still water level is to be used as the basic wind parameter to describe the long-term wind climate and the short-term wind speed fluctuations. Empirical statistical data used as a basis for design must cover a sufficiently long period of time.

2.2.1.2 Site-specific measured wind data over sufficiently long periods with minimum or no gaps are to be sought. For design, the wind climate data base should preferably cover a 10-year period or more of continuous data with a sufficient time resolution.

2.2.1.3 Wind speed data are height-dependent. The mean wind speed at 10 m height is often used as a reference. When wind speed data for other heights than the reference height are not available, the wind speeds for the other heights can be calculated from the wind speeds in the reference height in conjunction with a wind speed profile above the ground or above the still water level.

2.2.1.4 The long-term distributions of U_{10} and σ_U should preferably be based on statistical data for the same averaging period for the wind speed as the averaging period which is used for the determination of loads. If a different averaging period than 10 minutes is used for the determination of loads, the wind data may be converted by application of appropriate gust factors. The short-term distribution of the instantaneous wind speed itself is conditional on U_{10} and σ_U.

2.2.1.5 An appropriate gust factor to convert wind statistics from other averaging periods than 10 minutes depends on the frequency location of a spectral gap, when such a gap is present. Application of a fixed gust factor, which is independent of the frequency location of a spectral gap, can lead to erroneous results. A spectral gap separates large-scale motions from turbulent scale motions and refers to those spatial and temporal scales that show little variation in wind speed.

2.2.1.6 The latest insights for wind profiles above water should be considered for conversion of wind speed data between different reference heights or different averaging periods. Unless data indicate otherwise, the conversions may be carried out by means of the expressions given in 2.3.2.11.

2.2.1.7 The wind velocity climate at the location of the structure shall be established on the basis of previous measurements at the actual location and adjacent locations, hindcast wind data as well as theoretical models and other meteorological information. If the wind velocity is of significant importance to the design and existing wind data are scarce and uncertain, wind velocity measurements should be carried out at the location in question. Characteristic values of the wind velocity should be determined with due account of the inherent uncertainties.

2.2.1.8 When the wind velocity climate is based on hindcast wind data, it is recommended to use data based on reliable recognised hindcast models with specified accuracy. WMO (1983) specifies minimum requirements to hindcast models and their accuracy. Hindcast models and theoretical models can be validated by benchmarking to measurement data.

2.3 Wind modelling

2.3.1 Mean wind speed

2.3.1.1 The long-term probability distributions for the wind climate parameters U_{10} and σ_U that are derived from available data can be represented in terms of generic distributions or in terms of scatter diagrams. An example of a generic distribution representation consists of a Weibull distribution for the arbitrary 10-minute mean wind speed U_{10} in conjunction with a lognormal distribution of σ_U conditional on U_{10} (see 2.3.3.1). A scatter diagram provides the frequency of occurrence of given pairs (U_{10}, σ_U) in a given discretisation of the (U_{10}, σ_U) space.

2.3.1.2 Unless data indicate otherwise, a *Weibull distribution* can be assumed for the arbitrary 10-minute mean wind speed U_{10} in a given height z above the ground or above the sea water level,

$$F_{U_{10}}(u) = 1 - \exp(-(\frac{u}{A})^{k})$$

in which the scale parameter A and the shape parameter k are site- and height-dependent.

2.3.1.3 In areas where hurricanes occur, the Weibull distribution as determined from available 10-minute wind speed records may not provide an adequate representation of the upper tail of the true distribution of U_{10}. In such areas, the upper tail of the distribution of U_{10} needs to be determined on the basis of hurricane data.

2.3.1.4 Data for U_{10} are usually obtained by measuring the wind speed over 10 minutes and calculating the mean wind speed based on the measurements from these 10 minutes. Various sampling schemes are being used. According to some schemes, U_{10} is observed from every 10-minute period in a consecutive series of 10-minute periods, such that there are six U_{10} observations every hour. According to other schemes, U_{10} is observed from only one 10-minute period every hour or every third hour, such that there are only 24 or 8 U_{10} observations per day.

2.3.1.5 Regardless of whether U_{10} is sampled every 10 minutes, every hour or every third hour, the achieved samples – usually obtained over a time span of several years – form a data set of U_{10} values which are representative as a basis for estimation of the cumulative distribution function $F_{U10}(u)$ for U_{10}.

2.3.1.6 In areas where hurricanes do not occur, the distribution of the annual maximum 10-minute mean wind speed $U_{10,\max}$ can be approximated by

$$F_{U_{10,\max},1\,\text{year}}(u) = (F_{U_{10}}(u))^N$$

where $N = 52\,560$ is the number of consecutive 10-minute averaging periods in one year. Note that $N = 52\,595$ when leap years are taken into account. The approximation is based on an assumption of independent 10-minute events. The approximation is a good approximation in the upper tail of the distribution, which is typically used for prediction of rare mean wind speeds such as those with return periods of 50 and 100 years.

2.3.1.7 Note that the value of $N = 52\,560$ is determined on the basis of the chosen averaging period of 10 minutes and is not influenced by the sampling procedure used to establish the data for U_{10} and the distribution $F_{U10}(u)$; i.e. it does not depend on whether U_{10} has been sampled every 10 minutes, every hour or every third hour. Extreme value estimates such as the 99% quantile in the resulting distribution of the annual maximum 10-minute mean wind speed shall thus always come out as independent of the sampling frequency.

2.3.1.8 In areas where hurricanes occur, the distribution of the annual maximum 10-minute mean wind speed $U_{10,\max}$ shall be based on available hurricane data. This refers to hurricanes for which the 10-minute mean wind speed forms a sufficient representation of the wind climate.

2.3.1.9 The quoted power-law approximation to the distribution of the annual maximum 10-minute mean wind speed is a good approximation to the upper tail of this distribution. Usually only quantiles in the upper tail of the distribution are of interest, viz. the 98% quantile which defines the 50-year mean wind speed or the 99% quantile which defines the 100-year mean wind speed. The upper tail of the distribution can be well approximated by a Gumbel distribution, whose expression may be more practical to use than the quoted power-law expression.

2.3.1.10 The annual maximum of the 10-minute mean wind speed $U_{10,\max}$ can often be assumed to follow a *Gumbel distribution*,

$$F_{U_{10,\max},1\,\text{year}}(u) = \exp\{-\exp[-a(u-b)]\}$$

in which a and b are site- and height-dependent distribution parameters.

2.3.1.11 Experience shows that in many cases the *Gumbel distribution* will provide a better representation of the distribution of the *square* of the annual maximum of the 10-minute mean wind speed than of the distribution of the annual maximum of the mean wind speed itself. Wind loads are formed by wind pressures, which are proportional to the square of the wind speed, so for estimation of characteristic loads defined as the 98% or 99% quantile in the distribution of the annual maximum wind load it is recommended to work with the distribution of the square of the annual maximum of the 10-minute mean wind speed and extrapolate to 50- or 100-year values of this distribution.

2.3.1.12 The 10-minute mean wind speed with *return period* T_R in units of years is defined as the $(1-1/T_R)$ quantile in the distribution of the annual maximum 10-minute mean wind speed, i.e. it is the 10-minute mean wind speed whose probability of exceedance in one year is $1/T_R$. It is denoted U_{10,T_R} and is expressed as

$$U_{10,T_R} = F_{U_{10,\max},1\,\text{year}}^{-1}(1-\frac{1}{T_R}) \quad ; T_R > 1 \text{ year}$$

in which $F_{U10,\max,1\,\text{year}}$ denotes the cumulative distribution function of the annual maximum of the 10-minute mean wind speed.

2.3.1.13 The 10-minute mean wind speed with return period one year is defined as the mode of the distribution of the annual maximum 10-minute mean wind speed.

2.3.1.14 The 50-year 10-minute mean wind speed becomes

$$U_{10,50} = F_{U_{10,\max},1\,\text{year}}^{-1}(0.98)$$

and the 100-year 10-minute mean wind speed becomes

$$U_{10,100} = F_{U_{10,\max},1\,\text{year}}^{-1}(0.99)$$

Note that these values, calculated as specified, are to be considered as central estimates of the respective 10-minute wind speeds when the underlying distribution function $F_{U10,\max}$ is determined from limited data and is encumbered with statistical uncertainty.

2.3.2 Wind speed profiles

2.3.2.1 The wind speed profile represents the variation of the mean wind speed with height above the ground or above the still water level, whichever is applicable. When terrain conditions and atmospheric stability conditions are not complex, the wind speed profile may be represented by an idealised model profile. The most commonly applied wind profile models are the logarithmic profile model, the power law model and the Frøya model, which are presented in 2.3.2.4 through 2.3.2.12.

2.3.2.2 Complex wind profiles, which are caused by inversion and which may not be well represented by any of the most commonly applied wind profile models, may prevail over land in the vicinity of ocean waters.

2.3.2.3 The *friction velocity u** is defined as

$$u^* = \sqrt{\tau/\rho_a}$$

where τ is the surface shear stress and ρ_a is the air density.

The friction velocity u^* can be calculated from the 10-minute mean wind speed U_{10} at the height $H = 10$ m as

$$u^* = \sqrt{\kappa} \cdot U_{10}$$

where κ is a surface friction coefficient. The surface friction coefficient is defined in 2.3.2.6. Some sources refer to κ as a surface drag coefficient; however, it is important not to confuse κ with the drag coefficient used for calculations of wind forces on structures.

2.3.2.4 A *logarithmic* wind speed profile may be assumed for neutral atmospheric conditions and can be expressed as

$$U(z) = \frac{u*}{k_a} \ln \frac{z}{z_0}$$

where $k_a = 0.4$ is von Karman's constant, z is the height and z_0 is a terrain roughness parameter, which is also known as the *roughness length*. For locations on land, z_0 depends on the topography and the nature of the ground. For offshore locations z_0 depends on the wind speed, the upstream distance to land, the water depth and the wave field. Table 2-1 gives typical values for z_0 for various types of terrain.

Table 2-1 Terrain roughness parameter z_0 and power-law exponent α		
Terrain type	Roughness parameter z_0 (m)	Power-law exponent α
Plane ice	0.00001-0.0001	
Open sea without waves	0.0001	
Open sea with waves	0.0001-0.01	0.12
Coastal areas with onshore wind	0.001-0.01	
Snow surface	0.001-0.006	
Open country without significant buildings and vegetation	0.01	
Mown grass	0.01	
Fallow field	0.02-0.03	
Long grass, rocky ground	0.05	
Cultivated land with scattered buildings	0.05	0.16
Pasture land	0.2	
Forests and suburbs	0.3	0.30
City centres	1-10	0.40

Table 2-1 is based on Panofsky and Dutton (1984), Simiu and Scanlan (1978), JCSS (2001) and Dyrbye and Hansen (1997).

2.3.2.5 For offshore locations, the roughness parameter z_0 typically varies between 0.0001 m in open sea without waves and 0.01 m in coastal areas with onshore wind. The roughness parameter for offshore locations may be solved implicitly from the following equation

$$z_0 = \frac{A_C}{g} \left(\frac{k_a U(z)}{\ln(z/z_0)} \right)^2$$

where g is the acceleration of gravity and A_C is Charnock's constant. A_C is usually higher for "young" developing and rapidly growing waves than for "old" fully developed waves. For open sea with fully developed waves, $A_C = 0.011$-0.014 is recommended. For near-coastal locations, A_C is usually higher with values of 0.018 or more. Expressions for A_C, which include the dependency on the wave velocity and the available water fetch, are available in the literature, see Astrup et al. (1999).

2.3.2.6 An alternative formulation of the logarithmic profile, expressed in terms of the 10-minute mean wind speed $U(H)$ in the reference height $H = 10$ m, reads

$$U(z) = U(H) \cdot (1 + \frac{1}{k_a} \sqrt{\kappa} \cdot \ln \frac{z}{H})$$

in which

$$\kappa = \frac{k_a^2}{(\ln \frac{H}{z_0})^2}$$

is the surface friction coefficient.

This implies that the logarithmic profile may be rewritten as

$$U(z) = U(H) \cdot \left(1 + \frac{\ln\left(\frac{z}{H}\right)}{\ln\left(\frac{H}{z_0}\right)} \right)$$

2.3.2.7 The logarithmic wind speed profile implies that the scale parameter $A(z)$ at height z can be expressed in terms of the scale parameter $A(H)$ at height H as follows

$$A(z) = A(H) \frac{\ln \frac{z}{z_0}}{\ln \frac{H}{z_0}}$$

The scale parameter is defined in 2.3.2.1.

2.3.2.8 As an alternative to the logarithmic wind profile, a *power law profile* may be assumed,

$$U(z) = U(H)\left(\frac{z}{H}\right)^{\alpha}$$

where the exponent α depends on the terrain roughness.

2.3.2.9 Note that if the logarithmic and power law wind profiles are combined, then a height-dependent expression for the exponent α results

$$\alpha = \frac{\ln\left(\frac{\ln \frac{z}{z_0}}{\ln \frac{H}{z_0}}\right)}{\ln\left(\frac{z}{H}\right)}$$

2.3.2.10 Note also that the limiting value $\alpha = 1/\ln(z/z_0)$ as z approaches the reference height H has an interpretation as a turbulence intensity, cf. the definition given in 2.3.2.3. As an alternative to the quoted expression for α, values for α tabulated in Table 2-1 may be used.

2.3.2.11 The following expression can be used for calculation of the mean wind speed U with averaging period T at height z above sea level as

$$U(T, z) = U_{10} \cdot (1 + 0.137 \ln \frac{z}{H} - 0.047 \ln \frac{T}{T_{10}})$$

where $H = 10$ m and $T_{10} = 10$ minutes, and where U_{10} is the 10-minute mean wind speed at height H. This expression converts mean wind speeds between different averaging periods. When $T < T_{10}$, the expression provides the most likely largest mean wind speed over the specified averaging period T, given the original 10-minute averaging period with stationary conditions and given the specified 10-minute mean wind speed U_{10}. The conversion does not preserve the return period associated with U_{10}.

2.3.2.12 For offshore locations, the *Frøya wind profile* model is recommended unless data indicate otherwise. For extreme mean wind speeds corresponding to specified return periods in excess of approximately 50 years, the Frøya model implies that the following expression can be used for conversion of the one-hour mean wind speed U_0 at height H above sea level to the mean wind speed U with averaging period T at height z above sea level

$$U(T, z) = U_0 \cdot \left\{ 1 + C \cdot \ln \frac{z}{H} \right\} \cdot \left\{ 1 - 0.41 \cdot I_U(z) \cdot \ln \frac{T}{T_0} \right\}$$

where H = 10 m, T_0 = 1 hour and $T < T_0$, where

$$C = 5.73 \cdot 10^{-2} \sqrt{1 + 0.148 U_0}$$

and

$$I_U = 0.06 \cdot (1 + 0.043 U_0) \cdot \left(\frac{z}{H}\right)^{-0.22}$$

and where U will have the same return period as U_0.

2.3.2.13 Note that the Frøya wind speed profile includes a gust factor which allows for conversion of mean wind speeds between different averaging periods. The Frøya wind speed profile is a special case of the logarithmic wind speed profile in 2.3.2.4. The Frøya wind speed profile is the best documented wind speed profile for offshore locations and maritime conditions.

2.3.2.14 Over open sea, the coefficient C may tend to be about 10% smaller than the value that results from the quoted expression. In coastal zones, somewhat higher values for the coefficient C should be used, viz. 15% higher for U_0 = 10 m/s and 30% higher for U_0 = 40 m/s.

2.3.2.15 Both conversion expressions are based on winter storm data from a Norwegian Sea location and may not necessarily lend themselves for use at other offshore locations. The expressions should not be extrapolated for use beyond the height range for which they are calibrated, i.e. they should not be used for heights above approximately 100 m. Possible influences from geostrophic winds down to about 100 m height emphasises the importance of observing this restriction.

2.3.2.16 Both conversion expressions are based on the application of a logarithmic wind profile. For locations where an exponential wind profile is used or prescribed, the expressions should be considered used only for conversions between different averaging periods at a height equal to the reference height H = 10 m.

2.3.2.17 In the absence of information on tropical storm winds in the region of interest, the conversion expressions may also be applied to winds originating from tropical storms. This implies in particular that the expressions can be applied to winds in hurricanes.

2.3.2.18 The conversion expressions are not valid for representation of squall winds, in particular because the duration of squalls is often less than one hour. The representation of squall wind statistics is a topic for ongoing research.

2.3.2.19 Once a wind profile model is selected, it is important to use this model consistently throughout, i.e. the wind profile model used to transform wind speed measurements at some height z to wind speeds at a reference height H has to be applied for any subsequent calculation of wind speeds, both at the height z and at other heights, on the basis of wind speeds at the reference height H.

2.3.2.20 The wind profile models presented in 2.3.2.4 and 2.3.2.8 and used for conversion to wind speeds in heights without wind observations are idealised characteristic model profiles, which are assumed to be representative mean profiles in the short term. There is model uncertainty associated with the profiles and there is natural variability around them: The true mean profile may take a different form for some wind events, such as in the case of extreme wind or in the case of non-neutral wind conditions. This implies that conversion of wind data to heights without wind measurements will be encumbered with uncertainty. HSE (2002) gives an indication of the accu-

racy which can be expected when conversions of wind speeds to heights without wind data is carried out by means of wind profile models. It is recommended to account for uncertainty in such wind speed conversions by adding a wind speed increment to the wind speeds that result from the conversions.

2.3.2.21 The expressions in 2.3.2.11 and 2.3.2.12 contain gust factors for conversion of wind speeds between different averaging periods. As for conversion of wind speeds between different heights also conversion between different averaging periods is encumbered with uncertainty, e.g. owing to the simplifications in the models used for the conversions. HSE (2002) gives an indication of the accuracy which can be expected when conversions of wind speeds between different averaging periods is carried out by means of gust factors. It is recommended to account for uncertainty in such wind speed conversions by adding a wind speed increment to the wind speeds that result from the conversions.

2.3.3 Turbulence

2.3.3.1 The natural variability of the wind speed about the mean wind speed U_{10} in a 10-minute period is known as turbulence and is characterised by the standard deviation σ_U. For given value of U_{10}, the standard deviation σ_U of the wind speed exhibits a natural variability from one 10-minute period to another. Measurements from several locations show that σ_U conditioned on U_{10} can often be well represented by a lognormal distribution.

$$F_{\sigma_U | U_{10}}(\sigma) = \Phi\left(\frac{\ln \sigma - b_0}{b_1}\right)$$

in which $\Phi(\ )$ denotes the standard Gaussian cumulative distribution function

$$\Phi(x) = \frac{1}{\sqrt{2\pi}} \int_{-\infty}^{x} e^{-\xi^2/2} d\xi$$

The coefficients b_0 and b_1 are site-dependent coefficients dependent on U_{10}.

2.3.3.2 The coefficient b_0 can be interpreted as the mean value of $\ln \sigma_U$, and b_1 as the standard deviation of $\ln \sigma_U$. The following relationships can be used to calculate the mean value $E[\sigma_U]$ and the standard deviation $D[\sigma_U]$ of σ_U from the values of b_0 and b_1,

$$E[\sigma_U] = \exp\left(b_0 + \frac{1}{2}b_1^2\right)$$

$$D[\sigma_U] = E[\sigma_U]\sqrt{\exp(b_1^2) - 1}$$

Reference is made to *Guidelines for Design of Wind Turbines* (2001).

2.3.3.3 $E[\sigma_U]$ and $D[\sigma_U]$ will, in addition to their dependency on U_{10}, also depend on local conditions, first of all the terrain roughness z_0, which is also known as the roughness length. When different terrain roughnesses prevail in different directions, i.e. the terrain is not homogeneous, $E[\sigma_U]$ and $D[\sigma_U]$ may vary with the direction. This will be the case for example in the vicinity of a large building. Buildings and other "disturbing" elements will in general lead to more turbulence, i.e., larger values of $E[\sigma_U]$ and $D[\sigma_U]$, than will be found in smoother terrain. Figure 2-1 and Figure 2-2 give examples of the variation of $E[\sigma_U]$ and $D[\sigma_U]$ with U_{10} for an onshore and an offshore location, respectively. The difference between the two figures mainly consists in a different shape of the mean curve. This reflects the effect of the increasing roughness length for increasing U_{10} on the offshore location.
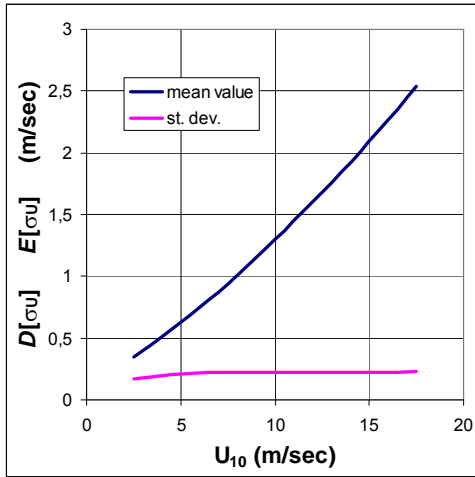
Figure 2-1
Example of mean value and standard deviation of σ_U as function of U_{10} – onshore location.
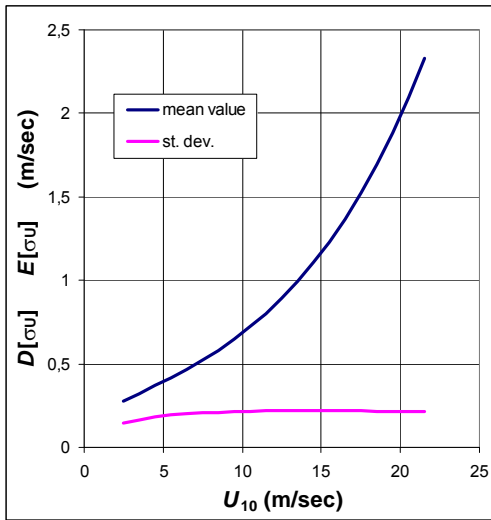
Figure 2-2
Example of mean value and standard deviation of σ_U as function of U_{10} – offshore location

2.3.3.4 In some cases, a lognormal distribution for σ_U conditioned on U_{10} will underestimate the higher values of σ_U. A *Frechet distribution* may form an attractive distribution model for σ_U in such cases, hence

$$F_{\sigma_U|U_{10}}(\sigma) = \exp(-(\frac{\sigma_0}{\sigma})^k)$$

The distribution parameter k can be solved implicitly from

$$(\frac{D[\sigma_U]}{E[\sigma_U]})^2 = \frac{\Gamma(1-\frac{2}{k})}{\Gamma^2(1-\frac{1}{k})} - 1$$

and the distribution parameter σ_0 then results as

$$\sigma_0 = \frac{E[\sigma_U]}{\Gamma(1-\frac{1}{k})}$$

where Γ denotes the gamma function

$$\Gamma(x) = \int_0^\infty t^{x-1}e^{-t}dt$$

2.3.3.5 Caution should be exercised when fitting a distribution model to data. Normally, the lognormal distribution provides a good fit to data, but use of a normal distribution, a Weibull distribution or a Frechet distribution is also seen. The choice of the distribution model may depend on the application, i.e., whether a good fit to data is required to the entire distribution or only in the body or the upper tail of the distribution. It is important to identify and remove data, which belong to 10-minute series for which the stationarity assumption for U_{10} is not fulfilled. If this is not done, such data may confuse the determination of an appropriate distribution model for σ_U conditioned on U_{10}.

2.3.3.6 The following expression for the mean value of the standard deviation σ_U, conditioned on U_{10}, can be applied

$$E[\sigma_U] = U_{10}A_x k_a \frac{1}{\ln\frac{z}{z_0}} = A_x u*$$

for homogeneous terrain, in which

k_a = 0.4 is von Karman's constant
z = the height above terrain
z_0 = the roughness parameter
A_x = constant which depends on z_0

Measurements from a number of locations with uniform and flat terrain indicate an average value of A_x equal to 2.4. In rolling terrain, A_x tends to be somewhat larger. Unless data indicate otherwise, the following approximation to A_x may be used for purely mechanical turbulence (neutral conditions) over uniform and flat terrain

$$A_x = \sqrt{4.5 - 0.856\ln z_0}$$

in which z_0 is to be given in units of m. Reference is made to Panofsky and Dutton (1984), Dyrbye and Hansen (1997), and Lungu and van Gelder (1997).

2.3.3.7 The 10-minute mean wind speed U_{10} and the standard deviation σ_U of the wind speed refer to the longitudinal wind speed, i.e. the wind speed in the constant direction of the mean wind during a considered 10-minute period of stationary conditions. During this period, in addition to the turbulence in the direction of the mean wind, there will be turbulence also laterally and vertically. The mean lateral wind speed will be zero, while the lateral standard deviation of the wind speed σ_{Uy} can be taken as a value between $0.75\sigma_U$ and $0.80\sigma_U$. The mean vertical wind speed will be zero, while the vertical standard deviation of the wind speed σ_{Uz} can be taken as $\sigma_{Uz} = 0.5\sigma_U$. These values all refer to homogeneous terrain. For complex terrain, the wind speed field will be much more isotropic, and values for σ_{Uy} and σ_{Uz} very near the value of σ_U can be expected.

2.3.3.8 When the wind climate at a location cannot be documented by site-specific measurements, the distribution of U_{10} can still, usually, be represented well, for example on the basis of wind speed measurements from adjacent locations. However, the distribution of σ_U will usually be harder to obtain, because it will be very dependent on the particular local roughness conditions, and it can thus not necessarily be inferred from known wind speed conditions at adjacent locations. At a location where wind speed measurements are not available, the determination of the distribution of the standard deviation σ_U of the wind speed is therefore often encumbered with ambiguity. It is common practice to account for this ambiguity by using conservatively high values for σ_U for design purposes.

2.3.4 Wind spectra

2.3.4.1 Short-term stationary wind conditions may be described by a wind spectrum, i.e. the power spectral density of the wind speed. Site-specific spectral densities of the wind speed process can be determined from available measured wind data.

2.3.4.2 When site-specific spectral densities based on measured data are used, the following requirement to the energy content in the high frequency range should be fulfilled, unless data indicate otherwise: The spectral density $S_U(f)$ shall asymptotically approach the following form as the frequency f in the high frequency range increases

$$S_U(f) = 0.14 \cdot \sigma_U^2 \left(\frac{L_u}{U_{10}}\right)^{-\frac{2}{3}} f^{-\frac{5}{3}}$$

in which L_u is the integral length scale of the wind speed process.

2.3.4.3 Unless data indicate otherwise, the spectral density of the wind speed process may be represented by a model spectrum. Several model spectra exist. They generally agree in the high frequency range, whereas large differences exist in the low frequency range. Most available model spectra are calibrated to wind data obtained over land. Only a few are calibrated to wind data obtained over water. Model spectra are often expressed in terms of the integral length scale of the wind speed process. The most commonly used model spectra with length scales are presented in 2.3.4.5 to 2.3.4.10.

2.3.4.4 Caution should be exercised when model spectra are used. In particular, it is important to be aware that the true integral length scale of the wind speed process may deviate significantly from the integral length scale of the model spectrum.

2.3.4.5 The *Davenport spectrum* expresses the spectral density in terms of the 10-minute mean wind speed U_{10} irrespective of the elevation. The Davenport spectrum gives the following expression for the spectral density

$$S_U(f) = \sigma_U^2 \frac{\frac{2}{3}(\frac{L_u}{U_{10}})^2 \cdot f}{(1 + (\frac{fL_u}{U_{10}})^2)^{4/3}}$$

in which f denotes the frequency and L_u is a length scale of the wind speed process. The Davenport spectrum is originally developed for wind over land with $L_u = 1200$ m as the proposed value.

2.3.4.6 The Davenport spectrum is not recommended for use in the low frequency range, i.e. for $f < 0.01$ Hz. There is a general difficulty in matching the Davenport spectrum to data in this range because of the sharp drop in the spectral density value of the Davenport spectrum near zero frequency.

2.3.4.7 The *Kaimal spectrum* gives the following expression for the spectral density,

$$S_U(f) = \sigma_U^2 \frac{6.868 \frac{L_u}{U_{10}}}{(1 + 10.32 \frac{fL_u}{U_{10}})^{5/3}}$$

in which f denotes frequency and L_u is an integral length scale. Unless data indicate otherwise, the integral length scale L_u can be calculated as

$$L_u = 300(\frac{z}{300})^{0.46+0.074 \ln z_0}$$

which corresponds to specifications in Eurocode 1 and where

z denotes the height above the ground or above the sea water level, whichever is applicable, and z_0 is the terrain roughness. Both z and z_0 need to be given in units of m.

2.3.4.8 An alternative specification of the integral length scale is given in IEC61400-1 for design of wind turbine generators and is independent of the terrain roughness,

$$L_u = \begin{cases} 3.33\,z & \text{for } z < 60 \text{ m} \\ 200 \text{ m} & \text{for } z \geq 60 \text{ m} \end{cases}$$

where z denotes the height above the ground or the sea water level, whichever is applicable.

2.3.4.9 The *Harris spectrum* expresses the spectral density in terms of the 10-minute mean wind speed U_{10} irrespective of the elevation. The Harris spectrum gives the following expression for the spectral density

$$S_U(f) = \sigma_U^2 \frac{4 \cdot \frac{L_u}{U_{10}}}{(1 + 70.8 \cdot (\frac{fL_u}{U_{10}})^2)^{5/6}}$$

in which L_u is an integral length scale. The integral length scale L_u is in the range 60-400 m with a mean value of 180 m. Unless data indicate otherwise, the integral length scale L_u can be calculated as for the Kaimal spectrum, see 2.3.4.6. The Harris spectrum is originally developed for wind over land and is not recommended for use in the low frequency range, i.e. for $f < 0.01$ Hz.

2.3.4.10 For design of offshore structures, the empirical *Simiu and Leigh spectrum* may be applied. This model spectrum is developed taking into account the wind energy over a seaway in the low frequency range. The Simiu and Leigh spectrum $S(f)$ can be obtained from the following equations

$$\frac{fS(f)}{u*^2} = \begin{cases} a_1 f_* + b_1 f_*^2 + d_1 f_*^3 & \text{for } f_* \leq f_m \\ c_2 + a_2 f_* + b_2 f_*^2 & \text{for } f_m < f_* \leq f_s \\ 0.26 f_*^{-2/3} & \text{for } f_* > f_s \end{cases}$$

where

$$f_* = \frac{f \cdot z}{U_{10}(z)}$$

f = frequency

z = height above the sea surface

U_{10} = 10-minute mean wind speed at height z

$$a_1 = \frac{4L_u \beta}{z}$$

$$\beta_1 = 0.26 f_s^{-2/3}$$

$$b_2 = \frac{\frac{1}{3} a_1 f_m + (\frac{7}{3} + \ln \frac{f_s}{f_m})\beta_1 - \beta}{\frac{5}{6}(f_m - f_s)^2 + \frac{1}{2}(f_m^2 - f_s^2) + 2f_m(f_s - f_m) + f_s(f_s - 2f_m)\ln \frac{f_s}{f_m}}$$

$$a_2 = -2b_2 f_m$$

$$d_1 = \frac{2}{f_m^3}(\frac{a_1 f_m}{2} - \beta_1 + b_2(f_m - f_s)^2)$$

$$b_1 = -\frac{a_1}{2f_m} - 1.5f_m d_1$$

$$c_2 = \beta_1 - a_2 f_s - b_2 f_s^2$$

$$\beta = \sigma_U^2 / u_*^2 = 6.0$$

f_m = dimensionless frequency at which $fS(f)$ is maximum

f_s = dimensionless frequency equivalent to the lower bound of the inertial subrange.

The magnitude of the integral length scale L_u typically ranges from 100 to 240 m for winds at 20-60 m above the sea surface. Unless data indicate otherwise, L_u can be calculated as for the Kaimal spectrum, see 2.3.4.7.

2.3.4.11 For design of offshore structures, the empirical *Ochi and Shin spectrum* may be applied. This model spectrum is developed from measured spectra over a seaway. The Ochi and Shin spectrum $S(f)$ can be obtained from the following equations

$$\frac{fS(f)}{u*^2} = \begin{cases} 583 f_* & \text{for} \quad 0 \leq f_* \leq 0.003 \\[2mm] \dfrac{420 f_*^{0.7}}{(1 + f_*^{0.35})^{11.5}} & \text{for} \quad 0.003 < f_* \leq 0.1 \\[2mm] \dfrac{838 f_*}{(1 + f_*^{0.35})^{11.5}} & \text{for} \quad 0.1 > f_* \end{cases}$$

where

$$f_* = \frac{f \cdot z}{U_{10}(z)}$$

The Ochi and Shin spectrum has more energy content in the low frequency range ($f < 0.01$ Hz) than the Davenport, Kaimal and Harris spectra which are spectral models traditionally used to represent wind over land.

Yet, for frequencies less than approximately 0.001 Hz, the Ochi and Shin spectrum has less energy content than the Frøya spectrum which is an alternative spectral model for wind over seaways. This is a frequency range for which the Ochi and Shin spectrum has not been calibrated to measured data but merely been assigned an idealised simple function.

2.3.4.12 For situations where excitation in the low-frequency range is of importance, the *Frøya model spectral density* proposed by Andersen and Løvseth (1992, 2006) is recommended for wind over water

$$S_U(f) = 320 \cdot \frac{(\frac{U_0}{10})^2 (\frac{z}{10})^{0.45}}{(1 + \tilde{f}^n)^{\frac{5}{3n}}}$$

where

$$\tilde{f} = 172 \cdot f \cdot (\frac{z}{10})^{2/3} \cdot (\frac{U_0}{10})^{-0.75}$$

and $n = 0.468$, U_0 is the 1-hour mean wind speed at 10 m height in units of m/s, and z is the height above sea level in units of m. The Frøya spectrum is originally developed for neutral conditions over water in the Norwegian Sea. Use of the Frøya spectrum can therefore not necessarily be recommended in regimes where stability effects are important. A frequency of 1/2400 Hz defines the lower bound for the range of application of the Frøya spectrum. Whenever it is important to estimate the energy in the low frequency range of the wind spectrum over water, the Frøya spectrum is considerably better than the Dav-

enport, Kaimal and Harris spectra, which are all based on studies over land, and it should therefore be applied in preference to these spectra.

The frequency of 1/2400 Hz, which defines the lower bound of the range of application of the Frøya spectrum, corresponds to a period of 40 minutes. For responses with natural periods of this order, the damping is normally quite small, and the memory time of the response process is several response periods. Since it cannot always be relied upon that the stochastic wind speed process remains stationary over time intervals of the order of 2 to 3 hours, the wind spectrum approach cannot necessarily be utilised for wind loads on structures, whose natural frequencies are near the limiting frequency of 1/2400 Hz of the wind spectrum.

2.3.5 Wind speed process and wind speed field

2.3.5.1 Spectral moments are useful for representation of the wind speed process $U(t)$, where U denotes the instantaneous wind speed at the time t. The j-th spectral moment is defined by

$$m_j = \int_0^\infty f^j S_U(f) df$$

It is noted that the standard deviation of the wind speed process is given by $\sigma_U = m_0^{1/2}$.

2.3.5.2 In the short term, such as within a 10-minute period, the wind speed process $U(t)$ can usually be represented as a Gaussian process, conditioned on a particular 10-minute mean wind speed U_{10} and a given standard deviation σ_U. The instantaneous wind speed U at a considered point in time will then follow a normal distribution with mean value U_{10} and standard deviation σ_U. This is usually the case for the turbulence in homogeneous terrain. However, for the turbulence in complex terrain a skewness of −0.1 is not uncommon, which implies that the Gaussian assumption, which requires zero skewness, is not quite fulfilled. The skewness of the wind speed process is the 3rd order moment of the wind speed fluctuations divided by σ_U^3.

2.3.5.3 Although the short-term wind speed process may be Gaussian for homogeneous terrain, it will usually not be a narrow-banded Gaussian process. This is of importance for prediction of extreme values of wind speed, and such extreme values and their probability distributions can be expressed in terms of the spectral moments.

2.3.5.4 At any point in time there will be variability in the wind speed from one point in space to another. The closer together the two points are, the higher is the correlation between their respective wind speeds. The wind speed will form a random field in space. The autocorrelation function for the wind speed field can be expressed as follows

$$\rho(r) = \frac{1}{\sigma_U^2} \int_0^\infty \sqrt{Coh(r,f)} S_U(f) df$$

in which r is the distance between the two points, f is the frequency, $S_U(f)$ is the power spectral density and $Coh(r,f)$ is the coherence spectrum. The coherence spectrum $Coh(r,f)$ is a frequency-dependent measure of the spatial connectivity of the wind speed and expresses the squared correlation between the power spectral densities at frequency f in two points separated a distance r apart in space.

2.3.5.5 The integral length scale L_u, which is a parameter in the models for the power spectral density, is defined as

$$L_u = \int_0^\infty \rho(r) dr$$

and is different for longitudinal, lateral and vertical separation.

2.3.5.6 Unless data indicate otherwise, the coherence spectrum may be represented by a model spectrum. Several model spectra exist. The most commonly used coherence models are presented in 2.3.5.7 to 2.3.5.17.

2.3.5.7 The exponential Davenport coherence spectrum reads

$$Coh(r, f) = \exp(-cf\frac{r}{u})$$

where r is the separation, u is the average wind speed over the distance r, f is the frequency, and c is a non-dimensional decay constant, which is referred to as the coherence decrement, and which reflects the correlation length of the wind speed field. The coherence decrement c is not constant, but depends on the separation r and on the type of separation, i.e. longitudinal, lateral or vertical separation. The coherence decrement typically increases with increasing separation, thus indicating a faster decay of the coherence with respect to frequency at larger separations. For along-wind turbulence and vertical separations in the range 10-20 m, coherence decrements in the range 18-28 are recommended.

2.3.5.8 The Davenport coherence spectrum was originally proposed for along-wind turbulence, i.e. longitudinal wind speed fluctuations, and vertical separations. Application of the Davenport coherence spectrum to along-wind turbulence and lateral separations usually entails larger coherence decrements than those associated with vertical separations.

2.3.5.9 It may not be appropriate to extend the application of the Davenport coherence spectrum to lateral and vertical turbulence components, since the Davenport coherence spectrum with its limiting value of 1.0 for $f = 0$ fails to account for coherence reductions at low frequencies for these two turbulence components.

2.3.5.10 It is a shortcoming of the Davenport model that it is not differentiable for $r = 0$. Owing to flow separation, the limiting value of the true coherence for $r = 0$ will often take on a value somewhat less than 1.0, whereas the Davenport model always leads to a coherence of 1.0 for $r = 0$.

2.3.5.11 The exponential IEC coherence spectrum reads

$$Coh(r, f) = \exp\left[-2a\sqrt{(\frac{fr}{u})^2 + (b\frac{r}{L_c})^2}\right]$$

where r is the separation, u is the average wind speed over the distance r, f is the frequency, and a and b are non-dimensional constants. L_C is the coherence scale parameter, which relates to the integral length scale L_u through $L_C = 0.742L_u$. Reference is made to IEC (2005). Except at very low frequencies, it is recommended to apply $a = 8.8$ and $b = 0.12$ for along-wind turbulence and relatively small vertical and lateral separations r in the range 7-15 m.

2.3.5.12 For along-wind coherence at large separations r, the exponential IEC model with these coefficient values may lead to coherence predictions which deviate considerably from the true coherences, in particular at low frequencies.

2.3.5.13 The isotropic von Karman coherence model reads

$$Coh(r, f) = \left\{\frac{2^{1/6}}{\Gamma(5/6)}\left[\zeta^{5/6}K_{5/6}(\zeta) - \frac{1}{2}\zeta^{11/6}K_{1/6}(\zeta)\right]\right\}^2$$

for the along-wind turbulence component for lateral as well as for vertical separations r.

2.3.5.14 For the lateral turbulence component and lateral separations r, the coherence model reads

$$Coh(r, f) = \left\{\frac{2^{1/6}}{\Gamma(5/6)}\left[\zeta^{5/6}K_{5/6}(\zeta) \right.\right.$$

$$\left.\left. + \frac{3\cdot(2\pi fr/u)^2}{3\zeta^2 + 5\cdot(2\pi fr/u)^2}\zeta^{11/6}K_{1/6}(\zeta)\right]\right\}^2$$

This expression also applies to the vertical turbulence component for vertical separations r.

2.3.5.15 For the vertical turbulence component and lateral separations r, the coherence model reads

$$Coh(r, f) = \left\{\frac{2^{1/6}}{\Gamma(5/6)}\left[\zeta^{5/6}K_{5/6}(\zeta) \right.\right.$$

$$\left.\left. + \frac{3\cdot(r/(aL))^2}{3\zeta^2 + 5\cdot(2\pi fr/u)^2}\zeta^{11/6}K_{1/6}(\zeta)\right]\right\}^2$$

This expression also applies to the lateral turbulence component for vertical separations r.

In these expressions

$$\Gamma(5/6) \approx 1.134062$$

$$\zeta = 2\pi\sqrt{(fr/u)^2 + (0.12r/L)^2}$$

$$a = \Gamma(1/3)/(\sqrt{\pi}\Gamma(5/6)) \approx 1.335381$$

apply. L is a length scale which relates to the integral length scale L_u through $L = 0.742L_u$, $\Gamma(\ )$ denotes the Gamma function and $K_\nu(\ )$ denotes the modified Bessel function of order ν.

2.3.5.16 The von Karman coherence model is based on assumptions of homogeneity, isotropy and frozen turbulence. The von Karman coherence model in general provides a good representation of the coherence structure of the longitudinal, lateral and vertical turbulence components for longitudinal and lateral separations. For vertical separations, measurements indicate that the model may not hold, possibly owing to a lack of vertical isotropy caused by vertical instability. Over large separations, i.e. separations in excess of about 20 m, the von Karman coherence model tends to overestimate the coherence.

For details about the von Karman coherence model, reference is made to Saranyansoontorn et al. (2004).

2.3.5.17 The Frøya coherence model is developed for wind over water and expresses the coherence of the longitudinal wind speed fluctuations between two points in space as

$$Coh(f, \Delta) = \exp\left\{-\frac{1}{U_0}\cdot\sqrt{\sum_{i=1}^{3}A_i^2}\right\}$$

where U_0 is the 1-hour mean wind speed and Δ is the separation between the two points whose coordinates are (x_1, y_1, z_1) and (x_2, y_2, z_2). Here, x_1 and x_2 are along-wind coordinates, y_1 and y_2 are across-wind coordinates, and z_1 and z_2 are levels above the still water level. The coefficients A_i are calculated as

$$A_i = \alpha_i \cdot f^{r_i} \cdot \Delta_i^{q_i} \cdot z_g^{-p_i}$$

with

$$z_g = \frac{\sqrt{z_1 \cdot z_2}}{H}$$

and $H = 10$ m is the reference height. The coefficients α, p_i, q_i and r_i and the separation components Δ_i, $i = 1, 2, 3$, are given in Table 2-2.

Table 2-2 Coefficients for Frøya coherence spectrum

i	Δ_i	q_i	p_i	r_i	α_i
1	$|x_2-x_1|$	1.00	0.4	0.92	2.9
2	$|y_2-y_1|$	1.00	0.4	0.92	45.0
3	$|z_2-z_1|$	1.25	0.5	0.85	13.0

2.3.5.18 As an alternative to represent turbulent wind fields by means of a power spectral density model and a coherence model, the turbulence model for wind field simulation by Mann (1998) can be applied. This model is based on a model of the spectral tensor for atmospheric surface-layer turbulence at high wind speeds and allows for simulation of two- and three-dimensional fields of one, two or three components of the wind velocity fluctuations. Mann's model is widely used for wind turbine design.

2.3.6 Wind profile and atmospheric stability

2.3.6.1 The wind profile is the variation with height of the wind speed. The wind profile depends much on the atmospheric stability conditions. Even within the course of 24 hours, the wind profile will change between day and night, dawn and dusk.

2.3.6.2 Wind profiles can be derived from the logarithmic model presented in 2.3.2.4, modified by a stability correction. The stability-corrected logarithmic wind profile reads

$$U(z) = \frac{u^*}{\kappa}(\ln\frac{z}{z_0} - \psi)$$

in which ψ is a stability-dependent function, which is positive for unstable conditions, negative for stable conditions, and zero for neutral conditions. Unstable conditions typically prevail when the surface is heated and the vertical mixing is increasing. Stable conditions prevail when the surface is cooled, such as during the night, and vertical mixing is suppressed. Figure 2-3 shows examples of stability-corrected logarithmic wind profiles for various conditions at a particular location.

2.3.6.3 The stability function ψ depends on the non-dimensional stability measure $\zeta = z/L_{MO}$, where z is the height and L_{MO} is the Monin-Obukhov length. The stability function can be calculated from the expressions

$\psi = -4.8\zeta$ for $\zeta \geq 0$

$\psi = 2\ln(1+x)+\ln(1+x^2)-2\tan^{-1}(x)$ for $\zeta < 0$

in which $x = (1-19.3\zeta)^{1/4}$.

2.3.6.4 The Monin-Obukhov length L_{MO} depends on the sensible and latent heat fluxes and on the momentum flux in terms of the frictional velocity u^*. Its value reflects the relative influence of mechanical and thermal forcing on the turbulence. Typical values for the Monin-Obukhov length L_{MO} are given in Table 2-3.

Table 2-3 Monin-Obukhov length

Atmospheric conditions	L_{MO}(m)
Strongly convective days	−10
Windy days with some solar heating	−100
Windy days with little sunshine	−150
No vertical turbulence	0
Purely mechanical turbulence	∞
Nights where temperature stratification slightly dampens mechanical turbulence generation	>0
Nights where temperature stratification severely suppresses mechanical turbulence generation	>>0
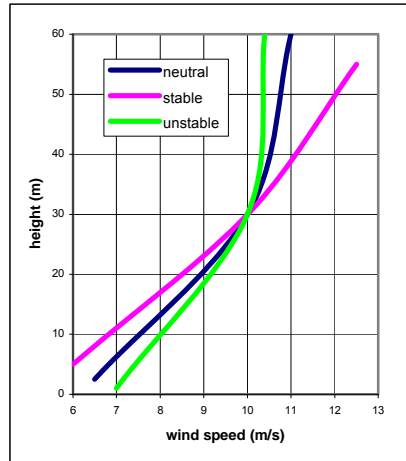
Figure 2-3
Example of wind profiles for neutral, stable and unstable conditions

2.3.6.5 The *Richardson number R* is a dimensionless parameter whose value determines whether convection is free or forced,

$$R = -\frac{g\frac{d\rho_0}{dz}}{\rho_0(\frac{dU}{dz})^2}$$

where g is the acceleration of gravity, ρ_0 is the unperturbed density, $d\rho_0/dz$ is the vertical density gradient and dU/dz is the vertical gradient of the horizontal wind speed. R is positive in stable air, i.e. when the heat flux is downward, and R is negative in unstable air, i.e. when the heat flux is upward.

2.3.6.6 When data for the Richardson number R are available, the following empirical relationships can be used to obtain the Monin-Obukhov length,

$$L_{MO} = \frac{z}{R} \quad \text{in unstable air}$$

$$L_{MO} = z\frac{1-5R}{R} \quad \text{in stable air}$$

2.3.6.7 When data for the Richardson number R are not available, the Richardson number can be computed from averaged conditions as follows

$$R = \frac{\frac{g}{T}(\gamma_d - \gamma)}{\left(\frac{\partial\overline{u}}{\partial z}\right)^2 + \left(\frac{\partial\overline{v}}{\partial z}\right)^2}(1+\frac{0.07}{B})$$

in which g is the acceleration of gravity, T is the temperature, $\gamma = -\partial T/\partial z$ is the lapse rate, and $\gamma_d \approx 9.8°C/km$ is the dry adiabatic lapse rate. Further, $\partial\overline{u}/\partial z$ and $\partial\overline{v}/\partial z$ are the vertical gradients of the two horizontal average wind speed components $\overline{u}$ and $\overline{v}$; and z denotes the vertical height. Finally, the Bowen ratio B of sensible to latent heat flux at the surface can near the ground be approximated by

$$B \approx \frac{c_p}{L_{MO}}\frac{(\overline{T}_2 - \overline{T}_1)}{(\overline{q}_2 - \overline{q}_1)}$$

in which c_p is the specific heat, L_{MO} is the Monin-Obukhov length, $\overline{T}_1$ and $\overline{T}_2$ are the average temperatures at two levels denoted 1 and 2, respectively, and $\overline{q}_1$ and $\overline{q}_2$ are the average

specific humidities at the same two levels. The specific humidity q is in this context calculated as the fraction of moisture by mass.

2.3.6.8 Application of the algorithm in 2.3.6.7 requires an initial assumption to be made for L_{MO}. An iterative approach is then necessary for solution of the Richardson number R. Convergence is achieved when the calculated Richardson number R leads to a Monin-Obukhov length L_{MO} by the formulas in 2.3.6.6 which equals the value of L_{MO}. Further details about atmospheric stability and its representation can be found in Panofsky and Dutton (1984).

2.3.6.9 Topographic features such as hills, ridges and escarpments affect the wind speed. Certain layers of the flow will accelerate near such features, and the wind profiles will become altered.

2.4 Transient wind conditions

2.4.1 General

2.4.1.1 When the wind speed changes or the direction of the wind changes, transient wind conditions may occur. Transient wind conditions are wind events which by nature fall outside of what can normally be represented by stationary wind conditions. Examples of transient wind conditions are:

— gusts
— squalls
— extremes of wind speed gradients, i.e. first of all extremes of rise times of gust
— strong wind shears
— extreme changes in wind direction
— simultaneous changes in wind speed and wind direction such as when fronts pass.

2.4.2 Gusts

2.4.2.1 Gusts are sudden brief increases in wind speed, characterised by a duration of less than 20 seconds, and followed by a lull or slackening in the wind speed. Gusts may be characterised by their rise time, their magnitude and their duration.

2.4.2.2 Gusts occurring as part of the natural fluctuations of the wind speed within a 10-minute period of stationary wind conditions – without implying a change in the mean wind speed level – are not necessarily to be considered as transient wind conditions, but are rather just local maxima of the stationary wind speed process.

2.4.3 Squalls

2.4.3.1 Squalls are strong winds characterised by a sudden onset, a duration of the order of 10-60 minutes, and then a rather sudden decrease in speed. Squalls imply a change in the mean wind speed level.

2.4.3.2 Squalls are caused by advancing cold air and are associated with active weather such as thunderstorms. Their formation is related to atmospheric instability and is subject to seasonality. Squalls are usually accompanied by shifts in wind direction and drops in air temperature, and by rain and lightning. Air temperature change can be a more reliable indicator of presence of a squall, as the wind may not always change direction.

2.4.3.3 Large uncertainties are associated with squalls and their vertical wind profile and lateral coherence. The vertical wind profile may deviate significantly from the model profiles given in 2.3.2.4 and 2.3.2.8. Assuming a model profile such as the Frøya wind speed profile for extreme mean wind speeds as given in 2.3.2.13 is a possibility. However, such an assumption will affect the wind load predictions and may or may not be conservative.

References

1) Andersen, O.J., and J. Løvseth, "The Maritime Turbulent Wind Field. Measurements and Models," Final Report for Task 4 of the Statoil Joint Industry Project, Norwegian Institute of Science and Technology, Trondheim, Norway, 1992.

2) Andersen, O.J., and J. Løvseth, "The Frøya database and maritime boundary layer wind description," *Marine Structures*, Vol. 19, pp. 173-192, 2006.

3) Astrup, P., S.E. Larsen, O. Rathmann, P.H. Madsen, and J. Højstrup, "WASP Engineering – Wind Flow Modelling over Land and Sea," in *Wind Engineering into the 21st Century*, eds. A.L.G.L. Larose and F.M. Livesey, Balkema, Rotterdam, The Netherlands, 1999.

4) Det Norske Veritas and RISØ, *Guidelines for Design of Wind Turbines*, Copenhagen, Denmark, 2001.

5) Dyrbye, C., and S.O. Hansen, *Wind Loads on Structures*, John Wiley and Sons, Chichester, England, 1997.

6) HSE (Health & Safety Executive), *Environmental considerations*, Offshore Technology Report No. 2001/010, HSE Books, Sudbury, Suffolk, England, 2002.

7) IEC (International Electrotechnical Commission), *Wind Turbines – Part 1: Design Requirements*, IEC61400-1, 3rd edition, 2005.

8) JCSS (Joint Committee on Structural Safety), *Probabilistic Model Code, Part 2: Loads*, 2001.

9) Lungu, D., and Van Gelder, P., "Characteristics of Wind Turbulence with Applications to Wind Codes," Proceedings of the 2nd European & African Conference on Wind Engineering, pp. 1271-1277, Genova, Italy, 1997.

10) Mann, J., "Wind field simulation," *Journal of Prob. Engng. Mech.*, Vol. 13, No. 4, pp. 269-282, Elsevier, 1998.

11) Panofsky, H.A., and J.A. Dutton, *Atmospheric Turbulence, Models and Methods for Engineering Applications*, John Wiley and Sons, New York, N.Y., 1984.

12) Saranyansoontorn, K., L. Manuel, and P.S. Veers, "A Comparison of Standard Coherence Models for Inflow Turbulence with Estimates from Field Measurements," *Journal of Solar Energy Engineering*, ASME, Vol. 126, pp. 1069-1082, 2004.

13) Simiu, E., and R.U. Scanlan, *Wind Effects on Structures; An Introduction to Wind Engineering*, John Wiley, New York, N.Y., 1978.

14) WMO (World Meteorological Organization), *Guide to Meteorological Instruments and Methods of Obser*vation, Publication No. 8, World Meteorological Organisation, Geneva, Switzerland, 1983.

3. Wave Conditions

3.1 General

3.1.1 Introduction

Ocean waves are irregular and random in shape, height, length and speed of propagation. A real sea state is best described by a random wave model.

A linear random wave model is a sum of many small linear wave components with different amplitude, frequency and direction. The phases are random with respect to each other.

A non-linear random wave model allows for sum- and difference frequency wave component caused by non-linear interaction between the individual wave components.

Wave conditions which are to be considered for structural design purposes, may be described either by deterministic design wave methods or by stochastic methods applying wave spectra.

For quasi-static response of structures, it is sufficient to use deterministic regular waves characterized by wave length and corresponding wave period, wave height and crest height. The deterministic wave parameters may be predicted by statistical methods.

Structures with significant dynamic response require stochastic modelling of the sea surface and its kinematics by time series. A sea state is specified by a wave frequency spectrum with a given significant wave height, a representative frequency, a mean propagation direction and a spreading function. In applications the sea state is usually assumed to be a stationary random process. Three hours has been introduced as a standard time between registrations of sea states when measuring waves, but the period of stationarity can range from 30 minutes to 10 hours.

The wave conditions in a sea state can be divided into two classes: *wind seas* and *swell*. Wind seas are generated by local wind, while swell have no relationship to the local wind. Swells are waves that have travelled out of the areas where they were generated. Note that several swell components may be present at a given location.

3.1.2 General characteristics of waves

A *regular* travelling wave is propagating with permanent form. It has a distinct wave length, wave period, wave height.

Wave length: The wave length λ is the distance between successive crests.

Wave period: The wave period T is the time interval between successive crests passing a particular point.

Phase velocity: The propagation velocity of the wave form is called phase velocity, wave speed or wave celerity and is denoted by $c = \lambda / T$.

Wave frequency is the inverse of wave period*: f = 1/T.*

Wave angular frequency: $\omega = 2\pi / T$.

Wave number: $k = 2\pi/\lambda$.

Surface elevation: The surface elevation $z = \eta(x,y,t)$ is the distance between the still water level and the wave surface.

Wave crest height A_C is the distance from the still water level to the crest.

Wave trough depth A_T is the distance from the still water level to the trough.

Wave height: The wave height H is the vertical distance from trough to crest. $H = A_C + A_T$.

Analytic wave theories (See 3.2) are developed for constant water depth d. The objective of a wave theory is to determine the relationship between T and λ and the water particle motion throughout the flow.

The *dispersion relation* is the relationship between wave period T, wave length λ and wave height H for a given water depth d.

Nonlinear regular waves are asymmetric, $A_C > A_T$ and the phase velocity depends on wave height, that is the dispersion relation is a functional relationship between T, λ and H.

The *average energy density E* is the sum of the average kinetic and potential wave energy per unit horizontal area. The *energy flux P* is the average rate of transfer of energy per unit width across a plane normal to the propagation direction of the wave. The group velocity $c_g = P/E$ is the speed of wave energy transfer.

In irregular or random waves, the free surface elevation $\eta(x,y,t)$ is a random process. The local wavelength of irregular waves can be defined as the distance between two consecutive zero up-crossings. The wave crest in irregular waves can be defined as the global maximum between a positive up-crossing through the mean elevation, and the following down-crossing through the same level. A similar definition applies to the wave trough.

3.2 Regular wave theories

3.2.1 Applicability of wave theories

Three wave parameters determine which wave theory to apply in a specific problem. These are the wave height H, the wave period T and the water depth d. These parameters are used to define three non-dimensional parameters that determine ranges of validity of different wave theories,

— Wave steepness parameter: $\quad S = 2\pi \dfrac{H}{gT^2} = \dfrac{H}{\lambda_0}$

— Shallow water parameter: $\quad \mu = 2\pi \dfrac{d}{gT^2} = \dfrac{d}{\lambda_0}$

— Ursell number: $\quad U_R = \dfrac{H\lambda^2}{d^3}$

where λ_0 and k_0 are the linear deep water wave length and wave number corresponding for wave period T. Note that the three parameters are not independent. When two of the parameters are given, the third is uniquely determined. The relation is

$$U_R = \frac{S}{\mu^3}$$

Note that the Ursell number can also be defined as

$$U_r = \frac{H}{k_0^2 d^3} = \frac{1}{4\pi^2} U_R$$

The range of application of the different wave theories are given in Figure 3-2.
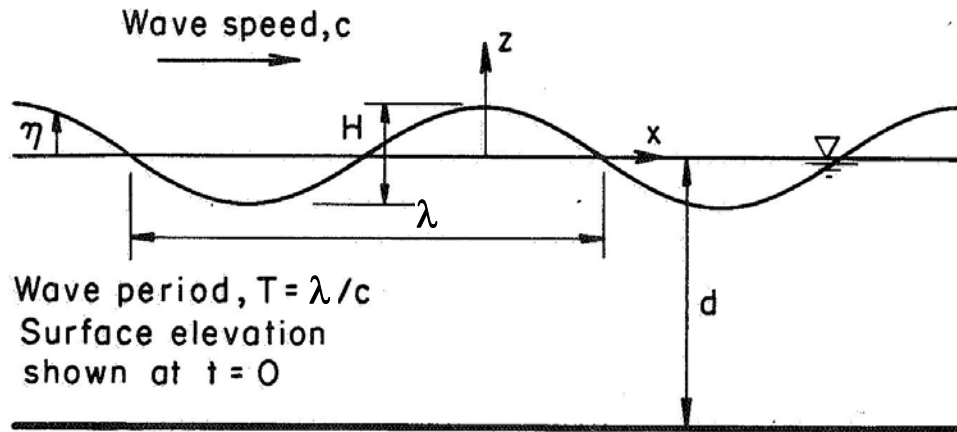
Figure 3-1
Regular travelling wave properties
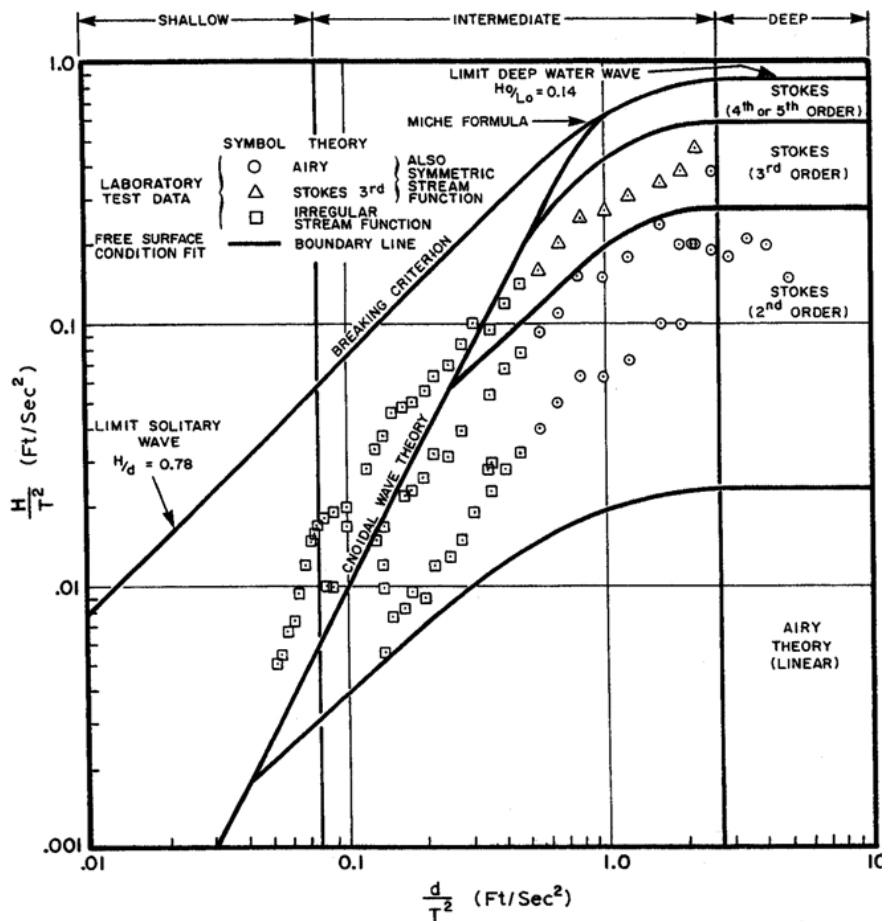
Figure 3-2
Ranges of validity for various wave theories. The horizontal axis is a measure of shallowness while the vertical axis is a measure of steepness (Chakrabarti, 1987)

3.2.2 Linear wave theory

3.2.2.1 The simplest wave theory is obtained by taking the wave height to be much smaller than both the wave length and the water depth. This theory is referred to as small amplitude wave theory, linear wave theory, sinusoidal wave theory or Airy theory.

3.2.2.2 For regular linear waves the wave crest height A_C is equal to the wave trough height A_H and is denoted the wave amplitude A, hence $H = 2A$.

The surface elevation is given by

$$\eta(x,y,t) = \frac{H}{2}\cos\Theta$$

where $\Theta = k(x\cos\beta + y\sin\beta) - \omega t$ is the phase and β is the direction of propagation, measured from the positive x-axis. c is the phase velocity.

3.2.2.3 The dispersion relationship gives the relationship between wave period T and wave length λ. For linear waves in

finite water depth d,

$$T = \left[\frac{g}{2\pi\lambda}\tanh\left(\frac{2\pi d}{\lambda}\right)\right]^{-1/2}$$

In terms of angular frequency $\omega = 2\pi/T$ and wave number $k = 2\pi/\lambda$ the dispersion relation is

$$\omega = \left[gk\tanh(kd)\right]^{1/2}$$

3.2.2.4 An accurate approximation for the wave length λ as a function of the wave period T is

$$\lambda = T(gd)^{1/2}\left(\frac{f(\varpi)}{1+\varpi f(\varpi)}\right)^{1/2}$$

where $f(\varpi) = 1 + \sum_{n=1}^{4}\alpha_n\varpi^n$, $\varpi = (4\pi^2 d)/(gT^2)$ and

$\alpha_1 = 0.666$, $\alpha_2 = 0.445$, $\alpha_3 = -0.105$, $\alpha_4 = 0.272$.

Figure 3-3 gives the wave length as a function of wave period for various water depths.

3.2.2.5 For linear waves the phase velocity only depends on wave length λ, it is independent of wave amplitude A.

$$c = \sqrt{\frac{g\lambda}{2\pi}\tanh(\frac{2\pi d}{\lambda})}$$

Figure 3-3 gives the phase velocity as a function of wave period for various water depths.

3.2.2.6 For deep water $d > \frac{\lambda}{2}$ the formula simplifies to

$$c = \sqrt{\frac{g\lambda}{2\pi}} = \frac{g}{\omega} = \frac{gT}{2\pi}$$

and the dispersion relationship is simplified to

$$\lambda = \frac{gT^2}{2\pi} \text{ or } \lambda = 1.56T^2 \text{ for } \lambda \text{ measured in meters and}$$

T in seconds

Formulae for fluid particle displacement, fluid velocity, fluid acceleration and sub surface fluid pressure in linear and second-order waves are given in Table 3-1.

3.2.3 Stokes wave theory

3.2.3.1 The Stokes wave expansion is an expansion of the surface elevation in powers of the linear wave height H. A first-order Stokes wave is identical to a linear wave, or Airy wave.

3.2.3.2 The surface elevation profile for a regular second-order Stokes wave is given by

$$\eta = \frac{H}{2}\cos\Theta + \frac{\pi H^2}{8\lambda}\frac{\cosh kd}{\sinh^3 kd}[2+\cosh 2kd]\cos 2\Theta$$

where $\Theta = k(x\cos\beta + y\sin\beta) - \omega t$.

3.2.3.3 In deep water, the Stokes second-order wave is given by

$$\eta = \frac{H}{2}\cos\Theta + \frac{\pi H^2}{4\lambda}\cos 2\Theta$$

3.2.3.4 Second-order and higher order Stokes waves are asymmetric with $A_C > A_T$. Crests are steeper and troughs are wider than for Airy waves.

For a second-order deep water Stokes wave

$$A_C = \eta(\Theta = 0) = \frac{H}{2}(1 + \frac{\pi H}{2\lambda})$$

$$A_T = |\eta(\Theta = \pi)| = \frac{H}{2}(1 - \frac{\pi H}{2\lambda})$$

Hence, the crest height is increased by a factor $1 + \pi H/2\lambda$

relative to a linear Airy wave. The linear dispersion relation holds for second-order Stokes waves, hence the phase velocity c and the wave length λ remain independent of wave height.
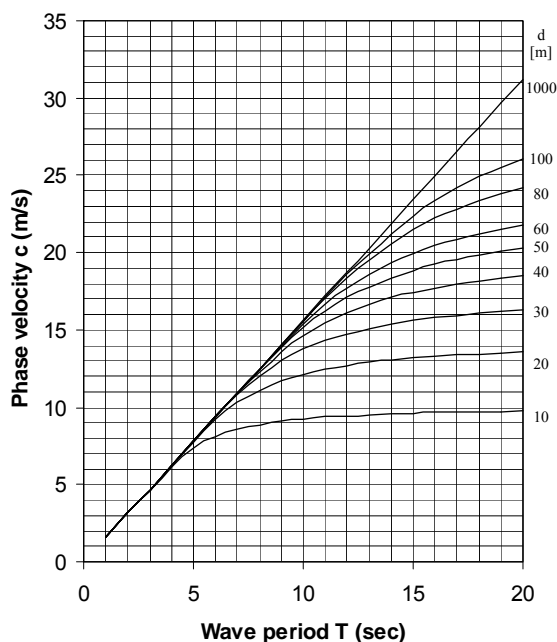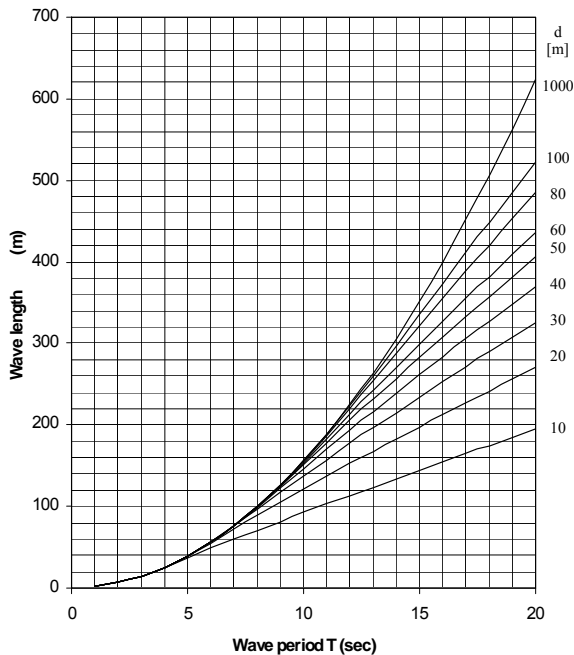
Figure 3-3
Wave length and phase velocity as function of wave period at various water depths for linear waves.

3.2.3.5 To *third order* however, the phase velocity depends on wave height according to

$$c^2 = \frac{g}{k}\tanh(kd)\left\{1 + \left(\frac{kH}{2}\right)^2\left[\frac{9 - 8\cosh^2(kd) + 8\cosh^4(kd)}{8\sinh^4(kd)}\right]\right\}$$

For deep water $d > \dfrac{\lambda}{2}$, the formula simplifies to

$$c^2 = \frac{g}{k}\left[1 + \left(\frac{kH}{2}\right)^2\right]$$

Formulae for fluid particle displacement, particle velocity and acceleration and sub surface pressure in a second-order Stokes wave are given in Table 3-1.

3.2.3.6 For regular steep waves $S < S_{max}$ (and Ursell number $U_R < 30$) Stokes 5th order wave theory applies, ref. Fenton (1985). A method for calculation of Stokes waves to any order n is presented by Schwartz (1974) and Longuet-Higgins (1985). The maximum crest to wave height ratio for a Stokes wave is 0.635.

Stokes wave theory is not applicable for very shallow water, $U_R > 30$, where cnoidal wave theory or stream function wave theory should be used.

For $U_R \sim 30$, both Stokes fifth order wave theory and cnoidal wave theory have inaccuracies. For such regular waves the stream function method is recommended.

3.2.4 Cnoidal wave theory

The cnoidal wave is a periodic wave with sharp crests separated by wide troughs. Cnoidal wave theory should be used when $\mu < 0.125$ and $U_R > 30$. A cnoidal wave has crest to wave height ratio between 0.635 and 1. The cnoidal wave theory and its application is described in Wiegel (1960) and Mallery & Clark (1972).

3.2.5 Solitary wave theory

For high Ursell numbers the wave length of the cnoidal wave goes to infinity and the wave is a solitary wave. A solitary wave is a propagating shallow water wave where the surface elevation lies wholly above the mean water level, hence $A_C = H$. The solitary wave profile can be approximated by

$$\eta(x,t) = H\cosh^{-2}\left[\frac{\sqrt{3\varepsilon}}{2d}\left(1 - \frac{5}{8}\varepsilon\right)(x - ct)\right]$$

where $\varepsilon = H/d$. The wave celerity is $c = 1.33\sqrt{gd}$.

More details on solitary wave theory is given by Sarpkaya & Isaacson (1981).

3.2.6 Stream function wave theory

The stream function wave theory is a purely numerical procedure for approximating a given wave profile and has a broader range of validity than the wave theories above.

A stream function wave solution has the general form

$$\Psi(x,z) = cz + \sum_{n=1}^{N} X(n)\sinh nk(z + d)\cos nkx$$

where c is the wave celerity and N is the order of the wave theory. The required order, N, of the stream function theory is determined by the wave parameters steepness S and shallow water parameter μ. For $N = 1$, the stream function theory reduces to linear wave theory.

The closer to the breaking wave height, the more terms are required in order to give an accurate representation of the wave. Reference is made to Dean (1965 & 1970).

3.3 Wave kinematics

3.3.1 Regular wave kinematics

3.3.1.1 For a specified regular wave with period T, wave height H and water depth d, two-dimensional regular wave kinematics can be calculated using a relevant wave theory valid for the given wave parameters.
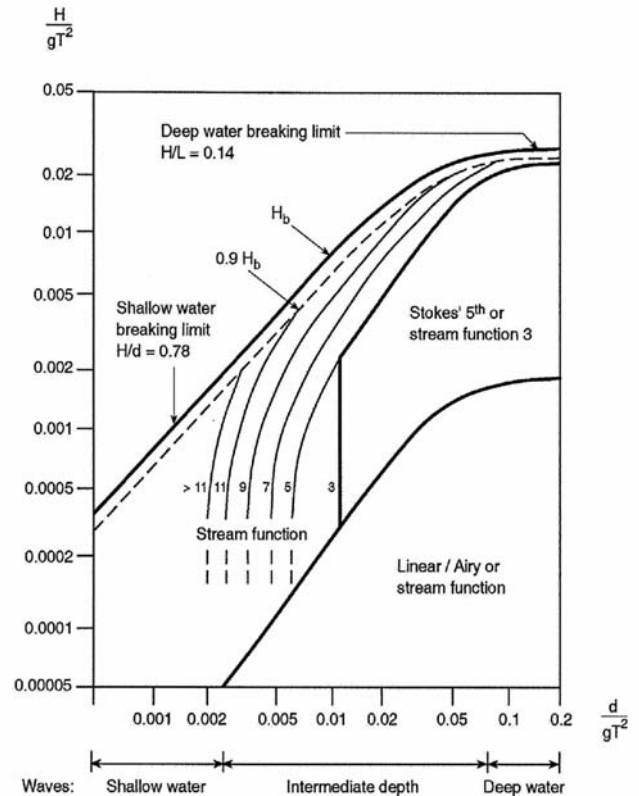
Figure 3-4
Required order, N, of stream function wave theory such that errors in maximum velocity and acceleration are less than one percent.

Table 3-1 gives expressions for horizontal fluid velocity u and vertical fluid velocity w in a linear Airy wave and in a second-order Stokes wave.

3.3.1.2 Linear waves and Stokes waves are based on perturbation theory and provide directly wave kinematics below $z = 0$. Wave kinematics between the wave crest and the still water level can be estimated by stretching or extrapolation methods as described in 3.3.3. The stream function theory (3.2.6) provides wave kinematics all the way up to the free surface elevation.

3.3.2 Modelling of irregular waves

3.3.2.1 Irregular random waves, representing a real sea state, can be modelled as a summation of sinusoidal wave components. The simplest random wave model is the linear long-crested wave model given by

$$\eta_1(t) = \sum_{k=1}^{N} A_k \cos(\omega_k t + \varepsilon_k)$$

where ε_k are random phases uniformly distributed between 0 and 2π, mutually independent of each other and of the random amplitudes A_k which are taken to be Rayleigh distributed with mean square value given by

$$E\left[A_k^2\right] = 2S(\omega_k)\Delta\omega_k$$

$S(\omega)$ is the wave spectrum and $\Delta\omega_k = \omega_k - \omega_{k-1}$ is the differ-

ence between successive frequencies.

3.3.2.2 The lowest frequency interval $\Delta\omega$ is governed by the total duration of the simulation t, $\Delta\omega = 2\pi/t$. The number of fre-

quencies to simulate a typical short term sea state should be at least 1 000. The influence of the maximum frequency ω_{max} should be investigated. This is particularly important when simulating irregular fluid velocities.
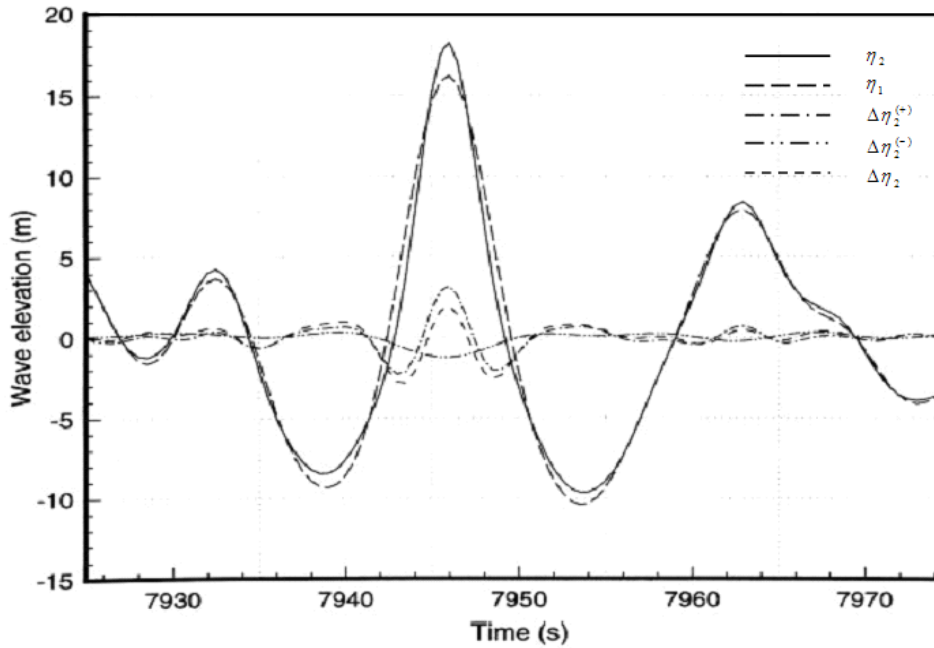
Figure 3-5
First- and second-order irregular wave simulation. H_s = 15.5 m, T_p = 17.8 s, γ = 1.7. N = 21 600, Δt = 0.5 s

3.3.2.3 The simplest nonlinear random wave model is the long-crested second-order model (Longuett-Higgins, 1963), where the second-order wave process has N^2 corrections spread over all sum-frequencies and another N^2 corrections over all difference frequencies. The second-order random wave is then modelled as $\eta_2 = \eta_1 + \Delta\eta_2$ where the second-order correction is given by

$$\Delta\eta_2 = \sum_{m=1}^{N}\sum_{n=1}^{N} A_m A_n E_{mn}^{(+)} \cos\left[(\omega_m + \omega_n)t + (\varepsilon_m + \varepsilon_n)\right]$$

$$+ \sum_{m=1}^{N}\sum_{n=1}^{N} A_m A_n E_{mn}^{(-)} \cos\left[(\omega_m - \omega_n)t + (\varepsilon_m - \varepsilon_n)\right]$$

where $E_{mn}^{(\pm)} = E^{(\pm)}(\omega_m, \omega_n)$ are quadratic surface elevation transfer functions. In deep water,

$$E^{(+)}(\omega_m, \omega_n) = \frac{1}{4g}(\omega_m^2 + \omega_n^2)$$

$$E^{(-)}(\omega_m, \omega_n) = -\frac{1}{4g}\left|\omega_m^2 - \omega_n^2\right|$$

The relative magnitudes between first and second order contributions to free surface elevation are shown in Figure 3-5.

3.3.2.4 The second order model has been shown to fit experimental data well if a cut-off frequency $\omega_{max} = \sqrt{2g/H_s}$ is applied. Numerical tools are available to simulate second-order short-crested random seas. The transfer functions for finite water depth is given by Sharma and Dean (1979) and Marthinsen & Winterstein (1992). Higher order stochastic wave models have been developed for special applications.

3.3.3 Kinematics in irregular waves

The kinematics in irregular waves can be predicted by one of the following methods:

— Grue's method
— Wheeler's method
— Second-order kinematics model.

A simple way of estimating the kinematics below the crest of a large wave in deep water is *Grue's method* (Grue et al. 2003). For a given wave elevation time-series, measured or simulated, the crest height $z = \eta_m$ and the corresponding trough-to-trough period T_{TT} are identified. A local angular frequency is defined by $\omega = 2\pi/T_{TT}$. The corresponding wave number k and the local wave slope ε are calculated by solving numerically the system of equations corresponding to a third-order Stokes wave

$$\frac{\omega^2}{gk} = 1 + \varepsilon^2 \quad , \quad k\eta_m = \varepsilon + \frac{1}{2}\varepsilon^2 + \frac{1}{2}\varepsilon^3$$

The first equation is the nonlinear dispersion relationship and the second equation is the expression for the non-dimensional free surface elevation. The horizontal velocity under the crest is then given by the exponential profile

$$u(z) = \varepsilon \sqrt{\frac{g}{k}} e^{kz}$$

where $z = 0$ is the mean water level and g is the acceleration of gravity. Grue's method as given above is limited to crest kinematics and valid for deep water waves.

3.3.3.1 The *Wheeler stretching method* is widely used. It is based on the observation that the fluid velocity at the still water level is reduced compared with linear theory. The basic principle is that from a given free surface elevation record, one com-

putes the velocity for each frequency component using linear theory and for each time step in the time series, the vertical co-ordinate is stretched according to

$$z = \frac{z_s - \eta}{1 + \eta/d} \quad ; \quad -d < z < 0 \; ; \; -d < z_s < \eta$$

where η is the free surface elevation and d is the water depth (Figure 3-6).
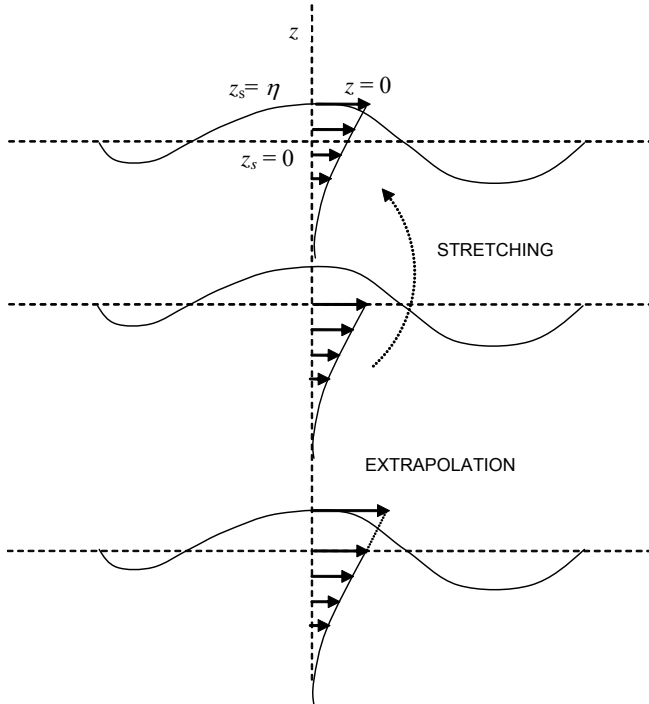
Figure 3-6
Stretching and extrapolation of velocity profile.

3.3.3.2 The Wheeler method should be used with a nonlinear (measured or second-order) elevation record and nonlinear kinematics components added as if they are independent.

Horizontal velocities can be consistently modelled up to the free surface elevation by use of a *second-orderkinematics model* which is a Taylor expansion (extrapolation) of the linear velocity profile including contributions from sum- and difference frequency wave components. Reference is made to Marthinsen & Winterstein (1992), Nestegård & Stokka (1995) and Stansberg & Gudmestad (1996). The horizontal velocity at a level z under a crest is given by

$$u(z) = u^{(1)}(z) + u^{(2+)}(z) + u^{(2-)}(z) \qquad ; \quad z \leq 0$$

$$u(z) = u^{(1)}(0) + (\partial u^{(1)}/\partial z)|_{z=0} \, z + u^{(2+)}(0) + u^{(2-)}(0) \; ; \quad z > 0$$

where $u^{(1)}(z)$, $u^{(2+)}(z)$, $u^{(2-)}(z)$ are the linear, second order sum- and second order difference-frequency velocity profiles. Similar expressions exist for vertical velocity and horizontal and vertical acceleration. Note that when calculating forces on risers attached to a floater, the kinematics must be consistent with the wave theory used for calculating the floater motion.

3.3.3.3 When using a measured input record, a low-pass filter must be applied to avoid the very high frequencies. It is advised to use a cut-off frequency equal to 4 times the spectral peak frequency.

3.3.3.4 A comparison of the three methods has been presented by Stansberg (2005):

— The second-order kinematics model performs well for all z-levels under a steep crest in deep water.
— Grue's method performs well for $z > 0$, but it overpredicts the velocity for $z < 0$.
— Wheeler's method, when used with a measured or a second-order input elevation record performs well close to the crest, but it underpredicts around $z = 0$ as well as at lower levels. If Wheeler's method is used with a linear input, it underpredicts also at the free surface.

3.3.4 Wave kinematics factor

When using two-dimensional design waves for computing forces on structural members, the wave particle velocities and accelerations may be reduced by taking into account the actual directional spreading of the irregular waves. The reduction factor is known as the *wave kinematics factor* defined as the ratio between the r.m.s. value of the in-line velocity and the r.m.s. value of the velocity in a unidirectional sea.

The wave kinematics factor can be taken as

$$F_s = \left[\frac{n+1}{n+2} \right]^{1/2}$$

for the directional spreading function $D(\theta) \sim \cos^n(\theta)$ defined in 3.5.8.4, or it can be taken as

$$F_s = \left[\frac{s^2 + s + 1}{(s+1)(s+2)} \right]^{1/2}$$

for the directional spreading function $D(\theta) \sim \cos^{2s}(\theta/2)$ defined in 3.5.8.7.

3.4 Wave transformation

3.4.1 General

Provided the water depth varies slowly on a scale given by the wave length, wave theories developed for constant water depth can be used to predict transformation of wave properties when water waves propagate towards the shore from deep to shallow water. Wave period T remains constant, while phase speed c and wave length λ decrease, and wave height H and steepness S increases. A general description of wave transformations is given by Sarpkaya & Isaacson.

3.4.2 Shoaling

For two-dimensional motion, the wave height increases according to the formula

$$\frac{H}{H_0} = K_s = \sqrt{\frac{c_{g,0}}{c_g}}$$

where K_s is the *shoaling coefficient* and c_g is the group velocity

$$c_g = \frac{1}{2}\left[1 + \frac{2kd}{\sinh(2kd)} \right]\sqrt{\frac{g}{k}\tanh(kd)}$$

and wave number k is related to wave period T by the dispersion relation. The zero subscript refer to deep water values at water depth $d = d_0$.

3.4.3 Refraction

The phase speed varies as a function of the water depth, d. Therefore, for a wave which is approaching the depth contours at an angle other than normal, the water depth will vary along the wave crest, so will the phase speed. As a result, the crest will tend to bend towards alignment with the depth contours and wave crests will tend to become parallel with the shore line.

For parallel sea bed contours, Snell's refraction law applies

$$\frac{\sin \alpha}{c(kd)} = \text{constant}$$

where $c = c(kd)$ is the phase velocity and α is the angle between the wave ray and a normal to the bed contour.

Refraction has also an affect on the amplitude. For depth contours parallel with the shore line, the change of wave height is given by

$$\frac{H}{H_0} = K_s K_r$$

where K_s is the shoaling coefficient as given in 3.4.2 and K_r is the refraction coefficient defined by

$$K_r = \left[\frac{1 - \sin^2 \alpha_0 \tanh^2 (kd)}{\cos^2 \alpha_0} \right]^{-1/4}$$

where α_0 is the angle between the wave crest and the depth contours at the deep water location. More details on shoaling and refraction can be found in Sarpkaya and Isaacson (1981).

3.4.4 Wave reflection

When surface waves encounter a subsurface or surface piercing vertical barrier, part of the wave energy is reflected. Regular waves of wave height H propagating normal to an infinite vertical wall ($x = 0$) lead to standing waves.

The free surface elevation for linear standing waves against a surface piercing vertical wall is given by

$$\eta = H \cos(kx) \cos(\omega t)$$

The pressure at the barrier is given by:

$$p = -\rho g z + \rho g H \frac{\cosh[k(z+d)]}{\cosh(kd)} \cos(\omega t)$$
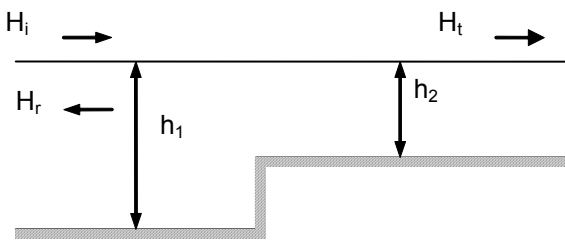
Figure 3-7
Waves passing over a subsurface barrier. Water depth changes from h_1 to h_2.

The reflection coefficient $R = H_r/H_i$ is defined as the ratio of reflected wave height to incident wave height. For long waves with wave length much larger than the water depth, propagating in a direction θ relative to the normal to the subsurface barrier ($\theta = 0$ is normal incidence), the reflection coefficient is given by

$$R = \frac{\alpha_1 h_1 - \alpha_2 h_2}{\alpha_1 h_1 + \alpha_2 h_2}$$

where $\alpha_i = k_i \cos \theta_i$, $k_1 \sin \theta_1 = k_2 \sin \theta_2$, $k_i = \omega \sqrt{g h_i}$, ω is the wave frequency and indices 1,2 correspond to values for depth 1 and 2 respectively.

The transmission coefficient $T = H_t/H_i$ is defined as the ratio of transmitted wave height to incident wave height.

$$R = \frac{2\alpha_1 h_1}{\alpha_1 h_1 + \alpha_2 h_2}$$

For $h_1 < h_2$ total reflection ($R = 1$) occurs for a critical angle of incidence,

$$(\theta_1)_{cr} = \tan^{-1} \frac{k_2}{\sqrt{k_1^2 - k_2^2}}$$

For general topographies numerical methods must be applied.

3.4.5 Standing waves in shallow basin

Natural periods of standing waves in a shallow basin of length L, width B and depth d are

$$T_{n,m} = \frac{2}{\sqrt{gd}} \left(\frac{n^2}{L^2} + \frac{m^2}{B^2} \right)^{-\frac{1}{2}}, n,m = 1,2,\cdots$$

Natural periods of standing waves in a shallow circular basin with radius a are given by

$$T_s = \frac{2\pi a}{j'_{0,s} \sqrt{gd}}$$

for symmetric modes and

$$T_s = \frac{2\pi a}{j'_{1,s} \sqrt{gd}}$$

for unsymmetrical modes where $j'_{0,s}$ and $j'_{1,s}$ are zeros of derivatives of Bessel function J'_0 and J'_1 respectively.

3.4.6 Maximum wave height and breaking waves

3.4.6.1 The wave height is limited by breaking. The maximum wave height H_b is given by

$$\frac{H_b}{\lambda} = 0.142 \tanh \frac{2\pi d}{\lambda}$$

where λ is the wave length corresponding to water depth d. In deep water the breaking wave limit corresponds to a maximum steepness $S_{\max} = H_b/\lambda = 1/7$.

3.4.6.2 The breaking wave height as a function of wave period for different water depths is given in Figure 3-8. In shallow water the limit of the wave height can be taken as 0.78 times the local water depth. Note that waves propagating over a horizontal and flat sea bed may break for a lower wave height. Laboratory data (Nelson, 1994) and theoretical analysis (Massel, 1996) indicate that under idealized conditions the breaking limit can be as low as 0.55.

3.4.6.3 Design of coastal or offshore structures in shallow water requires a reliable estimation of maximum wave height. More details on modelling of shallow water waves and their loads can be found in the Coastal Engineering Manual (2004).

3.4.6.4 Breaking waves are generally classified as *spilling, plunging, collapsing* or *surging*. Formation of a particular breaker type depends on the non-dimensional parameter

$$\beta = \frac{H_b}{gT^2 m}$$

where H_b is the wave height at breaking, m is the beach slope, assumed to be constant over several wave lengths.

Spilling breakers are characterized by foam spilling from the crest down on the forward face of the wave. They occur in deep water or on gentle beach slopes. Spilling breakers usually form when $\beta > 5$.
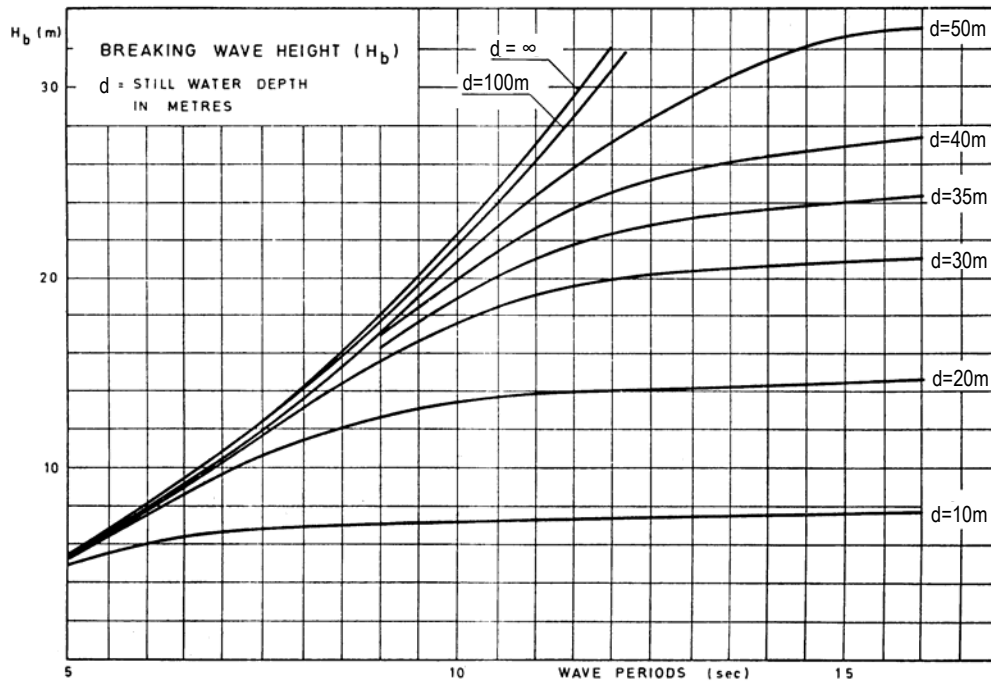
Figure 3-8
Breaking wave height dependent on still water depth

Plunging breakers occur on moderately steep beach slopes. They are characterized by a well defined jet of water forming from the crest and falling onto the water surface ahead of the crest. Plunging breakers form when $0.1 < \beta < 5$.

Surging breakers occur on relatively steep beaches in which there is considerable reflection with foam forming near the beach surface. Surging breakers form when $\beta < 0.1$.

The *collapsing wave* foams lower down the forward face of the wave and is a transition type between plunging and surging breakers, $\beta \sim 0.1$

3.5 Short term wave conditions

3.5.1 General

It is common to assume that the sea surface is stationary for a duration of 20 minutes to 3-6 hours. A stationary sea state can be characterised by a set of environmental parameters such as the *significant wave height H_s* and the *peak period T_p*.

The significant wave height H_s is defined as the average height (trough to crest) of the highest one-third waves in the indicated time period, also denoted $H_{1/3}$.

The peak period T_p is the wave period determined by the inverse of the frequency at which a wave energy spectrum has its maximum value.

The zero-up-crossing period T_z is the average time interval between two successive up-crossings of the mean sea level.

3.5.2 Wave spectrum - general

3.5.2.1 Short term stationary irregular sea states may be described by a wave spectrum; that is, the power spectral density function of the vertical sea surface displacement.

3.5.2.2 Wave spectra can be given in table form, as measured spectra, or by a parameterized analytic formula. The most appropriate wave spectrum depends on the geographical area with local bathymetry and the severity of the sea state.

3.5.2.3 The Pierson-Moskowitz (PM) spectrum and JON-SWAP spectrum are frequently applied for wind seas (Hasselmann et al. 1976; Pierson and Moskowitz, 1964). The PM-spectrum was originally proposed for fully-developed sea. The JONSWAP spectrum extends PM to include fetch limited seas, describing developing sea states. Both spectra describe wind sea conditions that often occur for the most severe seastates.

3.5.2.4 Moderate and low sea states in open sea areas are often composed of both wind sea and swell. A two peak spectrum may be used to account for both wind sea and swell. The Ochi-Hubble spectrum and the Torsethaugen spectrum are two-peak spectra (Ochi and Hubble, 1976; Torsethaugen, 1996).

3.5.2.5 The spectral moments m_n of general order n are defined as

$$m_n = \int_0^\infty f^n \, S\,(f) \, df$$

where f is the wave frequency, and $n = 0,1,2,\ldots$

3.5.2.6 If the power spectral density $S(\omega)$ is given as a function of the angular frequency ω, it follows that

$$S\,(\omega) = S(f)/2\pi$$

and for the corresponding spectral moment M_n, the relationship to m_n is

$$M_n = \int_0^\infty \omega^n \, S(\omega) \, d\omega = (2\pi)^n \, m_n$$

Table 3-1 Gravity wave theory

Parameter	Airy wave theory		Stokes second-order wave theory
	General water depth	*Deep water*	
Velocity potential, ϕ	$\dfrac{\pi H}{kT}\dfrac{\cosh[k(z+d)]}{\sinh(kd)}\sin\theta$ $=$ $\dfrac{gH}{2\omega}\dfrac{\cosh[k(z+d)]}{\cosh(kd)}\sin\theta$	$\dfrac{\pi H}{kT}e^{kz}\sin\theta$ $=$ $\dfrac{gH}{2\omega}e^{kz}\sin\theta$	$\phi_t+\dfrac{3}{8}\dfrac{\pi H}{kT}\left(\dfrac{\pi H}{\lambda}\right)\dfrac{\cosh[2k(z+d)]\sin 2\theta}{\sinh^4(kd)}$ Note that in deep water the Stokes second-order wave potential is equal to the first order Airy wave potential.
Phase velocity, celerity, c	$\sqrt{\dfrac{g}{k}\tanh(kd)}$	$gT/(2\pi)$	$\sqrt{\dfrac{g}{k}\tanh(kd)}$
Wavelength, λ	cT	$gT^2/(2\pi)$	cT
Surface elevation, η	$\dfrac{H}{2}\cos\theta$	$\dfrac{H}{2}\cos\theta$	$\eta_t+\dfrac{\pi H^2}{8\lambda}\dfrac{\cosh kd}{\sinh^3 kd}[2+\cosh 2kd]\cos 2\Theta$
Horizontal particle displacement, ξ	$-\dfrac{H}{2}\dfrac{\cosh[k(z+d)]}{\sinh(kd)}\sin\theta$	$-\dfrac{H}{2}e^{kz}\sin\theta$	$\xi_t+\dfrac{H}{8}\left(\dfrac{\pi H}{\lambda}\right)\dfrac{1}{\sinh^2(kd)}\left\{1-\dfrac{3\cosh[2k(z+d)]}{2\sinh^2(kd)}\right\}\sin 2\theta$ $+\dfrac{H}{4}\left(\dfrac{\pi H}{\lambda}\right)\dfrac{\cosh[2k(z+d)]}{\sinh^2(kd)}(\omega t)$
Vertical particle dis-placement, ζ	$-\dfrac{H}{2}\dfrac{\sinh[k(z+d)]}{\sinh(kd)}\cos\theta$	$\dfrac{H}{2}e^{kz}\cos\theta$	$\varsigma_t+\dfrac{3H}{16}\left(\dfrac{\pi H}{\lambda}\right)\dfrac{\sinh[2k(z+d)]}{\sinh^4(kd)}\cos 2\theta$
Horizontal particle velocity, u	$\dfrac{\pi H}{T}\dfrac{\cosh[k(z+d)]}{\sinh(kd)}\cos\theta$	$\dfrac{\pi H}{T}e^{kz}\cos\theta$	$u_t+\dfrac{3}{4}\dfrac{\pi H}{T}\left(\dfrac{\pi H}{\lambda}\right)\dfrac{\cosh[2k(z+d)]}{\sinh^4(kd)}\cos 2\theta$
Vertical particle velocity, w	$\dfrac{\pi H}{T}\dfrac{\sinh[k(z+d)]}{\sinh(kd)}\sin\theta$	$\dfrac{\pi H}{T}e^{kz}\sin\theta$	$w_t+\dfrac{3}{4}\dfrac{\pi H}{T}\left(\dfrac{\pi H}{\lambda}\right)\dfrac{\sinh[2k(z+d)]}{\sinh^4(kd)}\sin 2\theta$
Horizontal particle acceleration, $\dot u$	$\dfrac{2\pi^2 H}{T^2}\dfrac{\cosh[k(z+d)]}{\sinh(kd)}\sin\theta$	$\dfrac{2\pi^2 H}{T^2}e^{kz}\sin\theta$	$\dot u_t+\dfrac{3\pi^2 H}{T^2}\left(\dfrac{\pi H}{\lambda}\right)\dfrac{\cosh[2k(z+d)]}{\sinh^4(kd)}\sin 2\theta$
Vertical particle acceleration, $\dot w$	$-\dfrac{2\pi^2 H}{T^2}\dfrac{\sinh[k(z+d)]}{\sinh(kd)}\cos\theta$	$-\dfrac{2\pi^2 H}{T^2}e^{kz}\cos\theta$	$\dot w_t-\dfrac{3\pi^2 H}{T^2}\left(\dfrac{\pi H}{\lambda}\right)\dfrac{\sinh[2k(z+d)]}{\sinh^4(kd)}\cos 2\theta$
Subsurface pressure, p	$-\rho gz+\dfrac{1}{2}\rho gH\dfrac{\cosh[k(z+d)]}{\cosh(kd)}\cos\theta$	$-\rho gz+\dfrac{1}{2}\rho gHe^{kz}\cos\theta$	$p_t+\dfrac{3}{4}\rho gH\dfrac{\pi H}{\lambda\sinh(2kd)}\left\{\dfrac{\cosh[2k(z+d)]}{\sinh^2(kd)}-\dfrac{1}{3}\right\}\cos 2\theta$ $-\dfrac{1}{4}\rho gH\dfrac{\pi H}{\lambda\sinh(2kd)}\{\cosh[2k(z+d)]-1\}$
Group velocity, c_g	$\dfrac{c}{2}\left[1+\dfrac{2kd}{\sinh(2kd)}\right]$	$\dfrac{c}{2}$	$(c_g)_t$
Average energy density, E	$\dfrac{1}{8}\rho gH^2$	$\dfrac{1}{8}\rho gH^2$	$\dfrac{1}{8}\rho gH^2$
Energy flux, F	Ec_g	$\dfrac{1}{2}Ec$	Ec_g

Notation: d = mean water depth, g = acceleration of gravity, H = trough-to-crest wave height, $k=2\pi/\lambda$ = wave number, λ = wave length, T = wave period; t = time; x = distance of propagation; z = distance from mean free surface positive upward; $\theta = kx-\omega t = k(x-ct)$; $\omega = 2\pi/T$ = angular wave frequency. Subscript l denotes linear small-amplitude theory.

3.5.3 Sea state parameters

The following sea state parameters can be defined in terms of spectral moments:

3.5.3.1 The significant wave height H_s is given by:

$$H_{m0} = 4\sqrt{m_0} = 4\sqrt{M_0}$$

3.5.3.2 The zero-up-crossing period T_z can be estimated by:

$$T_{m02} = \sqrt{\frac{m_0}{m_2}} = 2\pi\sqrt{\frac{M_0}{M_2}}$$

3.5.3.3 The *mean wave period* T_1 can be estimated by:

$$T_{m01} = \frac{m_0}{m_1} = 2\pi\frac{M_0}{M_1}$$

3.5.3.4 The *mean crest period* T_c can be estimated by:

$$T_{m24} = \sqrt{\frac{m_2}{m_4}} = 2\pi\sqrt{\frac{M_2}{M_4}}$$

3.5.3.5 The significant wave steepness S_s can be estimated by:

$$S_{m02} = \frac{2\pi}{g}\frac{H_{mo}}{T_{m02}^2} = \frac{2}{\pi g}\frac{M_2}{\sqrt{M_0}}$$

3.5.3.6 Several parameters may be used for definition of *spectral bandwidth*:

$$\nu = \sqrt{\frac{M_0 M_2}{M_1^2} - 1}$$

$$\delta = \sqrt{1 - \frac{M_1^2}{M_0 M_2}} = \frac{\nu}{\sqrt{\nu^2 + 1}}$$

$$\alpha = \frac{M_2}{\sqrt{M_0 M_4}}$$

$$\varepsilon = \sqrt{1 - \frac{M_2^2}{M_0 M_4}} = \sqrt{1 - \alpha^2}$$

Note that the fourth order spectral moment, and consequently the spectral bandwidth parameters   and, do not exist for the Pierson-Moskowitz spectrum and for the JONSWAP spectrum.

3.5.4 Steepness criteria

The average wave steepness S_s, S_p and S_1 for short term irregular seastates are defined as

$$S_s = \frac{2\pi}{g}\frac{H_s}{T_z^2}$$

$$S_p = \frac{2\pi}{g}\frac{H_s}{T_p^2}$$

$$S_1 = \frac{2\pi}{g}\frac{H_s}{T_1^2}$$

The limiting values of S_s may, in absence of other reliable sources, be taken as

$S_s = 1/10$ for $T_z \leq 6$ s

$S_s = 1/15$ for $T_z \geq 12$s

and interpolated linearly between the boundaries. The limiting values of S_p may be taken as

$S_p = 1/15$ for $T_p \leq 8$ s

$S_p = 1/25$ for $T_p \geq 15$ s

and interpolated linearly between the boundaries.

The limiting values were obtained from measured data from the Norwegian Continental Shelf, but are expected to be of more general validity.

3.5.5 The Pierson-Moskowitz and JONSWAP spectra

3.5.5.1 The *Pierson-Moskowitz* (PM) spectrum $S_{PM}(\omega)$ is given by

$$S_{PM}(\omega) = \frac{5}{16} \cdot H_s^2 \omega_p^4 \cdot \omega^{-5} \exp\left(-\frac{5}{4}\left(\frac{\omega}{\omega_p}\right)^{-4}\right)$$

where $\omega_p = 2\pi/T_p$ is the angular spectral peak frequency.

3.5.5.2 The *JONSWAP* spectrum $S_J(\omega)$ is formulated as a modification of the Pierson-Moskowitz spectrum for a developing sea state in a fetch limited situation:

$$S_J(\omega) = A_\gamma S_{PM}(\omega)\ \gamma^{\exp\left(-0.5\left(\frac{\omega-\omega_p}{\sigma\,\omega_p}\right)^2\right)}$$

where

$$
\begin{array}{lll}
S_{PM}(\omega) & = & \text{Pierson-Moskowitz spectrum} \\
\gamma & = & \text{non-dimensional peak shape parameter} \\
\sigma & = & \text{spectral width parameter} \\
& & \sigma = \sigma_a \text{ for } \omega \leq \omega_p \\
& & \sigma = \sigma_b \text{ for } \omega > \omega_p \\
A_\gamma & = & 1\text{- }0.287\ln(\gamma) \text{ is a normalizing factor.}
\end{array}
$$

3.5.5.3 Average values for the JONSWAP experiment data are $\gamma = 3.3$, $\sigma_a = 0.07$, $\sigma_b = 0.09$. For $\gamma = 1$ the JONSWAP spectrum reduces to the Pierson-Moskowitz spectrum.

The JONSWAP spectrum is expected to be a reasonable model for

$$3.6 < T_p / \sqrt{H_s} < 5$$

where T_p is in seconds and H_s is in meters, and should be used with caution outside this interval. The effect of the peak shape parameter γ is shown in Figure 3-9.
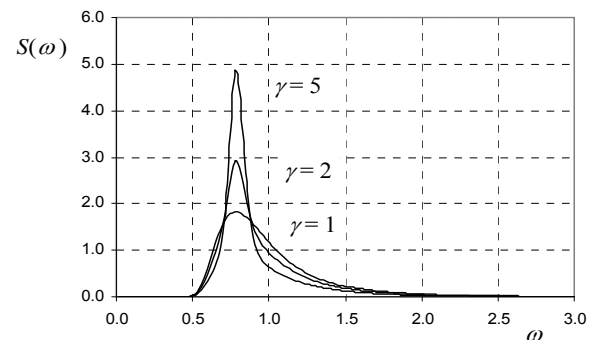
Figure 3-9
JONSWAP spectrum for H_s = 4.0 m, T_p = 8.0 s for γ= 1, γ= 2 and γ= 5.

3.5.5.4 The zero upcrossing wave period T_z and the mean wave period T_1 may be related to the peak period by the following approximate relations ($1 \le \gamma < 7$).

$$\frac{T_z}{T_p} = 0.6673 + 0.05037\gamma - 0.006230\gamma^2 + 0.0003341\gamma^3$$

$$\frac{T_1}{T_p} = 0.7303 + 0.04936\gamma - 0.006556\gamma^2 + 0.0003610\gamma^3$$

For $\gamma = 3.3$; $T_p = 1.2859T_z$ and $T_1 = 1.0734T_z$

For $\gamma = 1.0$ (PM spectrum); $T_p = 1.4049T_z$ and $T_1 = 1.0867T_z$

3.5.5.5 If no particular values are given for the peak shape parameter γ, the following value may be applied:

$$\gamma = 5 \quad \text{for} \quad T_P / \sqrt{H_s} \le 3.6$$

$$\gamma = \exp(5.75 - 1.15\frac{T_p}{\sqrt{H_s}}) \quad \text{for} \quad 3.6 < T_P / \sqrt{H_s} < 5$$

$$\gamma = 1 \quad \text{for} \quad 5 \le T_P / \sqrt{H_s}$$

where T_P is in seconds and H_S is in metres.

3.5.5.6 For the JONSWAP spectrum the spectral moments are given approximately as, see Gran (1995),

$$M_{-1} = \frac{1}{16} H_s^2 \omega_p^{-1} \frac{4.2+\gamma}{5+\gamma}$$

$$M_0 = \frac{1}{16} H_s^2$$

$$M_1 = \frac{1}{16} H_s^2 \omega_p \frac{6.8+\gamma}{5+\gamma}$$

$$M_2 = \frac{1}{16} H_s^2 \omega_p^2 \frac{11+\gamma}{5+\gamma}$$

3.5.5.7 Both JONSWAP and Pierson-Moskowitz spectra adopt ω^{-5} as the governing high frequency tail behaviour. There is empirical support for a tail shape closer to the theoretical shape ω^{-4}. The difference between ω^{-4} and ω^{-5} tail behaviour may be of importance for dynamic response of structures. For more information, confer ISO 19901-1.

3.5.6 TMA spectrum

The finite water depth TMA spectrum, for non-breaking waves, $S_{TMA}(\omega)$ is given as the JONSWAP spectrum multiplied by a depth function $\phi(\omega)$ (Bouws, et. al. *1985*),

$$S_{TMA}(\omega) = S_J(\omega) \; \phi(\omega)$$

where

$$\phi(\omega) = \frac{\omega^5 \frac{\partial k}{\partial \omega}}{2g^2 k^3}$$

Applying the dispersion relation

$$\omega^2 = gk \tanh(kd)$$

the depth function $\phi(\omega)$ can be written

$$\phi(\omega) = \frac{\cosh^2(kd)}{\sinh^2(kd) + \frac{\omega^2 d}{g}}$$

where d is the water depth.

3.5.7 Two-peak spectra

3.5.7.1 Combined wind sea and swell may be described by a double peak frequency spectrum, i.e.

$$S(\omega) = S_{wind\,sea}(\omega) + S_{swell}(\omega)$$

where wind sea and swell are assumed to be uncorrelated.

3.5.7.2 The spectral moments are additive,

$$M_n = M_{n,wind\,sea} + M_{n,swell}$$

from which it follows that the significant wave height is given as

$$H_{s,total} = \sqrt{H^2_{s,wind\,sea} + H^2_{s,swell}}$$

where

$$H_{s,wind\,sea}$$

is the significant wave height for the wind sea, and

$$H_{s,swell}$$

is the significant wave height for the swell.

3.5.7.3 The wind-sea component in the frequency spectrum is well described by a generalized JONSWAP function. Swell components are well described by either a generalized JONSWAP function or a normal function, Strekalov and Massel (1971), Ewans (2001).

3.5.7.4 The *Ochi-Hubble spectrum* is a general spectrum formulated to describe seas which is a combination of two different sea states (Ochi-Hubble, 1976). The spectrum is a sum of two Gamma distributions, each with 3 parameters for each wave system, viz. significant wave height $H_{s,j}$, spectral peak period $T_{p,j}$ and a shape factor λ_s. The parameters should be determined numerically to best fit the observed spectra.

3.5.7.5 The Ochi-Hubble spectrum is defined by:

$$S(\omega) = \sum_{j=1}^{2} E_j \cdot G_j \cdot \Gamma_j$$

where

$$E_j = \frac{H^2_{s,j}T_{p,j}}{32\pi}$$

$$\Gamma_j = \omega_{n,j}^{-4(\lambda_j + \frac{1}{4})} \cdot \exp^{-(\lambda_j + \frac{1}{4})\omega_{n,j}^{-4}}$$

$$G_j = \frac{4(\lambda_j + \frac{1}{4})^{\lambda_j}}{\Gamma(\lambda_j)}$$

$$\omega_{n,j} = \frac{\omega T_{p,j}}{2\pi}$$

in which $j = 1$ and $j = 2$ represents the lower and higher frequency components, respectively. The significant wave height for the sea state is

$$H_s = \sqrt{H^2_{s,1} + H^2_{s,2}}$$

For more information, confer ISO 19901-1.

3.5.7.6 The *Torsethaugen two-peaked spectrum* is obtained by fitting two generalized JONSWAP functions to averaged measured spectra from the Norwegian Continental Shelf (Torsethaugen,1996, 2004).

3.5.7.7 Input parameters to the Torsethaugen spectrum are significant wave height and peak period. The spectrum parameters are related to H_s and T_p according to empirical parameters. The Torsethaugen spectrum is given in Appendix A.

3.5.8 Directional distribution of wind sea and swell

3.5.8.1 Directional short-crested wave spectra $S(\omega,\theta)$ may be expressed in terms of the uni-directional wave spectra,

$$S(\omega,\theta) = S(\omega)D(\theta,\omega) = S(\omega)D(\theta)$$

where the latter equality represents a simplification often used in practice. Here $D(\theta,\omega)$ and $D(\theta)$ are directionality functions. θ is the angle between the direction of elementary wave trains and the main wave direction of the short crested wave system.

3.5.8.2 The directionality function fulfils the requirement

$$\int_\theta D(\theta,\omega)d\theta = 1$$

3.5.8.3 For a two-peak spectrum expressed as a sum of a swell component and a wind-sea component, the total directional frequency spectrum $S(\omega,\theta)$ can be expressed as

$$S(\omega,\theta) = S_{wind\,sea}(\omega)D_{wind\,sea}(\theta) + S_{swell}(\omega)D_{swell}(\theta)$$

3.5.8.4 A common directional function often used for wind sea is

$$D(\theta) = \frac{\Gamma(1 + n/2)}{\sqrt{\pi}\Gamma(1/2 + n/2)} \cos^n(\theta - \theta_p)$$

where Γ is the Gamma function and $| \theta - \theta_p |\leq \dfrac{\pi}{2}$.

3.5.8.5 The main direction θ_p may be set equal to the prevailing wind direction if directional wave data are not available.

3.5.8.6 Due consideration should be taken to reflect an accurate correlation between the actual sea-state and the constant n. Typical values for wind sea are $n = 2$ to $n = 4$. If used for swell, $n \geq 6$ is more appropriate.

3.5.8.7 An alternative formulation that is also often used is

$$D(\theta) = \frac{\Gamma(s + 1)}{2\sqrt{\pi}\Gamma(s + 1/2)} \cos^{2s}(\tfrac{1}{2}(\theta - \theta_p))$$

where $| \theta - \theta_p |\leq \pi$

Comparing the two formulations for directional spreading, s can be taken as $2n+1$.

Hence, typical values for wind sea are $s = 4$ to $s = 9$. If used for swell, $s > 13$ is more appropriate.

3.5.8.8 The directional spreading of swells can be modelled by a Poisson distribution (Lygre and Krogstad, 1986; Bitner-Gregersen and Hagen, 2003),

$$D(\theta) = \frac{1}{2\pi} \frac{1 - x^2}{1 - 2x\cos(\theta) + x^2} ;\ 0 < x < 1$$

It is often a good approximation to consider swell as long-crested.

For more information, confer ISO 19901-1.

3.5.9 Short term distribution of wave height

3.5.9.1 The peak-to-trough wave height H of a wave cycle is the difference between the highest crest and the deepest trough between two successive zero-upcrossings.

3.5.9.2 The wave heights can be modelled as Rayleigh distributed with cumulative probability function

$$F_H(h) = 1 - \exp\left[-\left(\frac{h}{\alpha_H H_S}\right)^2\right]$$

where (Næss, 1985)

$$\alpha_H = \frac{1}{2}\sqrt{1 - \rho}$$

3.5.9.3 The parameter ρ reflects band width effects, and typical values for ρ are in the range -0.75 to -0.6. Interpreting ρ as the autocorrelation function value at half the dominant wave period, the JONSWAP wave spectrum with peak enhancement factor 3.3, gives $\rho = -0.73$. Generally the presence of swell makes the wave process more broad banded, thus typically increasing the autocorrelation ρ (ρ closer to [-0.65,-0.6]).

3.5.9.4 A possible parameterization of ρ as function of the JONSWAP peak shape parameter is ($1 \leq \gamma \leq 10$)

$$\rho = -0.000191 \cdot \gamma^3 + 0.00488 \cdot \gamma^2 - 0.0525 \cdot \gamma - 0.605$$

3.5.9.5 An empirically based short term wave height distribution is the Weibull distribution

$$F_H(h) = 1 - \exp\left\{-\left(\frac{h}{\alpha_H \cdot H_s}\right)^{\beta_H}\right\}$$

The scale and shape parameters values are to be determined from data. The parameter values $\alpha_H = 0.681$ and $\beta_H = 2.126$ of the Forristall wave height distribution (Forristall, 1978) are originally based on buoy data from the Mexican Gulf, but have been found to have a more general applicability.

3.5.10 Short term distribution of wave crest above still water level

3.5.10.1 The nonlinearity of the sea surface elevations can be reasonably well modelled by second order theory. The Forristall crest distribution for wave crest above still water level is based on second order time domain simulations (Forristall, 2000),

$$F_C(x) = 1 - \exp\left[-\left(\frac{x}{\alpha_c H_s}\right)^{\beta_c}\right]$$

3.5.10.2 The Weibull parameters α_c, β_c in Forristall crest distribution are expressed as function of steepness S_1 and Ursell number U_{rs}:

$$S_1 = \frac{2\pi}{g} \frac{H_s}{T_1^2}$$

$$U_{rs} = \frac{H_s}{k_1^2 d^3}$$

where

$$k_1 = \frac{4\pi^2}{gT_1^2}$$

is the deep water wave number for a frequency $1/T_1$ and d is the water depth.

3.5.10.3 For long crested seas (2D) the Weibull parameters are given as

$$\alpha_c = 0.3536 + 0.2892 S_1 + 0.1060 U_{rs}$$

$$\beta_c = 2 - 2.1597 S_1 + 0.0968 U_{rs}^2$$

and for short-crested seas (3D)

$$\alpha_c = 0.3536 + 0.2568 S_1 + 0.0800 U_{rs}$$

$$\beta_c = 2 - 1.7912 S_1 - 0.5302 U_{rs} + 0.284 U_{rs}^2$$

3.5.10.4 It should be noted that the Forristall distribution is based on second order simulations. Higher order terms may result in slightly higher crest heights. Hence extremes predicted by this distribution are likely to be slightly on the low side.

3.5.10.5 If site specific crest height measurements are available, the short term statistics for crest heights may alternatively be modelled by a 3-parameter Weibull distribution with parameters fitted to the data.

3.5.10.6 It should be noted that wave crest data from wave rider measurements underestimate the height of the largest wave crests.

3.5.10.7 For the statistics of crest height above mean water level and for the crest height above lowest astronomic tide, the joint statistics of crest, storm surge and tide have to be accounted for.

3.5.10.8 Information on wave measurements and analysis can be found in Tucker and Pitt (2001).

3.5.11 Maximum wave height and maximum crest height in a stationary sea state

3.5.11.1 For a stationary sea state with N independent local maxima (for example wave heights, crest heights, response), with distribution function $F(x)$, the distribution of the extreme maximum is given as $F_E(x) = F(x)^N$

3.5.11.2 Assuming a 3-parameter Weibull distributed local maxima,

$$F(x) = 1 - \exp\left\{-\left(\frac{x-\gamma}{\alpha}\right)^\beta\right\}$$

where γ is the location parameter, α the scale parameter and β the shape parameter.

3.5.11.3 Some characteristic measures for the extreme maximum x_e in the sea state are:

Quantity	Value	$F_E(x_e)$
Mode x_c	$\gamma + \alpha \cdot (\ln N)^{1/\beta}$	0.368 $N \to \infty$
Mean x_{mean}	$\gamma + \alpha \cdot (\ln N)^{1/\beta}\left(1 + \dfrac{0.577}{\beta \ln N}\right)$ N large	0.570 $N \to \infty$
p-fractile x_p	$\gamma + \alpha\left[-\ln(1 - p^{1/N})\right]^{1/\beta}$	p
Median x_{median}	$\gamma + \alpha\left[-\ln(1 - p^{1/N})\right]^{1/\beta}$	$p = 0.5$
Std.dev.	$\dfrac{\pi}{\sqrt{6}} \dfrac{\alpha}{\beta} \cdot (\ln N)^{\frac{1}{\beta}-1}$ N large	

It follows that: $x_c < x_{median} < x_{mean}$.

3.5.11.4 The *mode* of the extreme value distribution is also called *the characteristic largest extreme*, and corresponds to the $1/N$ exceedance level for the underlying distribution, i.e.

$$F(x_c) = 1 - 1/N$$

giving $F_E(x_c) = (1 - 1/N)^N \approx 1/e$ for $N \to \infty$

For a narrow banded sea state, the number of maxima can be taken as $N = t/T_Z$ where t is the sea state duration.

3.5.11.5 The characteristic largest crest-to-trough wave height H_{max} in a stationary sea state of duration t can be taken as

$$H_{max,c} = \frac{H_s}{2}\sqrt{(1-\rho)\ln(t/T_z)}$$

where ρ is the band width parameter given in 3.5.9.2.

3.5.11.6 Assuming N independent maxima, the distribution of the extreme maximum can be taken as Gumbel distributed

$$F_{Ext}(x) \approx F(x)^N \approx \exp\{-\exp(-A_G \cdot (x - U_G))\}$$

where the parameters of the Gumbel distributions are

$$U_G = x_c = \gamma + a \cdot (\ln N)^{1/b}$$

$$A_G = \frac{b}{a} \cdot (\ln N)^{1 - \frac{1}{b}}$$

3.5.11.7 Improved convergence properties can often be obtained by considering the statistics for a transformed variable, for example by assuming that the quadratic processes H_{max}^2 or C_{max}^2 are Gumbel distributed.

3.5.12 Joint wave height and wave period

3.5.12.1 The short term joint probability distribution of wave height, H, and wave period, T, is obtained by

$$f_{HT}(H,T) = f_H(H) \cdot f_{T|H}(T \mid H)$$

3.5.12.2 The short term distribution of T for a given H, in a sea state with significant wave height H_s and wave period T_1, can be taken as normally distributed (Longuet-Higgins 1975, Krogstad 1985, Haver 1987)

$$F(t \mid h) = \Phi\left(\frac{t - \mu_T}{\sigma_{T|H}}\right)$$

where $\Phi(\ )$ is the standard Gaussian cumulative distribution function defined by

$$\Phi(x) = \frac{1}{\sqrt{2\pi}}\int_{-\infty}^{x} e^{-\xi^2/2}d\xi$$

and

$$\mu_T = C_1 \cdot T_1$$

$$\sigma_{T|H} = C_2 \frac{H_s}{H} \cdot T_1$$

Here T_1 is the mean wave period. The coefficients C_1 and C_2 may vary with T_1 (or T_Z), and should be determined from measured data.

3.5.12.3 In lack of site specific data, the following theoretical results can be applied for the wave period associated with large wave heights ($H > 0.6H_s$) (Tayfun;1993)

$$C_1 = 1 + \frac{\nu^2}{\left(1 + \nu^2\right)^{3/2}}$$

$$C_2 = \frac{1}{2} \frac{\nu}{1 + \nu^2}$$

where ν is the spectral bandwidth as defined in 3.5.3.

3.5.12.4 It is observed that for a stationary sea state, the most probable conditional wave period μ_T, which for the Normal distribution is equal to the mean wave period, is independent of H.

3.5.12.5 The following empirical values are suggested for the Norwegian Continental Shelf (Krogstad, 1985):

T_z [sec]	C_1	C_2
4.0	1.5	0.5-0.65
6.0	1.41-1.45	0.39
8.0	1.32-1.36	0.3
10.0	1.3-1.4	0.24
12.0	1.2-1.3	0.22

3.5.13 Freak waves

3.5.13.1 The occurrences of unexpectedly large and/or steep waves, so called freak or rogue waves, are reported. Even though the existence of freak waves themselves is generally not questioned, neither the probability of occurrence of these waves nor their physics is well understood. It has been suggested that freak waves can be generated by mechanisms like: wave-current interaction, combined seas, wave energy focusing. No consensus has been reached neither about a definition of a freak event nor about the probability of occurrence of freak waves.

3.5.13.2 Different definitions of freak waves are proposed in the literature. Often used as a characteristic, for a 20 minute sea elevation time series, is that $H_{max}/H_s > 2$ (maximum crest to trough wave height criterion), or that $C_{max}/H_s > 1.3$ (maximum crest criterion), or that both criteria are simultaneously fulfilled. Relevant references on freak waves are: Haver and Andersen (2000); Bitner-Gregersen, Hovem and Hørte (2003), EU-project MaxWave, Papers presented at Rogue Waves (2004).

3.6 Long term wave statistics

3.6.1 Analysis strategies

3.6.1.1 The long-term variation of wave climate can be described in terms of generic distributions or in terms of scatter diagrams for governing seastate parameters such as (H_S, T_z, θ) or $(\sigma, \gamma, H_S, T_p, \theta)$ that are interpreted from available data.

3.6.1.2 A scatter diagram provides the frequency of occurrence of a given parameter pair (e.g. (H_S, T_z)). Both marginal distributions and joint environmental models can be applied for wave climate description. The generic models are generally established by fitting distributions to wave data from the actual area.

3.6.1.3 Two different analysis strategies are commonly applied, viz. global models and event models.

— The *global model* (or initial distribution method) utilises all available data from long series of subsequent observations (e.g. all 3-hour data).
— In the *event model* observations over some threshold level are used (Peak Over Threshold (POT) method or storm analysis method). Alternatively, annual extremes or seasonal extremes are analysed.

3.6.1.4 The initial distribution method is typically applied for the distribution of sea state parameters such as significant wave height. The event based approaches can be applied for sea state parameters, but might also be used directly for maximum individual wave height and for the maximum crest height.

3.6.1.5 In selecting the method there is a trade-off between the all-sea-state models using all data, and the extreme event models based on a subset of the largest data points. While the initial distribution method utilises more data, there is correlation between the observations. Furthermore using the usual tests for fitting of distributions it may not be possible to discriminate adequately the tail behaviour. In contrast, extreme events are more independent, but their scarceness increases statistical uncertainty. The event approach is the preferred model for cases in which weather is relatively calm most of the time, and there are few very intense events.

3.6.1.6 When fitting probability distributions to data, different fitting techniques can be applied; notably Method Of Moments (MOM), Least Squares methods (LS) and Maximum Likelihood Estimation (MLE).

3.6.1.7 In MOM the distribution parameters are estimated from the two or three first statistical moments of the data sample (mean, variance, skewness). The method typically gives a good fit to the data at the mode of the distribution. The MLE has theoretical advantages, but can be cumbersome in practice. The idea is to maximise a function representing the likelihood for obtaining the numbers that are measured. In LS the sum of squared errors between the empirical distribution and the fitted probabilities are minimized. LS is typically more influenced by the tail behaviour than are MOM and MLE.

3.6.1.8 When estimating extremes, it is important that the tail of the fitted distribution honour the data, and for 3-parameter Weibull distribution the LS fit often gives better tail fit than the method of moments. For other applications, a good fit to the main bulk of data might be more important.

3.6.2 Marginal distribution of significant wave height

3.6.2.1 *Initial distribution method*: Unless data indicate otherwise, a 3-parameter Weibull distribution can be assumed for the marginal distribution of significant wave height H_S, Nordenstrøm (1973),

$$F_{H_s}(h) = 1 - \exp\left[-\left(\frac{h-\gamma}{\alpha}\right)^\beta\right]$$

where α is the scale parameter, β is the shape parameter, and γ is the location parameter (lower threshold). The distribution parameters are determined from site specific data by some fitting technique.

3.6.2.2 For Peak Over Threshold (POT) and storm statistics analysis, a 2-parameter Weibull distribution or an exponential distribution is recommended for the threshold excess values. It is recommended that the general Pareto distribution is not used.

For the exponential distribution

$$F_E(h) = \exp\left\{-\frac{h-h_0}{\theta}\right\}$$

the scale parameter can be determined from the mean value of the excess variable $y = H - h_0$, i.e. $\theta = E[H - h_0]$.

3.6.2.3 Peak Over Threshold (POT) statistics should be used with care as the results may be sensitive to the adopted threshold level. Sensitivity analysis with respect to threshold level should be performed. If possible, POT statistics should be

compared with results obtained from alternative methods. The storm statistics is appreciated if a sufficient number of storm events exists. Also, the storm statistics results may depend on the lower threshold for storms, and should be compared with results obtained from alternative methods.

3.6.2.4 The annual extremes of an environmental variable, for example the significant wave height or maximum individual wave height, can be assumed to follow a Gumbel distribution

$$F_C(x) = \exp\left\{-\exp\left[-\frac{(x-U)}{A}\right]\right\}$$

in which A and U are distribution parameters related to the standard deviation $\sigma = 1.283A$ and the mean $\mu = U + 0.557A$ of the Gumbel variable. The extreme value estimates should be compared with results from alternative methods.

3.6.2.5 It is recommended to base the annual statistics on at least 20-year of data points. It is further recommended to define the year as the period from summer to summer (not calendar year).

3.6.3 Joint distribution of significant wave height and period

3.6.3.1 Joint environmental models are required for a consistent treatment of the loading in a reliability analysis and for assessment of the relative importance of the various environmental variables during extreme load/response conditions and at failure.

3.6.3.2 Different approaches for establishing a joint environmental model exist. The Maximum Likelihood Model (MLM) (Prince-Wright, 1995), and the Conditional Modelling Approach (CMA) (e.g. Bitner-Gregersen and Haver, 1991), utilize the complete probabilistic information obtained from simultaneous observations of the environmental variables. The MLM uses a Gaussian transformation to a simultaneous data set while in the CMA, a joint density function is defined in terms of a marginal distribution and a series of conditional density functions.

3.6.3.3 If the available information about the simultaneously occurring variables is limited to the marginal distributions and the mutual correlation, the Nataf model (Der Kiuregihan and Liu, 1986) can be used. The Nataf model should be used with caution due to the simplified modelling of dependency between the variables (Bitner-Gregersen and Hagen, 1999).

3.6.3.4 The following CMA joint model is recommended: The significant wave height is modelled by a 3-parameter Weibull probability density function

$$f_{H_s}(h) = \frac{\beta_{Hs}}{\alpha_{Hs}}\left(\frac{h-\gamma_{Hs}}{\alpha_{Hs}}\right)^{\beta_{Hs}-1}\exp\left\{-\left(\frac{h-\gamma_{Hs}}{\alpha_{Hs}}\right)^{\beta_{Hs}}\right\}$$

and the zero-crossing wave period conditional on H_s is modelled by a lognormal distribution

$$f_{T_Z|H_s}(t\,|\,h) = \frac{1}{\sigma\,t\sqrt{2\pi}}\exp\left\{-\frac{(\ln t - \mu)^2}{2\sigma^2}\right\}$$

where the distribution parameters μ and σ are functions of the significant wave height (Bitner-Gregersen, 1988, 2005). Experience shows that the following model often gives good fit to the data:

$$\mu = E[\ln T_z] = a_o + a_1 h^{a_2}$$

$$\sigma = std[\ln T_z] = b_0 + b_1 e^{b_2 h}$$

The coefficients $a_i, b_i, i = 0,1,2$ are estimated from actual data.

3.6.3.5 Scatter diagram of significant wave height and zero-crossing period for the North Atlantic for use in marine structure calculations are given in Table C-2 (Bitner-Gregersen et.al. 1995). This scatter diagram covers the GWS ocean areas 8, 9, 15 and 16 (see Appendix B) and is included in the IACS Recommendation No. 34 "Standard Wave Data for Direct Wave Load Analysis". The parameters of the joint model fitted to the scatter diagrams are given in Table C-4.

3.6.3.6 Scatter diagram for World Wide trade is given in Table C-3. Distribution parameters for World wide operation of ships are given in Table C-5.

The world wide scatter diagram defines the average weighted scatter diagram for the following world wide sailing route: Europe-USA East Coast, USA West Coast - Japan - Persian Gulf - Europe (around Africa). It should be noted that these data are based on visual observations.

For the various nautic zones defined in Appendix B, the distribution parameters are given in Table C-1, where
$\gamma_{Hs} = 0$,
$\mu = 0.70 + a_1 H_s^{a_2}$ and $\sigma = 0.07 + b_1 e^{b_2 H_s}$

3.6.4 Joint distribution of significant wave height and wind speed

3.6.4.1 A 2-parameter Weibull distribution can be applied for mean wind speed U given sea state severity H_s (Bitner-Gregersen and Haver 1989, 1991)

$$f_{U|H_s}(u\,|\,h) = k\frac{u^{k-1}}{U_c^{\,k}}\exp\left[-\left(\frac{u}{U_c}\right)^k\right]$$

where the scale parameter U_c and the shape parameter k are estimated from actual data, for example using the models

$$k = c_1 + c_2 h_s^{c_3} \text{ and } U_c = c_4 + c_5 h_s^{c_6}$$

3.6.5 Directional effects

3.6.5.1 For wind generated sea it is often a good approximation to assume that wind and waves are inline.

For more detailed studies, the directional difference θ_r between waves and wind, i.e.

$$\theta_r = \theta_{waves} - \theta_{wind}$$

can be explicitly modelled. For omnidirectional data, θ_r can be assumed to be beta-distributed (Bitner-Gregersen, 1996). The beta distribution is a flexible tool for modelling the distribution of a bounded variable, but its applicability is not always straightforward.

3.6.5.2 It is common practice to model the distribution of absolute wave direction, i.e. the direction relative to the chart north, in terms of probability of occurrence p_{θ_i} of waves within direction bins. The 360° range is typically divided into eight 45°, twelve 30° or sixteen 22.5° directional sectors. The values p_{θ_i} and the required wave statistics for each sector, are determined from data.

3.6.5.3 If directional information is used in a reliability analysis of a marine structure, it is important to ensure that the overall reliability is acceptable. There should be consistency between omnidirectional and directional distributions so that the omnidirectional probability of exceedance is equal to the integrated exceedance probabilities from all directional sectors.

3.6.5.4 The concept of directional criteria should be used with caution. If the objective is to define a set of wave heights that accumulated are exceeded with a return period of 100-year, the wave heights for some or all sectors have to be increased. Note that if directional criteria are scaled such that the wave height

in the worst direction is equal to the omnidirectional value, the set of wave are still exceeded with a return period shorter than 100-year.

3.6.5.5 A set of directional wave heights that are exceeded with a period T_R can be established by requiring that the product of non-exceedance probabilities from the directional sectors is equal to the appropriate probability level.

3.6.5.6 An alternative approach for analysis of directional variability is to model the absolute wave direction using a continuous probability distribution, say the uniform distribution (Mathisen (2004), Sterndorff and Sørensen (2001), Forristall (2004)).

3.6.6 Joint statistics of wind sea and swell

3.6.6.1 Two approaches are described in the following. In the first approach, wind sea and swell are modelled as independent variables, which is generally a reasonable assumption with regard to the physics of combined seas. Use of this approach requires application of a wave spectrum which is fully described by the information provided by the wind sea and swell distributions, e.g. the JONSWAP spectrum. The total significant wave height is

$$H_s = \sqrt{H_{s,wind\,sea}^2 + H_{s,swell}^2}$$

(For more information, confer Bitner-Gregersen, 2005).

3.6.6.2 Often it is difficult to establish separate wind sea and swell distributions, and assumptions adopted to generate these distributions may lead to unsatisfactory prediction of extremes. For some applications, using the distribution of the total significant wave height and period combined with a procedure for splitting of wave energy between wind sea and swell, e.g. the Torsethaugen spectrum, is more appreciated. This procedure is based on wind sea and swell characteristics for a particular location. Although such characteristics to a certain extent are of general validity, procedures established using data from a specific location should be used with care when applied to other ocean areas. (For more information, confer Bitner-Gregersen and Haver, 1991).

3.6.7 Long term distribution of individual wave height

The long term distribution $F_H(x)$

of individual wave height can be obtained by integrating the short term distribution

$$F_{H|H_s}(x \mid h_s)$$

over all sea states, weighting for the number of individual wave cycles within each sea state (Battjes 1978)

$$F_H(x) =$$

$$\frac{1}{\bar{v}_0} \iint_{ht} T_z^{-1} \cdot F_{H|H_s}(x \mid h) f_{H_s T_z}(h,t) dh dt$$

$$= \frac{1}{\bar{v}_0} \int_h \left\langle T_z^{-1} \right\rangle_h F_{H|H_s}(x \mid h) f_{H_s}(h) dh$$

where

$$\left\langle T_z^{-1} \right\rangle_h = \int_t T_z^{-1} f_{T_z|H_s}(t \mid h) dt$$

$$\bar{v}_0 = \iint_{ht} T_z^{-1} f_{H_s T_z}(h,t) dh dt$$

$$= \int_h \left\langle T_z^{-1} \right\rangle_h f_{H_s}(h) dh$$

The individual wave height H_{T_R} with return period T_R (in years) follows from

$$1 - F_H(H_{T_R}) = \frac{1}{T_R \cdot 365.25 \cdot 24 \cdot 3600 \cdot \bar{v}_0}$$

3.7 Extreme value distribution

3.7.1 Design sea state

3.7.1.1 When $F_{Hs}(h)$ denotes the distribution of the significant wave height in an arbitrary t-hour sea state, the distribution of the annual maximum significant wave height $H_{S,max}$ can be taken as

$$F_{H_{S,max},1\,year}(h) = (F_{H_S}(h))^n$$

where n is the number of t-hour sea states in one year. For $t = 3$ hours, $n = 2922$. Alternatively, for a storm based approach, $F_{H_S}(h)$ denotes the distribution of the maximum significant wave height in storms, and n corresponds to the number of storms per year.

3.7.1.2 The significant wave height with return period T_R in units of years can be defined as the $(1-1/(nT_R))$ quantile of the distribution of significant wave heights, where n is the number of sea states per year. It is denoted H_{S,T_R}

and is expressed as

$$H_{S,T_R} = F_{H_S}^{-1}(1 - \frac{1}{nT_R})$$

3.7.1.3 Alternatively, H_{S,T_R} can be defined as the $(1-1/T_R)$ quantile in the distribution of the annual maximum significant wave height, i.e. it is the significant wave height whose probability of exceedance in one year is $1/T_R$. Then

$$H_{S,T_R} = F_{H_{S,max},1\,year}^{-1}(1 - \frac{1}{T_R}) \quad ; T_R > 1 \text{ year}$$

A T_R year design sea state is then a sea state of duration 3-6 hours, with significant wave height H_{S,T_R} combined with adequately chosen characteristic values for the other sea-state parameters. For example the accompanying T_p or T_Z values are typically varied within a period band about the mean or median period. The approach can be generalized by considering environmental contours as described in the next section.

3.7.1.4 The design sea state approximation amounts to assuming that the *n*-year extreme response can be estimated from the *n*-year maximum significant wave height condition. Generally, this requires some procedure that accounts for the short term variability of response within the sea state, such that inflating the significant wave height or using an increased fractile value for the short term extreme value distribution of response, confer 3.7.2.

3.7.2 Environmental contours

3.7.2.1 The *environmental contour* concept represents a rational procedure for defining an extreme sea state condition. The idea is to define contours in the environmental parameter space (usually H_s, T_p) along which extreme responses with given return period should lie. (Winterstein et al.,1993).

3.7.2.2 IFORM approach

— Determine the joint environmental model of sea state variables of interest

For H_s, T_z: $\qquad f_{H_s T_z}(h, t) = f_{H_s}(h) f_{T_Z | H_s}(t \mid h)$

— Transform the distribution to standard normalized U-space

$$\Phi(u_1) = F_{H_s}(h_s) \quad \Phi(u_2) = F_{T_z | H_s}(t_z)$$

— Establish the circle for prescribed return period in U-space. For observations recorded each 3rd hour, the radius for the 100-year contour is

$$\sqrt{u_1^2 + u_2^2} = \beta = -\Phi^{-1}\left[\frac{1}{100 \cdot 365 \cdot 8}\right] = 4.5$$

— Transform the circle into a contour in the environmental parameter space

$$h_s = F_{H_S}^{-1}(\Phi(u_1)) \qquad t_z = F_{Tz|H_S}^{-1}(\Phi(u_2))$$

3.7.2.3 Constant probability density approach

— Determine the joint environmental model of sea state variables of interest

For H_s, T_z: $\quad f_{H_s T_z}(h, t) = f_{H_s}(h) f_{T_Z | H_s}(t \mid h)$

— Estimate the extreme value for the governing variable for the prescribed return period, and associated values for other variables. For example 100-year value for H_s and the conditional median for T_z
— The contour line is estimated from the joint model or scatter diagram as the contour of constant probability density going through the above mentioned parameter combination.

3.7.2.4 An estimate of the *extreme response* is then obtained by searching along the environmental contour for the condition giving maximum characteristic extreme response.

3.7.2.5 This method will tend to underestimate extreme response levels because it neglects the response variability due to different short term sea state realisations. The short term variability can be accounted for in different ways (Winterstein et al., 1996).

3.7.2.6 One can estimate the indirectly and approximately account for the extreme response variability by *inflating* the return period and environmental contours (Winterstein et al.,1993).

3.7.2.7 Inflate response: One can replace the stochastic response by a fixed fractile level higher than the median value, or apply multipliers of the median extreme response estimates.

3.7.2.8 The appropriate fractile levels and multipliers will be case-specific, and should be specified for classes of structures and structural responses. Generally the relevant factor and fractile will be larger for strongly nonlinear problems. Values reported in the literature are fractiles 75% - 90% for 100-year response (Winterstein, Haver et al., 1998), and multiplying factors 1.1 - 1.3 (Winterstein at al., 1998).

3.7.3 Extreme individual wave height and extreme crest height

3.7.3.1 The maximum individual wave height in a random sea state can be expressed as

$$F_{H\max}(h_{\max}) = \iint_{h_s t_z} F_{H\max | H_s T_z}(h_{\max} \mid h_s, t_z) f_{H_s T_z}(h_s, t_z) dh_s dt_z$$

Here

$$f_{H_s T_z}(h_s, t_z)$$

is the joint probability density for H_s and T_z (alternatively T_p or T_1 could be used); and

$$F_{H\max | H_s T_z}(h_{\max} \mid h, t)$$

is the distribution of the maximum wave height in the sea state with parameters H_s, T_z. A corresponding expression applies for crest height and for storm events.

3.7.3.2 The following recipe is recommended to establish the distribution for the extreme waves based on storm statistics:

— step through storms, establish distribution of maximum wave height in the storm; fit a Gumbel distribution to $h_{\max}^2$, determine mode $h_{\max,m}$ and variance for the extreme value distribution within each storm
— carry out POT analysis for the modes
— establish distribution for the maximum wave height in a random storm as

$$F_{H\max}(h_{\max}) \approx \exp\left\{-\exp\left(-\ln(N) \cdot \left[(\frac{h_{\max}}{h_{\max,m}})^2 - 1\right]\right)\right\}$$

The parameter ln (N) is a function of the coefficient of variation of $h_{\max}^2$; a typical value for North Sea storms is $\ln(N) = 8$. A similar expression applies for maximum crest height. For more information confer Tromans and Vanderschuren(1995).

3.7.3.3 The annual extreme value distributions for wave height are obtained by integrating the short term statistics weighted by the long term distributions, viz:

$$F_{H_{annual}}(h_{\max}) = [F_{H\max}(h_{\max})]^n$$

Here n is the number of events (sea states or storms) per year. A similar expression applies for crest height.

3.7.3.4 Assuming a sea state duration 3-hours, the value H_{T_R} with return period T_R (in years) follows from

$$1 - F_{H\max}(H_{T_R}) = \frac{1}{T_R \cdot 2922}$$

The wave height H_{T_R} can alternatively be expressed as the $1/T_R$ fractile for the distribution of annual maximum wave height,

$$1 - F_{H_{annual}}(H_{T_R}) = \frac{1}{T_R}$$

E.g., the 100-year individual wave height H_{100} corresponds to the wave height with an annual exceedance probability of 10^{-2}.

As discussed in 3.5.11, the distribution of the annual maximum wave height or annual maximum crest height, can be assumed to follow a Gumbel distribution.

3.7.3.5 In lack of more detailed information, for sea states of duration 3-hours, the H_{100} may be taken as 1.9 times the significant wave height $H_{s,100}$.

3.7.4 Wave period for extreme individual wave height

3.7.4.1 The most probable individual wave period T_{Hmax} to be used in conjunction with a long term extreme wave height

H_{max}, can be expressed as

$$T_{H\,max} = a \cdot H_{max}^{b}$$

where a and b are empirical coefficients. For the Norwegian Continental Shelf, the following values may be applied,

$a = 2.94$, $b = 0.5$

giving

$$T_{H\,max} = 2.94 \cdot \sqrt{H_{max}}$$

3.7.4.2 The period T_{Hmax} used in conjunction with H_{100} should be varied in the range

$$2.55\sqrt{H_{100}} \le T_{H\,max} \le 3.32\sqrt{H_{100}}$$

3.7.5 Temporal evolution of storms

In evaluation of the foundation's resistance against cyclic wave loading, the temporal evolution of the storm should be taken into account. This should cover a sufficient part of the growth and decay phases of the storm.

If data for the particular site is not available, the storm profile in Figure 3-10 may be applied.
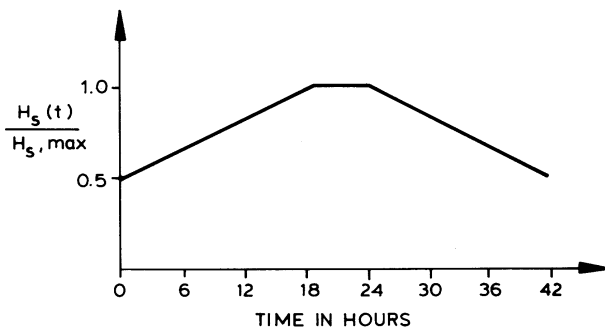

Figure 3-10
Significant wave height relative to maximum value as a function of time during a storm, for evaluation of foundation resistance against cyclic wave loading.

References

1) Battjes, J. A. (1978), "Engineering Aspects of Ocean Waves and Currents", Seminar on Safety of Structures under Dynamic Loading, Trondheim, Norway.

2) Bitner-Gregersen and Ø. Hagen (1999), "Extreme value analysis of wave steepness and crest using joint environmental description", Proc. of OMAE 99 Conference, No. 6033.

3) Bitner-Gregersen E.M. (1996), "Distribution of Multidirectional Environmental Effects", Proceedings of 15th International Conference of Offshore Mechanics and Arctic Engineering; OMAE 1996; Florence, Italy.

4) Bitner-Gregersen, E. (1988), Appendix "Joint Long Term Distribution of Hs, Tp", Det Norske Veritas Report No. 87-31, "Probabilistic Calculation of Design Criteria for Ultimate Tether Capacity of Snorre TLP" by Madsen, H. O., Rooney, P., and Bitner-Gregersen, E. Høvik.

5) Bitner-Gregersen, E. M. and S. Haver (1991) "Joint Environmental Model for Reliability Calculations", Proceedings of the 1st International Offshore and Polar Engineering Conference, Edinburgh, United Kingdom, August 11-15, 1991.

6) Bitner-Gregersen, E. M., Hovem, L., and Hørte, T. (2003) "Impact of Freak Waves on Ship Design Practice", WMO J., Geneva, 2003.

7) Bitner-Gregersen, E.M. (2005) Joint Probabilistic Description for Combined Seas, Proceedings of 24th International Conference on Offshore Mechanics and Arctic Engineering (OMAE 2005), June 12-17, 2005, Halkidiki, Greece OMAE 2005-67382.

8) Bitner-Gregersen, E.M. and Haver, S. (1989), "Joint Long Term Description of Environmental Parameters for Structural Response Calculation". Proc. 2nd Int. Workshop on Wave Hindcasting and Forecasting, Vancouver, B.C. Canada, April 25-28, 1989.

9) Bitner-Gregersen, E.M., Cramer, E. and Korbijn, F. (1995) "Environmental Description for Long-term Load Response", Proc. ISOPE-95 Conf., The Hague, June 11-16, 1995.

10) Bitner-Gregersen, E.M., Guedes Soares, C., Machado, U. and Cavaco, P. (1998) "Comparison Different Approaches to Joint Environmental Modelling", Proceedings of OMAE'98 conference, Lisboa, Portugal, July 1998.

11) Bitner-Gregersen. E.M. and Hagen. Ø. (2002) "Directional Spreading in Two-peak Spectrum at the Norwegian Continental Shelf". Proc. OMAE'2002 Conference. Oslo. June 23-28, 2002.

12) Bouws, E., Günther, H., Rosenthal, W. and Vincent, C.L. (1985) Similarity of the wind wave spectrum in finite depth water: 1. Spectral form. J. Geophys. Res., 90, C1, pp. 975-86.

13) Chakrabarti, S.K. (1987) "Hydrodynamics of Offshore Structures". WIT Press.

14) Coastal Engineering Research Center (1984) "Shore Protection Manual", Vols I-II.

15) Dean, R.G. (1965) "Stream function representation of nonlinear ocean waves". Journal of Geophysical Research, Vol. 70, No. 8.

16) Dean, R.G. (1970) "Relative validities of water wave theories". Journ. of the Waterways and Harbours Div., ASCE.

17) Der Kiuregihan and Liu, (1986), "Structural Reliability under Incomplete Probability Information", J. Eng. Mechaincs, ASCE, Vol.113, No.8, pp.1208-1225.

18) Fenton, J.D. (1985) "A fifth order Stokes theory for steady waves". J. Waterway, Port, Coast. and Ocean Eng. ASCE, 111 (2).

19) Forristal, G.Z. (1978). "On the statistical distribution of wave heights in a storm.", J. Geophysical Res., 83, 2353-2358.

20) Forristall, G.Z., 2004, "On the use of directional wave criteria", Journal of Waterway, Port, Coastal and Ocean Engineering.

21) Forristall, George Z., (2000), "Wave Crest Distributions: Observations and Second Order Theory", Journal of Physical Oceanography, Vol. 30, pp 1931-1943.

22) Grue, J. Clamond, D., Huseby, M. and Jensen, A. (2003) "Kinematics of extreme waves in deep water". Applied Ocean Research, Vol. 25, pp.355-366.

23) Gudmestad, O.T. (1993) "Measured and predicted deep water wave kinematics in regular and irregular seas". Marine Structures, Vol. 6, pp.1-73.

24) Hasselman et al., (1973), "Measurements of Win-Wave Growth and Swell Decay During the Joint North sea Wave Project" (JONSWAP), Deutschen Hydro-graphischen Institut, No. 12, Hamburg, Germany.

25) Haver S. and G. Kleiven (2004), "Environmental Contour Lines for Design Purposes- Why and When", 23rd Int. Conf. Offshore Mechanics and Arctic Engineering, OMAE, June 20-25. Vancouver, British Columbia, Canada.

26) Haver, S. (1987), "On the distribution of heights and periods of sea waves"; Ocean Engng. Vol. 14, No. 5, pp. 359-376, 1987.

27) Haver, S. and Andersen, O.J., "Freak Waves Rare Realizations of a Typical Population or Typical Realizations of a rare Population?", Proc. ISOPE-2000 Conference, June 2000, Seattle, USA.

28) Hurdle, D.P. and Stive, M.J.F. (1989). "Revision of SPM 1984 wave hindcast model to avoid inconsistencies in engineering applications". Coastal Engineering, 12:339-357.

29) ISO 19901-1 (2005) "Metocean design and operating considerations".

30) Kleiven, G. and S. Haver (2004) "Met-Ocean Contour Lines for Design; Correction for Omitted Variability in the Response Process", Proc. of 14th Int. Offshore and Polar Engineering Conference, Toulon, France, May 23-28, 2004.

31) Krogstad, Harald (1985), Height and Period Distributions of Extreme Waves; Applied Ocean Research, 1985; Vol. 7, No 3., pp 158-165.

32) Longuet-Higgins, M.S. (1975). "On the joint distribution of the periods and amplitudes of sea waves". Journal of the Geophysical Research, 80, 2688-2694.

33) Longuet-Higgins, M.S. (1980). "On the Distribution of Heights of Sea Waves: Some Effects of Non-linearities and Finite Band Width", Journal of Geophysical Research, Vol. 85, No. C3, pp 1519-1523.

34) Longuet-Higgins, M.S. (1984) "Bifurcation in gravity waves". J. Fluid Mech. Vol. 151, pp. 457-475.

35) Longuet-Higgins, M.S., (1983), "On the joint distribution of wave periods and amplitudes in a random wave field", Proc. R. Soc. Lond., A 389, pp.241-258.

36) Longuett-Higgins, M.S. (1963) "The effect of non-linearities on statistical distributions in the theory of sea waves". J. Fluid Mech., Vol. 13.

37) Lygre, A. and H.E. Krogstad (1986), "Maximum Entropy Estimation of the Directional Distribution in Ocean wave Spectra", J. Phys. Ocean., Vol.16, pp. 2052-2060.

38) Mallery, G.O. and Clark, G.C. (1972) "Cnoidal wave theory for application to offshore structural design". OTC Paper No. 1614.

39) Marthinsen, T. and Winterstein, S. (1992) "On the skewness of random surface waves". Proc. vol. 3, 2nd ISOPE Conf., San Franciisco, California, USA, pp. 472-478.

40) Marthinsen, T. and Winterstein, S.R. (1992) "On the skewness of random surface waves". Proc. ISOPE Conf., San Francisco, USA.

41) Massel, S. (1996) "On the largest wave height in water of constant depth", Ocean Eng. Vol 23, No. 7, pp 553-573.

42) Mathisen, J. K. Ronold, G. Sigurdssson (2004), "Probabilistic modelling for reliability analysis of jackets", 23rd International Conference on Offshore Mechanics and Arctic Engineering, June 20-25, 2004, Vancouver, British Columbia, Canada, paper 51227.

43) MAXWAVE; European Commission under the Fifth Framework Programme; Key Action 3: Sustainable Marine Ecosystems within the Energy, Environment and Sustainable Development (2000-2003); http://w3g.gkss.de/projects/maxwave/

44) Næss, A. (1985): "The joint crossing frequency of stochastic processes and its application to wave theory", Journal of Applied Ocean Research, Vol. 7, No. 1, 1985.

45) Nelson, R.C. (1994) "Depth limited design wave heights in ver yflat regions". Coastal Eng. Vol. 23, pp. 43-59.

46) Nestegård, A. and Stokka, T. (1995). "Third-order random wave model". Proc. of the 5th Int. Offshore and Polar Engineering Conference, The Hague, Netherlands.

47) Nordenstrøm, N. : "A Method to Predict Long-Term Distributions of Waves and Wave-Induced Motions and Loads on Ships and Other Floating Structures". Det Norske Veritas. Publication No. 81. April 1973.

48) Ochi, M.K. and Hubble, E.N., (1976), "On Six-Parameters Wave Spectra", Proc. 15th Coastal Eng. Conf., Vol 1, pp-301-328.

49) Pierson-Moskowitz (1964), "A Proposed Spectral Form for Fully Developed Wind Seas Based on Similarity Theory of S.A. Kitaigorodskii", J. Geoph. Res., 69, pp.5181-5190.

50) Prince-Wright, R., "Maximum Likelihood Models of Joint Environmental Data for TLP Design", OMAE, Safety and Reliability, volume II, ASME 1995.

51) Proceedings Rogue Waves 2004, Brest, France 20-22 October 2004.

52) Sarpkaya, T. and Isaacson, M. (1981) "Mechanics of Offshore Structures". Van Nostrand Reinhold Company.

53) Sarpkaya, T. and Isaacson, M. (1981). "Mechanics of wave forces on offshore structures". Van Nostrand Reinhold Company.

54) Schwartz, L. (1974) "Computer extension and analytical continuation of Stokes' expansion for gravity waves". J. Fluid Mech. 62, pp. 553-578.

55) Sharma, J.N. and Dean, R.G. (1979) "Second-order directional seas and associated wave forces". OTC 3645. Houston.

56) Stansberg, C.T. (2005) "Comparing models for kinematics under irregular waves". Marintek Report 570023.00.01.

57) Stansberg, C.T. and Gudmestad, O.T. (1996). "Nonlinear random wave kinematics models verified against measurements in steep waves". Proc. Vol. 1A 15th OMAE Conf., Florence, Italy, pp. 15-24.

58) Sterndorff, M.J. and J.D. Sørensen, 2001. A rational procedure for determination of directional individual design wave heights. OMAE'2001, Paper No. OMAE01/S&R-2173.

59) Strekalov, S.S. and S. Massel (1971), "On the Spectral Analysis of Wind Waves", Arch. Hydrot. 18, pp.457-485.

60) Tayfun, M.A. (1981). "Distribution of Crest-to-trough Wave Heights", J. Wtrway, Port, Coastal and Ocean Engng., 107(3), 149-158.

61) Tayfun, M.A. (1993). "Distribution of Large Wave Heights", J. Wtrway, Port, Coastal and Ocean Engng., 116(6), 686-707.

62) Torsethaugen, K. and S. Haver (2004), "Simplified Double Peak Spectral Model for Ocean Waves", Proceedings of the Fourteenth International Offshore and Polar Engineering Conference, Toulon, France, May 23-28, 2004.

63) Torsethaugen, K.(1996), "Model for Double Peaked Wave Spectrum", SINTEF Civil and Envir. Engineering, Rep. No. STF22 A96204, Trondheim, Norway.

64) Tromans, P.S. and Vanderschuren, L. (1995) "Response based design conditions in the North Sea: Application of a new method". OTC 7683.

65) Tucker, M.J. and Pitt, E.G. (2001) "Waves in Ocean Engineering". Elsevier Ocean Engineering Book Series. Volume 5.

66) U.S. Army Corps of Engineers (2004) "Coastal Engineering Manual".

67) Wheeler, J.D.E. (1970) "Method for calculating forces produced by irregular waves". Journal of Petroleum Tech., Vol. 249, pp.359-367.

68) Wiegel, R.L. (1960) "A presentation of cnoidal wave theory for practical application". Journal of Fluid Mechanics. Vol. 7, No. 18.

69) Winterstein, S., Ude, T.C., Cornell. C.A., Bjerager, P., Haver, S., "Environmental Parameters for Extreme Response: Inverse FORM with omission Sensitivity", Proc. ICOSSAR-93, Innsbruck, 1993.

70) Winterstein, S.R., and K. Engebretsen (1998): "Reliability-Based Prediction of Design Loads and Responses for Floating Ocean Structures", OMAE-1998, Lisbon, Portugal.

4. Current and Tide Conditions

4.1 Current conditions

4.1.1 General

4.1.1.1 The effects of currents should be considered for design of ships and offshore structures, their construction and operation.

4.1.1.2 The following items should be considered in design of offshore structures:

— Currents can cause large steady excursions and slow drift motions of moored platforms.
— Currents give rise to drag and lift forces on submerged structures.
— Currents can give rise to vortex induced vibrations of slender structural elements and vortex induced motions of large volume structures.
— Interaction between strong currents and waves leads to change in wave height and wave period.
— Currents can create seabed scouring around bottom mounted structures.

4.1.1.3 Information on statistical distribution of currents and their velocity profile is generally scarce for most areas of the world. Current measurement campaigns are recommended during early phases of an offshore oil exploration development. Site specific measurements should extend over the water column and over the period that captures several major storm events. Some general regional information on current conditions are given in ISO 19901-1 (2005) "Metocean design and operating considerations".

4.1.1.4 If sufficient joint current-wave data are available, joint distributions of parameters and corresponding contour curves (or surfaces) for given exceedance probability levels can be established. Otherwise conservative values, using combined events should be applied (NORSOK N-003, DNV-OS-C101).

4.1.2 Types of current

4.1.2.1 The most common categories of ocean currents are:

— wind generated currents
— tidal currents
— circulational currents
— loop and eddy currents
— soliton currents
— longshore currents.

4.1.2.2 *Wind-generated currents* are caused by wind stress and atmospheric pressure gradient throughout a storm.

4.1.2.3 *Tidal currents* are regular, following the harmonic astronomical motions of the planets. Maximum tidal current precedes or follows the highest and lowest astronomical tides, HAT and LAT. Tidal currents are generally weak in deep water, but are strengthened by shoreline configurations. Strong tidal currents exist in inlets and straights in coastal regions.

4.1.2.4 *Circulational currents* are steady, large-scale currents of the general oceanic circulation (i.e. the Gulf Stream in the Atlantic Ocean). Parts of the circulation currents may break off from the main circulation to form large-scale eddies. Current velocities in such eddies (*loop and eddy currents*) can exceed that of the main circulation current (i.e. Loop Current in GoM).

4.1.2.5 *Soliton currents* are due to internal waves generated by density gradients.

4.1.2.6 *Loop/eddy currents* and soliton currents penetrate deeply in the water column.

4.1.2.7 *Longshore current* – in coastal regions runs parallel to the shore as a result of waves breaking at an angle on the shore, also referred to as *littoral* current.

4.1.2.8 Earthquakes can cause unstable deposits to run down continental slopes and thereby set up gravity driven flows. Such flows are called *turbidity currents*. Sediments in the flow gives a higher density than the ambient water. Such currents should be accounted for in the design of pipelines crossing a continental slope with unstable sediments. Strong underwater earthquakes can also lead to generation of *tsunamis* which in coastal regions behaves like a long shallow water wave similar to a strong horizontal current.

4.1.3 Current velocity

4.1.3.1 The current velocity vector varies with water depth. Close to the water surface the current velocity profile is stretched or compressed due to surface waves (see Figure 4-1). In general the current velocity vector varies in space and time

$$\mathbf{v}_c = \mathbf{v}_c(x, y, z; t)$$

The time-dependence is due to flow fluctuations caused by turbulence.

4.1.3.2 For most applications the current velocity can be considered as a steady flow field where the velocity vector (magnitude and direction) is only a function of depth. Design of certain dynamic current sensitive structures should take into account turbulence effects.

4.1.3.3 The total current velocity at a given location (*x,y*) should be taken as the vector sum of each current component present, wind generated, tidal and circulational currents,

$$\mathbf{v}_c(z) = \mathbf{v}_{c,\text{wind}}(z) + \mathbf{v}_{c,\text{tide}}(z) + \mathbf{v}_{c,\text{circ}}(z) + \dots$$

4.1.4 Design current profiles

4.1.4.1 When detailed field measurements are not available the variation in shallow of tidal current velocity water with depth may be modelled as a simple power law, assuming unidirectional current,

$$\text{v}_{c,\text{tide}}(z) = \text{v}_{c,\text{tide}}(0)\left(\frac{d+z}{d}\right)^{\alpha} \text{ for } z \le 0$$

4.1.4.2 The variation of *wind* generated current can be taken as either a linear profile from $z = -d_0$ to still water level,

$$\text{v}_{c,\text{wind}}(z) = \text{v}_{c,\text{wind}}(0)\left(\frac{d_0+z}{d_0}\right) \text{for} - d_0 \le z \le 0$$

or a slab profile

$$\text{v}_{c,\text{wind}}(z) = \text{v}_{c,\text{wind}}(0) \text{ for} - d_0 < z < 0$$

The profile giving the highest loads for the specific application should be applied.

4.1.4.3 Wind generated current can be assumed to vanish at a distance below the still water level,

$$\text{v}_{c,\text{wind}}(z) = 0 \text{ for } z < -d_0$$

where

$\text{v}_c(z)$	=	total current velocity at level z
z	=	distance from still water level, positive upwards
$\text{v}_{c,\text{tide}}(0)$	=	tidal current velocity at the still water level
$\text{v}_{c,\text{wind}}(0)$	=	wind-generated current velocity at the still water level
d	=	water depth to still water level (taken positive)

d_0 = reference depth for wind generated current,
$d_0 = 50$ m

α = exponent – typically $\alpha = 1/7$

4.1.4.4 In deep water along an open coastline, wind-generated current velocities at the still water level may, if statistical data are not available, be taken as follows:

$v_{c,wind}(0) = k\ U_{1\ hour,\ 10\ m}$ where $k = 0.015 - 0.03$

$U_{1\ hour,\ 10\ m}$ is the 1 hour sustained wind speed at height 10 m above sea level as defined in Ch.2.

4.1.4.5 The variation of current velocity over depth depends on the local oceanographic climate, the vertical density distribution and the flow of water into or out of the area. This may vary from season to season. Deep water profiles may be complex. Current direction can change 180 degrees with depth.

4.1.4.6 When long-term measured current profile data sets are available, design current profiles can be derived by parametrizing the data using so-called empirical orthogonal functions (EOF). This technique is used for representing a set of spatially distributed time series as a sum of orthogonal spatial functions b_m (EOFs) multiplied by their temporal amplitudes $w_m(t)$. A current profile at location x can then be expressed as

$$\mathbf{v}_c(\mathbf{x},t) = \sum_{m=1}^{M} \boldsymbol{b}_m(\mathbf{x}) \cdot \mathbf{w}_m(t)$$

4.1.4.7 Profiles with required return periods can be selected by applying EOFs and inverse first order reliability method IFORM (see 3.9.2) methods as described by Foristall and Cooper (1997).

4.1.4.8 While frequency power spectra are extensively used for wave loading (close to the wave surface boundary) and for wind loading (close to the ground or sea surface), such spectra are not in general available for current loading. An exception is current loading (e.g. pipelines) in the turbulent boundary layer close to the sea bed. Current conditions close to the sea bed are discussed in DNV-RP-F105 Free Spanning Pipelines.

4.1.5 Stretching of current to wave surface

4.1.5.1 The variation in current profile with variation in water depth due to wave action should be accounted for. In such cases the current profile may be stretched or compressed vertically, but the current velocity at any proportion of the instantaneous depth is constant, see Figure 4-1. By this method the surface current component remains constant.

4.1.5.2 Stretching is expressed formally by introducing a stretched vertical coordinate z_s such that the current speed $v(z)$ at depth z in the still water profile is at the stretched coordinate z_s.

4.1.5.3 Linear stretching is defined by

$z_s = (d+\eta)(1+z/d) - d$; $\quad -d \le z_s \le \eta$

where η is the water surface elevation and d is the still water depth. This is the essentially the same as Wheeler stretching used for wave kinematics above z = 0 for linear waves (see 3.5.2).

4.1.5.4 Non-linear stretching is defined by relating z_s and z through linear Airy wave theory as

$z_s = z + \eta \dfrac{\sinh[k_{nl}(z+d)]}{\sinh(k_{nl}d)}$; $\quad -d \le z_s \le \eta$

where k_{nl} is the non-linear wave number corresponding to the wavelength λ_{nl} for the regular wave under consideration for water depth d and wave height H. Non-linear stretching provides the greatest stretching at the sea surface where the wave orbital motion has the greatest radii.
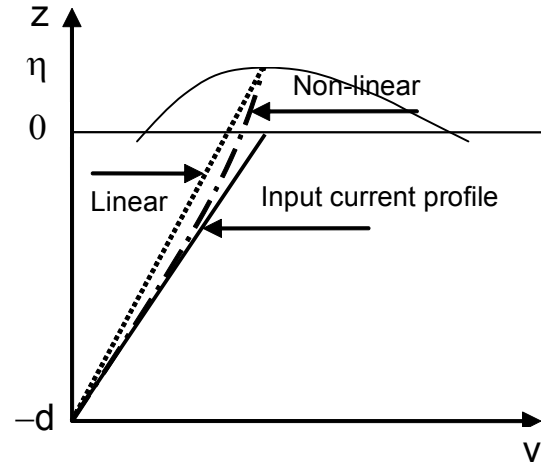
Figure 4-1
Linear and non-linear stretching of current profile to wave surface

4.1.5.5 In most cases linear stretching produces accurate estimates of global hydrodynamic loads. However if the current profile has very high speed at the sea surface, with a strong shear to lower speeds just below the surface, the non-linear stretching should be used.

4.1.5.6 If the current is not in the same direction as the wave, both in-line and normal components of the current may be stretched. For irregular waves, the stretching method applies to each individual crest-trough.

4.1.6 Numerical simulation of current flows

Reliable numerical ocean models can be used for prediction of current flow fields at locations where no measurements are available. Input to these models are site measurements at a finite number of locations or observations from satellites.

Numerical ocean models should be used with care. Such models should be validated by measurements before they can be used with confidence. Recent references on numerical ocean modelling are Heidvogel and Beckman (2000) and Kantha and Clayson (2000).

4.1.7 Current measurements

4.1.7.1 Two different types of measurements are available for obtaining information about ocean current velocity:

— *Direct measurements* provides information about the current velocity at a finite number of fixed points. Examples are *rotor current meters*, using a propeller rotating around a vertical axis, and *acoustic current meters*, emitting a series of short sound wave pulses, and then measuring the reflected signal from particles which travels with the current.
— *Indirect measurements* where measurements of salinity and temperature for a number of locations are used to estimate the density and then the mean current velocities can be derived from the geostrophic equations (Pickard and Emery, 1990).

4.1.7.2 For estimates of mean current velocities in circulation currents, large loop/eddy currents and tidal currents, it is sufficient to use averaging periods of 10 minutes and longer when recording the current velocity. In order to resolve variations on time scales corresponding to dynamic response periods of marine structures, short averaging periods are necessary. When developing design criteria for free-spanning pipelines close to the seabed it may be necessary to record data with a sampling frequency of 1 Hz.

4.2 Tide conditions

4.2.1 Water depth

4.2.1.1 The water depth at any offshore location consists of a stationary component and a time-varying component. The variations are due to *astronomical tide*, to wind and the atmospheric pressure. Wind and variations in atmospheric pressure create *storm surges*, positive or negative. Other variations in water depth can be due to long-term climatic changes, sea floor subsidence or an episodic increase of water level events like tsunamis.

4.2.1.2 Best estimates of water depth and its variations are derived from site-specific measurements with a tide gauge measuring pressure from sea floor. Accurate estimates of extreme tides, including HAT and LAT, require at least one year of measurements.

4.2.1.3 It is recommended that when receiving measured water level data, it should always be checked whether the tide has been removed or not. This is important for being able to establish a surge model.

4.2.2 Tidal levels

4.2.2.1 The tidal range is defined as the range between the highest astronomical tide (HAT) and the lowest astronomical tide (LAT), see Figure 4-2.

4.2.2.2 The Highest Astronomical Tide (HAT) is the highest level, and Lowest Astronomical Tide (LAT) is the lowest level that can be expected to occur under average meteorological conditions and under any combination of astronomical conditions.

4.2.2.3 The values of Lowest Astronomical Tide (LAT) and Highest Astronomical Tide (HAT) are determined by inspection over a span of years.

4.2.2.4 Spring tides are tides of increased range occurring near the times of full moon and new moon. The gravitational forces of the moon and the sun act to reinforce each other. Since the combined tidal force is increased the high tides are higher and the low tides are lower than average. Spring tides is a term which implies a welling up of the water and bears no relationship to the season of the year.

4.2.2.5 Neap tides are tides of decreased range occurring near the times of first and third quarter phases of the moon. The gravitational forces of the moon and the sun counteract each other. Since the combined tidal force is decreased the high tides are lower and the low tides are higher than average.

4.2.2.6 The height of mean high water springs (MHWS) is the average of the heights of two successive high waters during those periods of 24 hours (approximately once a fortnight) when the range of the tide is greatest. The height of mean low water springs (MLWS) is the average height obtained by the two successive low waters during the same period.

4.2.2.7 The height of mean high water neaps (MHWN) is the average of the heights of two successive high waters during those periods (approximately once a fortnight) when the range of the tide is least. The height of mean low water neaps (MLWN) is the average height obtained from the two successive low waters during the same period.

4.2.2.8 The values of MHWS, MLWS, MHWN and MLWN vary from year to year in a cycle of approximately 18.6 years. In general the levels are computed from at least a year's predictions and are adjusted for the long period variations to give values which are the average over the whole cycle.

4.2.3 Mean still water level

Mean still water level (MWL) is defined as the mean level between the highest astronomical tide (HAT) and the lowest astronomical tide (LAT), see Figure 4-2.

4.2.4 Storm surge

The storm surge includes wind-induced and pressure-induced effects. Accurate estimates of the storm surge require long-term measurements on the order of 10 years or more. The relation between storm surge and significant wave height can be established by a regression model. Negative storm surge may be important for coastal navigation and port activities, especially in shallow water.

4.2.5 Maximum still water level

Maximum (or highest) still water level (SWL) is defined as the highest astronomical tide including storm surge, see Figure 4-2. Minimum (or lowest) still water level is defined as the lowest astronomical tide including negative storm surge
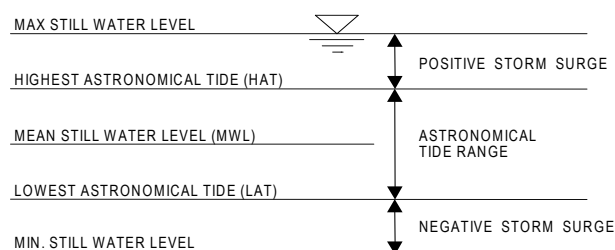
Figure 4-2
Definition of water levels

References

1) ISO 19901-1 Petroleum and natural gas industries – Specific requirements for offshore structures – Part 1: Metocean design and operating considerations (2005)

2) Coastal Engineering Research Center (1984) "Shore Protection Manual", Vols I-II.

3) DNV-OS-C101 "Design of offshore steel structures. General (LRFD method). October 2000.

4) DNV-RP-F105 "Free Spanning Pipelines".

5) Foristall, G.Z. and Cooper, C.K. (1997) "Design current profiles using Empirical Orthogonal Functions (EOF) and Inverse FORM methods": Proc. 29th OTC Conference, OTC 8267, Houston, May 1997.

6) Heidvogel, D.B. and Beckman, A. (2000) "Numerical ocean circulation modeling". Imperial College Press, London, UK.

7) Kantha, L.H. and Clayson, C.A. (2000) "Numerical models of oceans and oceanic processes". Academic Press.

8) NORSOK N-003 "Action and action effects" (2004)

9) Pickard, G.L. and Emery, W.J. (1990) "Descriptive Physical Oceanography". Oxford OX2 8DP: Butter-worth-Heinemann.

5. Wind Loads

5.1 General

Wind induced loads on structures are in general time dependent loads due to fluctuations in the wind velocity. Wind loads act on the external surfaces of the closed structures and may also act on internal surfaces of open structures. Wind pressure loads act in a direction normal to the surface. When a large surface is swept by wind, frictional forces due to tangential drag should be considered also.

The response of a structure due to wind loading is a superposition of a static response and resonant response due to excitation close to natural frequencies.

The dynamic effects can be

— resonant response due to turbulence in wind (see 5.6)
— response due to vortex shedding (see Ch.9)
— galloping / flutter.

Guidance on galloping and flutter can be found in Blevins (1990).

As the wind speed varies with elevation, the height of the structure or component considered shall be taken into account. Vertical wind profiles that can be used are discussed in 2.3.2.

Global wind loads on structures shall be determined using a time-averaged design speed in the form of a sustained wind speed. For design of individual components, a time-averaged wind speed is also adequate, but the averaging time interval should be reduced to allow for smaller turbulence scales.

For design of offshore structures that exhibit considerable dynamic response, the time and spatial variation of the wind speed should be accounted for. When the wind field contains energy at frequencies near the natural frequencies of the structure, a dynamic analysis using a wind frequency spectrum should be carried out.

A general introduction to wind engineering is presented by Simiu and Scanlan (1978).

5.2 Wind pressure

5.2.1 Basic wind pressure

The basic wind pressure is defined by the following equation:

$$q = \frac{1}{2} \rho_a U_{T,z}^2$$

where

q = the basic wind pressure or suction
ρ_a = the mass density of air; to be taken as 1.226 kg/m^3 for dry air at 15°C. See also Appendix F.
$U_{T,z}$ = $U(T,z)$ = the wind velocity averaged over a time interval T at a height z meter above the mean water level or onshore ground.

5.2.2 Wind pressure coefficient

ny external horizontal or vertical surfaces of closed structures, which are not efficiently shielded, should be checked for local wind pressure or suction using the following equation:

$$p = \pm C_p \, q$$

where

p = wind pressure or suction
q = basic wind pressure or suction, as defined in 5.2.1
C_p = pressure coefficient.

The pressure coefficient may be chosen equal to 1.0 for horizontal and vertical surfaces.

5.3 Wind forces

5.3.1 Wind force - general

The wind force F_W on a structural member or surface acting normal to the member axis or surface may be calculated according to:

$$F_W = C \, q \, S \sin \alpha$$

where

C = shape coefficient
q = basic wind pressure or suction, as defined in 5.2.1
S = projected area of the member normal to the direction of the force
α = angle between the direction of the wind and the axis of the exposed member or surface.

The most unfavourable wind direction in the horizontal plane should be used when calculating the stresses in a member due to wind. The spatial correlation of the wind may be taken into consideration for large surfaces. Local wind pressure may be important for design of the exterior panels on topsides. Lift forces due to wind induced pressures on the structure may be an important design issue. Ref. Eurocode EN 1991-1-4. Shape coefficient for various structures are given in Eurocode EN 1991-1-4 General actions - Wind actions.

5.3.2 Solidification effect

If several members are located in a plane normal to the wind direction, as in the case of a plane truss or a serie of columns, the solidification effect ϕ must be taken into account. The wind force is

$$F_{W,SOL} = C_e \, q \, S \, \phi \sin \alpha$$

where

C_e = the effective shape coefficient, see 5.4.7
q = the basic wind pressure according to 5.2.1
S = as defined in 5.3.1. To be taken as the projected area enclosed by the boundaries of the frame
ϕ = *solidity ratio*, defined as the projected exposed solid area of the frame normal to the direction of the force divided by the area enclosed by the boundary of the frame normal to the direction of the force
α = angle between the wind direction and the axis of the exposed member, as defined in 5.3.1.

5.3.3 Shielding effects

If two or more parallel frames are located behind each other in the wind direction, the shielding effect may be taken into account. The wind force on the shielded frame $F_{W,SHI}$ may be calculated as

$$F_{W,SHI} = F_W \eta$$

(if equation in 5.3.1 is applicable)

or as

$$F_{W,SHI} = F_{W,SOL} \eta$$

(if equation in 5.3.2 is applicable)

where

η = shielding factor.

The *shielding factor* η depends on the solidity ratio ϕ of the windward frame, the type of member comprising the frame and the spacing ratio of the frames. The shielding factor may be chosen according to Table 5-1.

If more than two members or frames are located in line after each other in the wind direction, the wind load on the rest of the members or frames should be taken equal to the wind load on the second member or frame.

5.4 The shape coefficient

5.4.1 Circular cylinders

The shape coefficient $C\infty$ for circular cylinders of infinite length may be chosen according to Figure 6-6. Reynolds number R_e is then defined as:

$$R_e = \frac{DU_{T,z}}{v_a}$$

where

D = diameter of member

$U_{T,z}$ = mean wind speed

v_a = kinematic viscosity of air, may be taken as 1.45×10^{-5} m²/s at 15ºC and standard atmospheric pressure. See also Appendix F.

Table 5-1 The shielding factor η as function of spacing ratio α and aerodynamic solidity ratio β.

β α	0.1	0.2	0.3	0.4	0.5	0.6	0.7	0.8
< 1.0	1.0	0.96	0.90	0.80	0.68	0.54	0.44	0.37
2.0	1.0	0.97	0.91	0.82	0.71	0.58	0.49	0.43
3.0	1.0	0.97	0.92	0.84	0.74	0.63	0.54	0.48
4.0	1.0	0.98	0.93	0.86	0.77	0.67	0.59	0.54
5.0	1.0	0.98	0.94	0.88	0.80	0.71	0.64	0.60
> 6.0	1.0	0.99	0.95	0.90	0.83	0.75	0.69	0.66

The *spacing ratio* α is the distance, centre to centre, of the frames, beams or girders divided by the least overall dimension of the frame, beam or girder measured at right angles to the direction of the wind. For triangular or rectangular framed structures diagonal to the wind, the spacing ratio should be calculated from the mean distance between the frames in the direction of the wind.

The *aerodynamic solidity ratio* is defined by $\beta = \phi a$ where

ϕ = solidity ratio, see 5.3.2

a = constant

= 1.6 for flat-sided members

= 1.2 for circular sections in subcritical range and for flat-sided members in conjunction with such circular sections

= 0.6 for circular sections in the supercritical range and for flat-sided members in conjunction with such circular sections.

5.4.2 Rectangular cross-section

The shape coefficients for smooth members with rectangular cross-section ($b_1 \geq b_2$, ref. Figure 5-1) may be taken as:

$$C_{S1} = 2 K_R \sin \alpha$$

$$C_{S2} = \left(1 + \frac{b_2}{b_1}\right) K_R \cos \alpha \quad \text{for } b_2 \leq b_1 \leq 2b_2$$

$$= 1.5 K_R \cos \alpha \qquad \text{for } b_1 > 2b_2$$

$$K_R = 1.0 \qquad\qquad \text{for } \frac{r}{b} \leq 0.10$$

$$= \frac{1}{3}(4.3 - 13\frac{r}{b}) \text{ for } 0.10 < \frac{r}{b} < 0.25$$

$$= 0.35 \qquad\qquad \text{for } \frac{r}{b} \geq 0.25$$

b_1 = longer side of rectangle

b_2 = shorter side of rectangle

r = corner radius of the section

α = angle between side b_1 of the rectangle and the flow component in the cross-sectional plane.

b_1, b_2 and α are also shown in Figure 5-1.

For wide rectangular cross-sections it may be necessary to take into account that the resultant drag force P_{d1} is assumed to be acting at a distance $b_1/3$ from the leading edge of the surface. See Figure 5-1.

The shape coefficients and characteristic dimensions for various smooth members with irregular cross-sections may be taken in accordance with Table 5-2 where dimensions perpendicular to P_{d1} and P_{d2} are to be understood as b_1 and b_2 respectively.
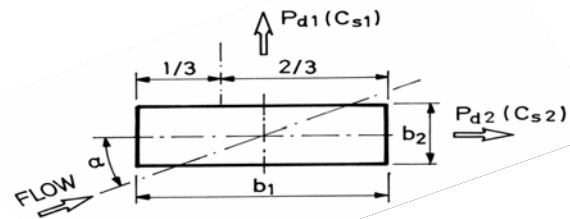
Figure 5-1
Drag forces on rectangular cross-sections

5.4.3 Finite length effects

The shape coefficient C for individual members of finite length may be obtained as: $C = \kappa C_\infty$

where κ is the reduction factor as a function of the ratio l/d (may be taken from Table 6-2, where d is the cross-sectional dimension of a member normal to the wind direction and l is the length of the member).

For members with one end abuting on to another member or a wall in such a way that free flow around that end of the member is prevented, the ratio l/d should be doubled for the purpose of determining κ. When both ends are abuted as mentioned, the shape coefficient C should be taken equal to that for an infinite long member.

5.4.4 Spherical and parabolical structures

For spherical and parabolical structures like radar domes and antennas, the shape coefficient C may be taken from Table 5-3.

5.4.5 Deck houses on horizontal surface

For three-dimensional bodies such as deck houses and similar structures placed on a horizontal surface, the shape coefficients may be taken from Table 5-5.

Table 5-2 Shape coefficient C∞ for irregular cross sections

Profile	α (deg)	C_{S1}	C_{S2}	Profile	α (deg)	C_{S1}	C_{S2}
	0 45 90 135 180	1.9 1.8 2.0 -1.8 -2.0	1.0 0.8 1.7 -0.1 0.1		0 45 90 135 180	2.1 1.9 0 -1.6 -1.8	0 0.6 0.6 0.4 0
	0 45 90 135 180	1.8 2.1 -1.9 -2.0 -1.4	1.8 1.8 -1.0 0.3 -1.4		0 45 90	2.1 2.0 0	0 0.6 0.9
	0 45 90 135 180	1.7 0.8 0 -0.8 -1.7	0 0.8 1.7 0.8 0		0 45 90	1.6 1.5 0	0 1.5 1.9
	0 45 90 135 180	2.0 1.2 -1.6 -1.1 -1.7	0 0.9 2.2 -2.4 0		0 180	1.8 -1.3	0 0

5.4.6 Global wind loads on ships and platforms

Isherwood (1972) has presented drag coefficients for passenger ships, ferries, cargo ships, tankers, ore carriers, stern trawlers and tugs. Aquiree & Boyce (1974) have estimated wind forces on offshore drilling platforms.

5.4.7 Effective shape coefficients

The effective shape coefficient C_e for single frames is given in Table 5-4.

Table 5-3 Shape coefficients C for sphere-shaped structures

Structures		Shape coefficient
	Hollow hemisphere, concavity to wind	1.40
	Hollow hemisphere	0.35
	Hollow or solid hemisphere, concavity to leeward	0.40
	Solid hemisphere and circular disc	1.20
	Hemisphere on horizontal plane	0.50

Table 5-3 Shape coefficients C for sphere-shaped structures (Continued)

Structures		Shape coefficient
	Sphere	Re $\leq 4.2 \cdot 10^5$ → 0.50
		$4.2 \cdot 10^5 < \text{Re} < 10^6$ → 0.15
		Re $\geq 10^6$ → 0.20
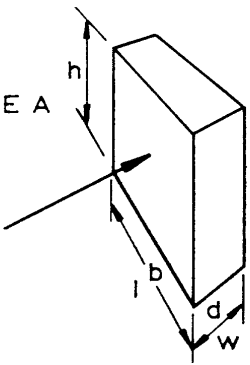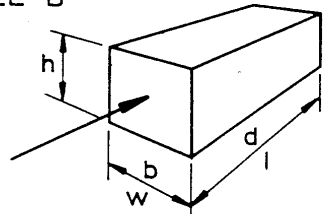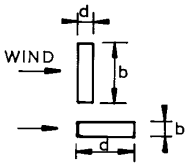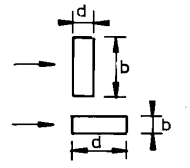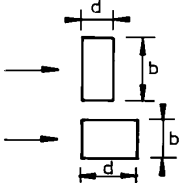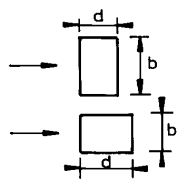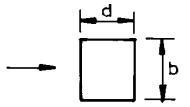
For hollow spherical cupolas with a rise f less than the radius r, one can interpolate linearly for the ratio f/r between the values for a circular disc and a hemisphere.

Table 5-4 Effective shape coefficient C_e for single frames

Solidity ratio ϕ	Effective shape coefficient Ce		
	Flat-side members	Circular sections	
		Re $< 4.2 \times 10^5$	Re $\geq 4.2 \times 10^5$
0.10	1.9	1.2	0.7
0.20	1.8	1.2	0.8
0.30	1.7	1.2	0.8
0.40	1.7	1.1	0.8
0.50	1.6	1.1	0.8
0.75	1.6	1.5	1.4
1.00	2.0	2.0	2.0

All shape coefficients given in 5.4.1 through 5.4.6 include the effect of suction on the leeward side of the member.

Table 5-5 Shape coefficient C for three-dimensional bodies placed on a horizontal surface

EXAMPLE A   EXAMPLE B

Plan shape	l/w	b/d	C for height/breadth ratio h/b				
			Up to 1	1	2	4	6
	≥ 4	≥ 4	1.2	1.3	1.4	1.5	1.6
		≤ 1/4	0.7	0.7	0.75	0.75	0.75
	3	3	1.1	1.2	1.25	1.35	1.4
		1/3	0.7	0.75	0.75	0.75	0.8
	2	2	1.0	1.05	1.1	1.15	1.2
		0.5	0.75	0.75	0.8	0.85	0.9
	1.5	1.5	0.95	1.0	1.05	1.1	1.15
		2/3	0.8	0.85	0.9	0.95	1.0

Plan shape	l/w	b/d	C for height/breadth ratio h/b						
			Up to 0.5	1	2	4	6	10	20
	1	1	0.9	0.95	1.0	1.05	1.1	1.2	1.4

b = the dimension of the member normal to the wind
d = the dimension of the member measured in the direction of the wind
l = the greater horizontal dimension.
w = the lesser horizontal dimension of a member
Example A: l = b, w = d. Example B: w = b, l = d.

5.5 Wind effects on helidecks

The wind pressure acting on the surface of helidecks may be calculated using a pressure coefficient $C_p = 2.0$ at the leading edge of the helideck, linearly reducing to $C_p = 0$ at the trailing edge, taken in the direction of the wind. The pressure may act both upward and downward.

5.6 Dynamic analysis

5.6.1 Dynamic wind analysis

5.6.1.1 A detailed dynamic wind analysis considering the time variation of wind forces should be performed for wind exposed equipment and objects sensitive to varying wind loads. Typically, high towers, flare booms, compliant platforms like ten-

sion leg platforms and catenary anchored platforms etc. should be considered for such analysis.

5.6.1.2 Time varying component of wind force can induce low frequency resonant surge, sway and yaw motion of floating catenary anchored platforms. Low frequency wind forces are computed from a wind energy spectrum. Method for estimating wind forces on ships are given in OCIMF (1994).

5.6.1.3 The gust variation of the wind field can be described as the sum of a sustained wind component (see 2.1.1) and a gust component. The fluctuating gust velocity can be described by a gust spectrum as given in Ch.2.

5.6.1.4 The spatial correlation (or distribution) of the gust in a plane normal to the sustained wind direction can be described by a coherence function using a horizontal decay factor, normal to the sustained wind direction, and a vertical decay factor.

5.6.1.5 The instantaneous wind force on a wind exposed structure can be calculated by summation of the instantaneous force on each wind exposed member. The instantaneous wind pressure q can be calculated by the formula

$$q = \frac{1}{2} \rho_a \left| U_{T,z} + u - \dot{x} \right| (U_{T,z} + u - \dot{x})$$

where

u	=	the gust speed and direction variation
$U_{T,z}$	=	the mean wind speed
$\dot{x}$	=	the instantaneous velocity of the structural member.

5.6.1.6 For time domain calculations, time histories of wind velocities corresponding to spectra as given in Ch.2 can be used in combination with the force calculations given in 5.6.1.5 to establish time histories of the wind forces.

5.6.1.7 When using a frequency domain calculation, the instantaneous wind pressure can normally be linearized to

$$q = \frac{1}{2} \rho_a U_{T,z}^2 + \rho_a U_{T,z} u$$

for structures where the structural velocity $\dot{x}$ is negligible compared to the wind velocity. This means that the fluctuating wind force is linear in the fluctuating velocity.

5.6.1.8 In direct frequency domain analysis, the solution can be obtained by multiplication of the cross spectral density for the dynamic wind load with the transfer function of response.

5.6.1.9 In a frequency domain analysis a modal formulation may be applied. The modal responses may be combined with the Square-Root-of-Sum-of-Squares (SRSS) method if the modes are not too closely related. In case of modes having periods close to each other, the Complete-Quadratic-Combination (CQC) method can be applied.

5.6.1.10 The SRSS method assumes that all of the maximum modal values are statistically independent of each other. The CQC method assumes that all of the maximum modal values occur at the same point in time. The peak value of the load is estimated by the formulae

$$F = \sqrt{\sum_n \sum_m f_n \rho_{nm} f_m}$$

where f_n is the modal force associated with mode n and the summation is over all the modes. The cross-modal coefficients

ρ_{nm} with constant damping ζ are

$$\rho_{mn} = \frac{8\zeta^2 (1+r) r^{3/2}}{(1-r^2)^2} + 4\zeta^2 r (1+r)^2$$

where r is the ratio between modal frequencies $r = \omega_n / \omega_m \le 1$.

5.6.1.11 All relevant effects as structural damping, aerodynamic damping and hydrodynamic damping should normally be considered in the analysis.

5.6.1.12 For the structural design, the extreme load effect due to static and dynamic wind can be assessed by:

$$F_e = F_s + g \, \sigma(f)$$

where

F_s	=	the static response due to the design average wind speed
$\sigma(f)$	=	the standard deviation of the dynamic structural responses
g	=	wind response peak factor.

5.7 Model tests

Data obtained from reliable and adequate model tests are recommended for the determination of pressures and resulting loads on structures of complex shape.

Tests should be carried out on a properly scaled model of the full scale shape of the structure.

The actual wind should be modelled to account for the variation of the mean wind speed with height above ground or sea water and the turbulence level in the wind.

5.8 Computational Fluid Dynamics

Wind loads on structures can be calculated using Computational Fluid Dynamics (CFD), solving the Navier Stokes Equations for the motion of air, taking into account compressibility and turbulence effects. One should be aware of the following when applying CFD to calculate wind induced forces on structures:

— results may depend strongly on the turbulence model used
— input wind velocity field should be properly modelled, including boundary layer effects
— exposed area of the structure(s) should be a small fraction of the computational domain outflow area
— grid resolution should be at least 10 cells per cubic root of structure volume and at least 10 cells per separation distance between structures
— grid convergence studies should be carried out
— results should be validated with results from wind tunnel tests.

References

1) Aquiree, J.E. & Boyce, T.R. (1974) "Estimation of wind forces on offshore drilling platforms". Trans. Royal Inst. Nav. Arch. (RINA), 116, 93-119.

2) Blevins, R.D. (1990) "Flow-Induced Vibrations". Krieger Publishing Company.

3) Eurocode EN 1991-1-4 General actions - Wind actions (2005).

4) Isherwood, R. M., 1972: "Wind resistance of merchant ships". Trans. of the Royal Institution of Naval Architects. 115, 327- 338.

5) OCIMF (1994) "Prediction of wind and current loads on VLCCs". Oil Companies International Marine Forum. 2nd Edition.

6) Simiu, E., and R.U. Scanlan (1978) "Wind Effects on Structures". An Introduction to Wind Engineering, John Wiley, New York, 1978.

6. Wave and Current Induced Loads on Slender Members

6.1 General

6.1.1 Sectional force on slender structure

The hydrodynamic force exerted on a slender structure in a general fluid flow can be estimated by summing up sectional forces acting on each strip of the structure. In general the force vector acting on a strip can be decomposed in a *normal force* f_N, a *tangential force* f_T and a *lift force* f_L being normal to both f_N and f_T, see Figure 6-1. In addition a *torsion moment* m_T will act on non-circular cross-sections.

6.1.2 Morison's load formula

6.1.2.1 For slender structural members having cross-sectional dimensions sufficiently small to allow the gradients of fluid particle velocities and accelerations in the direction normal to the member to be neglected, wave loads may be calculated using Morison's load formula (6.2.1-6.2.4) being a sum of an inertia force proportional to acceleration and a drag force being proportional to the square of velocity.

6.1.2.2 Normally, Morison's load formula is applicable when the following condition is satisfied:

$$\lambda > 5\,D$$

where λ is the wave length and D is the diameter or other projected cross-sectional dimension of the member. When the length of the member is much larger than the transverse dimension, the end-effects can be neglected and the total force can be taken as the sum of forces on each cross-section along the length.

6.1.2.3 For combined wave and current flow conditions, wave and current induced particle velocities should be added as vector quantities. If available, computations of the total particle velocities and accelerations based on more exact theories of wave/current interaction are preferred.

6.1.3 Definition of force coefficients

The following definitions apply:

The drag coefficient C_D is the non-dimensional drag force

$$C_D = \frac{f_{\text{drag}}}{\frac{1}{2}\rho D \text{v}^2}$$

where

f_{drag} = sectional drag force [N/m]
ρ = fluid density [kg/m³]
D = diameter (or typical dimension) [m]
v = velocity [m/s]

In general the fluid velocity vector will be in a direction relative to the axis of the slender member (Figure 6-1). The drag force f_{drag} is decomposed in a normal force f_N and a tangential force f_T.

The added mass coefficient C_A is the non-dimensional added mass

$$C_A = \frac{m_a}{\rho A}$$

where

m_a = the added mass per unit length [kg/m]
A = cross-sectional area [m²]

The mass coefficient is defined as

$$C_M = 1 + C_A$$

The lift coefficient is defined as the non-dimensional lift force

$$C_L = \frac{f_{\text{lift}}}{\frac{1}{2}\rho D \text{v}^2}$$

where

f_{lift} = sectional lift force [N/m]
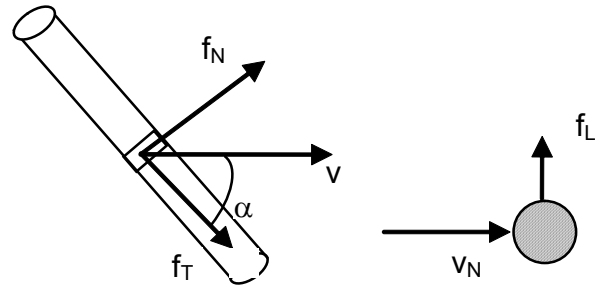
Figure 6-1
Definition of normal force, tangential force and lift force on slender structure.

6.2 Normal force

6.2.1 Fixed structure in waves and current

The sectional force f_N on a *fixed* slender structure in two-dimensional flow normal to the member axis is given by

$$f_N(t) = \rho(1 + C_A)A\dot{\text{v}} + \frac{1}{2}\rho C_D D\text{v}|\text{v}|$$

v = fluid particle (waves and/or current) velocity [m/s]
$\dot{\text{v}}$ = fluid particle acceleration [m/s²]
A = cross sectional area [m²]
D = diameter or typical cross-sectional dimension [m]
ρ = mass density of fluid [kg/m³]
C_A = added mass coefficient (with cross-sectional area as reference area) [-]
C_D = drag coefficient [-]

6.2.2 Moving structure in still water

The sectional force f_N on a *moving* slender structure in still water can be written as

$$f_N(t) = -\rho C_A A\ddot{r} - \frac{1}{2}\rho C_d D\dot{r}|\dot{r}|$$

where

$\dot{r}$ = velocity of member normal to axis [m/s]

$\ddot{r}$ = acceleration of member normal to axis [m/s²]

C_d = hydrodynamic damping coefficient [-]

6.2.3 Moving structure in waves and current

The sectional force f_N on a *moving* slender structure in two-dimensional non-uniform (waves and current) flow normal to the member axis can be obtained by summing the force contributions in 6.2.1 and 6.2.2,

$$f_N(t) = -\rho C_A A \ddot{r} + \rho(1+C_A)A\dot{v} + \frac{1}{2}\rho C_D D v|v| - \frac{1}{2}\rho C_d D\dot{r}|\dot{r}|$$

This form is known as the *independent flow field model*. In a response analysis, solving for $r = r(t)$, the added mass force

$$\rho C_A A \ddot{r} = m_a \ddot{r}$$

adds to the structural mass m_s times acceleration on the left hand side of the equation of motion. When the drag force is expressed in terms of the relative velocity, a single drag coefficient is sufficient. Hence, the *relative velocity formulation* (6.2.4) is most often applied.

6.2.4 Relative velocity formulation

The sectional force can be written in terms of relative velocity

$$f_N(t) = -\rho C_A A \ddot{r} + \rho(1+C_A)A\dot{v} + \frac{1}{2}\rho C_D D v_r|v_r|$$

or in an equivalent form when relative acceleration is also introduced,

$$f_N(t) = \rho A a + \rho C_A A a_r + \frac{1}{2}\rho C_D D v_r|v_r|$$

where

$a = \dot{v}$ is the fluid acceleration [m/s^2]
$v_r = v - \dot{r}$ is the relative velocity [m/s]
$a_r = \dot{v} - \ddot{r}$ is the relative acceleration [m/s^2]

When using the relative velocity formulation for the drag forces, additional hydrodynamic damping should normally not be included.

6.2.5 Applicability of relative velocity formulation

The use of relative velocity formulation for the drag force is valid if

$r/D > 1$

where r is the member displacement amplitude and D is the member diameter.

When $r/D < 1$ the validity is depending on the value of the *parameter* $V_R = vT_n/D$ as follows:

$20 \le vT_n/D$ Relative velocity recommended
$10 \le vT_n/D < 20$ Relative velocity may lead to an over-estimation of damping if the displacement is less than the member diameter.
$vT_n/D < 10$ It is recommended to discard the velocity of the structure when the displacement is less than one diameter, and use the drag formulation in 6.2.1.

For a vertical surface piercing member in combined wave and current field, the velocity can be calculated using

$v = v_c + \pi H_s/T_z$ approximation of particle velocity close to wave surface [m/s]
$v_c = $ current velocity [m/s]
$T_n = $ period of structural oscillations [s]
$H_s = $ significant wave height
$T_z = $ zero up-crossing period

6.2.6 Normal drag force on inclined cylinder

6.2.6.1 For incoming flow with an angle of attack of 45–90 degrees, the *cross flow principle* is assumed to hold. The normal force on the cylinder can be calculated using the normal component of the water particle velocity

$v_n = v \sin \alpha$

where α is the angle between the axis of the cylinder and the velocity vector. The drag force normal to the cylinder is then given by

$$f_{dN} = \frac{1}{2}\rho C_{Dn} D v_n|v_n|$$

6.2.6.2 In general C_{Dn} depends on the Reynolds number and the angle of incidence. For sub-critical and super-critical flow C_{Dn} can be taken as independent of α. For flow in the critical flow regime (Figure 6-5), C_{Dn} may vary strongly with flow direction, Sarpkaya & Isaacson (1981), Ersdal & Faltinsen (2006).

6.3 Tangential force on inclined cylinder

6.3.1 General

6.3.1.1 For bare cylinders the tangential drag force is mainly due to skin friction and is small compared to the normal drag force. However for long slender elements with a considerable relative tangential velocity component the tangential drag force may be important.

6.3.1.2 The tangential drag force per unit length can be written as

$$f_T = \frac{1}{2}\rho C_{Dt} D v^2$$

where C_{Dt} is the tangential drag coefficient and v is the magnitude of the total velocity. The tangential force is generally not proportional to the square of the tangential component of the velocity $v_T = v \cos \alpha$ although this is used in some computer codes. Some computer codes also use the skin friction coefficient C_{Df} defined by

$C_{Dt} = \pi C_{Df} \cos(\alpha)$

6.3.1.3 The following formula (Eames, 1968) for C_{Dt} can be used for the dependence on angle between velocity vector and cylinder axis,

$C_{Dt} = C_{Dn}(m + n \cdot \sin \alpha)\cos \alpha$

where C_{Dn} is the drag coefficient for normal flow. The following values for m and n are based on published data:

	m	n
Bare cables, smooth cylinders	0.02-0.03	0.04-0.05
Faired cables	0.25-0.50	0.50-0.25
6-stranded wire	0.03	0.06

6.3.1.4 For risers with some surface roughness it is recommended to use $m = 0.03$ and $n = 0.055$. The variation of C_{Dt} with α for these values of m and n is given in Figure 6-2.
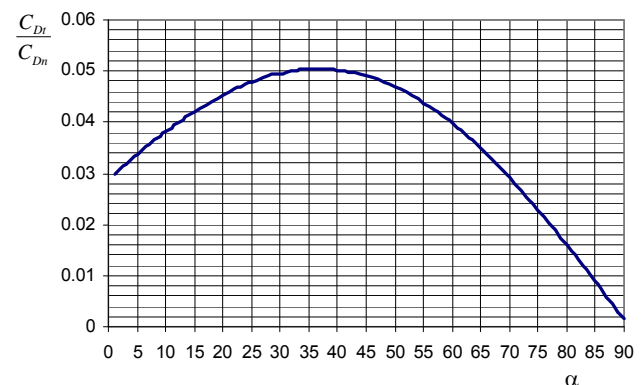

Figure 6-2
Variation of C_{Dt} with angle of attack α.

6.4 Lift force

6.4.1 General

A lift force f_L, in the normal direction to the fluid flow direction, on a slender structure may be due to

— unsymmetrical cross-section
— wake effects
— wall effects
— vortex shedding.

6.4.1.1 Unsymmetrical cross-section. Lift and drag forces and torsional moment (6.5) on slender structures with unsymmetrical cross-section (relative to the flow direction) can lead to large amplitude galloping and flutter (Blevins, 1990).

6.4.1.2 Wake effects. The velocity field in the wake of one or several cylinders is non-uniform (Figure 6-12). Position dependent lift and drag forces on a cylinder in the wake may lead to *wake induced oscillations* (WIO).

6.4.1.3 Wall effects. The unsymmetrical flow past a cylinder close to a wall gives rise to a non-zero lift force. A narrow gap between the cylinder and the wall leads to increased velocity and reduced pressure in the gap with a resulting lift force acting towards the wall.

6.4.1.4 Vortex shedding. The lift force due to vortex shedding oscillates with the Strouhal frequency. Guidance on vortex shedding and vortex induced vibrations (VIV) is given in Ch.9.

6.5 Torsion moment

The inviscid moment per unit length about the longitudinal axis of a non-circular cross-section with two planes of symmetry is

$$m_t = -m_{66}\dot{\Omega} + \rho A(C_A^y - C_A^z)(v - \dot{y})(w - \dot{z})$$

where

v, w = fluid particle velocity in directions y and z [m/s]

$\dot{y}, \dot{z}$ = normal velocity of cross-section in directions y and z [m/s]

m_{66} = added moment of inertia for cross-section [kg × m], see Appendix D.

$\dot{\Omega}$ = angular acceleration of cross-section [rad/s^2]

C_A^y, C_A^z = added mass coefficient in directions y and z [-]

In a response analyses the term $m_t = -m_{66}\, \Omega$ adds to the moment of inertia times angular acceleration on the left hand side of the equations of motion.

The last term is the so-called Munk moment (Faltinsen, 1990). Note that the Munk moment does not appear on cross-sections with three or more planes of symmetry. The inviscid force and moment for a general cross-section is discussed by Newman (1977).

6.6 Hydrodynamic coefficients for normal flow

6.6.1 Governing parameters

6.6.1.1 When using Morison's load formula to calculate the hydrodynamic loads on a structure, one should take into account the variation of C_D and C_A as function of Reynolds number, the Keulegan-Carpenter number and the roughness.

$C_D = C_D(R_e, K_C, \Delta)$
$C_A = C_A(R_e, K_C, \Delta)$

The parameters are defined as:

— Reynolds number: $R_e = vD/\nu$
— Keulegan-Carpenter number: $K_C = v_m\, T/D$
— Non-dimensional roughness: $\Delta = k/D$

where

D = diameter [m]
T = wave period or period of oscillation [s]
k = roughness height [m]
v = total flow velocity [m/s]
ν = fluid kinematic viscosity [m^2/s]. See Appendix F
v_m = maximum orbital particle velocity [m/s]

The effect of R_e, K_C and Δ on the force coefficients is described in detail in Sarpkaya (1981).
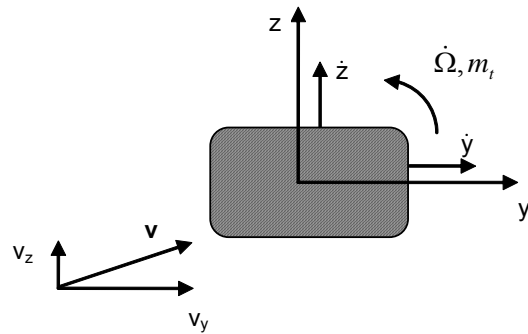
Figure 6-3
Torsion moment exerted on non-circular cross-section

6.6.1.2 For oscillatory fluid flow a *viscous frequency parameter* is often used instead of the Reynolds number. This parameter is defined as the ratio between the Reynolds number and the Keulegan-Carpenter number,

$$\beta = R_e/K_C = D^2/\nu T = \omega D^2/(2\pi\nu)$$

where

D = diameter [m]
T = wave period or period of structural oscillation [s]
ω = $2\pi/T$ = angular frequency [rad/s]
ν = fluid kinematic viscosity [m^2/s]

Experimental data for C_D and C_M obtained in U-tube tests are often given as function of K_C and β since the period of oscillation T is constant and hence β is a constant for each model.

6.6.1.3 For a circular cylinder, the ratio of maximum drag force $f_{D,max}$ to the maximum inertia force $f_{I,max}$ is given by

$$\frac{f_{D,max}}{f_{I,max}} = \frac{C_D}{\pi^2(1 + C_A)}K_C$$

The formula can be used as an indicator on whether the force is drag or inertia dominated.

6.6.1.4 For combined regular wave and current conditions, the governing parameters are Reynolds number based on maximum velocity, $v = v_c + v_m$, Keulegan-Carpenter number based on maximum orbital velocity v_m and the *current flow velocity ratio*, defined as

$$\alpha_c = v_c/(v_c + v_m)$$

where v_c is the current velocity. In a general sea state the significant wave induced velocity should be used instead of the

maximum orbital velocity. More details on the effect of the current flow velocity ratio is given by Sumer and Fredsøe (1997) and in DNV RP-F105 Free spanning pipelines.

6.6.1.5 For sinusoidal (harmonic) flow the Keulegan-Carpenter number can also be written as

$$K_C = 2\pi\eta_0 / D$$

where η_0 is the oscillatory flow amplitude. Hence, the K_C-number is a measure of the distance traversed by a fluid particle during half a period relative to the member diameter.

For fluid flow in the wave zone η_0 in the formula above can be taken as the wave amplitude so that the K_C number becomes

$$K_C = \frac{\pi H}{D}$$

where H is the wave height.

6.6.1.6 For an oscillating structure in still water, which for example is applicable for the lower part of the riser in deep water, the Keulegan-Carpenter number is given by

$$K_C = \frac{\dot{r}_m T}{D}$$

where $\dot{r}_m$ is the maximum velocity of the riser, T is the period of oscillation and D is the cylinder diameter.

6.6.2 Wall interaction effects

6.6.2.1 The force coefficients also depend on the distance to a fixed boundary defined by the gap ratio between the cylinder and the fixed boundary ($e = H/D$) where H is the clearance between the cylinder and the fixed boundary, see Figure 6-7. The lift coefficient C_L for flow around a smooth cylinder in the

vicinity of a boundary is given in Figure 6-4. More information on force coefficients on cylinders close to a boundary can be found in Sumer & Fredsøe (1997) and Zdravkovich (2003).
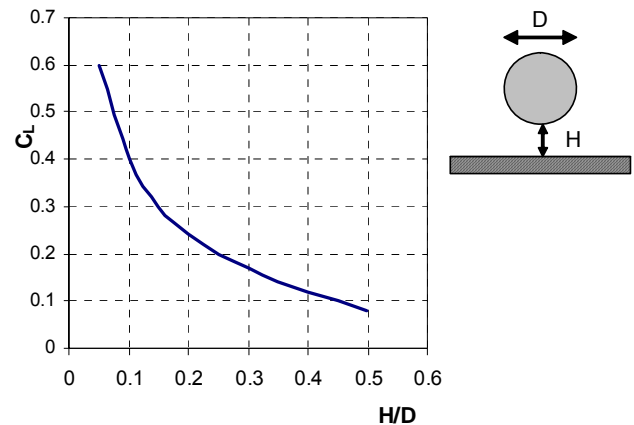
Figure 6-4
Lift coefficient for cylinder close to boundary. Re = 250 000. From Zdravkovich (2003).

6.6.2.2 A free surface may have a strong effect on the added mass coefficient C_A if the structure is close to the surface. C_A is then also a function of the frequency of oscillation. The relevant non-dimensional frequency parameter is

$$\omega(D / g)^{1/2}$$

where ω is the angular frequency of oscillation and g is the acceleration of gravity. See 6.9.3.
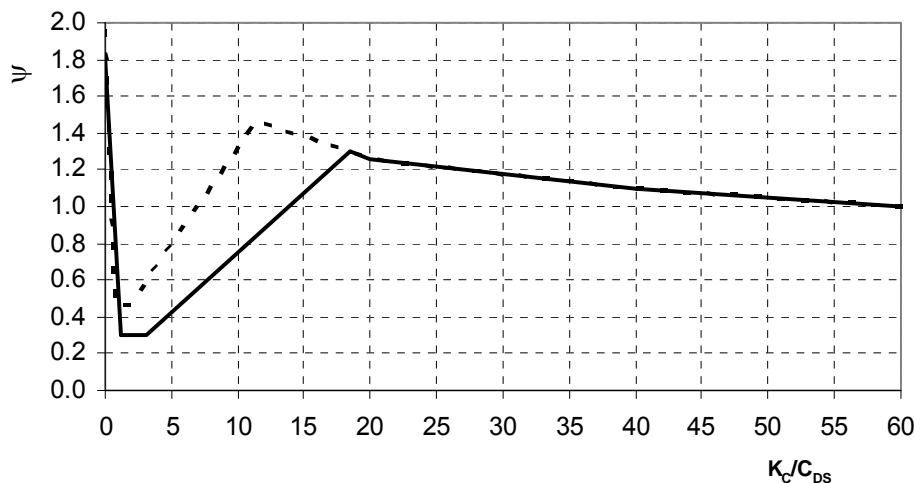
Figure 6-5
Wake amplification factor ψ as function of K_C-number for smooth (C_{DS} = 0.65 - solid line) and rough (C_{DS} = 1.05 - dotted line).

6.7 Drag coefficients for circular cylinders

6.7.1 Effect of Reynolds number and roughness

6.7.1.1 Two-dimensional drag coefficients for smooth circular cylinders and cylinders of various roughnesses in steady uniform flow as a function of Reynolds number are given in Figure 6-6. There is a distinct drop in the drag coefficient in a certain Reynolds number range. This is referred to as the critical flow regime and is very pronounced for a smooth circular cylinder.

6.7.1.2 One usually defines four different flow regimes: *subcritical* flow, *critical* flow, *supercritical* flow and *transcritical* flow. The term *post-critical* is also used and covers super- and transcritical flow.

6.7.1.3 As guidance for the surface roughness used for determination of the drag coefficient, the following values may be used:

Table 6-1 Surface roughness

Material	k (meters)
Steel, new uncoated	5×10^{-5}
Steel, painted	5×10^{-6}
Steel, highly corroded	3×10^{-3}
Concrete	3×10^{-3}
Marine growth	$5 \times 10^{-3} - 5 \times 10^{-2}$

6.7.1.4 The effect of marine growth and appurtenances as anodes etc. should be considered when selecting effective diameters and drag coefficients.

6.7.1.5 For high Reynolds number ($R_e > 10^6$) and large K_C number, the dependence of the drag-coefficient on roughness $\Delta = k/D$ may be taken as

$$C_{DS}(\Delta) = \begin{cases} 0.65 & ; \Delta < 10^{-4} \text{(smooth)} \\ (29 + 4 \cdot \log_{10}(\Delta))/20 & ; 10^{-4} < \Delta < 10^{-2} \\ 1.05 & ; \Delta > 10^{-2} \text{(rough)} \end{cases}$$

The above values apply for both irregular and regular wave analysis.

6.7.1.6 In the post-critical flow regime the coefficients may be considered independent of Reynolds number. For a riser operating in an extreme design environment, the Reynolds number is normally in the post-critical flow regime.

6.7.1.7 For fatigue calculations in less severe environments, the riser may drop down in the critical flow regime, at least for smooth riser segments. For rough cylinders however, the critical regime is shifted to much lower Reynolds number so that the riser can still be considered to be in the post-critical regime.

6.7.2 Effect of Keulegan Carpenter number

6.7.2.1 The variation of the drag coefficient as a function of Keulegan-Carpenter number K_C for smooth and marine growth covered (rough) circular cylinders for supercritical Reynolds numbers can be approximated by

$$C_D = C_{DS}(\Delta) \cdot \psi(K_C)$$

where the *wake amplification factor* $\psi(K_C)$ is given in Figure 6-5 and in 6.7.2.2. $C_{DS}(\Delta)$ is given in 6.7.1.5. This applies for free flow field without any influence of a fixed boundary. The curve in Figure 6-5 is obtained as the best fit to experimental data presented in API RP 2A-LRFD (1993).

6.7.2.2 For low Keulegan-Carpenter numbers ($K_C < 12$) the wake amplification factor can be taken as (Figure 6-5),

$$\psi(K_C) = \begin{cases} C_\pi + 0.10(K_C - 12) & 2 \le K_C < 12 \\ C_\pi - 1.00 & 0.75 \le K_C < 2 \\ C_\pi - 1.00 - 2.00(K_C - 0.75) & K_C \le 0.75 \end{cases}$$

where

$$C_\pi = 1.50 - 0.024 \cdot (12 / C_{DS} - 10)$$

For intermediate roughness the values are found by linear interpolation between the curves for smooth and rough cylinder corresponding to $C_{DS} = 0.65$ and $C_{DS} = 1.05$.

6.7.2.3 The wake amplification factor defined above can be applied to non circular cylinders provided the C_{DS} value is the appropriate steady drag coefficient for the cylinder.

6.7.2.4 The drag coefficient for steady current is equal to the asymptotic value for infinitely large K_C. For combined wave and in-line current action, the increase of K_C due to the current may be taken into account; $K_C^* = (v_m + v_c)T/D$ where v_m is the maximum wave velocity and v_c is the current velocity. Hence the effect of a steady in-line current added to the oscillatory wave motion is to push C_D towards C_{DS}, its steady value.

When $v_c > 0.4 v_m$ ($\alpha_c > 0.3$) C_D can be taken equal to C_{DS}. A current component normal to the wave direction also moves C_D towards C_{DS}.

6.7.2.5 For dynamic analysis of lower riser segments in deep water responding at low K_C numbers due to low riser velocity, the K_C-adjusted drag coefficient should not exceed 0.8 since the hydrodynamic force in still water is a damping force and one should use a lower drag coefficient to be conservative.
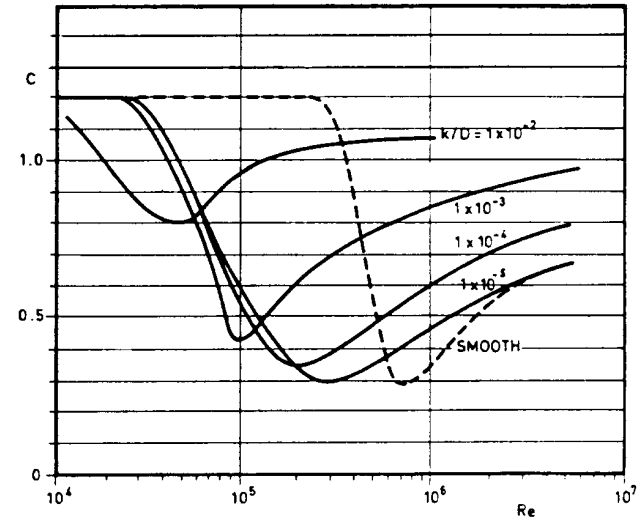
Figure 6-6
Drag coefficient for fixed circular cylinder for steady flow in critical flow regime, for various roughnesses.

6.7.3 Wall interaction effects

To determine the drag coefficients for circular cylinders close to a fixed boundary, the drag coefficients given in unbounded fluid may be multiplied by a correction factor obtained from Figure 6-7.
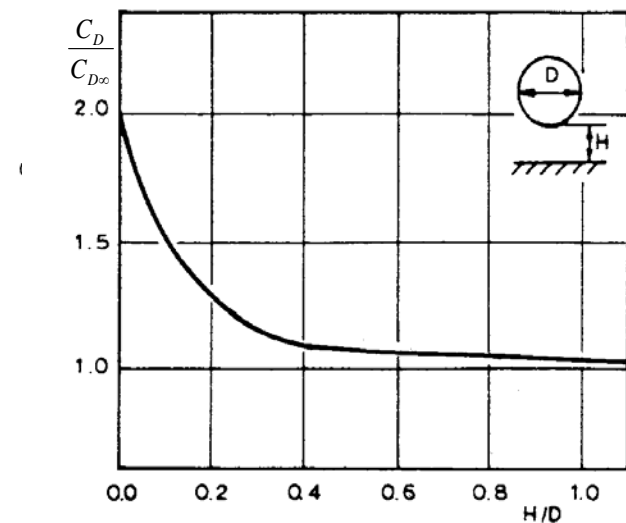
Figure 6-7
Influence of a fixed boundary on the drag coefficient of a circular cylinder in oscillatory supercritical flow
$K_C > 20, R_e = 10^5 - 2 \times 10^6$. $C_{D\infty}$ is the drag coefficient for $H \to \infty$.

6.7.4 Marine growth

6.7.4.1 The cross-sectional dimensions of structural elements are increased due to thickness of marine growth. This should be accounted for when calculating forces on slender members like jacket tubulars, risers, umbilicals and conductors. The thickness of marine growth depends on location. Some site specific information on marine growth is given in ISO 19901-1 (2005).

The thickness may be assumed to increase linearly to the given value over a period of 2 years after the member has been placed in the sea.

The effective diameter (or cross-sectional width for non-circular members) is given by

$$D = D_C + 2t$$

where

D_C = "clean" outer diameter

t = thickness of marine growth

6.7.4.2 In lack of site specific information the thickness of marine growth can be taken as (NORSOK N-003):

	56-59 ^{o} N	*59-72 ^{o} N*
Water depth (m)	*Thickness (mm)*	*Thickness (mm)*
+2 to -40	100	60
below -40	50	30

The density of marine growth may be set to 1325 kg/m^3.

6.7.5 Drag amplification due to VIV

An increase in the drag coefficient due to cross flow vortex shedding should be evaluated, see Ch.9.

6.7.6 Drag coefficients for non-circular cross-section

Drag coefficient for cross-sections with sharp corners can be taken as independent of roughness.

Drag coefficients for various cross-sections are listed in Appendix E. Reference is also made to 5.4.

6.8 Reduction factor due to finite length

When estimating the total drag force on a slender member with characteristic cross-sectional dimension d and finite length $l,$ the integrated sum of sectional force contributions shall be multiplied by a reduction factor according to Table 6-2.

Table 6-2 Values of reduction factor κ for member of finite length and slenderness.

A - Circular cylinder – subcritical flow
B - Circular cylinder – supercritical flow
C - Flat plate perpendicular to flow

l/d	*2*	*5*	*10*	*20*	*40*	*50*	*100*
A	0.58	0.62	0.68	0.74	0.82	0.87	0.98
B	0.80	0.80	0.82	0.90	0.98	0.99	1.00
C	0.62	0.66	0.69	0.81	0.87	0.90	0.95

For members with one end abuting on to another member or a wall in such a way that free flow around that end of the member is prevented, the ratio l/d should be doubled for the purpose of determining κ. When both ends are abuted as mentioned, the drag coefficient C_D should be taken equal to that for an infinitely long member.

6.9 Added mass coefficients

6.9.1 Effect of K_C-number and roughness

For cylinders in unbounded fluid, far from the free surface and seabed, the following added mass coefficients can be applied:

6.9.1.1 For $K_C < 3$, C_A can be assumed to be independent of K_C number and equal to the theoretical value $C_A = 1.0$ for both smooth and rough cylinders.

6.9.1.2 For $K_C > 3$, the added mass coefficient can be found from the formula

$$C_A = \max\begin{Bmatrix} 1.0 - 0.044(K_C - 3) \\ 0.6 - (C_{DS} - 0.65) \end{Bmatrix}$$

where C_{DS} is given 6.7.1.5. The variation of C_A with K_C for smooth ($C_{DS} = 0.65$) and rough ($C_{DS} = 1.05$) cylinder is shown in Figure 6-8. For intermediate roughness the values are found by formula above or linear interpolation between the curves for smooth and rough cylinder.

The curve in Figure 6-8 is obtained as the best fit to experimental data presented in API RP 2A-LRFD (1993).

6.9.1.3 The asymptotic values for large K_C-number are

$$C_A = \begin{cases} 0.6 & \text{smooth cylinder} \\ 0.2 & \text{rough cylinder} \end{cases}$$

For large K_C-number, the drag force is the dominating force compared with the inertia force.
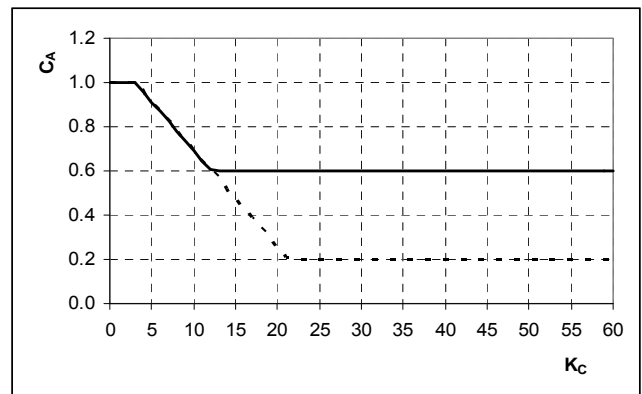
Figure 6-8
Added mass coefficient as function of K_C-number for smooth (solid line) and rough (dotted line) cylinder.

6.9.1.4 The variation of added mass coefficient for non-circular cylinders is obtained by multiplying the C_A value defined in 6.9.1.1 - 6.9.1.3 by C_{A0}, the theoretical value of C_A for zero $K_C = 0$.

6.9.2 Wall interaction effects

The added mass coefficients for a circular cylinder close to a fixed boundary, is obtained from Figure 6-9. The figure applies to motion normal to the boundary as well as motion parallel to the boundary. The analytic value for zero gap $H/D = 0$ is $C_A = \pi^2/3 - 1 = 2.29$.
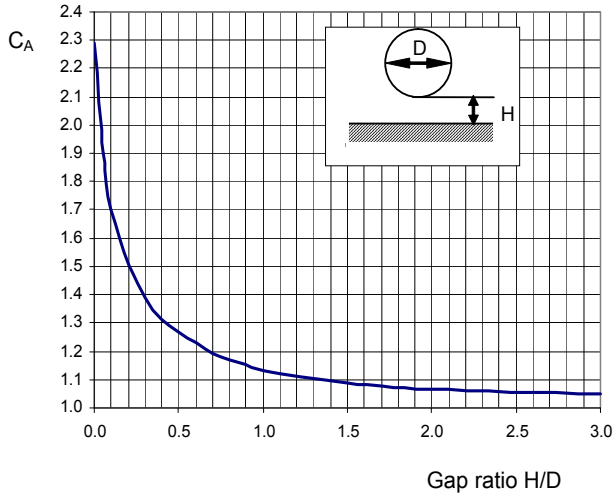
Figure 6-9
Recommended value for the added mass coefficient, C_A of a circular cylinder in the vicinity of a fixed boundary moving normal to or parallel to the boundary.

6.9.3 Effect of free surface

6.9.3.1 The added mass of a fully submerged oscillating cylinder in the vicinity of a free surface is strongly dependent on the frequency of oscillation ω and the distance h (defined in Figure 6-11) to the free surface. See Figure 6-10.
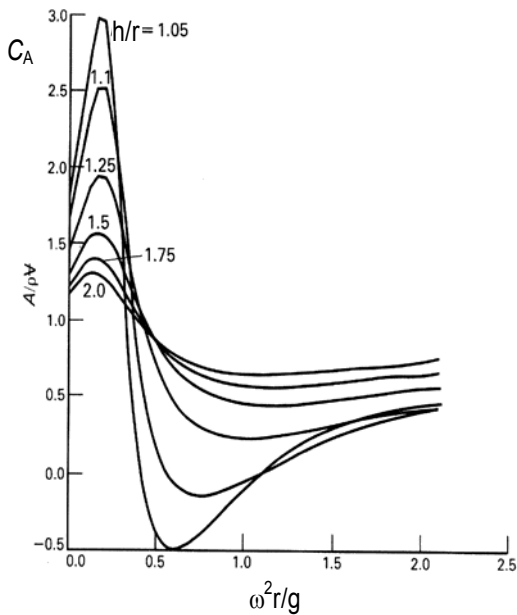
Figure 6-10
Vertical added mass coefficient for circular cylinder at different distances from free surface. r is the cylinder radius. From Greenhow & Ahn (1988).

6.9.3.2 The added mass coefficient for a surface piercing vertical cylinder is given by

$$C_A = \frac{4}{\pi(kR)^2 \sqrt{A_1(kR)}} - 1$$

where k is the wave number related to the angular frequency of oscillation, ω by the dispersion relation (3.2.2.3), R is the cylinder

radius and

$$A_1(kR) = J'_1{}^2(kR) + Y'_1{}^2(kR)$$

where J'_1 and Y'_1 are the derivatives of Bessel functions of first order. In the limit of very long periods of oscillation, $kR \to 0$ and $C_A \to 1.0$.

6.9.3.3 For high speed entry of a circular cylinder through a free surface the vertical added mass can be taken as its high frequency limit $m_A(\infty)$.

The slamming force is given by

$$f_s = \frac{d}{dt}(m_a v) = m_a \dot{v} + \frac{dm_a}{dh} v^2$$

where the first term on the right hand side vanishes for constant velocity v. The variation of m_a with depth of submergence h from free surface to centre of cylinder (dm_a/dh) is shown in Figure 6-11. Water entry and slamming of circular cylinders is covered in Ch.8.
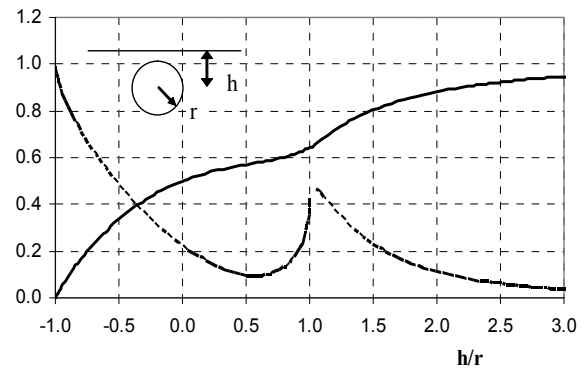
Figure 6-11
High frequency limit of added mass and its derivative close to a free surface. Solid line: $m_a/\rho\pi r^2$. Dotted line: $(dm_a/dh)/\rho\pi r$.

6.10 Shielding and amplification effects

6.10.1 Wake effects

6.10.1.1 The force on a cylinder downstream of another cylinder is influenced by the wake generated by the upstream cylinder. The main effects on the mean forces on the downstream cylinder are

— reduced mean drag force due to shielding effects
— non-zero lift force due to velocity gradients in the wake field.

Hence, the mean drag and lift coefficients depend on the relative distance between the cylinders.

6.10.1.2 The velocity in the wake can be taken as

$$v_w(x, y) = v_0 - v_d(x, y)$$

where v_0 denotes the free-stream current velocity acting on the upstream riser and $v_d(x,y)$ is the deficit velocity field. For a super-critical (turbulent) wake the following formula applies (Schlicting, 1968),

$$v_d(x, y) = k_2 v_0 \sqrt{\frac{C_D D}{x_s}} e^{-0.693\left(\frac{y}{b}\right)^2}$$

where

$$x_s = x + \frac{4D}{C_D}$$

$$b = k_1\sqrt{C_D D x_s}$$

k_1 and k_2 are empirical constants, $k_1 = 0.25$ and $k_2 = 1.0$. D is the upstream cylinder diameter and C_D is the drag coefficient of the upstream cylinder. The origin of the coordinate system (x,y) is in the center of the upstream cylinder, see Figure 6-12.
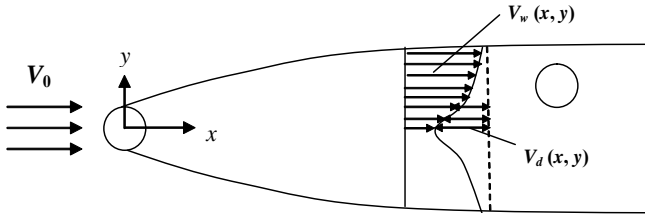
Figure 6-12
Time-averaged turbulent wake behind a cylinder.

6.10.2 Shielding from multiple cylinders

6.10.2.1 For several cylinders close together, group effects may be taken into account. If no adequate documentation of group effects for the specific case is available, the drag coefficients for the individual cylinder should be used.
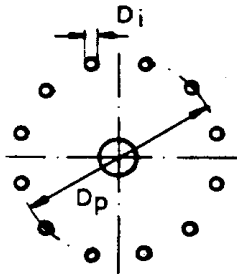
Figure 6-13
Parameters of typical composite cylindrical shapes

6.10.2.2 For frame structures, the current may be reduced due to interference from the structure on the flow field of the current (Taylor, 1991). The current may be reduced as follows

$$\frac{v_c}{v_c(\infty)} = \left[1 + \frac{\sum_i C_D^{(i)} D_i}{4D_p}\right]^{-1}$$

but not less than 0.7

v_c = steady state current to be used in calculations
$v_c(\infty)$ = the observed far field current
$C_D^{(i)}$ = the drag coefficient of element i

D_i = the element diameter of element i
D_p = the width of the structure or cluster of members considered.

6.10.3 Effects of large volume structures

6.10.3.1 For slender structures (e.g. riser) close to a large volume floater, due regard shall be given to radiation/diffraction effects on wave fluid kinematics. To account for radiation/diffraction effects both in ULS and FLS analysis, it is recommended to calculate consistent transfer functions for fluid velocity and acceleration at selected locations along the slender structure. This applies both to regular and irregular waves.

6.10.3.2 For risers operated from floating structures kinematics used in Morison's load formula for hydrodynamic loading on the riser should be consistent with the kinematics in incoming waves exciting the motions of the floater. Airy waves with kinematics in the splash zone derived from Wheeler stretching can be used with drag coefficients adjusted for K_C-effects.

6.11 Risers with buoyancy elements

6.11.1 General

The hydrodynamic force coefficients for riser buoyancy sections depend on:

— geometry of the buoyancy elements
— spacing between elements
— riser inclination angle α relative to the flow
— flow parameters (R_e, K_C).

As α becomes small, approaching tangential flow, shielding effects for elements positioned in the wake of each other will be important.

6.11.2 Morison load formula for riser section with buoyancy elements

The normal and tangential forces on a riser section with buoyancy elements can be written

$$f_N = \rho A_1 C_M^N \dot{v}_n - \rho A_1 C_A^N \ddot{r}_n + \frac{1}{2}\rho C_D^N D_1 v_r \,|\,v_r\,|$$

$$f_T = \rho A_1 C_M^T \dot{v}_t - \rho A_1 C_A^T \ddot{r}_t + \frac{1}{2}\rho C_D^T D_1 v_r \,|\,v_r\,|$$

where

C_M^N, C_M^T	=	mass coefficients for flow in normal and tangential direction
C_A^N, C_A^T	=	added mass coefficients for flow in normal and tangential direction ($C_A = C_M - 1$)
C_D^N, C_D^T	=	drag coefficients for flow in normal and tangential direction
$\ddot{r}_n, \ddot{r}_t$	=	components of riser accelerations [m/s²]
$\dot{v}_n, \dot{v}_t$	=	components of wave particle accelerations [m/s²]
v_r	=	relative velocity [m/s]
A_1	=	V/L, reference cross-sectional area [m²]
D_1	=	A/L, reference 'drag diameter' [m]
V	=	volume displacement of riser + buoyancy elements of riser section of length L [m³]
L	=	length of riser segment [m]
A	=	total projected area for normal flow ($\alpha = 90°$) [m²]

6.11.3 Added mass of riser section with buoyancy element

6.11.3.1 The added mass coefficient C_A^N for normal flow past a riser section with buoyancy elements can be estimated from two-dimensional added mass coefficients according to 6.9.

6.11.3.2 The tangential added mass for each buoyancy element can be estimated by

$$m_a^T = \frac{1}{6}\rho\pi D_b^3\left(1 - \frac{D}{D_b}\right)^2$$

where D_b is the outer diameter of the buoyancy element and D is the riser (or umbilical) diameter. The tangential added mass coefficient for the total riser segment is

$$C_A^T = \frac{Nm_a^T}{\rho V}$$

6.11.4 Drag on riser section with buoyancy elements

6.11.4.1 The drag coefficient C_D^N for normal flow past a riser section with buoyancy elements can be estimated from two-dimensional drag coefficients corrected for finite length effects according to Table 6-1.

6.11.4.2 The tangential drag coefficient is given by

$$C_D^T = C_{D1}N \cdot I \cdot \frac{\pi}{4}D_b^2 /(D_1 L)$$

where

C_{D1} = drag coefficient of one single buoyancy element for $\alpha = 0^o$ and the geometry in question, referring to the area $\pi D_b^2/4$.

D_b = diameter of buoyancy element [m]

N = number of buoyancy elements

I = $I(K_C,N,S/D_b)$ = interaction factor depending on K_C, N and the element spacing S/D_b

S = length between element centres [m]

Figure 6-15 shows the interaction factor as function of K_C-number and length between buoyancy element, from "Handbook of hydrodynamic coefficients of flexible risers" (1991).

The tangential drag coefficient C_{D1} for one single buoyancy element is a function of the length to diameter ratio l/D_b to be interpolated from Table 6-3. l is the length of the buoyancy element.

Table 6-3 Tangential drag coefficient

l/D_b	0.5	1.0	2.0	4.0	8.0
C_{D1}	1.15	0.90	0.85	0.87	0.99
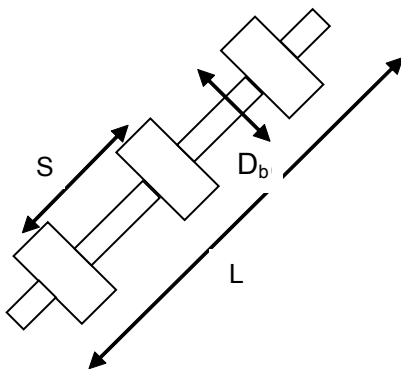
Figure 6-14
Dimensions of buoyancy elements
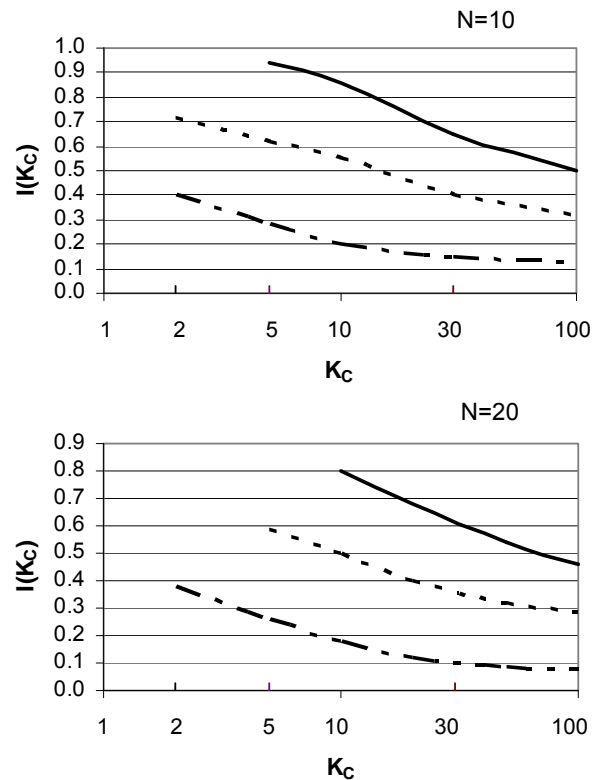
Figure 6-15
Interaction factor I versus K$_C$-number for N = 10, N = 20 and different values of *S/D*. Solid curve: S/D_b = 2.88. Dotted curve: S/D_b = 1.44. Dash-dotted curve S/D_b = 0.87.

6.12 Loads on jack-up leg chords

6.12.1 Split tube chords

For split tube chords (Jack-up leg chords) the hydrodynamic coefficients may, in lieu of more detailed information be taken in accordance with Figure 6-16 and corresponding formulae, as appropriate.

For a split tube chord as shown in Figure 6-16, the drag coefficient C_D related to the reference dimension D, the diameter of the tubular including marine growth may be taken as:

$$C_D = \begin{cases} C_{D0} & \text{for } 0^o < \theta \leq 20^o \\ C_{D0} + (C_{D1}\frac{W}{D} - C_{D0})\sin^2\left(\frac{9}{7}(\theta - 20^o)\right) & \text{for } 20^o < \theta \leq 90^o \end{cases}$$

where:

θ = angle in degrees, see Figure 6-16

C_{D0} = the drag coefficient for tubular with appropriate roughness as defined in 6.7

C_{D1} = the drag coefficient for flow normal to the rack ($\theta = 90^o$), related to the projected diameter, W. C_{D1} is given by
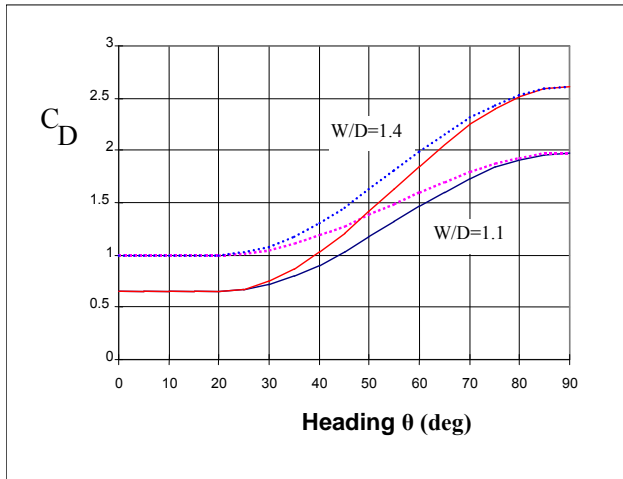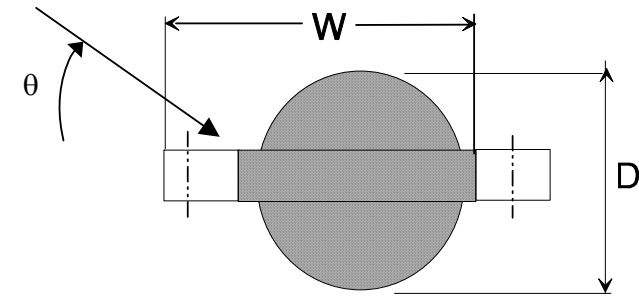
Figure 6-16
Split tube chord and typical values for C_D (SNAME 1997)
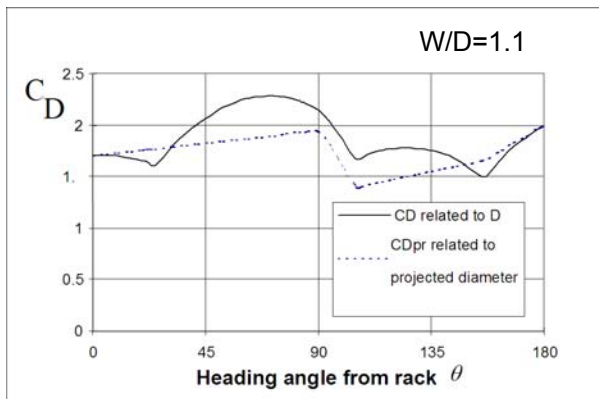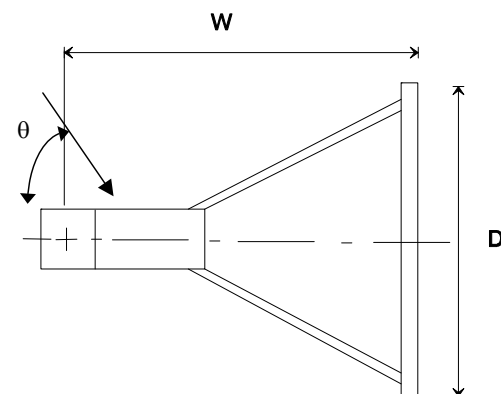
Figure 6-17
Triangular chord and typical values of C_D

$$C_{D1} = \begin{cases} 1.8 & : & W/D < 1.2 \\ 1.4 + W/3D & : & 1.2 < W/D < 1.8 \\ 2 & : & 1.8 < W/D \end{cases}$$

The added mass coefficient $C_m = 1.0$ may be applied for all headings, related to the equivalent volume $\pi D^2/4$ per unit length.

6.12.2 Triangular chords

For a triangular chord (Jack-up leg chords) the hydrodynamic coefficients may, in lieu of more detailed information be taken in accordance with Figure 6-17 corresponding formulae, as appropriate.

The drag coefficient C_D related to the reference dimension D may be taken as

$$C_D = C_{Dpr}(\theta)\frac{D_{pr}}{D}$$

where the drag coefficient related to the projected diameter, C_{Dpr} is determined from

$$C_{Dpr} = \begin{cases} 1.70 & \text{for} & \theta = 0^o \\ 1.95 & \text{for} & \theta = 90^o \\ 1.40 & \text{for} & \theta = 105^o \\ 1.65 & \text{for} & \theta = 180^o - \theta_0 \\ 2.00 & \text{for} & \theta = 180^o \end{cases}$$

Linear interpolation is to be applied for intermediate headings. The projected diameter, D_{pr}, may be determined from:

$$D_{pr} = \begin{cases} D\cos\theta & 0^0 < \theta < \theta_0 \\ W\sin\theta + 0.5D\,|\cos\theta| & \theta_0 < \theta < 180^0 - \theta_0 \\ D\,|\cos\theta| & 180^0 - \theta_0 < \theta < 180^0 \end{cases}$$

The angle, $\theta_0 = \arctan(D/2W)$, describes when half the rack-plate is hidden. The added mass coefficient $C_m = 1.0$ may be applied for all eadings, related to the equivalent volume $\pi D^2/4$ per unit length.

6.13 Small volume 3D objects

6.13.1 General

6.13.1.1 A Morison type formulation may also be used to estimate the drag and inertia loads on three dimensional objects in waves and current. It is required that the characteristic dimensions of the object are small relative to the wave length as defined in 6.1.2.

6.13.1.2 In the load formulae in 6.2.1-6.2.3 the cross-sectional area A is substituted by the displaced volume V and the cross-sectional dimension (diameter) D is substituted by the projected area S normal to the force direction.

$$f(t) = \rho V(1 + C_A)\dot{v} + \frac{1}{2}\rho C_D Sv|v|$$

Added mass coefficients for some 3D objects are given in Appendix D. Drag coefficients are given in Appendix E.

6.13.1.3 For some typical subsea structures which are perforated with openings (holes), the added mass may depend on motion amplitude or equivalently, the K_C-number (Molin & Nielsen, 2004). A summary of force coefficients for various 3D and 2D objects can be found in Øritsland (1989).

References

1) API RP 2A-LRFD (1993): Planning, Designing and Constructing Fixed Offshore Platforms – Load and Resistance Factor Design.

2) Blevins, R.D. (1990) "Flow-induced vibration". Krieger Publishing Company.

3) DNV RP-F105 "Free spanning pipelines". Det Norske Veritas.

4) Eames, M.C (1968) "Steady state theory of towing cables". Trans. of the Royal Inst. of Naval Architects, Vol. 10.

5) Ersdal, S. and Faltinsen, O.M. (2006) "Normal forces on cylinders in near-axial flow". Journal of Fluids and Structures. No. 8.

6) Faltinsen, O.M. (1990) "Sea loads on ships and offshore structures". Cambridge University Press.

7) Greenhow, M. and Ahn, S.I. (1988) "Added mass and damping of horizontal circular cylinder sections". Ocean Engng, Vol. 15, No. 5, pp. 495-504.

8) "Handbook of hydrodynamic coefficients of flexible risers" (1991). FPS2000 / Flexible risers and pipes. Report 2.1-16. Marintek report no. 511201.00.05.

9) Heidemann, Olsen and Johansen (1978), "Local Wave Force Coefficients", ASCE Civil Engineering in the Ocean IV, September 1978.

10) Hoerner, S.F. (1965) "Fluid-Dynamic Drag".

11) ISO 19901-1 (2005) "Metocean design and operating considerations"

12) ISO/CD 19902 "Fixed Steel Offshore Structures" (2004).

13) Molin, B. and Nielsen, F.G. (2004) "Heave added mass and damping of a perforated disk below the free surface". 19th IWWWFB, Cortona, Italy, March 2004.

14) Newman, J.N. (1977) "Marine Hydrodynamics". MIT Press, Cambridge, MA, USA.

15) Sarpkaya, T. (1977), "In-line and Transverse Force on Cylinders near a Wall in Oscillatory Flow at High Reynolds Numbers", OTC Paper No. OTC 2980, May 1977.

16) Sarpkaya, T. and Rajabi, F. (1979), "Hydrodynamic Drag on Bottom mounted Smooth and Rough Cylinder in Periodical Flow", OTC Paper No. OTC 3761, May 1979.

17) Sarpkaya, T. and Isaacson, M. (1981), "Mechanics of Wave Forces on Offshore Structures", Van Nostrand, Reinhold Company, New York, 1981.

18) Schlichting, H. (1968) "Boundary Layer Theory". McGraw Hill Book Company Inc., New York.

19) SNAME, Technical & Research Bulletin 5-5A, Site Specific Assessment of Mobile Jack-up Units, The Society of Naval Architects and Marine Engineers, Jersey City, New York, May 1997.

20) Sumer, B.M and Fredsøe, J. (1997) "Hydrodynamics around cylindrical structures". World Scientific.

21) Taylor, P. (1991), "Current Blockage - Reduced Forces on Steel Platforms in Regular and Irregular Waves with a Mean Current", Offshore Technology Conference, OTC 6519, Houston, 1991.

22) Zdravkovich, M.M. (2003) "Flow around cylinders. Vol 2: Applications". Oxford Science Publications.

23) Øritsland, O. (1989) "A summary of subsea module hydrodynamic data". marine Operations Part III.2. Report No. 70. Marintek Report MT51 89-0045.

7. Wave and Current Induced Loads on Large Volume Structures

7.1 General

7.1.1 Introduction

7.1.1.1 The term large volume structure is used for offshore structures with dimensions D on the same order of magnitude as typical wave lengths λ of ocean waves exciting the structure, usually $D > \lambda/6$. This corresponds to the *diffraction* wave force regimes II and IV shown in Figure 7-1 below where this boundary is equivalently defined as $\pi D/\lambda > 0.5$.

7.1.1.2 A large volume structure can be fixed or floating. Examples of large volume fixed structures are GBS platforms and LNG terminals. Examples of large volume floating structures are ships, FPSOs, Spars, TLPs and Semi-submersibles.

7.1.1.3 In this Recommended Practice the main focus is on hydrodynamic and aerodynamic *loads*. For guidance on *response* of offshore systems, reference is made to DNV-RP-F205. Inclusion of some response description is nevertheless necessary in the present document.

7.1.1.4 Understanding the response characteristics of the system is important for correct treatment and inclusion of all relevant load effects. The response itself may also be important for the loads (e.g. hydroelastic effects and coupled effects between floater and mooring/risers).

7.1.1.5 Key references on wave induced loads and response of large volume structures are Newman (1977), Sarpkaya & Isaacson (1981), Chakrabarti (1987) and Faltinsen (1990).

7.1.2 Motion time scales

7.1.2.1 A floating, moored structure may respond to wind, waves and current with motions on three different time scales,

— wave frequency (WF) motions
— low frequency (LF) motions
— high frequency (HF) motions.

7.1.2.2 The largest wave loads on offshore structures take place at the same frequencies as the waves, causing wave frequency (WF) motions of the structure. To avoid large resonant effects, offshore structures and their mooring systems are often designed in such a way that the resonant frequencies are shifted well outside the wave frequency range.

7.1.2.3 A floating structure responds mainly in its six rigid modes of motions including translational modes, surge, sway, heave, and rotational modes, roll, pitch, yaw. In addition, wave induced loads can cause high frequency elastic response, i.e. springing and whipping of ships.

7.1.2.4 Due to non-linear load effects, some responses always appear at the natural frequencies. Slowly varying wave and wind loads give rise to low frequency (LF) resonant horizontal motions, also named slow-drift motions.

Higher-order wave loads yield high frequency (HF) resonant motions, springing and ringing, of tensioned buoyant platforms like TLPs. The WF and HF motions are mainly governed by inviscid fluid effects, while viscous fluid effects are relatively important for LF motions. Different hydrodynamic effects are important for each floater type, and must be taken into account in the analysis and design.
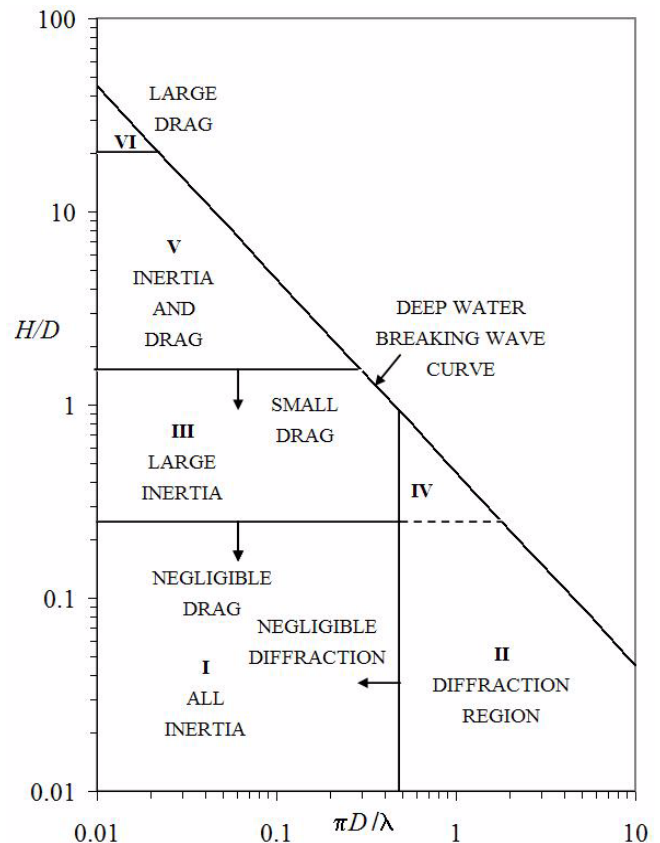
Figure 7-1
Different wave force regimes (Chakrabarti, 1987). *D* = characteristic dimension, *H* = wave height, *λ* = wave length.

7.1.3 Natural periods

7.1.3.1 Natural periods for a moored offshore structure in surge, sway and yaw are typically more than 100 seconds. Natural periods in heave, roll and pitch of semi-submersibles are usually above 20 seconds. On the other hand, for a Tension Leg Platform (TLP), which is a buoyant tethered platform, the natural periods for vertical motions are typically below 5 seconds.

7.1.3.2 The natural periods T_j, j = 1,2,...6 of a moored offshore structure are approximately given by

$$T_j = 2\pi \left(\frac{M_{jj} + A_{jj}}{C_{jj} + K_{jj}} \right)^{\frac{1}{2}}$$

where M_{jj}, A_{jj}, C_{jj} and K_{jj} are the diagonal elements of the mass, added mass, hydrostatic and mooring stiffness matrices.

7.1.3.3 Natural periods may depend on coupling between different modes and the amount of damping.

7.1.3.4 The uncoupled natural period in heave for a freely floating semi-submersible or an FPSO is

$$T_3 = 2\pi \left(\frac{M + A_{33}}{\rho g S} \right)^{\frac{1}{2}}$$

where M is the mass, A_{33} the heave added mass and S is the waterplane area.

7.1.3.5 For a TLP the tendon stiffness K_{33} is much larger than the hydrostatic stiffness C_{33}. Hence the natural period in heave

for a TLP is

$$T_3 = 2\pi \left(\frac{M + A_{33}}{EA/L} \right)^{\frac{1}{2}}$$

where E is the modulus of elasticity, A is the total cross-sectional area of all the tendons and L is the length of each tendon.

7.1.3.6 he natural period in pitch for a freely floating body like a semi-submersible or an FPSO is

$$T_5 = 2\pi \left(\frac{Mr_{55}^{\,2} + A_{55}}{\rho g V \, GM_L} \right)^{\frac{1}{2}}$$

where r_{55} is the pitch radius of gyration, A_{55} is the pitch added moment and GM_L is the longitudinal metacentric height. The natural period in roll is

$$T_4 = 2\pi \left(\frac{Mr_{44}^{\,2} + A_{44}}{\rho g V \, GM_T} \right)^{\frac{1}{2}}$$

where r_{44} is the roll radius of gyration, A_{44} is the roll added moment and GM_T is the transversal metacentric height.

Typical natural periods for moored deep water floaters are given in Table 7-1.

Table 7-1 Typical natural periods [s] of deep water floaters

Floater Mode	FPSO	Spar	TLP	Semi
Surge	> 100	> 100	> 100	> 100
Sway	> 100	> 100	> 100	> 100
Heave	5 – 12	20 – 35	< 5	20 – 50
Roll	5 – 30	50–90	< 5	30 - 60
Pitch	5 – 12	50 –90	< 5	30 - 60
Yaw	> 100	> 100	> 100	> 50-60

7.1.4 Coupled response of moored floaters

7.1.4.1 A moored floating system is an integrated dynamic system of one or several floaters, risers and moorings responding to wind, wave and current loadings in a complex way. The floater motions in shallow and intermediate water depth are to a large extent excited and damped by fluid forces on the floater itself.

7.1.4.2 As the water depth increases the coupling between the slender structures and the large volume floater becomes more important. In this case a coupled analysis, in which the dynamics of the floater, mooring lines and risers are solved simultaneously, is recommended. The most important coupling effects are:

— Restoring from stationkeeping system is a function of floater offset.
— Effect of current loading on restoring force due to mooring and riser system.
— Damping from riser and stationkeeping system due to dynamics, current etc.
— Inertia forces due to mooring and riser system.
— Damping due to possible contact friction between hull (Spar) and riser.
— Seafloor friction, if mooring system has sea-bottom contact.

A response analysis taking into account these effects is called a *coupled analysis*.

7.1.4.3 Coupled analysis is often necessary in the design of deepwater floating systems. Guidance on coupled analysis is given in DNV-RP-F205 "Global performance analysis of deep water floating structures".

7.1.5 Frequency domain analysis

7.1.5.1 The wave induced loads in an irregular sea can be obtained by linearly superposing loads due to regular wave components. Analysing a large volume structure in regular incident waves is called a *frequency domain analysis*.

7.1.5.2 Assuming steady state, with all transient effects neglected, the loads and dynamic response of the structure is oscillating harmonically with the same frequency as the incident waves, or with the frequency of encounter in the case of a forward speed.

7.1.5.3 Within a linear analysis, the hydrodynamic problem is usually divided into two sub-problems:

— *Radiation problem* where the structure is forced to oscillate with the wave frequency in a rigid body motion mode with no incident waves. The resulting loads are usually formulated in terms of *added mass*, *damping* and *restoring* loads

$$F_k^{\,(r)} = -A_{kj}\frac{d^2\xi_j}{dt^2} - B_{kj}\frac{d\xi_j}{dt} - C_{kj}\xi_j$$

where A_{kj} and B_{kj} are added mass and damping, and C_{kj} are the hydrostatic restoring coefficients, $j,k = 1,2,...6$, for the six degrees of rigid body modes. A_{kj} and B_{kj} are functions of wave frequency ω.

— *Diffraction problem* where the structure is restrained from motions and is excited by incident waves. The resulting loads are *wave excitation* loads

$$F_k^{\,(d)} = f_k(\omega)e^{-i\omega t} \; ; \; k = 1,2,...6$$

7.1.5.4 The part of the wave excitation loads that is given by the undistorted pressure in the incoming wave is called the *Froude-Krylov* forces/moments. The remaining part is called *diffraction* forces/moments.

Frequency domain analysis of hydroelastic response of large volume structures is covered in 7.3.7.

7.1.6 Time domain analysis

7.1.6.1 Some hydrodynamic load effects can be linearised and included in a frequency domain approach, while others are highly non-linear and can only be handled in time-domain.

7.1.6.2 The advantage of a time domain analysis is that it can capture higher order load effects. In addition, a time domain analysis gives the response statistics without making assumptions regarding the response distribution.

7.1.6.3 A time-domain analysis involves numerical integration of the equations of motion and should be used when non-linear effects are important. Examples are

— transient slamming response
— simulation of low-frequency motions (slow drift)
— highly non-linear high-frequency response (e.g. ringing)
— coupled floater, riser and mooring response.

7.1.6.4 Time-domain analysis methods are usually used for prediction of extreme load effects. In cases where time-domain analyses are time-consuming, critical events can be analysed by a refined model for a time duration defined by a simplified model.

7.1.6.5 Time-domain analyses of structural response due to random load effects must be carried far enough to obtain stationary statistics.

Methods for estimation of extremes are given in Ch.3.

7.1.7 Forward speed effects

7.1.7.1 If the large volume structure has a mean forward speed or if the structure is exposed to a combined wave and current environment, this will influence the hydrodynamic loads. The loads and dynamic response of the structure will oscillate harmonically with the *frequency of encounter* ω_e.

7.1.7.2 For a general heading β between the ship and the wave propagation direction, the oscillation frequency is

$$\omega_e = \omega - \frac{\omega^2 U}{g}\cos\beta$$

where U is the forward speed, and $\beta = 0^o$ is following seas. For a ship course against the waves ($\beta > 90^o$) the frequency of encounter is higher than the incident wave frequency. For a course in the wave direction ($\beta < 90^o$) the frequency of encounter is normally lower than the wave frequency. An exception may occur when short following waves are passed by the ship. The condition for the ship passing the waves is given by

$$U\cos\beta > \sqrt{\frac{g\lambda}{2\pi}}$$

where λ is the wave length of incoming waves.

7.1.7.3 For small mean forward speed, typical for slow drift motion of stationary platforms, linear wave induced loads can be evaluated at zero speed. However the effect on the mean drift force should be included (see also 7.4.5).

7.1.8 Numerical methods

7.1.8.1 Wave-induced loads on large volume structures can be predicted based on potential theory which means that the loads are deduced from a velocity potential of the irrotational motion of an incompressible and inviscid fluid.

7.1.8.2 The most common numerical method for solution of the potential flow is boundary element method (BEM) where the velocity potential in the fluid domain is represented by a distribution of sources over the mean wetted body surface. The source function satisfies the free surface condition and is called a *free surface Green function*. Satisfying the boundary condition on the body surface gives an integral equation for the source strength.

7.1.8.3 An alternative is to use elementary *Rankine sources* ($1/R$) distributed over both the mean wetted surface and the mean free surface. A Rankine source method is preferred for forward speed problems.

7.1.8.4 Another representation is to use a mixed distribution of both sources and normal dipoles and solve directly for the velocity potential on the boundary.

7.1.8.5 The mean wetted surface is discretized into flat or curved panels, hence these methods are also called panel methods. A *low-order* panel method uses flat panels, while a *higher order* panel method uses curved panels. A higher order method obtains the same accuracy with less number of panels (Lee et al., 1997).

Requirements to discretisation are given in 7.3, 7.4 and 7.5.

7.1.8.6 The potential flow problem can also be solved by the finite element method (FEM), discretizing the volume of the fluid domain by elements. For infinite domains, an analytic representation must be used a distance away from the body to reduce the number of elements. An alternative is to use so-called infinite finite element.

7.1.8.7 For fixed or floating structures with simple geometries like sphere, cylinder, spheroid, ellipsoid, torus, etc. semi-analytic expressions can be derived for the solution of the potential flow problem. For certain offshore structures, e.g. a Spar platform, such solutions can be useful approximations.

7.1.8.8 Wave-induced loads on slender ship-like large volume structures can be predicted by *strip theory* where the load is approximated by the sum of loads on two-dimensional strips. One should be aware that the numerical implementation of the strip theory must include a proper treatment of head sea ($\beta = 180^o$) wave excitation loads. Strip theory is less valid for low encounter frequencies.

7.1.8.9 Motion damping of large volume structures is due to wave radiation damping, hull skin friction damping, hull eddy making damping, viscous damping from bilge keels and other appendices, and viscous damping from risers and mooring. Wave radiation damping is calculated from potential theory. Viscous damping effects are usually estimated from simplified hydrodynamic models or from experiments. For simple geometries Computational Fluid Dynamics (CFD) can be used to assess viscous damping.

7.2 Hydrostatic and inertia loads

7.2.1 General

7.2.1.1 The structure weight and buoyancy force balance is the starting point for hydrodynamic analyses. Influence from risers and mooring mass and pretensions is part of this load balance.

7.2.1.2 The static balance is trivial for a linear analysis, but important for the success of subsequent hydro-dynamic analyses. Buoyancy of large volume structures is calculated directly from the wetted surface geometry described by the radiation/diffraction model. In cases where a dual model, including Morison elements, is applied, this may also be handled automatically by the computer program as long as the actual location and dimensions of the Morison elements are implemented. For non-linear hydrodynamic analyses special consideration should be given to hydrostatic loads.

7.2.1.3 A moonpool needs special considerations if the moonpool area is large and reduces the waterplane area significantly. In the case of a Spar with air-can supported riser system, using a model with closed bottom of the hard tank or at keel level will result in too high waterplane stiffness.

7.2.1.4 The elements of the mass matrix [M] and hydrostatic stiffness matrix [C] are given in Figure 7-2. For a freely floating body the mass is $M = \rho V$ where ρ is the mass density of water and V is the submerged volume of the structure. In this case equilibrium of static forces require that the center of gravity and center of buoyancy must lie on the same vertical line $x_B = x_G$ and $y_B = y_G$. This implies $C_{46} = C_{64} = C_{56} = C_{65} = 0$. Usually the origin of the coordinate system is chosen on a vertical line going through the center of gravity so that $x_G = y_G = 0$.

$$
M_{jk} = \begin{bmatrix}
M & 0 & 0 & 0 & Mz_G & -My_G \\
0 & M & 0 & -Mz_G & 0 & Mx_G \\
0 & 0 & M & My_G & -Mx_G & 0 \\
0 & -Mz_G & My_G & I_{11} & I_{12} & I_{13} \\
Mz_G & 0 & -Mx_G & I_{21} & I_{22} & I_{23} \\
-My_G & Mx_G & 0 & I_{31} & I_{32} & I_{33}
\end{bmatrix}
$$

$$
C_{jk} = \begin{bmatrix}
0 & 0 & 0 & 0 & 0 & 0 \\
0 & 0 & 0 & 0 & 0 & 0 \\
0 & 0 & \rho g S & \rho g S_2 & -\rho g S_1 & 0 \\
0 & 0 & \rho g S_2 & \rho g(S_{22}+Vz_B)-Mgz_G & -\rho g S_{12} & -\rho g Vx_B + Mgx_G \\
0 & 0 & -\rho g S_1 & -\rho g S_{12} & \rho g(S_{11}+Vz_B)-Mgz_G & -\rho g Vy_B + Mgy_G \\
0 & 0 & 0 & -\rho g Vx_B + Mgx_G & -\rho g Vy_B + Mgy_G & 0
\end{bmatrix}
$$

Figure 7-2
Inertia matrix [M] and hydrostatic stiffness matrix [C] for a floating body. M = mass, V = submerged volume of body, (x_G,y_G,z_G) = centre of gravity, (x_B,y_B,z_B) = centre of buoyancy, I_{ij} = moments of inertia, S = water plane area, S_i, S_{ij} = first and second moments of water plane area.

7.2.1.5 The metacentric heights are defined by

$$
GM_T = \frac{S_{22}}{V} + z_B - z_G
$$

$$
GM_L = \frac{S_{11}}{V} + z_B - z_G
$$

Hence the hydrostatic stiffness in roll and pitch for a freely floating body are given by

$$
C_{44} = \rho g V \cdot GM_T
$$
$$
C_{55} = \rho g V \cdot GM_L
$$

7.2.1.6 Applying the correct metacentric height in the analyses is just as important as the location of the centre of buoyancy. Influence from free surface effects in internal tanks needs to be taken into account while determining the metacentric height.

7.2.1.7 The additional restoring effects due to the reaction from buoyancy cans on the riser guides also need to be taken into account.

7.2.1.8 Closed cushions provide additional restoring. The heave restoring for a wallsided cushion of horizontal area A_c and volume V_c is given by

$$
C_{33} = \gamma \frac{p_0 A_c^2}{V_c}
$$

where γ = 1.4 is the gas constant for air and p_0 is the atmospheric pressure.

7.2.1.9 Stiffness contributions from tethers, mooring lines, risers and possible additional restoring from thrusters must also be accounted for.

7.2.1.10 The mass distribution of the floater may either be entered as a global mass matrix, in terms of mass and mass moments of inertia, or from a detailed mass distribution (e.g. FE model). The input coordinate system varies depending on

software and may be referred to the vertical centre of gravity, or the water plane.

7.2.1.11 The moments of inertia in the global mass matrix are given by

$$
I_{ij} = \int_{body} (r^2 \delta_{ij} - x_i x_j) dm
$$

where with $x_1 = x$, $x_2 = y$ and $x_3 = z$.

$$
r^2 = \sum_{i=1}^{3} x_i^2
$$

The diagonal elements of the moment of inertia matrix I_{jj} are often given in terms of radii of gyration, r_4, r_5 and r_6,

$$
I_{jj} = M r_{j+3}^2
$$

7.2.1.12 Input of roll, pitch and yaw radii of gyration is very often a source of error in computer programs. If the origin of the coordinate system is not in the centre of gravity, off-diagonal terms appear in the body mass matrix. Applying the correct reference axis system is usually the challenge in this context.

7.3 Wave frequency loads

7.3.1 General

7.3.1.1 Large volume structures are inertia-dominated, which means that the global loads due to wave diffraction are significantly larger than the drag induced global loads. Some floaters, such as semi-submersibles and Truss Spars, may also require a Morison load model for the slender members/braces in addition to the radiation/diffraction model, ref. Ch.6.

7.3.1.2 A linear analysis will usually be sufficiently accurate for prediction of global wave frequency loads. Hence, this section focuses on first order wave loads. The term *linear* means that the fluid dynamic pressure and the resulting loads are pro-

portional to the wave amplitude. This means that the loads from individual waves in an arbitrary sea state can be simply superimposed.

7.3.1.3 Only the wetted area of the floater up to the mean water line is considered. The analysis gives first order excitation forces, hydrostatics, potential wave damping, added mass, first order motions in rigid body degrees of freedom and the mean drift forces/moments. The mean wave drift force and moments are of second order, but depends on first order quantities only.

7.3.1.4 The output from a frequency domain analysis will be transfer functions of the variables in question, e.g. exciting forces/moments and platform motions per unit wave amplitude. The first order or linear force/ moment transfer function (LTF) is usually denoted $H^{(1)}(\omega)$. The linear motion transfer function,

$$\xi^{(1)}(\omega)$$

also denoted the response transfer function $H_R(\omega)$ or the Response Amplitude Operator (RAO). The RAO gives the response per unit amplitude of excitation, as a function of the wave frequency,

$$\xi^{(1)}(\omega) = H^{(1)}(\omega)L^{-1}(\omega)$$

where $L(\omega)$ is the linear structural operator characterizing the equations of motion,

$$L(\omega) = -\omega^2 [M + A(\omega)] + i\omega B(\omega) + C$$

M is the structure mass and inertia, A the added mass, B the wave damping and C the stiffness, including both hydrostatic and structural stiffness. The equations of rigid body motion are, in general, six coupled equations for three translations (surge, sway and heave) and three rotations (roll, pitch and yaw).

7.3.1.5 The concept of RAOs is also used for global forces and moments derived from rigid body motions and for diffracted wave surface elevation, fluid pressure and fluid kinematics.

7.3.2 Wave loads in a random sea

7.3.2.1 The frequency domain method is well suited for systems exposed to random wave environments, since the random response spectrum can be computed directly from the transfer function and the wave spectrum in the following way:

$$S_R(\omega) = \left|\xi^{(1)}(\omega)\right|^2 S(\omega)$$

where

ω = angular frequency ($= 2\pi/T$)
$\xi^{(1)}(\omega)$ = transfer function of the response
$S(\omega)$ = wave spectrum
$S_R(\omega)$ = response spectrum

7.3.2.2 Based on the response spectrum, the short-term response statistics can be estimated. The method limitations are that the equations of motion are linear and the excitation is linear.

7.3.2.3 Linear assumption is also employed in the random process theory used to interpret the solution. This is inconvenient for nonlinear effects like drag loads, damping and excitation, time varying geometry, horizontal restoring forces and variable surface elevation. However, in many cases these nonlinearities can be satisfactorily linearised.

7.3.2.4 Frequency domain analysis is used extensively for floating units, including analysis of both motions and forces. It is usually applied in fatigue analyses, and analyses of more moderate environmental conditions where linearization gives satisfactory results. The main advantage of this method is that the computations are relatively simple and efficient compared to time domain analysis methods.

7.3.3 Equivalent linearization

7.3.3.1 Linear superposition can be applied in the case of nonlinear damping or excitation if the non-linear terms are linearized. In general a non-linear force term $|\dot{x}|^n \dot{x}$

can be written in a linearized form $B_1 \dot{x}$

where

$$B_1 = \sqrt{\frac{2}{\pi}} 2^{\frac{n+1}{2}} \Gamma\left(\frac{n+3}{2}\right) \sigma_{\dot{x}}^n$$

where $\sigma_{\dot{x}}$

is the root mean square structural velocity (Chakrabarti, 1990). For a quadratic drag force $n = 1$, the equivalent linear force is

$$\sqrt{\frac{8}{\pi}} \sigma_{\dot{x}} \dot{x}$$

Since $\sigma_{\dot{x}}$

is a function of the response of the structure, iteration is needed.

7.3.4 Frequency and panel mesh requirements

7.3.4.1 Several wave periods and headings need to be selected such that the motions and forces/moments can be described as correctly as possible. Cancellation, amplification and resonance effects must be properly captured.

7.3.4.2 Modelling principles related to the fineness of the panel mesh must be adhered to. For a low-order panel method (BEM) with constant value of the potential over the panel the following principles apply:

— Diagonal length of panel mesh should be less than 1/6 of smallest wave length analysed.
— Fine mesh should be applied in areas with abrupt changes in geometry (edges, corners).
— When modelling thin walled structures with water on both sides, the panel size should not exceed 3-4 times the modelled wall thickness.
— Finer panel mesh should be used towards water-line when calculating wave drift excitation forces.
— The water plane area and volume of the discretized model should match closely to the real structure.

7.3.4.3 Convergence tests by increasing number of panels should be carried out to ensure accuracy of computed loads. Comparing drift forces calculated by the pressure integration method and momentum method provides a useful check on numerical convergence for a given discretisation.

7.3.4.4 Calculating wave surface elevation and fluid particle velocities require an even finer mesh as compared to a global response analysis. The diagonal of a typical panel is recommended to be less than 1/10 of the shortest wave length analysed. For low-order BEM, fluid kinematics and surface elevation should be calculated at least one panel mesh length away from the body boundary, preferably close to center of panels. For details related to wave elevation analysis, reference is made to Ch.8.

7.3.4.5 For a motion analysis of a floater in the frequency domain, computations are normally performed for at least 30 frequencies. Special cases may require a higher number. This applies in particular in cases where a narrow-band resonance peak lies within the wave spectral frequency range. The fre-

quency spacing should be less than $\zeta\omega_0$ to achieve less than about 5% of variation in the standard deviation of response. ζ is the damping ratio and ω_0 the frequency.

7.3.4.6 Fine frequency discretisation is required near resonance and in other areas with abrupt changes in forces with frequency due to wave trapping, cancellation effects etc.

7.3.4.7 First order near trapping is defined as a massive upwelling of water in the basin enclosed by a cylinder array, corresponding to a trapping of surface wave energy around the columns. The trapped energy leads to high wave forces on the column sides facing the basin and also high wave amplification. The phenomenon should be considered when selecting wave frequencies in computer analysis.

7.3.4.8 For an array of vertical cylinders located at the vertices of a square and with a wave travelling along the diagonal, first order near trapping in deep water occurs at the incident wave frequency with wave length approximately equal to

$$\lambda \approx \sqrt{2}d - 2a$$

where d is the shortest distance between adjacent cylinder centres and a is the cylinder radius.

7.3.4.9 The sensitivity of wave loads to the discretization of bodies is presented by Newman et al. (1992). Practical procedures for computing motion response of fixed and floating platforms including modelling requirements are discussed by Herfjord & Nielsen (1992).

7.3.5 Irregular frequencies

7.3.5.1 For radiation/diffraction analyses, using free surface Green function solvers, of large volume structures with large water plane area like FPSOs and Spars, attention should be paid to the existence of so-called *irregular frequencies*.

7.3.5.2 These frequencies correspond to fictitious eigenmodes of an internal problem (inside the numerical model of the structure) and do not have any direct physical meaning. It is a deficiency of the integral equation method used to solve for the velocity potential.

7.3.5.3 At irregular frequencies a standard BEM method may give unreliable values for added mass and damping. Methods are available in some commercial software tools to remove the unwanted effects of the irregular frequencies (Lee and Sclavounos, 1989). The Rankine source method avoids irregular frequencies.

7.3.5.4 Irregular wave numbers v_{ij} of a rectangular barge with length L, beam B and draft T are given by the relations

$$v_{ij} = k_{ij} \coth(k_{ij}T)$$

where

$$k_{ij} = \pi\sqrt{(i/L)^2 + (j/B)^2}\;;\; i, j = 0,1,2,...;\; i + j \geq 1$$

7.3.5.5 Irregular wave numbers v_{ms} of a vertical cylinder with radius R and draft T are given by the relations

$$v_{ms} = k_{ms} \coth(k_{ms}T)$$

where $k_{ms} = j_{ms}/R$ are given by the zeros of the mth order Bessel function $J_m(j_{ms}) = 0$; $m = 0,1,2,\ldots, s = 1,2,\ldots$ The lowest zeros are $j_{01} = 2.405$, $j_{11} = 3.832$, $j_{21} = 5.136$, $j_{02} = 5.520$. The corresponding irregular frequencies are then given by the dispersion relation

$$\omega^2 = g\,v\,\tanh(vd)$$

where d is the water depth.

7.3.5.6 Note that for bottom mounted structures the hyperbolic cotangent function coth in the formulae above (7.3.5.4-7.3.5.5) is replaced by hyperbolic tangent function tanh.

7.3.6 Multi-body hydrodynamic interaction

7.3.6.1 Hydrodynamic interactions between multiple floaters in close proximity and between a floater and a large fixed structure in the vicinity of the floater, may also be analysed using radiation/diffraction software through the so-called multi-body options. The n floaters are solved in an integrated system with motions in $n \times 6$ DOFs.

7.3.6.2 An example of a two-body system is an LNG-FPSO and a side-by-side positioned LNG carrier during offloading operations where there may be a strong hydrodynamic interaction between the two floaters. The interaction phenomena may be of concern due to undesirable large relative motion response between the two floaters, ref. Kim et al. (2003).

7.3.6.3 An important non-linear interaction effect is a trapped standing wave between the floaters that can excite sway and roll motions. Some radiation-diffraction codes have means to damp trapped standing waves.

7.3.6.4 The discretisation of the wetted surfaces in the area between the floaters must be fine enough to capture the variations in the trapped wave. Additional resonance peaks also appear in coupled heave, pitch and roll motions.

7.3.6.5 Another effect is the sheltering effect which leads to smaller motions on the leeside than on the weather side. Hydrodynamic interaction effects between multiple surface piercing structures should be included if the excitation loads on each structure is considerable influenced by the presence of the other structures.

7.3.7 Generalized body modes

7.3.7.1 Wave induced global structural deformations can be analysed in the frequency domain by defining a set of generalised modes. These modes are defined by specifying the normal velocity on the wetted surface in the form

$$v_n = u_j n_x + v_j n_y + w_j n_z$$

where $j > 6$ is the index of the generalized mode. (n_x, n_y, n_z) is the normal to the surface and (u_j, v_j, w_j) can be any physically relevant real vector function of (x,y,z).

7.3.7.2 As an example, the transverse and vertical bending of a ship can be represented by

$$v_7 = w_8 = P_2(q) = (3q^2 - 1)/2$$

where $q = 2x / L \in [-1,1]$

$$u_7 = w_7 = u_8 = v_8 = 0$$

P_2 is the Legendre polynomial and q is the normalized horizontal coordinate over the length of the ship. Higher order modes can be represented by introducing several generalized modes.

7.3.7.3 Generalized restoring must be supplied in terms of elastic stiffness matrix, and damping must include structural damping. More details on wave induced response of flexible modes is found in Newman (1994).

7.3.8 Shallow water and restricted areas

7.3.8.1 Special attention should be paid to analysis of wave induced loads in very shallow water and in restricted waters.

7.3.8.2 In cases where the keel of an FPSO or ship is very close to the sea bed, the vertical added mass may change considerably during its motion. Since the narrow gap restricts fluid flow beneath the hull, nonlinear diffraction effects may occur.

Similar effects occur for waves over shallow horizontal surfaces, e.g. a shallow pontoon.

7.3.8.3 Since the wave frequency analysis is based on incoming Airy waves, the validity of this wave theory should be checked for the actual wave lengths and wave heights, see Ch.3.

7.3.8.4 Shallow water effects may have a strong influence on mean drift loads, see 7.4.3.

7.3.8.5 For floating structures in shallow water coastal areas where the water depth varies along the length of the structure, this variation should be accounted for in the wave frequency analysis by modelling the sea bed in addition to the wetted surface of the floater.

7.3.9 Moonpool effects

7.3.9.1 The radiation/diffraction analysis for a floating structure with a moonpool should be treated with some care. Moonpool effects are most relevant for turret moored ships and Spar platforms. Depending on the dimensions of the moonpool, the heave motion transfer function may be strongly influenced by the fluid motion inside the moonpool.

7.3.9.2 The motion of the water in the moonpool has a resonance at a wave frequency corresponding to the eigenfrequency of an vertically oscillating water column, *pumping mode*. For a moonpool with constant cross-sectional area A the resonance period is given by the

$$T_0 = 2\pi \sqrt{\frac{h + \kappa\sqrt{A}}{g}}$$

where h is the height of the water column and g is the acceleration of gravity. The factor κ depends on the cross-sectional shape. $\kappa = 8/(3\pi^{3/2}) = 0.479$ for a circle, $\kappa = 0.460$ for a rectangle ($\delta = b/l = 0.5$) and $\kappa = 0.473$ for a square.

7.3.9.3 The κ-factor for a general rectangular moonpool is given by (Molin, 2001)

$$\kappa = \frac{\sqrt{\delta}}{\pi}\left[\sinh^{-1}(\delta^{-1}) + (\delta^{-1})\sinh^{-1}\delta + \frac{1}{3}(\delta + \delta^{-2}) \right.$$
$$\left. -\frac{1}{3}(1+\delta^{-2})\sqrt{1+\delta^2}\right] \quad ; 0 < \delta < 1$$

7.3.9.4 The resonant period for a moonpool of varying cross-sectional area $A(z)$ can be approximated by

$$T_0 = 2\pi \sqrt{\frac{M_{eq}}{\rho A(-h)g}}$$

where the equivalent mass M_{eq} is given by

$$M_{eq} = \rho A(-h)\left\{\int_{-h}^{0}\frac{A(0)}{A(z)}\,dz + \frac{A(0)}{A(-h)}\cdot\kappa\sqrt{A(-h)}\right\}$$

$A(0)$ is the cross-sectional area at still water level and $A(-h)$ is the cross-sectional area at moonpool opening.

7.3.9.5 Neglecting viscous damping of the water motion in the moonpool will result in unrealistic large motions and free surface elevation in the moonpool close to resonance. Discretisation of the wetted area within the moonpool must be done with care in order to capture the flow details.

7.3.9.6 The fluid motion in the moonpool can be calculated by a radiation/diffraction panel program. A simplified approach is to calculate the fluid pressure over the cross-sectional area at the lower end of the moonpool and then find the resulting vertical motion of the water plug. A more accurate method is to treat the vertical fluid motion in the moonpool as a generalized mode. In both cases viscous damping should be introduced. The damping level may be estimated from model tests but one should be aware of viscous scale effects, see Ch.10.

7.3.9.7 Sloshing motion may occur in large moonpools. The natural angular frequencies ω_n of longitudinal sloshing modes in a rectangular moonpool with length l, breadth b and draught (height) h is approximated by (Molin, 2001)

$$\omega_n^2 = g\lambda_n\frac{1 + J_n\tanh(\lambda_n h)}{J_n + \tanh(\lambda_n h)}$$

where $\lambda_n = n\pi/l$ and function J_n for $n = 1,2$ is given in Figure 7-3. The resonance periods are then given by $T_n = 2\pi/\omega_n$. One should note that these natural modes are different from sloshing modes in a tank.
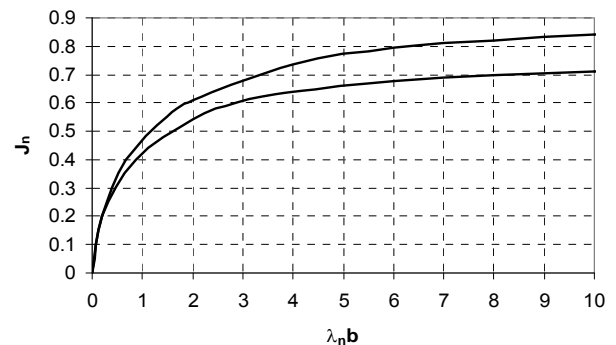

Figure 7-3
Function J_n for $n = 1$ lower curve, $n = 2$ upper curve (from Molin, 2001).

7.3.10 Fluid sloshing in tanks

7.3.10.1 Wave induced motions of ships and floating platforms will generate motion of fluid in internal tanks containing oil or water. Depending on the resonant rigid body motions and the resonant oscillation of the fluid in the tanks, dynamic amplification of pressure on fluid walls may occur. Such sloshing motion can also cause high local impact pressures.

7.3.10.2 The resonant frequencies for sloshing mode in a rectangular tank of length L, width B and depth h are

$$\omega_{mn} = \sqrt{gk_{mn}\tanh(k_{mn}h)}$$

where

$$k_{mn} = \sqrt{(m\pi/L)^2 + (n\pi/B)^2} \quad , m,n = 0,1,2\ldots.$$

For a circular tank of radius a,

$$k_{mn} = \frac{j'_{mn}}{a}, \quad n = 1,2,3,\ldots, m = 0,1,2,3$$

where j'_{mn} is the nth zero of the derivative of Bessel function of order m, $\quad J'_m$.

7.3.10.3 Numerical predictions of loads due to sloshing in internal tanks should be combined with model test. Computer programs (CFD) are still not able to predict wave breaking in tanks and resulting local impact loads.

7.3.10.4 Some radiation-diffraction programs are able to capture the natural sloshing modes in tanks and predict coupled wave induced response of rigid body motion and sloshing (non-breaking) wave motion by modelling the wetted surface of the internal tanks.

7.4 Mean and slowly varying loads

7.4.1 Difference frequency QTFs

7.4.1.1 Low frequency motions of a moored floating structure are caused by slowly varying wave, wind and current forces. The wave-induced drift force consists of an inviscid part and a viscous part. The inviscid wave drift force is a second-order wave force, proportional to the square of the wave amplitude.

7.4.1.2 In a random sea-state represented by a sum of N wave components ω_i, $i = 1, N$ this force oscillates at difference frequencies $\omega_i - \omega_j$ and is given by the expression

$$q_{WA}^{(2-)}(t) = \text{Re} \sum_{i,j}^{N} a_i a_j H^{(2-)}(\omega_i, \omega_j) e^{i(\omega_i - \omega_j)t}$$

where a_i, a_j are the individual wave amplitudes and $H^{(2-)}$ is the quadratic transfer function (QTF) for the difference frequency load. The QTF is here presented as a complex quantity with amplitude $|H^{(2-)}|$ and phase $\alpha^{(2-)}$. Re denotes the real part.

7.4.1.3 Commercial computer tools exist for calculating the difference frequency QTF. This is a second-order problem requiring discretisation of the free surface in addition to the floater body surface. The QTFs depend weakly on the first order motions $\xi^{(1)}$.

7.4.1.4 The QTF also depends on the directions of propagation β_i of the wave components. For short-crested sea-states this means that it may be necessary to solve the complete bi-chromatic and bi-directional second-order problem, ref. Kim et al. (1997).

7.4.2 Mean drift force

7.4.2.1 The mean drift force is obtained by keeping only diagonal terms ($\omega_i = \omega_j$) in the sum above. The mono-chromatic drift force is defined by

$$F_d(\omega_i) = \frac{1}{2} a_i^2 \text{Re}\left[H^{(2-)}(\omega_i, \omega_i)\right]$$

The bi-directional mean drift force $F_d(\omega; \beta_i, \beta_j)$ can also be calculated from first order velocity potentials.

7.4.2.2 The mean wave drift force and moments are of second order, but depends on first order quantities only. They can therefore be predicted from a linear analysis. The accuracy is dependent on the accurate prediction of the first order motions.

7.4.2.3 The horizontal components (surge, sway) and the moment about the vertical axis (yaw) can be calculated in a robust manner by a far-field method, also called the momentum method.

7.4.2.4 The mean drift force/moment in heave, roll and pitch must be calculated by integrating the 2nd order mean wave pressure over the wetted surface of the structure. This usually requires a finer discretisation of the geometry. The vertical mean drift force is usually only of interest for structures with small water plane area (e.g. semisubmersible) having natural periods in heave and pitch well above peak period of the wave spectrum.

7.4.2.5 Restricted waters may have a strong influence on mean drift loads, e.g.

— vertical drift forces in shallow water may be important for structures where these are normally neglected
— sway drift forces in head sea for a structure near other structure is in general non-zero.

7.4.2.6 For low frequencies, i.e. long waves, diffraction effects are small and the wave drift force is zero. Conversely, at high frequencies, the structure reflects the waves completely and the drift force has a finite asymptotic value. In between these asymptotic cases, the drift force has peaks associated with resonance effects in heave, roll and pitch or in the case of a multi-column platform, interference effects between the columns.

7.4.2.7 Special considerations have to be made for multi-vessel systems when calculating individual mean drift forces. The momentum approach gives only the total drift force on the global system. Direct pressure integration of second-order fluid pressure on each body is required.
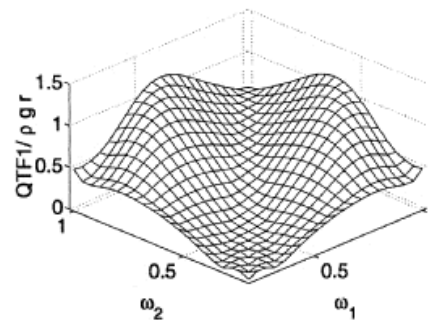
(a) Surge QTF
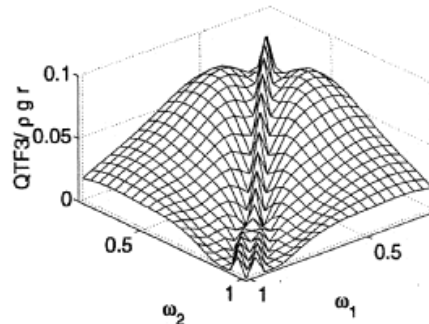
(b) Heave QTF

(c) Pitch QTF (ref VCG)

Figure 7-4
Difference frequency QTF for 228 m classical Spar.
From Haslum (1999).

7.4.3 Newman's approximation

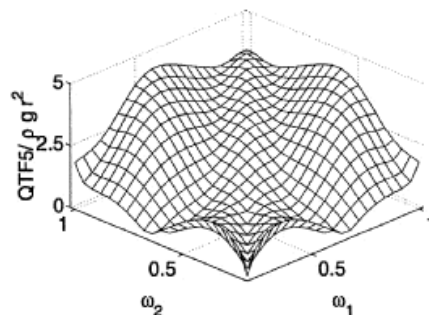*7.4.3.1* In general all frequencies in the $\omega_i\omega_j$-plane may contribute to the second order difference frequency wave forces $q_{WA}^{(2-)}$. As the second order wave forces are small, their most important contribution is in the vicinity of resonance. For a floater with low damping, the force components with difference frequencies close to the natural frequency are the most important for the response. Difference frequencies equal to the natural frequency ω_N represent two lines in the $\omega_i\omega_j$-plane:

$$\omega_i = \omega_j \pm \omega_N.$$

7.4.3.2 If the natural frequency of the floater is very low, which is the case for horizontal motions, these lines are close to the 'diagonal' $\omega_i = \omega_j$. One can then take advantage of Newman's approximation (Newman 1974), which states that the off-diagonal elements in the full QTF matrix can be approximated by the diagonal elements, i.e.

$$H^{(2-)}(\omega_i, \omega_j) \cong \frac{1}{2}\left[H^{(2-)}(\omega_i, \omega_i) + H^{(2-)}(\omega_j, \omega_j)\right]$$

7.4.3.3 Another requirement is that the QTF function is smooth in the region close to the diagonal. Figure 7-4 shows that for a classical SPAR the surge QTF satisfies this requirement, while the heave QTF does not.

7.4.3.4 Using Newman's approximation to calculate slow-drift forces significantly reduces computation time since a linear analysis is sufficient. Newman's approximation usually gives satisfactory results for slow-drift motions in the horizontal plane since the natural period is much larger than the wave period. For slow-drift motions in the vertical plane, e.g. the heave/pitch motions of a Spar, Newman's approximation may underestimate the slow-drift forces and in such case the solution of a full QTF matrix is required.

7.4.3.5 For floater concepts such as TLPs, Newman's approximation has been commonly accepted and used in calculation of slow drift forces/moments due to its efficiency in comparison with the computation of the full matrix of quadratic transfer functions (QTF). However, for some other types of floaters caution should be exercised when applying Newman's approximation.

7.4.3.6 If slowly varying heave, roll or pitch is important or if the structure has relatively large natural frequencies, it is recommended to apply the full difference frequency QTFs.

7.4.4 Viscous effect on drift forces

7.4.4.1 In severe weather conditions the viscous contribution to the wave induced drift forces shall be included. This may be particularly important for column based structures like semi-submersibles and TLPs. For a vertical circular cylinder in regular waves, the contribution to the mean viscous drift force in the splash zone (from MWL to crest) is proportional to the cube of the wave amplitude,

$$F_d^{(v)} = \frac{2}{3\pi}\rho g k C_D D A^3$$

where k is the wave number, C_D is the drag coefficient, D is the diameter and A is the wave amplitude. The viscous contribution to mean drift force is discussed by Dev & Pinkster (1997) and Stansberg et al. (1998).

7.4.5 Damping of low frequency motions

7.4.5.1 While for wave-frequency response, most of the damping is provided by the radiation of free surface waves, several other damping effects come into play for the slow drift response of moored floating structures. As the motion frequency decreases, the structure radiates less and less wave energy, hence for most practical slow-drift problems radiation damping is negligible. Hydrodynamic and aerodynamic damping of slow-drift motions comprise:

— wave drift damping
— damping due to viscous loads on the hull (skin friction and form drag)
— damping due to drag forces on mooring lines and risers
— damping due to variation of the wind loads with the velocity of the structure
— damping due to thrusters.

7.4.5.2 These damping effects are non-linear, and the total damping used in frequency domain estimation of slow-drift response must be determined by stochastic linearization.

7.4.5.3 Wave drift damping (i) and viscous hull damping (ii) are large volume structure load effects. Damping due to drag forces on mooring lines and risers is covered in Ch.6 while wind damping is covered in Ch.5.

7.4.5.4 An important potential flow effect for low frequency motions is the *wave drift damping* force. The wave drift damping force is defined as the increase in the second-order difference frequency force experienced by a structure moving with a small forward speed in waves.

7.4.5.5 By expanding the difference frequency force in a Taylor series in terms of the forward velocity, and retaining the linear term only, the wave drift damping is proportional to the forward velocity. The wave drift therefore behaves like a linear damping, provided that the increase with forward speed is positive. This is usually the case. In some special cases, however, the wave drift damping may be negative.

7.4.5.6 When the slow-drift frequency is much smaller than the wave frequency, the slow-drift velocity varies little over a few wave periods and can be interpreted as an apparent forward speed. The wave drift damping force can therefore also be defined as the first order correction of the mean drift force in terms of the slow drift velocity $\dot{x}$ of the floating structure. Usually, only the mean wave drift damping is considered, based on an expansion of the mean drift force F_d,

$$F_d(\omega, \dot{x}) = F_d(\omega, 0) - B(\omega)\dot{x} + O(\dot{x}^2)$$

where

$$B(\omega) = -\frac{\partial F_d}{\partial \dot{x}}\Big|_{\dot{x}=0}$$

7.4.5.7 For single- and multi-column structures (Spar, TLP, Semi) consisting of vertical circular cylinders, software is available to calculate the full bi-chromatic wave drift damping,

$$G(\omega_i, \omega_j) = -\frac{\partial}{\partial \dot{x}}H^{(2-)}(\omega_i, \omega_j; \dot{x})\Big|_{\dot{x}=0}$$

7.4.5.8 For floaters like TLPs and Spars it is sufficient to consider wave drift damping for uncoupled translational modes of motion (surge, sway). But for FPSOs undergoing large slow drift yaw motions as well, the complete 3x3 wave drift damping matrix for coupled surge, sway and yaw damping is needed. In the general case the coupled wave drift damping forces (F_{dx}, F_{dy}) and moment M_{dz} in the horizontal plane is given by

$$\begin{pmatrix} F_{dx} \\ F_{dy} \\ M_{dz} \end{pmatrix} = \begin{pmatrix} B_{xx} & B_{xy} & B_{xz} \\ B_{yx} & B_{yy} & B_{yz} \\ B_{zx} & B_{zy} & B_{zz} \end{pmatrix} \begin{pmatrix} \dot{x} \\ \dot{y} \\ \dot{\theta} \end{pmatrix}$$

where $\dot{x}, \dot{y}$ are the surge and sway velocities and $\dot{\theta}$ is the yaw angular velocity. A numerical method for calculating three-dimensional wave drift damping matrix B_{ij} for general offshore structures was presented by Finne *et al* (2000).

7.4.5.9 For column-based structures (TLP, Spar) in deep water a simplified method is widely used. The formula is called Aranha's formula (Aranha, 1994),

$$B(\omega) = \frac{\omega^2}{g}\frac{\partial F_d}{\partial \omega} + \frac{4\omega}{g}F_d$$

The formula can be generalised to the case of combined surge-sway motion and waves from an arbitrary direction β (see Molin, 1994). No such simple formula exists for yaw wave drift damping. For most deepwater floaters wave drift damping of low frequency heave, roll and pitch motions can be neglected.

7.4.5.10 Wave drift damping can also be applied to quantify the effect of current on wave drift forces. Wave drift forces are sensitive to the superposition of a current, which affects the way wave energy is scattered by the floating structure. Assuming the current is weak enough so that flow separation does not occur, potential theory can be applied. Flow separation does not occur if the following condition holds (deep water)

$$\frac{U_c}{\omega A} < 1$$

where U_c is the current speed, ω is the wave frequency and A is the wave amplitude.

7.4.5.11 The drift force in waves and current can be simply related to the drift force in waves only by:

$$F_d(\omega, U_c) = F_d(\omega, 0) + B(\omega)U_c + O(U_c^2)$$

where $B(\omega)$ is the wave drift damping. If waves and current propagate in the same direction, the drift force is increased.

7.4.5.12 A simple example can be used to quantify the effect of current on the mean drift force. Taking U_c = 1 m/s, a wave with a period of 10 seconds and assuming this corresponds to a peak in the mean drift force as a function of frequency ($\partial F_d/\partial\omega = 0$), the use of Aranha's formula above gives a 25% increase in the drift force. When $\partial F_d/\partial\omega > 0$, the increase is even larger.

7.4.5.13 The constant wave drift damping to be used in a frequency domain analysis can be taken as

$$\overline{B}_{ij} = 2\int_0^\infty B_{ij}(\omega)S(\omega)d\omega$$

where B_{ij} is the wave drift damping coefficient and $S(\omega)$ is the wave spectrum.

7.4.5.14 The contribution to damping from viscous forces acting on the floater is often the most difficult to quantify and its part of the total damping may differ significantly from one structure to another. For an FPSO in surge motion linear skin friction dominates the viscous forces while for a TLP or semi-submersible quadratic drag dominates.

7.4.5.15 The linear skin friction can be estimated by assuming the hull surface to be a flat plate in oscillatory turbulent flow. But analytic results should be used cautiously. Viscous damping is usually based on decay model tests.

7.4.5.16 For a TLP or semi-submersible viscous damping can be simplified by reducing the problem to the case of two-dimensional cylinders performing a combination of low frequency and wave frequency motions. This is also relevant for an FPSO in slow sway or yaw motions. The K_C number ($K_C = 2\pi a/D$ where a is motion amplitude and D is diameter)

for flow around the hull is in the range 0 to 5. Special care is required when selecting drag coefficients in this regime. It is common to use an 'independent flow' form of Morison equation, where the drag forces due to wave frequency and low frequency motions are separated, so that two drag coefficients are required. The low frequency drag force is then given by

$$dF = \frac{1}{2}\rho C_{dU}DU|U|ds$$

where U is the slow-drift velocity.

7.4.5.17 A propeller at constant rate of revolution will experience a decrease in thrust when the vessel moves forward and an increase in thrust when the vessel moves backwards. The effect of variation of thrust due to a slow drift motion is a net force acting against the motion, i.e. a damping force.

The thrust loss dT due to a change in speed dU is expressed as

$$\frac{dT}{T_0} = K_a dV$$

where

$$T_0 = a_0\rho n^2 D^4$$

is the thrust at zero speed of advance and

ρ = water density
n = number of revolutions per unit time
D = propeller diameter
a_0 = constant.

Typical values for K_a are:

Thruster, ducted propeller:	$K_a = 0.1$
Open propeller at constant rate of revolution:	$K_a = 0.1$
Open propeller at constant power:	$K_a = 0.05$

Figure 7-5
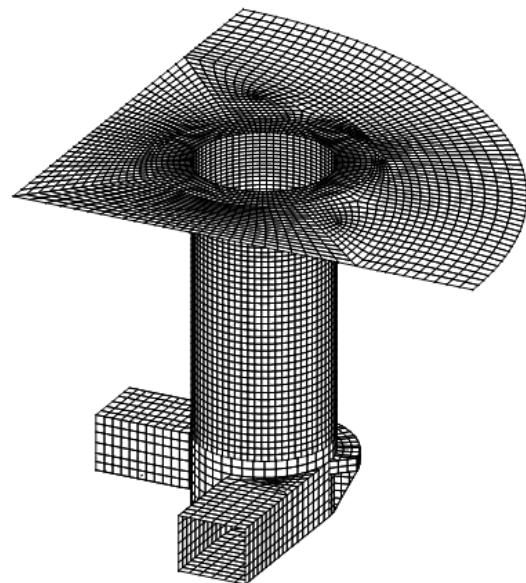**Example of discretisation of one quarter of TLP hull and free surface for calculation of second order sum-frequency wave loads.**

7.5 High frequency loads

7.5.1 General

7.5.1.1 Higher-order wave loads yield high frequency resonant vertical motions of tensioned buoyant platforms like TLPs. Similarly, slender gravity based structures (GBS) can be excited in high-frequency resonant elastic motions.

7.5.1.2 Due to its stiff tendons, tension leg platforms experience vertical mode (heave, roll, pitch) resonance at relatively low eigenperiods, T_N. The heave eigenperiod is in the range 2 – 5 seconds. Waves in this range do not carry enough energy to excite such structures in resonant response. However, due to non-linear wave effects and non-linear wave-body interaction effects, the structure will also be excited by waves of periods $2T_N$, $3T_N$, etc. which in a typical sea-state carry more energy. This non-linear transfer of energy to higher order (super-harmonic) response of the structure can equivalently be described by saying that regular waves of frequency ω excite the structural response at 2ω, 3ω, etc.

7.5.1.3 The high-frequency stationary time-harmonic oscillation of a TLP is called *springing*. Large resonant high frequency transient response is called *ringing*.

7.5.2 Second order wave loads

7.5.2.1 Second-order wave forces in a random sea-state oscillating at the sum-frequencies $\omega_i + \omega_j$ excite resonant response in heave, roll and pitch of TLPs. The high-frequency stationary time-harmonic oscillation of a TLP is called *springing*. Springing loads are essential for prediction of fatigue of TLP tendons.

7.5.2.2 Computer tools are available for calculating the sum-frequency quadratic force transfer functions (QTF) $H^{(2+)}(\omega_i, \omega_j)$. The high-frequency, or sum-frequency, force in a random sea-state is given by

$$q_{WA}^{(2+)}(t) = \text{Re} \sum_{i,j}^{N} a_i a_j H^{(2+)}(\omega_i, \omega_j) e^{i(\omega_i + \omega_j)t}$$

The most important aspects to be considered for springing analyses are:

— Discretisation (mesh) of wetted floater surface geometry.
— Discretisation of free surface and its extension. Detailed guidance on this should be given for the computer program used to calculate QTFs.
— Number of frequency pairs in the QTF matrix.
— Damping level for the tendon axial response.

7.5.2.3 For multi-column based structures like a TLP, the QTF exhibits rapid oscillations at high frequencies due to second order interaction effects between the columns. Hence, a very fine frequency mesh must be used for high frequencies (short waves). It could be misleading to only consider the diagonal terms when selecting wave periods. The diagonal term may be well represented, without capturing all peaks outside the diagonal.

Numerical tests are required to ensure that the body mesh and free surface mesh are sufficiently detailed.

7.5.3 Higher order wave loads

7.5.3.1 In high seastates deep water TLPs can experience large resonant high frequency transient response, called *ringing*. Ringing response can also occur at the 1st global bending mode of a GBS monotower.

7.5.3.2 Ringing exciting waves have a wavelength considerably longer than a characteristic cross section of the structure (e.g. diameter of column). Therefore, long wave approximations may be applied for higher-order load contribution. See Faltinsen *et al* 1995 and Krokstad *et al* (1998).

7.5.3.3 Since ringing is a transient phenomenon, the response must be solved in time domain. However, a linear structural model can usually be applied.

7.5.3.4 Due to its strongly non-linear nature, numerical models for ringing do often not provide accurate enough predictions. Model tests should be carried out to assess ringing load effects.

7.6 Steady current loads

7.6.1 General

7.6.1.1 A steady current gives rise to a steady force in the horizontal plane and a yaw moment. The moment about a horizontal axis may also be of importance. Empirical formulae are most often used to calculate current forces and moments on offshore structures. The forces and moments are normally a function of the current velocity squared given in the general form

$$F = C \cdot U_c^2$$

where C is an empirical current coefficient, and U_c is the current velocity. The current coefficients can be established by model tests, either in wind tunnel or water basin/towing tank. If the current forces are important, it is recommended to perform model tests.

The current loads increase in shallow water. Proximity effects should be accounted for.

The current coefficients in surge and sway can be used to include damping on the hull by using the relative velocity between water and structure to calculate the forces.

The influence of current on the mean wave drift force is dealt with in 7.4.5.

The current may induce vortex induced motions (VIM) of a floater. VIM is dealt with in Ch.9.

The viscous current loads are similar to the viscous wind loads. A discussion on current loads on offshore structures is given in Faltinsen (1990).

7.6.2 Column based structures

7.6.2.1 Viscous current forces on offshore structures that consist of relatively slender large volume structural parts can be calculated using the strip-theory approximation. Although these structures are classified as large-volume structures relative to the incoming waves, they may be treated as slender structures for prediction of pure current loads. This applies for instance to columns and pontoons of semi-submersibles and of TLPs.

7.6.2.2 The current velocity is decomposed into one component U_{cN} in the cross flow direction of the slender structural part and one component in the longitudinal direction. The latter component causes only shear forces and is usually neglected. The cross flow velocity component causes high Reynolds number separation and gives rise to an inline drag force

$$F_c^N = \frac{1}{2} \rho C_d D U_{cN}^2$$

where C_d is the sectional drag coefficient and D is the diameter.

7.6.2.3 There may be hydrodynamic interaction between structural parts. If a structural part is placed in the wake behind another part, it will experience a smaller drag coefficient if the free stream is used to normalize the drag coefficient. Such current blockage effects should be considered when calculating the steady current forces. More details can be found in Ch.6 on Wave and current forces on slender structures.

7.6.3 Ships and FPSOs

7.6.3.1 For moored ship-shaped structures, it is common to represent current forces in surge, sway and yaw by empirical global current coefficients, given as a function of the current heading β,

$$F_{1,2,6}(\beta, U_c) = C_{1,2,6}(\beta)U_c^2$$

The coefficients C_i can be estimated based on acknowledged published or in-house data for similar ships scaling to the size of the current ship. This will normally give sufficiently accurate forces. For instance, for Very Large Crude Carriers (VLCCs), a well established set of coefficients are published by OCIMF (1994). However, these coefficients should be used with care for other structures.

The horizontal current forces can also be estimated as described below.

7.6.3.2 The drag force on an FPSO in the longitudinal direction is mainly due to skin friction forces and it can be expressed as

$$F_{cx} = \frac{1}{2}\rho S U_c^2 C_d(R_e\, d, \beta)$$

where S is the wetted surface. The drag coefficient is a function of the Reynolds number R_e and the angle β between the current and the longitudinal axis of the ship, see Hughes (1954).

7.6.3.3 The transverse current force and current yaw moment on an FPSO can be calculated using the cross flow principle. The assumption is that the flow separates due to cross flow past the ship, that the longitudinal current components do not influence the transverse forces on the cross-section, and that the transverse force on a cross-section is mainly due to separated flow effects. The transverse current force on the ship then can be written as

$$F_{cy} = \frac{1}{2}\rho\left[\int_L dx\, C_D(x)D(x)\right]U_c^2 \sin\beta\,|\sin\beta|$$

where the integration is over the length of the ship. $C_D(x)$ above is the drag coefficient for flow past an infinitely long cylinder with the cross-sectional area of the ship at position x. $D(x)$ is the sectional draught.

7.6.3.4 The viscous yaw moment due to current flow is simply obtained by integrating the moments due to sectional drag forces along the ship. It is important to note that the yaw moment has an additional inviscid part, called the Munk moment,

$$M_c = U_c^2 \cos\beta \sin\beta(A_{11} - A_{22})$$

where U_c is the current velocity in a direction β with the x-axis and A_{11} and A_{22} are the added mass coefficients in the x- and y-directions. For a ship with transom stern A_{22} in the formula above shall be substituted by

$$A_{22} + x_{stern}A_{22,stern}^{2D}$$

where x_{stern} is the position of stern and

$$A_{22,stern}^{2D}$$

is the 2D added mass of the stern section. x is measured from the position of the moment point.

References

1) Aranha, J. A. P. (1994): "A formula for wave damping in the drift of floating bodies". J. Fluid Mech., Vol. 275, pp. 147-55.

2) Chakrabarti, S.K. (1987): "Hydrodynamics of Offshore Structures". Springer Verlag.

3) Chakrabarti, S.K. (1990): "Nonlinear Methods in Offshore Engineering". Developments in Marine Technology, 5. Elsevier Science Publishers B.V.

4) Dev, A.K. and Pinkster, J.A. (1997) "Viscous Mean and Low Frequency Drift Forces on Semisubmersibles". Proc. Vol. 2, 8th BOSS Conf., Delft, The Netherlands, pp. 351-365.

5) Faltinsen, O.M. (1990): "Sea Loads on Ships and Offshore Structures", Cambridge University Press.

6) Faltinsen, O.M., Newman, J.N., Vinje, T., (1995), Nonlinear wave loads on a slender vertical cylinder, Journal of Fluid Mechanics, Vol. 289, pp. 179-198.

7) Finne, S., Grue, J. and Nestegård, A. (2000) "Prediction of the complete second order wave drift damping force for offshore structures". 10th ISOPE Conference. Seattle, WA, USA.

8) Haslum, H. A. and Faltinsen O. M, "Alternative Shape of Spar Platforms for Use in Hostile Areas", OTC 1999.

9) Herfjord, K. & Nielsen, F.G., "A comparative study on computed motion response for floating production platforms: Discussion of practical procedures.", Proc. 6th. International Conf. Behaviour of Offshore Structures (BOSS '92), Vol. 1, London, 1992.

10) Hughes, G. (1954) "Friction and form resistance in turbulent flow, and a proposed formulation for use in model and ship correlation". Transaction of the Institution of Naval Architects, 96.

11) Kim, M-S., Ha, M-K. and Kim, B-W. (2003): "Relative motions between LNG-FPSO and side-by-side positioned LNG carriers in waves". 13th ISOPE Conference, Honolulu.

12) Kim, S., Sclavounos, P.D. and Nielsen, F.G. (1997) "Slow-drift responses of moored platforms". 8th Int. BOSS Conference, Delft.

13) Krokstad, J.R., Stansberg, C.T., Nestegård, A., Marthinsen, T (1998): "A new nonslender ringing load approach verified against experiments". Transaction of the ASME, Vol. 120, Feb. 1998

14) Lee, C.-H. and Sclavounos P.D. (1989) "Removing the irregular frequencies from integral equations in wave-body interactions". Journal of Fluid Mechanics, Vol. 207: pp. 393-418.

15) Lee, C-H., Maniar, H. and Zhu, X. (1997) "Computationas of wave loads using a B-spline panel method". Proc. of 21st Symp. on Naval Hydrodynamics. Trondheim, Norway.

16) Molin, B. (1994): "Second-order hydrodynamics applied to moored structures. A state-of-the-art survey". Ship Technology Research, Vol. 41, pp. 59-84.

17) Molin, B. (2001) "On the piston and sloshing modes in moonpools". J. Fluid Mech, Vol.430. pp. 27-50.

18) Newman, J.N. (1974): "Second Order, Slowly Varying Forces in Irregular Waves". Proc. Int. Symp. Dynamics of Marine Vehicles and Structures in Waves, London.

19) Newman, J.N. (1977) "Marine Hydrodynamics". MIT Press.

20) Newman, J.N., & Lee, C.-H., "Sensitivity of wave loads to the discretization of bodies.", Proc. 6th. Conf. on the Behaviour of Offshore Structures (BOSS '92), Vol. 1, London, 1992.

21) Newman, J.N. (1994) "Wave effects on deformable bodies," Applied Ocean Research, 16, 1, pp. 47-59.

22) NORSOK Standard N-003 (2004) "Action and action effects".

23) OCIMF (Oil Companies Int. Marine Forum) (1994) "Prediction of wind and current loads on VLCCs". 2nd Edition.

24) Sarpkaya, T. and Isaacson, M. (1981) "Mechanics of Offshore Structures". Van Nostrand Reinhold Company.

25) Stansberg, C.T., Yttervik, R. and Nielsen, F.G. (1998) "Wave Drift Forces and Responses in Storm Waves". OMAE'98.

8. Air gap and Wave Slamming

8.1 General

Parts of the structure that are near the water surface are susceptible to forces caused by wave slamming when the structural part is being submerged.

Wave slamming may have both global and local effect. The impact of a massive bulk of water from a wave crest hitting the platform deck is a global load effect while wave slamming on a brace in the splash zone is a local load effect which usually does not influence the global structural capacity.

Slamming is due to sudden retardation of a volume of fluid. The retardation causes a considerable force to act on the structure.

8.2 Air gap

8.2.1 Definitions

8.2.1.1 Consider a floating structure where the still-water air gap, a_0, represents the difference in elevation between the bottom of the deck, or some other relevant part of the structure, and the mean water level. In the presence of waves and corresponding wave induced response of the structure, the instantaneous air gap, $a(x,y,t)$, at a given horizontal location (x,y) is different from a_0.

8.2.1.2 The instantaneous air gap is defined by

$$a(x, y, t) = a_0 + z(x, y, t) - \eta(x, y, t)$$

where $z(x,y,t)$ is the vertical displacement of the structure at (x,y) and $\eta(x,y,t)$ is the instantaneous surface elevation at the same horizontal position.

8.2.1.3 Negative air gap, $a(x,y,t) < 0$, means that there is impact between the wave and the structure.

8.2.2 Surface elevation

8.2.2.1 The surface elevation $\eta(x,y,t)$ includes global *upwelling* due to diffraction of incoming waves with the structure and local *run-up* in the form of jets and other strongly non-linear effects close to a vertical surface of the surface piercing structure.

8.2.2.2 To second order, the global upwelling for a floating structure includes first- and second-order contributions from incident (I), radiated (R) and diffracted (D) waves and may be written as follows:

$$\eta = \eta_I^{(1)} + \eta_{R,D}^{(1)} + \eta_I^{(2)} + \eta_{R,D}^{(2)}$$

For a fixed structure the there is no effect of radiated waves. Both sum- and difference-frequency (set-down) effects may contribute to $\eta^{(2)}$.

8.2.2.3 For a jacket or jack-up type of structure, where the surface piercing elements have small horizontal dimensions, diffraction effects can usually be neglected and the free surface elevation taken as the incident wave.

8.2.2.4 Tidal variations of mean sea water level, storm surge and subsidence of sea bed will affect air gap.

8.2.3 Local run-up

8.2.3.1 The evaluation of air gap at locations very close to vertical surfaces is challenging because of local run-up in the form of jets. Radiation-diffraction solutions based on a perturbation approach do not give reliable results closer than 0.15-0.20 times column diameter.

8.2.3.2 The run-up height, the volume of the jet and its kinematics is a function of the wave steepness and the wave height to diameter ratio.

8.2.3.3 Wave run-up factors derived from model tests should be used to account for local wave run-up or alternatively, direct measurements of run-up induced force.

8.2.4 Vertical displacement

8.2.4.1 For a floating structure the vertical displacement of the structure may be written as

$$z(x, y, t) = \xi_3(t) - x \sin[\xi_5(t)] + y \sin[\xi_4(t)]$$

where

$\xi_3(t)$ = heave translational motion

$\xi_4(t)$ = roll rotational motion

$\xi_5(t)$ = pitch rotational motion.

8.2.4.2 The sign convention adopted here is that the displacement ξ_3 is positive when directed in the positive z-direction, while the rotations ξ_4 and ξ_5 are positive with respect to the positive x and y directions respectively, using the right hand rule. The roll and pitch contributions to the heave displacement depend on the location of the field point.

8.2.4.3 Depending on the direction of the wave heading relative to the structure and the location of the field point in question, one or more of the rotational motion contributions to the displacement z can be zero.

8.2.4.4 The vertical displacement z of the structure at a field point (x,y) also consists of first- and second-order contributions, since

$$\xi_i = \xi_i^{(1)} + \xi_i^{(2)}, i = 3,4,5$$

8.2.4.5 Most structures have negligible 2nd order sum-frequency vertical motions, but certain floating platforms like semisubmersibles can exhibit considerable 2nd order slowly varying heave, pitch and roll motions.

8.2.4.6 For a structure with stiff mooring (TLP), set-down effects due to increased vertical tension for large horizontal excursions, must be taken into account when analysing air gap for such structures. For moored floaters in deep water, coupled analysis (7.1.4) may be necessary for prediction of displacement of the floater.

8.2.4.7 In some cases a static vertical displacement $\xi_t^{(0)}$ due to ballasting of the structure to even keel against the weather, must be accounted for.

8.2.5 Numerical free surface prediction

8.2.5.1 Numerically predicted second-order diffracted free surface elevation should be applied only after careful verification by convergence checks have been carried out.

8.2.5.2 The sum frequency radiated and diffracted wave elevation computed by a radiation-diffraction program is sensitive to the discretisation of the free surface, yielding the following recommendations:

— There should be at least 15 panels per second order wave length due to sum frequencies, i.e. 60 panels per linear wave length.
— The aspect ratio of the free surface panels should not be larger than 2. For panels bordering the structure, the longest side should face the body.
— The free surface should be discretized with a uniform and dense mesh.
— Special care should be given to the extent of the free surface mesh, ensuring that the numerical integration over the infinite free surface is being evaluated with necessary accuracy. Depending on the specific numerical method used in each program, detailed advice on this should be

given in the User's Manual.

— A structured and dense mesh is more crucial for convergence than a large extension of the free surface mesh.

8.2.5.3 The validity of second-order perturbation modelling of the diffracted free surface in vicinity of structures can be questioned for steep waves. Comparing with model tests Kristiansen et al. (2005) found deviations in the range 10-50% although there is a clear improvement relative to linear analysis. For short wave diffraction deviations can be even larger and model tests should be used, ref. Stansberg and Kristiansen (2006).

8.2.6 Simplified analysis

8.2.6.1 A simplified method to investigate air gap is to employ linear radiation-diffraction analysis to determine the diffracted wave field and the linearized platform motion. The surface elevation is then modified by a coefficient to account for the asymmetry of crests and troughs. The air gap is then defined by

$$a = \alpha \eta^{(1)} - z$$

where α is an asymmetry factor, $\eta^{(1)}$ is the linear local surface elevation and z is the vertical displacement at the location. a is then treated as a RAO for each location and for each frequency and each direction. The simplified method is not to be used very close to vertical columns (within one radius).

8.2.6.2 The use of an asymmetry factor $\alpha = 1.2$ is generally found to yield conservative results for standard floater concepts like TLP and semisubmersibles. For very special geometries, a higher value may be required. α varies along the $H_s(T_p)$ contour, generally decreasing as T_p increases.

8.2.6.3 The above simplified method is inaccurate for platforms with small draft, where shallow water effects may be expected above the pontoons or caisson. Also, for sea states having shorter wave periods the 'trapped' waves between multiple columns may be of importance. In such case these phenomena need to be investigated separately.

8.2.7 Wave current interaction

8.2.7.1 Wave-current interactions should be taken into account for strong currents in relatively steep waves. No exact criteria for when this effect is important in terms of current velocity and wave frequencies can be given. A measure of linear wave-current interaction effects is given by the Brard number $\tau = U_c \omega / g$ where U_c is current velocity, ω is the wave angular frequency and g is the acceleration of gravity.

8.2.7.2 Free surface elevation in pure current without waves is governed by the Froude number $Fn = U_c / \sqrt{gD}$ where D is a characteristic dimension of the structure at the water level.

8.2.7.3 Computer programs based on the sink-source technique are available for prediction of linear diffracted surface elevation where terms of order current velocity squared are neglected. This is a good estimate if the Brard number τ and the Froude number are small. Theoretically, τ must be less than 0.25 for upstream waves to exist, and the wave-current interaction theory to be valid since it assumes waves propagating in all directions. This means that the theory gets more inaccurate for lower periods. $\tau = 0.15$ is suggested as a higher limit of reliable results As an example this means that the theory gets more inaccurate for periods on the order of 6.5 sec and below for a current speed of 1.5 m/s. This may be within a range of wave periods where the relative wave elevation is large.

8.2.8 Air gap extreme estimates

8.2.8.1 When estimating air gap extreme values it is convenient to define a new air gap response variable $\tilde{a}$,

$$\tilde{a}(t) = a_0 - a(t)$$

so that extreme minimum air gap corresponds to maximum $\tilde{a}$. One should note that in a random sea, the two processes $\eta(t)$ and $z(t)$ are not independent since the vertical displacement of a specific location on the floater is a function of the wave motion.

8.2.8.2 When estimating air gap extremes, the static, wave frequency and slowly varying contributions shall be combined. The correlation between slowly varying and wave frequency contributions to air gap is low, on the order of 0.1.

8.3 Wave-in-deck

The following is a physical interpretation of the wave-in-deck interaction, as observed for a wave crest hitting head-on a simple box-type deck structure attached to a fixed jacket-type platform. It illustrates the main contributions to the global force identifying local and global structural impacts and the time instants for maximum and minimum wave-in-deck forces.

8.3.1 Horizontal wave-in-deck force

8.3.1.1 The horizontal wave-in-deck force has contributions from slamming, drag and inertia. Slamming and drag contributions are quadratic in velocity and governed by the high wave particle velocity in the crest. Inertia contributions are proportional to fluid particle acceleration. The slamming contribution is of short duration and drops to zero shortly after the initial impact.

8.3.1.2 The fluid particles underneath the deck are accelerated in a jet-like flow when the wave crest hits the deck (see also 8.3.7). The drag contribution remains reasonably steady as the wave passes the deck.

8.3.1.3 The magnitude of the inertia contribution depends on the horizontal acceleration and the rate of change of the wetted vertical area. As the horizontal acceleration is zero at the crest and increases at lower elevations, the inertia term contribution is dependent on the immersion of the structure.

8.3.1.4 The negative water exit forces (Figure 8-1) is due to the low pressure at the frontal wall caused by the vertical downward fluid velocity. The magnitude is dependent on the crest velocity and the immersion of the structure.

8.3.2 Vertical wave-in-deck force

8.3.2.1 The vertical upward force is critical for local structural details because the force acts over a small area, leading to high local pressures. It is dominated by slamming forces, which is proportional to the wetted length times the wave particle velocity squared.

8.3.2.2 As the wave runs along the underside of the deck, the wave front causes slamming loads at each new location. The magnitude of the slamming load is largest at the inflow side and reduces moderately as the wave reaches the other side, resulting in a relatively wide global force peak (Figure 8-1). The global vertical impact force has its maximum when the wave crest passes the front of the deck, at the minimum (negative) air gap. The local impact force has its maximum at a slightly earlier stage.

8.3.2.3 The inertia force acts downwards as the wave passes by, since the vertical fluid acceleration in the crest is negative. During the initial stage of the wave cycle, the inertia term is small due to the small wet area, and it acts in opposite direction

of the slam and drag forces. When the whole underside of the deck structure is wet, the inertia term is at its maximum due to the maximum added mass force. At this time instant, which is important for global effects due to the large exposed area, the crest has passed the centre of the structure and the vertical velocity has changed to negative, i.e. acting downward in the same direction as the inertia force.
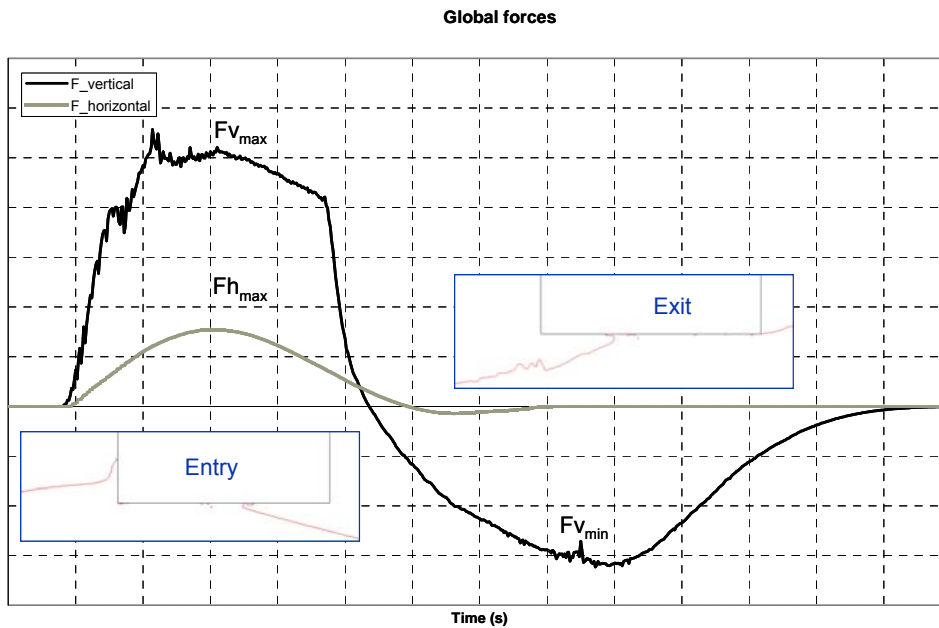

Figure 8-1
Vertical and horizontal wave-in-deck load on a rectangular box.

8.3.2.4 The vertical force at water exit is dependent on the wetted length of the structure and to a lesser degree of the impact condition and the immersion. Slamming is not defined for water exit. When girders are present, the flow is disturbed, which in turn reduces the wetted length and the magnitude of the vertical downward force.

8.3.2.5 When assessing the structural resistance, it is important to consider the transient nature of the wave-in deck loads.

8.3.2.6 It should be noted that negative pressure force during water exit means that the normal pressure is lower than atmospheric pressure, resulting in a downward acting force.

8.3.3 Simplified approach for horizontal wave-in-deck force

8.3.3.1 A simplified method for predicting horizontal global wave-in-deck forces is the API method (API RP2A-WSD). The method is a drag formulation. The simplified procedure relies on a given crest height. The crest height should be calculated using methods in Ch.3. The steps for predicting wave-in-deck force and its point of application are as follows:

8.3.3.2 For a given crest height, compute the wetted "silhouette" deck area, A, projected in the wave direction, θ_w.

8.3.3.3 The silhouette is defined as the shaded area in Figure 8-2 i.e. the area between the bottom of the scaffold deck and the top of the "solid" equipment on the main deck. The areas of deck legs and bracings above cellar deck are part of the silhouette area. The area, A is calculated as follows:

$$A = A_x \cos\theta_w + A_y \sin\theta_w$$

where θ_w, A_x and A_y are defined in Figure 8-3.

8.3.3.4 Calculate the maximum wave-induced horizontal fluid velocity, V, at the crest elevation or the top of the main deck silhouette, whichever is lower.

8.3.3.5 The wave-in-deck horizontal force on the deck is calculated by the following formula

$$F_h = \frac{1}{2}\rho C_h V^2 A$$

where ρ is the mass density of water and the horizontal force coefficient for a heavily equipped (solid) deck is given by

$$C_h = \begin{cases} 2.5 \text{ for end - on and broadside} \\ 1.9 \quad \text{for diagonal}\,(\theta_w = 45°) \end{cases}$$

8.3.3.6 The force F_h should be applied at an elevation above the bottom of the cellar deck, defined as 50 percent of the distance between the lowest point of the silhouette area and the lower of the wave crest or top of the main deck.

8.3.3.7 The simplified method should be used with care for structures with overhanging parts, where water may be trapped. In such cases the horizontal force might be significantly higher, possibly doubled for head-on and broad-side waves.

8.3.3.8 The force coefficient will also be larger for low impact heights when there are multiple obstacles along the deck underside, e.g. a number of girders, which the projected area approach does not reflect. In such cases the force coefficient should be larger, up to $C_h = 3.5$ for head-on waves.
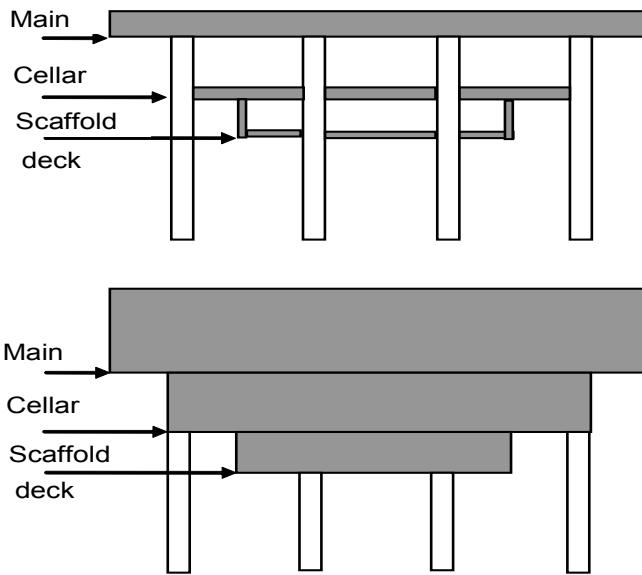
Figure 8-2
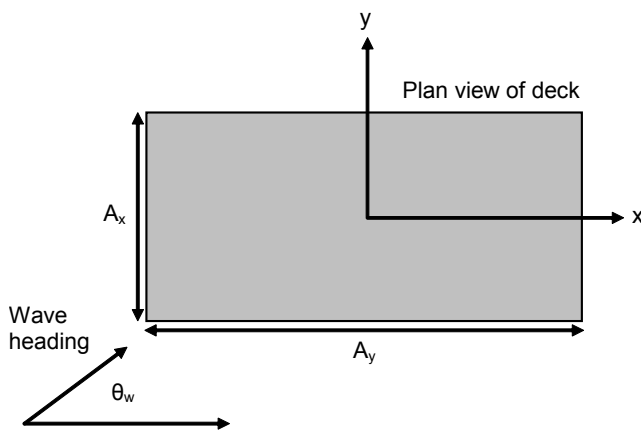**Definition of silhouette area (from API RP2A-WSD)**

Figure 8-3
Wave heading and direction convention (from API RP2A-WSD)

8.3.4 Momentum method for horizontal wave-in-deck force

8.3.4.1 A robust method for predicting wave impact forces on deck structures is the method of Kaplan et al. (1995). The method is limited to 2D and an undisturbed incoming wave field. An expression for the wave-in-deck force is found from the principle of conservation of fluid momentum.
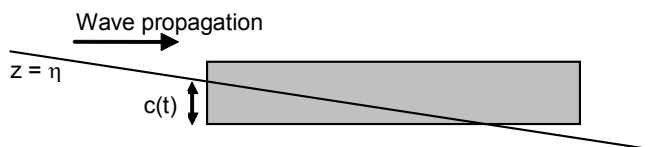

Figure 8-4
Definition of vertical wetted length

8.3.4.2 The horizontal wave impact force on a solid deck structure can be estimated assuming that the deck has effectively a solid vertical short plating around the outer boundary of the deck. The sectional lateral added mass of a vertical plate surface with wetted vertical length *c*, is given by (Kaplan, 1995),

$$m_{a,x} = (2/\pi)\rho c^2$$

8.3.4.3 Assuming that the maximum value of the vertical wetted length *c* is much smaller than the horizontal width *B*, normal to the wave propagation direction, the total lateral added mass is given by (see Figure 8-4),

$$M_{a,x} = (2/\pi)\rho c^2 B.$$

8.3.4.4 Including both inertia momentum change and drag, the horizontal force time history in the wave propagation direction is given by

$$F_h(t) = M_{a,x}\dot{u} + \frac{dM_{a,x}}{dt}u + \frac{1}{2}\rho c C_D B u|u|$$

where

c = $c(t)$ is the instantaneous vertical wetted length
u = $u(t)$ is the instantaneous horizontal particle velocity in undisturbed wave
$dM_{a,x}/dt$ = $(4/\pi)\rho c(dc/dt)B$ is the rate of change of lateral added mass
C_D = drag coefficient

8.3.5 Simplified approach for vertical wave impact force

8.3.5.1 The vertical wave-in-deck force on a heavily equipped or solid deck can be predicted from the vertical velocity in the wave at the point of initial contact and the wetted deck area at the time instant of maximum vertical impact force. The method is developed for a simple box-type deck. For other types of deck configurations, such as decks with overhanging parts or multiple crosswise girders, the vertical wave impact force may be significantly larger. The wave profile and wave kinematics should be computed by the wave theory recommended in Ch.3.

8.3.5.2 For a given crest height defined from a specified storm condition, determine the phase at which the lowest part of the deck encounters the wave.

8.3.5.3 Compute the vertical (upwards) velocity, v_z, in the wave at this location. The wetted deck length, *L*, should be taken as the horizontal distance from the point of encounter to where the wave crest is at maximum. The wetted deck area, *A*, is determined by the wetted length and deck configuration, see Figure 8-5.

8.3.5.4 The vertical upwards wave-in-deck force is then calculated by the formula

$$F_v = \frac{1}{2}\rho C_v A v_z^{\,2}$$

where

C_v = 5 for head-on and broadside waves

C_v = 10 for 45° oblique waves.

8.3.5.5 The vertical upwards force should be distributed evenly over the wetted deck area. The simplified method is valid for global forces, while local impact forces of nearly the same magnitude occurs along the whole deck underside, see 8.3.2 above.

8.3.5.6 The vertical downwards force should also be considered. The magnitude of the downwards force can be larger than the upwards force if the underside of the deck is smooth, which may be the case when a large bottom tank is present.
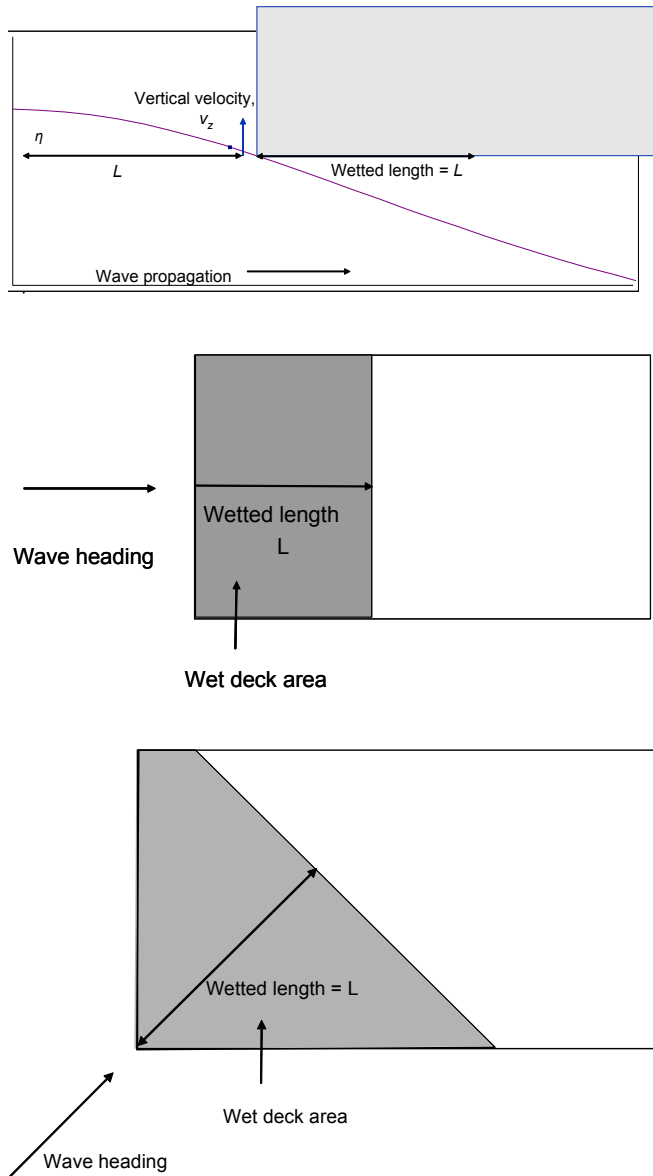
Figure 8-5
Definition of wetted length and vertical velocity in wave for max vertical impact force

8.3.6 Momentum method for vertical wave-in-deck force

8.3.6.1 The vertical impact force on a solid horizontal deck structure is given by the combined effect of rate of change of momentum and a drag force. Approximating the wetted part of deck structure by a flat plate of length *L* and width *B*, and assuming waves propagating in a direction along the length of the plate, the vertical impact force is given by

$$F_v(t) = \frac{d}{dt}(M_{a,z}w) + \frac{1}{2}\rho BLC_D w|w|$$

8.3.6.2 The three-dimensional vertical added mass of the rectangular flat plate deck structure is given by

$$M_{a,z}(t) = \rho \frac{\pi}{8} BL^2 \left[1 + (L/B)^2\right]^{-1/2}$$

w = *w*(*t*) is the vertical velocity at the deck underside and

L = *L*(*t*) is the wetted length. The quantities *L* and *dL/dt* are determined from the relative degree of wetting of the flat deck underside, which occurs as the incident wave travels along the deck from its initial contact location.

8.3.6.3 In the free field case, i.e. for the deck of a jacket structure, where the incoming wave is not disturbed by the platform, the quantity *dL/dt* can be approximate by the wave phase velocity. The term

$w dM_{a,z}/dt$ varies continuously up to the time when the wetted length *L* reaches the end of the plate, after which *dL/dt* = 0 and that term is then zero throughout the remaining time that the particular wave elevation is contacting the deck. The term is also taken to be zero when $w_z < 0$, that is when the wave leaves the plate. This contributes to the sign reversal of the vertical force.

8.3.6.4 The value of the drag coefficient C_D can be taken as 2.0. The value of vertical velocity w_z and vertical acceleration dw_z/dt is that corresponding to the vertical location of the deck. During the impact, the kinematics is found at each time instant at the location of the geometric centre of the wetted region being considered.

8.3.6.5 For a general deck geometry the wetted area can be approximated by a flat plate with a boundary determined by the instantaneous intersection between the deck and the incident wave.

8.3.6.6 The added mass of the arbitrary shaped plate can be approximated by the added mass of an elliptical plate in the free surface. The axes of the ellipse is found by requiring the area and aspect ratio equal for the two geometries, Baarholm (2005).

8.3.6.7 The high frequency limit of the added mass of a thin elliptical plate with axes *a*/2 and *b*/2 oscillating in the free surface is given by half its value in unbounded fluid,

$$M_{a,z} = \frac{1}{6}\rho C_A \pi a^2 b$$

where the coefficient C_A can be found by interpolation in Table D-2 in Appendix D.

8.3.6.8 When the wave is just reaching the deck, great accuracy in both the wave elevation and the fluid particle kinematics are required in order to predict forces with acceptable accuracy. The resulting force for mild impacts is however small, and the absolute errors in the computed force is therefore also small.

8.3.6.9 Kaplan's method may underestimate the magnitude of the upwards directed wave-in-deck force because diffraction due to the deck is omitted and thus the $dM_{a,z}/dt$ is underestimated.

8.3.7 Diffraction effect from large volume structures

8.3.7.1 An extension of Kaplan's method to include first and second-order three-dimensional large volume diffraction effects, general deck geometries and arbitrary incoming wave direction was proposed by Baarholm (2005).

8.3.7.2 Large volume diffraction effects can be due to large diameter columns supporting the deck (e.g. GBS, Semi) or due to other large volume structures in the vicinity of the deck, e.g. a vertical barrier.

8.3.7.3 When the wave kinematics is strongly affected by the large volume structure, the fluid impact velocity and acceleration should be computed by a diffraction analysis.

8.3.7.4 When a wave crest hits the deck, the kinematics in the wave beneath the deck is strongly influenced by the deck itself. A jet effect may occur, increasing the horizontal fluid particle velocity to values even higher than the phase velocity of the wave. This increased velocity should be accounted for when assessing the load on obstructions located in a zone beneath the deck. The vertical extension of the disturbed velocity field is dependent on the smoothness of the structure, e.g. tank bottom or girders, and the immersion of the structure.

8.4 Wave-in-deck loads on floating structure

8.4.1 General

8.4.1.1 The inertia momentum method can also be used to predict the vertical water impact loads on a floating structure such as a semisubmersible. There are three main differences between impact on a floater and on a bottom-mounted platform.

— the platform motion contribute to the relative impact velocity and acceleration
— the deck height varies in time and space
— the impact will to some extent influence the motion of the platform.

8.4.1.2 All these three items should in principle be accounted for. A wave diffraction program should be used to compute first and second order platform motion and the relative fluid kinematics.

8.4.1.3 If the water impact loads are significant in magnitude and duration, they may introduce rigid body motions that cannot be disregarded in the computation of the wave-in-deck load.

8.4.1.4 The impact induced motion may contribute to the relative velocity and acceleration, and therefore also affects the instantaneous deck height.

8.5 Computational Fluid Dynamics

8.5.1 General

8.5.1.1 Computational Fluid Dynamics (CFD) can be used to assess the distribution of forces on a general three-dimensional platform deck of arbitrary geometry. A suitable method for simulation of wave-in-deck loads is the Volume-of-Fluid (VOF) method which allows for break-up of fluid particles and changing topology of fluid domain (Kleefsman, 2004). A fully nonlinear Boundary Element Method (BEM) may also be used, but special boundary conditions must be applied at intersection points (Baarholm, 2004).

8.5.1.2 Three-dimensional analyses is required. When applying CFD, convergence tests must be carried out to ensure that the fluid cells are sufficiently small. The computational domain should be large enough to avoid reflections from boundaries.

8.5.1.3 The software applied should have means to identify whether simulated pressure spikes are physical or purely numerical.

8.5.1.4 An incoming non-linear wave with appropriate crest height, wave period and corresponding wave kinematics is applied at the inflow boundary. CFD results should be validated with benchmark model tests results.

8.6 Wave impact loads on slender structures

8.6.1 Simplified method

8.6.1.1 For a cylindrical shaped structural member the slamming force per unit length may be calculated as:

$$F_s = \frac{1}{2} \rho C_s D v^2$$

where F_S is the slamming force per unit length in the direction of the velocity, ρ is mass density of the fluid, C_S is the slamming coefficient, D is member diameter, v is relative velocity between water and member normal to the member surface.

8.6.1.2 For a smooth circular cylinder the slamming coefficient can be taken as $C_S = 5.15$ (see also 8.6.3.4).

8.6.1.3 If dynamic effects are important both the water entry and the exit phases should be modelled. Modelling of water exit of a horizontal circular cylinder is described in Zhu et al. (2005).

8.6.2 Slamming on horizontal slender structure

8.6.2.1 A method to predict time history of slamming forces on horizontal slender structure is given by Kaplan (1992). Assuming waves propagating normal to the cylinder horizontal axis, the vertical force per unit length of the cylinder can be expressed by

$$F_z(t) = \rho g A_1 + (m_{a,3} + \rho A_1)\ddot{\eta} + \frac{\partial m_{a,z}}{\partial z}\dot{\eta}^2 + \frac{\rho}{2}\dot{\eta}|\dot{\eta}|d(z/r)C_D^z(z/r)$$

where

$\rho g A_1$	is the buoyancy force
$\rho A_1 \ddot{\eta}$	represents the effect of the spatial pressure gradient in the waves
$m_{a,3}$	is the vertical added mass which is a function of the degree of immersion (as is A_1)
$d(z/r)$	is the varying cross-section horizontal length reference for drag force evaluation (with a maximum value equal to the cylinder diameter). See Figure 8-6.
$C_D^z(z/r)$	is a drag coefficient for vertical flow, being a function of immersion, but can be taken to have a constant value 1.0

8.6.2.2 The terms involving m_3 are found from the time rate of change of vertical fluid momentum; and the last term in the equation represents a drag force. The inertia term proportional to $\dot{\eta}^2$ is only evaluated when $\dot{\eta} > 0$, corresponding to condition of increasing immersion. When $\dot{\eta} < 0$ this term is set to zero.
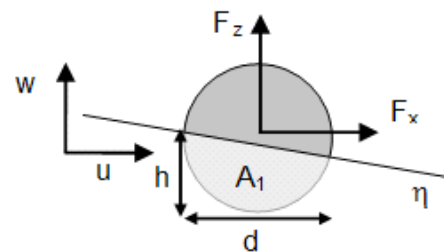

Figure 8-6
Slamming on horizontal cylinder

8.6.2.3 A similar expression is available for the horizontal impact force per unit length

$$F_x(t) = (\rho A_1 + m_{a,1})\dot{u} + \frac{\partial m_{a,1}}{\partial z}\dot{\eta}u + \frac{\rho}{2}u|u|h(z/r)C_D^x(z/r)$$

where

$m_{a,1}$ is the horizontal added mass ($m_{a,1} = \rho\pi R^2$)

u is the horizontal fluid particle velocity

$h(z/r)$ is the vertical reference length which varies with immersion and has a maximum value equal to the cylinder diameter

$C_D^x(z/r)$ is the lateral drag coefficient, which physically varies in accordance with the degree of immersion, but can be taken as the constant value 1.0.

For a circular cylinder the rate of change of horizontal added mass is given by $\partial m_1/\partial z = 4\rho R/\pi$.

8.6.3 Slamming on vertical slender structure

8.6.3.1 Slamming forces on a vertical cylinder can be predicted in a strip-wise manner by summing up the force acting on each strip of the cylinder as it penetrates the wave surface (Nestegård et al. 2004).

8.6.3.2 The dominating contribution to sectional force F_x at height z when the wave hits the cylinder, is the rate of change of added mass momentum

$$F_x(z,t) = \frac{d}{dt}\left[A^{2D}(t;z)\,u\right] = \frac{d}{ds}\left[A^{2D}(s;z)\right]u^2 = \frac{1}{2}\rho C_s D u^2$$

where A^{2D} is the high-frequency limit of the added mass for a 2D cylindrical section as a function of submergence $s = s(t)$ relative to the wave surface and u is the relative horizontal velocity between wave surface and cylinder. u is assumed constant during penetration.

8.6.3.3 Experimental values for the rate of change of added mass of a circular cylinder with respect to penetration distance s are available and have been represented by an analytical formula by Campbell & Weynberg (1980). The slamming or *impact coefficient* is defined by

$$C_s = \frac{2}{\rho D}\frac{dA^{2D}}{ds}$$

where D is the cylinder diameter. An analytic fit to the experiments is

$$C_s(s) = 5.15\left[\frac{D}{D+19s} + \frac{0.107s}{D}\right]$$

8.6.3.4 At start of impact $C_s(0) = 5.15$. The above model is a good approximation when the impacting wave is steep. The formula above shall be applied only during penetration of the wave surface, i.e. for $0 < s < D$. When the cylinder is fully submerged, $C_s(D) = 0.8$.

8.6.3.5 The formulae above give the distributed impact forces along the cylinder. When the cylinder section is fully submerged, the appropriate load model is the conventional Morison's equation with mass and drag terms using constant mass and drag coefficients.

8.7 Wave impact loads on plates

8.7.1 Slamming loads on a rigid body

8.7.1.1 Parameters characterizing slamming on a rigid body with a small deadrise angle are the position and value of the maximum pressure, the time duration and the spatial extent of high slamming pressures. Figure 8-7 gives a schematic view of water entry of a two-dimensional body onto a calm free surface. The free surface is deformed resulting in spray and the formation of a jet.

8.7.1.2 The local deadrise angle is an important parameter, but the effect of local curvature and the time history of the deadrise angle and curvature matter as well. Three-dimensional effects will tend to reduce the slamming pressure. Cushioning effects may significantly reduce the peak pressure when the angle between the impacting body and free surface is less than 2-3°.

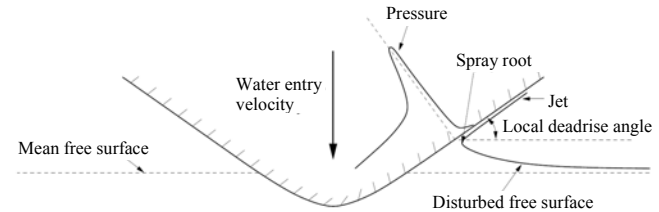**Figure 8-7**
Schematic view of water entry of a body onto a calm free surface

8.7.1.3 Figure 8-8 presents definition of parameters characterizing slamming pressures on a rigid wedge shaped body during water entry. The body enters the undisturbed free surface with a constant downward velocity V. The mean free surface is located at $z = 0$ and the spray root is at (y_{max}, z_{max}).

β =   deadrise angle

C_{Pmax} =   pressure coefficient at maximum pressure

z_{max} =   z-coordinate of maximum pressure

ΔS_S =   spatial extent of slamming pressure exceeding 50% of maximum pressure

F_3 =   vertical hydrodynamic force on the wedge

t =   time

8.7.1.4 The wetted length of a symmetric wedge (from vertex to spray root) can be approximated by the formula

$$c(t) = \frac{\pi V t}{2\tan\beta}$$

The formula is based on the Wagner method (1932) and gives a good estimate for low deadrise angles ($\beta < 15\text{-}20°$).

8.7.1.5 Table 8-1 presents values for the parameters characterizing the slamming pressure, including the total vertical hydrodynamic force, z-coordinate of the maximum pressure and spatial extent of slamming pressure exceeding 50% of maximum pressure. When the deadrise angle β is below about 20°, the pressure distribution has a pronounced peak close to the spray root.

8.7.1.6 Experiments may be needed in order to give accurate estimates of impact loads, ref. 10.6.8 Slamming loads can also be predicted by the method described in 8.6.2 which is based on the rate of change of added mass.

8.7.2 Space averaged slamming pressure

8.7.2.1 The highest pressure during water entry of a wedge with a small deadrise angle is usually not relevant for steel structures. As described in 8.7.1 the pressure peak is localised in time and space.

Table 8-1 Calculation of slamming parameters by similarity solution during water entry of a wedge with constant vertical velocity V (Zhao and Faltinsen 1993)

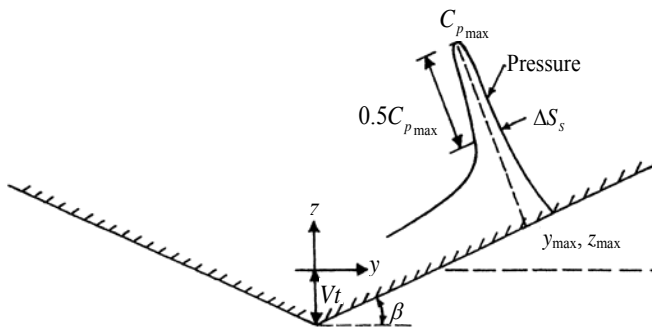| β	C_{Pmax}	z_{max}/Vt	$\Delta S_S/c$	$F_3/\rho V^3 t$
4°	503.030	0.5695	0.0150	1503.638
7.5°	140.587	0.5623	0.0513	399.816
10°	77.847	0.5556	0.0909	213.980
15°	33.271	0.5361	0.2136	85.522
20°	17.774	0.5087	0.4418	42.485
25°	10.691	0.4709		23.657
30°	6.927	0.4243		14.139
40°	3.266	0.2866		5.477

Figure 8-8
Definition of parameters characterizing slamming pressure during water entry of a blunt 2D rigid body. The pressure coefficient is given by $C_{Pmax} = (p-p_a)/(0.5\rho V^2)$. From Faltinsen (2005)

8.7.2.2 Space average slamming pressure over a broader area (i.e. several plate fields of a ship) can be calculated from:

$$p_s = \frac{1}{2}\rho C_{Pa} v^2$$

where

p_s = space average slamming pressure
ρ = mass density of fluid
C_{Pa} = space average slamming pressure coefficient
v = relative normal velocity between water and surface

8.7.2.3 The space average slamming pressure coefficient should be determined using recognised theoretical and/or experimental methods. One example is the exact solution of the two-dimensional water entry problem by (Zhao and Faltinsen 1993). A simplification which is numerically faster, more robust and gives satisfactory results is developed by (Zhao et al. 1996) for two-dimensional geometries.

8.7.2.4 The values presented in the following should not be used to predict extreme local slamming pressure.

8.7.2.5 For a smooth circular cylinder the slamming pressure coefficient should not be taken less than $C_{Pa} = 5.15$. For flat bottom slamming taking account of cushioning and three dimensional effects, the slamming pressure coefficient should not be taken less than $C_{Pa} = 2\pi$. This applies to deadrise angle β less than 4°.

8.7.2.6 For a wedge shaped body with deadrise angle β above 15°, taking account of three dimensional effects the slamming pressure coefficient should not be taken less than:

$$C_{Pa} = \frac{2.5}{(\tan\beta)^{1.1}}$$

where β is the wedge angle at the intersection between body and water surface. This empirical formula is based on a curve-fit of the apex pressure in Figure 8-9.
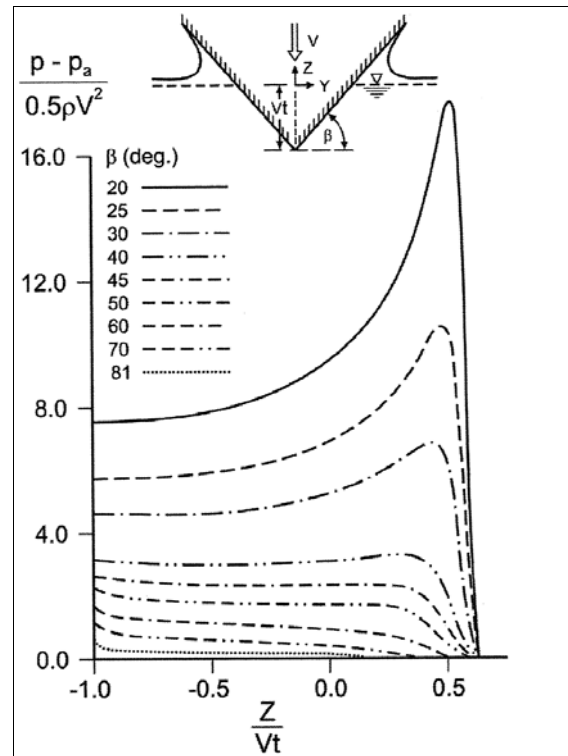

Figure 8-9
Predictions of pressure (*p*) distribution during water entry of a rigid wedge with constant vertical velocity *V*. p_a = atmospheric pressure, β = deadrise angle. From Faltinsen (2005), Zhao and Faltinsen (1993)

8.7.2.7 For a wedged shaped body with $0 < \beta < 15°$, taking account of cushioning and three dimensional effects, a linear interpolation between results for flat bottom ($C_{Pa} = 2\pi$ for $\beta = 0°$) and $\beta = 15°$ can be applied, see Figure 8-9.
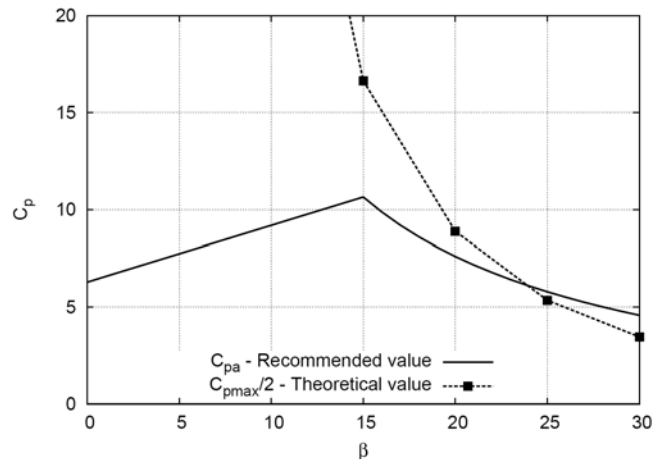

Figure 8-10
Space average slamming pressure coefficient C_{Pa} compared with $C_{Pmax}/2$ from Table 8-1 for a wedge shaped body as a function of local deadrise angle β.

8.7.2.8 In a practical analysis of slamming loads on ships, it is challenging to estimate the relevant angle between the structure and impinging water surface. When impacts with a local deadrise angle β less than 15° can be expected, the stiffeners and larger structures may be dimensioned based on the space average slamming coefficient for $\beta = 15°$, $C_{Pa} = 10.64$ (calculated from formula in 8.7.2.6). For the local structure, i.e. plate, a twice as large slamming coefficient $C_{P\,local} = 21.28$ should be applied.

8.7.3 Hydroelastic effects

When slamming loads cause structural deformations or vibrations of the structure, the hydrodynamic loading is affected. The slamming pressure is a function of the structural deflections. In such cases hydroelastic effects should be accounted for. In general it is conservative to neglect hydroelastic effects.

8.7.3.1 For slamming on stiffened plates between bulkheads, hydroelastic effects is important when

$$\sqrt{\frac{EI}{\rho L^2}} \frac{\tan \beta}{|V_R|} < 0.25$$

where *EI* is the bending stiffness of a representative beam, *L* is the length of the beam (Figure 8-11), β is the angle of impact and V_R is the relative normal velocity (Faltinsen, 1999).
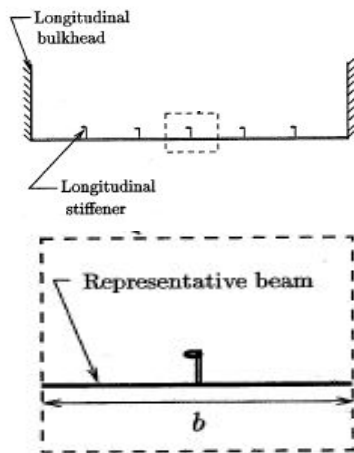

Figure 8-11
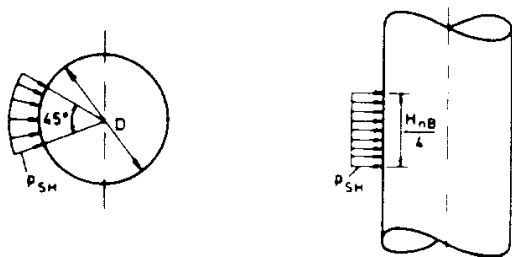**Representative beam for stiffened panel (Faltinsen, 1999)**

Figure 8-12
Area to be considered in evaluating the loads due to shock pressure on circular cylinders

8.8 Breaking wave impact

8.8.1 Shock pressures

8.8.1.1 Shock pressures due to breaking waves on vertical surfaces should be considered. The procedure described in 8.6.3 may be used to calculate the shock pressure. The coefficient C_s depends on the configuration of the area exposed to shock pressure.

8.8.1.2 For undisturbed waves the impact velocity (*u*) should be taken as 1.2 times the phase velocity of the most probable highest breaking wave in *n* years. The most probable largest breaking wave height may be taken as 1.4 times the most probable largest significant wave height in *n* years. For impacts in the vicinity of a large volume structure, the impact velocity is affected by diffraction effects.

8.8.1.3 For a circular vertical cylinder, the area exposed to shock pressure may be taken as a sector of 45° with a height of $0.25\,H_b$, where H_b is the most probable largest breaking wave height in *n* years. The region from the still water level to the top of the wave crest should be investigated for the effects of shock pressure.

8.8.1.4 For a plunging wave that breaks immediately in front of a vertical cylinder of diameter *D*, the duration *T* of the impact force on the cylinder may be taken as

$$T = \frac{13D}{64c}$$

where *c* is the phase velocity of the wave (Wienke, 2000).

8.9 Fatigue damage due to wave impact

8.9.1 General

The fatigue damage due to wave slamming may be determined according to the following procedure:

— Determine minimum wave height, H_{min}, which can cause slamming
— Divide the long term distribution of wave heights, in excess of H_{min}, into a reasonable number of blocks
— For each block the stress range may be taken as:

$$\Delta \sigma_j = 2\left[A\,\sigma_{slam} - (\sigma_b + \sigma_w)\right]$$

where

σ_{slam} = stress in the element due to the slam load given in 6.4.2

σ_b = stress due to the net buoyancy force on the element

σ_w = stress due to vertical wave forces on the element

A = factor accounting for dynamic amplification.

— Each slam is associated with 20 approximate linear decaying stress ranges.
— The contribution to fatigue from each wave block is given as:

$$y_j = R\,\frac{n_j}{N_j} \sum_{i=20-n_i}^{i=20} \left(\frac{i}{20}\right)^k$$

where

n_j = number of waves within block j

N_j = critical number of stress cycles (from relevant S-N curve) associated with $\Delta\sigma_j$

n_i = number of stress ranges in excess of the limiting stress range associated with the cut off level of the S-N curve

R = reduction factor on number of waves. For a given element only waves within a sector of 10° to each side of the normal direction to the member have to be accounted for. In case of an unidirectional wave distribution, R equals 0.11

k = slope of the S-N curve (in log-log scale)

8.9.1.1 The calculated contribution to fatigue due to slamming has to be added to the fatigue contribution from other variable loads.

8.9.1.2 The method of Ridley (1982) can be used to estimate fatigue damage of inclined slender structures in the splash-zone.

References

1) API RP 2A-WSD "Recommended practice for planning, designing and constructing fixed offshore platforms – Working Stress Design".

2) Baarholm, R. and Faltinsen, O. M. (2004) "Wave impact underneath horizontal decks". J. Mar. Sci. Technol. Vol. 9, pp. 1-13.

3) Baarholm, R. (2005) "A simple numerical method for evaluation of water impact loads on decks of large-volume offshore platforms". Proc. OMAE Conf., June 12-17, 2005, Halkidiki.

4) Campbell, I.M.C. and Weynberg, P.A. (1980): "Measurement of Parameters Affecting Slamming", Rep. 440, Tech. Rep. Centre No. OT-R-8042, Southampton University.

5) Faltinsen, O.M. (1999) "Water entry of a wedge by hydroelastic orthotropic plate theory". J. Ship Research, 43(3).

6) Faltinsen, O.M. (2005) "Hydrodynamics of high-speed marine vehicles". Cambridge University Press.

7) Kaplan, P. (1992) "Wave Impact Forces on Offshore Structures. Re-examination and New Interpretations". OTC 6814.

8) Kaplan, P., Murray, J.J. and Yu, W.C. (1995) "Theoretical Analysis of Wave Impact Forces on Platform Deck Structures", Proc. OMAE Conf., Vol. I-A, pp 189-198.

9) Kleefsman, T., Fekken, G., Veldman, A. and Iwanowski, B. (2004). "An improved Volume-of-Fluid Method for Wave Impact Problems. ISOPE Paper No. 2004-JSC-365.

10) Kristiansen, T., Brodtkorb, B., Stansberg, C.T. and Birknes, J. (2005) "Validation of second-order free surface elevation prediction around a cylinder array". Proc. MARINE 2005, Oslo.

11) Nestegård, A., Kalleklev, A.J., Hagatun, K., Wu, Y-L., Haver, S. and Lehn, E. (2004) "Resonant vibrations of riser guide tubes due to wave impact". Proc. 23rd Int. Conf. Offshore Mechanics and Arctic Engineering, Vancouver, Canada, 20-25 June 2004.

12) Ridley J.A., 1982: "A study of some theoretical aspects of slamming", NMI report R 158, OT-R-82113, London.

13) Stansberg, C.T., Baarholm, R., Kristiansen, T., Hansen, E.W.M. and Rørtveit, G., (2005), "Extreme wave amplifications and impact loads on offshore structures", Paper 17487, *Proc. OTC 2005*, Houston, TX, USA.

14) Stansberg, C.T. and Kristiansen, T. (2006), "Non-linear scattering of steep surface waves around vertical columns". To appear in Applied Ocean Research.

15) Wagner, H. (1932) "Über Stoss- und Gleitvorgänge an der Oberfläche von Flüssigkeiten". Zeitschr. f. Angewandte Mathematik und Mechanik, 12, 4, 193-235.

16) Wienke, J., Sparboom, U. and Oumeraci, H. "Breaking wave impact on a slender cylinder". Proc. 27th ICCE, Sydney, 2000.

17) Zhao, R. and Faltinsen, O.M. (1993) "Water entry of two-dimensional bodies". Journal of Fluid Mechanics; Vol. 246: pp. 593-612.

18) Zhao, R., Faltinsen, O.M. and Aarsnes, J.V. (1996) "Water entry of arbitrary two-dimensional sections with and without flow separation". 21st Symp. on Naval Hydrodynamics, Trondheim, Norway.

19) Zhu, X., Faltinsen, O.M. and Hu, C. (2005) "Water entry and exit of a horizontal circular cylinder". Proc. OMAE2005. June 12-17, 2005, Halkidiki, Greece.

9. Vortex Induced Oscillations

9.1 Basic concepts and definitions

9.1.1 General

Wind, current or any fluid flow past a structural component may cause unsteady flow patterns due to vortex shedding. This may lead to oscillations of slender elements normal to their longitudinal axis. Such vortex induced oscillations (VIO) should be investigated.

Important parameters governing vortex induced oscillations are

— geometry (L/D)
— mass ratio ($m^* = m/(\frac{1}{4}\pi\rho D^2)$)
— damping ratio (ζ)
— Reynolds number ($R_e = uD/\nu$)
— reduced velocity ($V_R = u/f_n D$)
— flow characteristics (flow profile, steady/oscillatory flow, turbulence intensity (σ_u/u) etc.).

where

L	=	member length (m)
D	=	member diameter (m)
m	=	mass per unit length (kg/m)
ζ	=	ratio between damping and critical damping
ρ	=	fluid density (kg/m³)
ν	=	fluid kinematic viscosity (m²/s)
u	=	(mean) flow velocity (m/s)
f_n	=	natural frequency of the member (Hz)
σ_u	=	standard deviation of the flow velocity (m/s)

This chapter provides guidance on methods for determining the motion amplitude and/or forces on the member due to vortex shedding.

9.1.2 Reynolds number dependence

For rounded hydrodynamically smooth stationary members, the vortex shedding phenomenon is strongly dependent on Reynolds number for the flow, as given below.

$10^2 < R_e < 0.6 \times 10^6$	Periodic shedding
$0.6 \times 10^6 < R_e < 3 \times 10^6$	Wide-band random shedding
$3 \times 10^6 < R_e < 6 \times 10^6$	Narrow-band random shedding
$R_e > 6 \times 10^6$	Quasi-periodic shedding

For rough members and for smooth vibrating members, the vortex shedding shall be considered strongly periodic in the entire Reynolds number range.

9.1.3 Vortex shedding frequency

The vortex shedding frequency in steady flow or flow with K_C numbers greater than 40 may be calculated as follows:

$$f_s = St \frac{u}{D}$$

where

f_s	=	vortex shedding frequency (Hz)
St	=	Strouhal number
u	=	fluid velocity normal to the member axis (m/s)
D	=	member diameter (m)

9.1.3.1 Vortex shedding is related to the drag coefficient of the member considered. High drag coefficients usually accompany strong regular vortex shedding or vice versa.

9.1.3.2 For a smooth stationary cylinder, the Strouhal number is a function of Reynolds number (R_e). The relationship between St and Re for a circular cylinder is given in Figure 9-1.
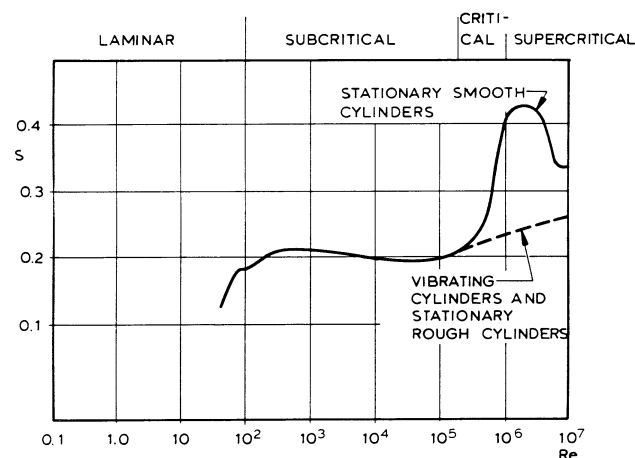

Figure 9-1
Strouhal number for a circular cylinder as a function of Reynolds number

9.1.3.3 Rough surfaced cylinders or vibrating cylinders (both smooth and rough surfaced) have Strouhal numbers which are relatively insensitive to the Reynolds number.

9.1.3.4 For cross sections with sharp corners, the vortex shedding is well defined for all velocities, giving Strouhal numbers that are independent of flow velocity (R_e). Strouhal numbers for some cross sectional shapes are shown in Table 9-1.

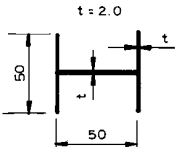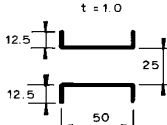**Table 9-1 Strouhal number for different cross section shapes. Reproduced after ASCE (1961)**
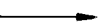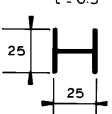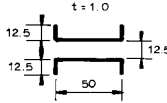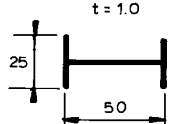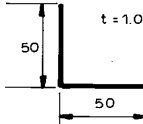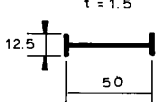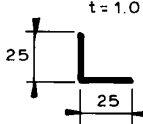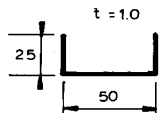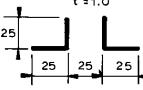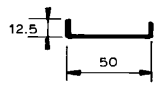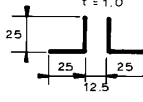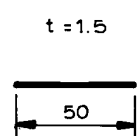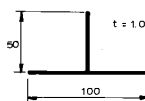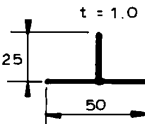
Flow direction	Profile dimensions [mm]	Value of St	Flow direction	Profile dimensions [mm]	Value of St
→	t = 2.0, 50, 50	0.120	↓	t = 1.0, 12.5, 25, 12.5, 50	0.147
↓		0.137			
→	t = 0.5, 25, 25	0.120	↓	t = 1.0, 12.5, 12.5, 12.5, 50	0.150
↓	t = 1.0, 25, 50	0.144	←	t = 1.0, 50, 50	0.145
			↑		0.142
			↘		0.147
↓	t = 1.5, 12.5, 50	0.145	←	t = 1.0, 25, 25	0.131
			↑		0.134
			↘		0.137
↓	t = 1.0, 25, 50	0.140	→	t = 1.0, 25, 25, 25, 25	0.121
↑		0.153	↓		0.143
↓	t = 1.0, 12.5, 50	0.145	→	t = 1.0, 25, 25, 25, 12.5	0.135
↑		0.168			

Table 9-1 Strouhal number for different cross section shapes. Reproduced after ASCE (1961) (Continued)

Flow direction	Profile dimensions [mm]	Value of St	Flow direction	Profile dimensions [mm]	Value of St
→	t = 1.5 / 50	0.156	→	t = 1.0 / 50 / 100	0.180
↓		0.145			
→	t = 1.0 / 25 / 50	0.114			
↑		0.145			

9.1.4 Lock-in

9.1.4.1 At certain critical flow velocities, the vortex shedding frequency may coincide with a natural frequency of motion of the member, resulting in resonance vibrations.

9.1.4.2 When the flow velocity is increased or decreased so that the vortex shedding frequency f_s approaches the natural frequency f_n, the vortex shedding frequency locks onto the structure natural frequency and the resultant vibrations occur at or close to the natural frequency. It should be noted that the eigen frequency during lock-in may differ from the eigen frequency in still water. This is due to variation in the added mass with flow velocity as described in 9.1.12.

9.1.4.3 In the lock-in region, the vortex shedding frequency is dictated by the member's eigen frequency, while for lower and higher velocities the vortex shedding frequency follows the Strouhal relationship.

9.1.4.4 Lock-in to the eigen frequencies can take place both parallel with the flow (in-line) and transverse to the flow (cross flow).

9.1.4.5 For flexible cylinders that respond at multiple modes, the response is typically broad banded and pronounced lock-in does not occur.

9.1.5 Cross flow and in-line motion

Vortex induced vibrations may be split into:

— Cross flow (CF) vibrations with vibration amplitude in the order of 1 diameter
— Pure In-Line (IL) vibrations with amplitudes in the order of 10-15% of the diameter
— CF induced IL vibrations with amplitudes of 30-50% of the CF amplitude.
— Pure IL motion will occur at the lowest reduced velocities, and will be the first response to occur. When the velocity is large enough for CF response (and CF induced IL response) to occur, pure IL motion is normally no longer of interest since the response amplitudes are smaller.

9.1.6 Reduced velocity

For determination of the velocity ranges where the vortex shedding will be in resonance with an eigen frequency of the member, a parameter V_R, called the reduced velocity, is used. V_R is defined as

$$V_R = \frac{u}{f_i D}$$

where

u = $u(x)$ = instantaneous flow velocity normal to the member axis (m/s)
f_i = the i'th natural frequency of the member (Hz)
D = $D(x)$ = member diameter (m)
x = distance along member axis (m)

9.1.7 Mass ratio

The mass ratio is a measure of the relative importance of buoyancy and mass effects on the model, and is defined as:

$$m^* = \frac{m}{\pi \rho D^2 / 4}$$

Note that another definition of mass ratio can be found in the literature, using ρD^2 in denominator. The lock-in region is larger for low mass ratios than for high mass ratios. This is due to the relative importance of added mass to structural mass. Typically, the vibrations occur over the reduced velocity range $3 < V_R < 16$ for low mass ratios (e.g. risers, pipelines), while for high mass ratios the vibrations occur over the range $4 < V_R < 8$ (wind exposed structures).

9.1.8 Stability parameter

Another parameter controlling the motions is the stability parameter, K_s. It is also termed Scrouton number. This parameter is proportional to the damping and inversely proportional to the total exciting vortex shedding force. Hence the parameter is large when the damping is large or if the lock-in region on the member is small compared with the length of the pipe.

For uniform member diameter and uniform flow conditions over the member length the stability parameter is defined as

$$K_S = \frac{2 m_e \delta}{\rho D^2}$$

where

ρ = mass density of surrounding medium (air/gas or liquid) (kg/m^3)
D = member diameter (m)
m_e = effective mass per unit length of the member, see 9.1.11 (kg/m)

δ =   the logarithmic decrement (= $2\pi\zeta$)

ζ =   the ratio between damping and critical damping

δ = $\delta_s + \delta_{other} + \delta_h$

δ_s =   structural damping, see 9.1.9

δ_{other} =   soil damping or other damping (rubbing wear)

δ_h =   hydrodynamic damping, see 9.1.10

9.1.9 Structural damping

Structural damping is due to internal friction forces of the member material and depends on the strain level and associated deflection. For wind exposed steel members, the structural damping ratio ($\delta_s/2\pi$) may be taken as 0.0015, if no other information is available. For slender elements in water, the structural damping ratio at moderate deflection is typically ranging from 0.005 for pure steel pipes to 0.03-0.04 for flexible pipes.

Damping ratios for several structures and materials can be found in Blevins (1990).

9.1.10 Hydrodynamic damping

9.1.10.1 The generalised logarithmic decrement for the hydrodynamic damping can be found as

$$\overline{\delta_h} \approx \frac{\int_0^{l_1} \rho C_D D(x)|u(x)|y^2(x)dx + \int_{l_1+\Delta}^{d} \rho C_D D(x)|u(x)|y^2(x)dx}{4 f_i M_i}$$

M_i is the generalized (modal) mass for mode i;

$$M_i = \int_0^L m[y(x)]^2 dx$$

where

m = $m(x)$, mass per unit length including structural mass, added mass, and the mass of any fluid contained within the member (kg/m)

L =   length of member (m)

$y(x)$ =   normalized mode shape

9.1.10.2 The drag coefficient C_D is a function of x. The integral limits (l_1, $l_1 +\Delta$ and d) are defined in Figure 9-2.

$\overline{\delta_h}$ is the generalised logarithmic decrement of hydrodynamic damping *outside* the lock-in region for cross flow vibrations. The contribution to hydrodynamic damping *within the lock-in region* shall be set to zero in the calculation of K_S.

For cross flow vortex induced vibrations $\delta_h = \overline{\delta_h}$, and for in-line vortex induced vibrations the contribution is double, i.e. $\delta_h = 2\overline{\delta_h}$.

9.1.11 Effective mass

The effective mass per unit length of the member is found as

$$m_e = \frac{\int_L m[y(x)]^2 dx}{\int_L [y(x)]^2 dx}$$

The added mass entering into the expression for m can be determined from the expressions in Ch.6. The added mass will vary with the reduced velocity due to the separation of flow

behind the pipe. This variation can be neglected when calculating K_S. It should however be noted that variation in hydrodynamic mass (added mass) will affect the response frequency of the member.
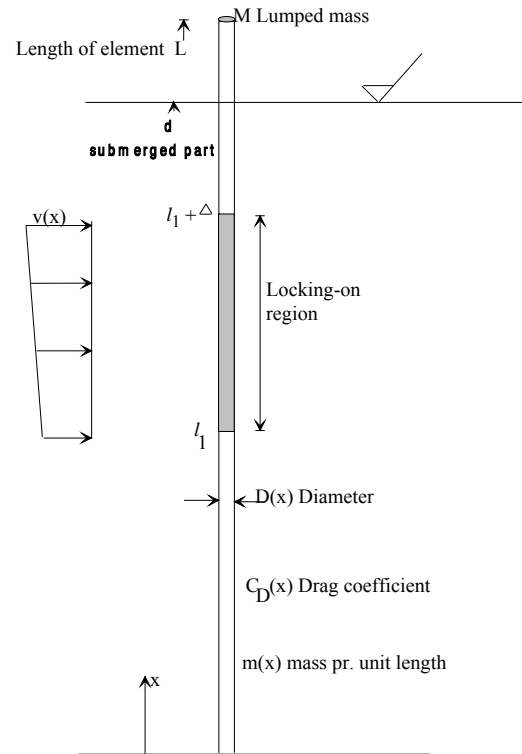
Figure 9-2
Definition of parameters

9.1.12 Added mass variation

The added mass varies with the reduced velocity due to the separation of flow behind the pipe, see Figure 9-3. The variation in added mass will affect the response frequency of the member.
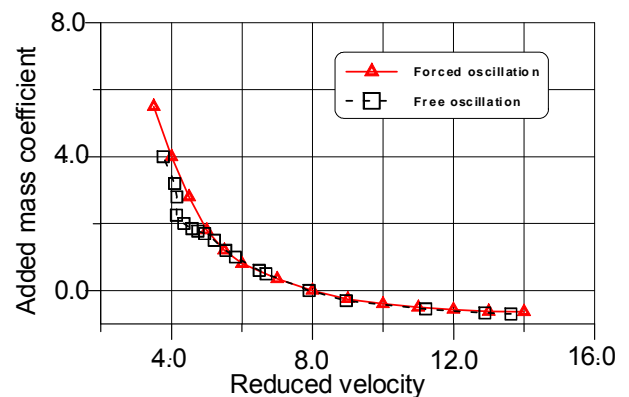
Figure 9-3
Added mass variation with reduced velocity found from forced oscillations (Gopalkrishnan, 1993) and free oscillation tests (Vikestad, et.al., 2000)

9.2 Implications of VIV

9.2.1 General

9.2.1.1 Vortex induced oscillations (VIO) may be a design issue (both ALS/ULS and FLS) for a wide range of objects such as bridges, topsides, floaters, jackets, risers, umbilicals and pipelines exposed to wind, ocean currents and/or waves. The basic principles for prediction of VIO are the same for dif-

ferent fluid flows and objects, however, some special conditions may apply. It may be convenient to differ between rigid body motions and elastic motions. Rigid body motion due to vortex shedding is often termed vortex induced motion (VIM), while elastic motion is commonly termed vortex induced vibrations (VIV).

9.2.1.2 Vortex induced motions of floaters may induce additional loads on mooring and risers system. Both extreme loads and fatigue damage may be affected. Vortex induced oscillations of floaters are described in 9.4.

9.2.1.3 Important effects of VIV on slender elements are:

— The system may experience significant fatigue damage due to VIV.
— VIV may increase the mean drag coefficient of the member, affecting the global analysis of the member and possible interference with other members.
— VIV may influence Wake Induced Oscillations (WIO) of cylinder arrays (onset and amplitude). Guidance on wake induced oscillations are given in DNV-RP-F203.
— VIV may contribute significantly to the relative collision velocity of two adjacent cylinders.

9.2.1.4 Specific guidance for risers and pipelines can be found in

— DNV-RP-F204 Riser fatigue
— DNV-RP-F203 Riser interference
— DNV-RP-F105 Free spanning pipelines.

9.2.2 Drag amplification due to VIV

9.2.2.1 Drag amplification due to VIV must be accounted for. Drag amplification is important for global behaviour of the member and for possible interference between cylinders in a cylinder array. Several expressions for the increase in drag coefficient with vibration exist in literature, based on estimated VIV amplitude *A* normalised by the diameter *D*. A simple formulation applicable for fixed cylinders is (Blevins, 1990):

$$C_D = C_{Do}\left[1 + 2.1\frac{A}{D}\right]$$

where

A = Amplitude of cross flow vibration
C_{Do} = the drag coefficient for the stationary cylinder
D = member diameter

9.2.2.2 Good correspondence with experiments on flexible risers has been found for the following expression (Vandiver, 1983):

$$C_D = C_{Do}\left[1 + 1.043\left(\frac{2A_{rms}}{D}\right)^{0.65}\right]$$

where A_{rms} is the root-mean-square of VIV-amplitude. For sinusoidal motion.

$$A_{rms} = A/\sqrt{2}$$

9.2.2.3 The drag amplification in wave dominated flows is smaller than in pure current conditions. Drag amplification in waves may be taken as (Jacobsen et.al., 1985):

$$C_D = C_{Do}\left[1 + \frac{A}{D}\right]$$

9.3 Principles for prediction of VIV

9.3.1 General

Vortex induced oscillations may be determined by model tests. Scale effects should be given due consideration, see Ch.10 for details.

The following computational models can be used for prediction of vortex induced vibrations:

1) *Response based models*
   Empirical models providing the steady state VIV amplitude as a function of hydrodynamic and structural parameters.

2) *Force based models*
   Excitation, inertia and damping forces are obtained by integrated force coefficients established from empirical data. The response is computed according to structural parameters.

3) *Flow based models*
   The forces on the structure and corresponding dynamic response are computed from fluid flow quantities (velocity and its gradients, fluid pressure). The response is computed according to structural parameters.

9.3.2 Response based models

9.3.2.1 Response based models are empirical models providing the steady state VIV amplitude as a function of hydrodynamic and structural parameters. These models rely on relevant high quality experimental data. The amplitude models aim at enveloping the experimental data, yielding conservative predictions. The response based models for prediction of VIV are simple and therefore well suited for screening analyses.

9.3.2.2 Response based methods for pipelines and risers, respectively, are described in

— Recommended Practice DNV-RP-F105 "Free spanning pipelines"
— Recommended Practice DNV-RP-F204 "Riser Fatigue".

Both Cross Flow and In-Line VIV are considered.

9.3.2.3 The fundamental principles given in these Recommended Practices may also be applied and extended to other subsea cylindrical structural components at the designer's discretion and judgement. The assumptions and limitations that apply should be carefully evaluated. Frequencies and mode shapes should be based on finite element analysis. DNV-RP-F105 applies primarily to low mode response and uniform flow, while DNV-RP-F204 applies to high mode response in a general current profile. For more detailed description of the assumptions and limitations applicable to the response models for pipelines and risers, reference is made to the two above mentioned RPs.

9.3.3 Force based models

9.3.3.1 Excitation, inertia and damping forces are obtained by integrated force coefficients established from empirical data. The response is computed according to structural parameters.

9.3.3.2 The excitation forces on a cross section due to vortex shedding are oscillating lift and drag forces. The lift force is oscillating with the vortex shedding frequency, while the drag force oscillates around a mean drag with twice the vortex shedding frequency.

9.3.3.3 Force based models rely on pre-established forces to use in the computation. Forces are stored as non-dimensional coefficients. The force coefficients are established from numerous experiments, mostly 2D model tests using flexibly

mounted rigid cylinder sections in uniform flow. Most of the tests are performed at low Reynolds number (subcritical flow), while full scale situations often imply high Reynolds numbers.

9.3.3.4 At present, most VIV programs using pre-defined force coefficients are designed to predict only cross flow VIV for a single pipe (riser). This means that lift force coefficients are included but not the oscillating drag coefficients. In-line response may be equally important for fatigue life for e.g. risers responding at high modes.

9.3.4 Flow based models

9.3.4.1 Flow based models mean that the fluid flow around the structure is modelled, and that the forces on the structure is deduced from properties of the flow. The solution of Navier-Stokes equations falls into this definition, and is referred to as Computational Fluid Dynamics (CFD). However, not all of the methods that are considered flow based models solve Navier-Stokes equations in a complete and consistent manner. Boundary layer equations may be used for one part of the problem, while other parts of the problem rely on inviscid flow methods, i.e. the solution is made of discrete vortex particles in otherwise potential flow.

9.3.4.2 Examples of flow based models are:

— viscous sheet method
— discrete vortex method (DVM)
— vortex-in-cell (VIC)
— Navier-Stokes solvers.

The first three methods use discrete vortices in the flow; the latter solve all parts of the problem on a grid. The Navier-Stokes solvers are usually based on either finite difference (FD), finite volume (FV) or finite element (FE) methods.

9.3.4.3 At high Reynolds numbers, the flow becomes turbulent, that is small fluctuations on top of the stationary or slowly varying velocity component. The effect of these fluctuations is an apparent increase in viscosity. In the computational methods, this effect may be included by resolving all details in the flow, or by using a model for the turbulent viscosity. It is not considered feasible to use direct numerical simulations, so a turbulence model is necessary. A universally acknowledged turbulence model is still not established, many models exist. Therefore there will be differences between the individual computer programs.

9.3.4.4 Even if many CFD programs exist in 3D, only 2D computations and use of strip theory are at present considered feasible for long and slender structures. The coupling between the sections is due to the global response of the structure. One improvement of this is done by Willden and Graham (2000), who implemented a weak hydrodynamic coupling between the 2D sections.

9.3.4.5 The possibility to assess the effect of strakes is depending on 3D representation. To compute the effect of strakes in 2D (in 2D, strakes would appear as fins) is considered meaningless. 3D representation is in principle not difficult for a CFD program. The difficulty is connected to the vast amount of grid points and the corresponding size of the numerical problem.

9.4 Vortex induced hull motions

9.4.1 General

9.4.1.1 Vortex shedding may introduce cross flow and in-line hull motions of platforms constructed from large circular cylinders, such as Spars and other deep draught floaters. These motions are commonly termed vortex-induced-motions (VIM).

9.4.1.2 Hull VIM is important to consider as it will influence the mooring system design as well as the riser design. Both extreme loading (ULS and ALS) and fatigue (FLS) will be influenced. VIM is a strongly non-linear phenomenon, and it is difficult to predict from numerical methods. Model testing has usually been the approach to determine the hull VIM responses.

9.4.1.3 Cross flow oscillations are considered most critical due to the higher oscillation amplitude compared to the in-line component.

9.4.1.4 The most important parameters for hull VIM are the A/D ratio and the reduced velocity $V_R = u_c/(f_n D)$.

where

A = transverse oscillation amplitude (m)
D = hull diameter (m)
u_c = current velocity (m/s)
f_n = eigen frequency for rigid body modes transverse to the current direction (Hz)

9.4.1.5 For $V_R < 3\sim4$ VIM oscillations are small and in-line with the current flow. For $V_R > 3\sim4$ the hull will start to oscillate transverse to the current flow and increase in magnitude compared to in-line.

9.4.1.6 An important effect from the transverse oscillations is that the mean drag force increases (drag amplification). This is also confirmed by model tests and full scale measurements. The in-line drag coefficient can be expressed as:

$C_D = C_{Do}[1 + k (A/D)]$

where

C_{Do} = initial drag coefficient including influence of strakes
k = amplitude scaling factor
A/D = cross flow amplitude/hull diameter

9.4.1.7 The amplitude scaling factor is normally around 2, see also 9.2.2. For a reduced velocity around 5, A/D can be up to 0.7-0.8 if the hull has no suppression devices such as strakes. Strakes effectively reduce the VIM response down to A/D ~ 0.3-0.4.

9.4.1.8 The coupled analysis approach, see 7.1.4, can be an effective way of checking out the responses in moorings and risers by introducing the known (analytical, model tests, or full-scale) in-line and cross flow oscillations as forces/moments onto the floater.

9.4.1.9 Since the vortex shedding is more or less a sinusoidal process, it is reasonable to model the cross flow force imposed on the hull as harmonic in time at the shedding frequency f_s, (see 9.1.3). VIM lock-in occurs when the vortex shedding frequency locks on to the eigen frequency, f_n.

9.4.1.10 In general the transverse (lift) force may be written

$$q_{VIM}(t) = \frac{1}{2} \rho u_c D C_L \sin(2\pi f_s t)$$

where C_L is the lift force coefficient. The oscillating in-line force is given by the same expression, except that the oscillation frequency is twice the vortex shedding frequency $f_{IL} = 2f_s$.

9.4.1.11 The in-line VIM response may be in the order of 0.2 times the cross flow VIM response. Hence, the hull VIM response curves are typically in the shape of a skewed '8' or a crescent (half moon).

9.4.1.12 Floaters with single columns like Spars are most likely to be exposed to VIM oscillations. Therefore, these types of floaters are designed with vortex shedding suppression devices like strakes. The inclusion of strakes makes it challenging to perform CFD simulations as it will require simulation of 3-dimensional effects, and this increases the simulation time considerably, see 9.3.4. One alternative to CFD simulations is to use results from a bare cylinder and use empirical data to estimate the reduction in oscillation amplitude due to the strakes. Full-scale data is, however, the ultimate solution and should be used to correlate with analytical predictions.

9.5 Wind induced vortex shedding

9.5.1 General

9.5.1.1 Wind induced vibrations of pipes may occur in two planes, in-line with or perpendicular (cross-flow) to the wind direction.

9.5.2 In-line vibrations

9.5.2.1 In-line vibrations may occur when

$$\frac{0.3}{St} < V_R < \frac{0.65}{St}$$

In-line vibrations may only occur for small stability parameters, i.e. $K_s < 2$. The stability parameter is defined in (9.1.8).

9.5.3 Cross flow vibrations

9.5.3.1 Cross flow vibrations may occur when

$$\frac{0.8}{St} < V_R < \frac{1.6}{St}$$

where

V_R = $U_w /(f_n D)$ is the reduced velocity [-]
St = Strouhal number [-]
U_w = wind velocity [m/s]
f_n = natural frequency of member [1/s]
D = characteristic cross-sectional dimension [m]

9.5.3.2 The amplitude as a function of K_s for fully developed cross flow oscillations may be found from Figure 9-4. The mode shape parameter, γ (see Table 9-2 for typical values), used in this figure is defined as:

$$\gamma = y_{max} \left[\frac{\int_0^L y^2(x)\,dx}{\int_0^L y^4(x)\,dx} \right]^{1/2}$$

where

$y(x)$ = mode shape
y_{max} = maximum value of the mode shape
L = length of the element

9.5.3.3 For strongly turbulent wind flow, the given amplitudes are conservative.

$$\frac{A_{CF}}{\gamma D} = \frac{0.31}{\sqrt{0.062 + 0.077 K_S^2}}$$

$$K_S = \frac{m_e 2\delta}{\rho D^2}$$
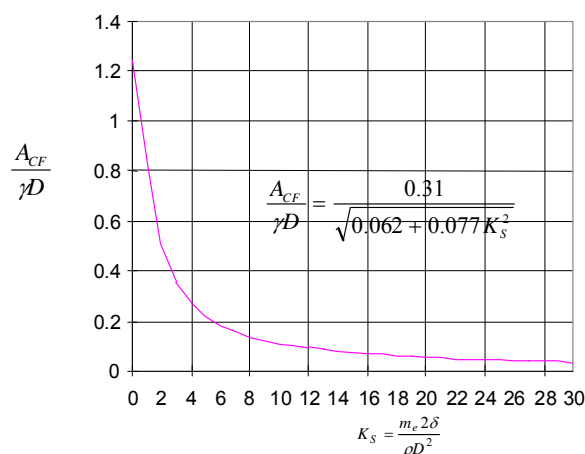
Figure 9-4
Amplitude of cross flow motions as function of K_S (Sarpkaya, 1979)

Table 9-2 The mode shape parameter of some typical structural elements	
Structural element	γ
Rigid cylinder	1.00
Pivoted rod	1.29
String and cable	1.16
Simply supported beam	1.16
Cantilever, 1st mode	1.31
Cantilever, 2nd mode	1.50
Cantilever, 3rd mode	1.56
Clamped-clamped, 1st mode	1.17
Clamped-clamped, 2nd mode	1.16
Clamped-pinned, 1st mode	1.16
Clamped-pinned, 2nd mode	1.19

9.5.3.4 The oscillatory cross-flow excitation force on a stationary cylinder can be expressed in terms of a sectional lift force coefficient C_L,

$$F = \frac{1}{2} \rho_a C_L D U_w^2$$

where

ρ_a = density of air [kg/m³]
C_L = lift coefficient [-]

9.5.4 VIV of members in space frame structures

9.5.4.1 The problem of wind induced VIV of members in space frame offshore structures should be treated as an on-off type. Either the member will experience vibrations and then there is a fatigue problem or it will not experience vibrations and then there is no danger of fatigue cracks.

9.5.4.2 Such members should therefore be designed according to an avoidance criterion that will ascertain that the structure will not vibrate.

9.5.4.3 It may be assumed that the cross-flow vibrations occur only in the plane defined by the member and that is perpendicular to the direction of the wind. One should allow for the possibility that the wind may attack at an angle ± 15 degrees from the horizontal plane.

9.5.4.4 The natural frequency of the member is a key parameter and needs to be determined as accurate as possible. The

largest source of uncertainty is the fixation the member is given by the adjoining structure. This should be assessed in each case.

Guidance note:

For traditional tubular trusses the following guidelines may be used: Brace members can be assumed to have 80% of fully fixed end conditions if the diameter ratio between the brace and the chord is above 0.6 and the diameter to thickness ratio of the chord is less than 40. For other cases the joint flexibility should be assessed specifically or a fixation ratio that is obviously conservative should be selected. Chord members should be assessed as hinged members in the case the chord have equal length and same diameter over several spans. The length between the nodes of the neutral lines should be used in the calculation of the natural frequency.

---e-n-d---of---G-u-i-d-a-n-c-e---n-o-t-e---

9.5.4.5 Cross-flow vibrations of several elements vibrating in phase may be more likely to occur than individual member vibrations. Multiple member vibrations (MMV) can be analysed by assuming the member normal to the wind being subject to cross-flow vortex shedding at the natural frequency of the system. It may be necessary to check more than one member of the same MMV system.

Guidance note:

Calculation of the natural frequency of a system of members may be done by FEM eigenvalue analysis using beam elements.

---e-n-d---of---G-u-i-d-a-n-c-e---n-o-t-e---

9.5.4.6 The lower limit for wind velocity inducing cross-flow vibrations of the member is given by the reduced velocity, defined in (9.5.3),

$$V_R^* = \frac{0.8}{St}$$

or equivalently in terms of the limiting wind velocity

$$U_w^* = 0.8 \frac{D f_n}{St}$$

where

St = Strouhal number
f_n = natural frequency of member [1/s]
D = characteristic cross-sectional dimension [m]

Guidance note:

The Strouhal number may be taken as 0.2 for circular cross sections and as 0.12 for rectangular cross-sections. Strouhal numbers for other beam profiles are given in Table 9-1.

---e-n-d---of---G-u-i-d-a-n-c-e---n-o-t-e---

9.5.4.7 Members of a space frame structure can be assumed to be without risk to wind induced VIV if

$$U_{1year,1min}(z) < U_w^*$$

where

$U_{1year,1min}(z)$ = 1 minute mean speed at the location z of the member with a return period of 1 year.

The variation of wind velocity with height z and conversion between different averaging periods are given in 2.3.2.

9.5.4.8 When the 1-year wind velocity defined above exceeds U_w^*, the member can still be assumed to be without risk to VIV if the following criteria in terms of Reynolds number and sta-bility parameter K_s are fulfilled,

$$K_s \cdot R_e^* \geq 7.5 \cdot 10^6 \text{ for } 3 \cdot 10^5 < R_e^* < 5 \cdot 10^5$$

$$K_s \geq 15 \qquad \text{for } R_e^* > 5 \cdot 10^5$$

where

$$R_e^* = \frac{U_w^* D}{\nu}$$

is the Reynolds number at the wind velocity U_w^*.

Guidance note:

The criteria above are based on the fact that the oscillating lift force on the member is drastically reduced in the critical flow range occurring at Reynolds number around $3 \cdot 10^5$ and the fact that the amplitude of the transverse oscillations is limited when the stability parameter is large.

---e-n-d---of---G-u-i-d-a-n-c-e---n-o-t-e---

Guidance note:

For steel tubular members the stability parameter is given by

$$K_s = 2\pi\delta \frac{\rho_s}{\rho} \left[(t/D) - (t/D)^2 \right]$$

where

ρ_s = density of steel [kg/m³]
ρ = density of air (1.25 kg/m³ at 10°C) [kg/m³]
δ = structural damping $\delta = 2\pi\zeta$ where $\zeta = 0.0015$
D = member diameter [m]
t = thickness [m]

---e-n-d---of---G-u-i-d-a-n-c-e---n-o-t-e---

9.6 Current induced vortex shedding

9.6.1 General

9.6.1.1 In response models in-line and cross flow vibrations are considered separately. The response models described here are primarily intended for single-mode lock-in situations. However, modifications applying when response at several modes may occur are also presented.

9.6.1.2 The response models are developed for uniform flow conditions. For strongly sheared flow, or flow where only parts of the member are subjected to current, it is recommended to use a force model where spatial variation of excitation and damping is accounted for.

9.6.1.3 For response at high modes in uniform or weakly sheared currents, reference is made to the simplified response model presented in RP-F204 Riser Fatigue.

9.6.1.4 In situations where the member is placed in shear flow and has overlapping lock-in regions one vortex frequency will normally dominate and the other frequencies are suppressed in the overlapping region.

9.6.1.5 In general the frequency associated with the highest local response will dominate. The investigation shall be made for all the lock-in modes. The modes giving the largest response shall be used as the final result.

9.6.1.6 For cables or for very long pipes the lock-in may take place with "travelling" waves in the cable or pipe. Both the response in the stationary mode shape and in the travelling wave may be investigated by methods given in the literature, for instance Vandiver (1991). The result of the two analyses which gives the largest response shall be used for design. For screening of VIV induced fatigue damage in long slender pipes responding at high modes, the simplified methodology in RP-F204 Riser Fatigue may be used.

9.6.1.7 The vortex shedding can be considered to be shed in cells. A statistical measure for the length of the cells is the correlation between forces for sections at different length apart. This is formulated by the correlation length, l_c.

$$l_c = l_{c0} + l_{c1} \frac{A(y(x))}{0.5D - A(y(x))} \quad \text{for } A\left(y(x)\right) < \frac{D}{2}$$

$$l_c = \infty \qquad\qquad \text{for } A\left(y(x)\right) \geq \frac{D}{2}$$

where A is the amplitude of mode $y(x)$. The lack of correlation over the length of the cylinder influences the transverse forces. The lengths l_{c0} and l_{c1} can be taken as $l_{c0} \approx 3D$ and $l_{c1} \approx 35D$.

9.6.1.8 In a vortex cell the transverse force, F_{cell} can be determined by

$$F_{cell} = \frac{1}{2}\rho C_f u^2 D \sin(2\pi f_i t) \cdot sign\left[y(x)\right]$$

where $C_f \cong 0.9$. C_f shall always be assigned this value irrespective of Reynolds number, because even small vibrations will tune the vortex shedding and separation points. The force will always work together with the motion in the higher modes. This is the reason for the sign(y(x)).

9.6.1.9 For a long pipe where the correlation length is small compared with the length, Δ, over which the lock-in conditions are satisfied, i.e. ($l_c << \Delta$) the lack of correlation modifies the average force per unit length, F, to be

$$F_{cell} = \sqrt{l_c/\Delta}\, C_f \frac{1}{2}\rho u^2 D \sin(2\pi f_i t) \cdot sign\left[y(x)\right]$$

for $l_c > \Delta$, $\sqrt{l_c/\Delta} \approx 1$ (as approximation).

The above expressions are the forces on a fixed cylinder.

9.6.2 Multiple cylinders and pipe bundles

9.6.2.1 Multiple cylinders and pipe bundles can experience vortex shedding as global vortex shedding (on the total enclosed volume) or as local vortex shedding on individual members.

9.6.2.2 When the pipes are widely spaced the vortex shedding will be local on each member. However, when the pipes are spaced so densely that the drag coefficient for the total *enclosed* volume exceeds 0.7, the total bundle can be exposed to global vortex shedding.

9.6.2.3 The vortex shedding excitation will grow with the total drag coefficient on the bundle. For a circular pipe bundle the vortex shedding excitation will be the same as for a solid circular cylinder when the total bundle drag coefficient rises above 1.2. In this case a $C_f = C_{f0}$ defined in 9.6.1 can be used acting on the pitch diameter of the bundle. For total bundle drag coefficients, C_D, smaller than 1.2, as determined in Ch.6, the transverse lift coefficient, C_f, will depend on the total drag coefficient roughly as

$$C_f \cong C_{f0} \frac{C_D - 0.7}{1.2 - 0.7} \quad (C_D > 0.7)$$

in which C_{f0} is the transverse flow coefficient for the enclosed body if it is solid. In addition there may be local vortex shedding on individual members.

9.6.2.4 Pipes spaced so that the drag coefficient for the total enclosed volume is below 0.7 will only be exposed to local vortex shedding on members.

9.6.3 In-line VIV response model

9.6.3.1 In-line VIV is separated into *pure in-line* and *cross flow induced in-line* motion. Contributions from both first and second in-line instability regions are included in the pure in-line model. Cross flow induced additional VIV motion is considered approximately.

9.6.3.2 *Pure in-line* vortex shedding resonance (lock-in) may occur when:

$$1.0 \leq V_R \leq 4.5$$

$$K_S \leq 1.8$$

Depending on the flow velocity the vortices will either be shed symmetrically or alternatively from either side of the cylinder.

9.6.3.3 For $1.0 < V_R < 2.2$, in the *first instability region*, the shedding will be symmetrical. The criterion for onset of the motion in the first instability region is given in Figure 9-6. The onset criterion is only valid when the reduced velocity V_R is increasing. In non-steady flow where V_R may go from high values to low values lock-in vibrations will exist for all $V_R \geq 1.0$.

9.6.3.4 For $V_R > 2.2$ the shedding will be unsymmetrical, the motion will take place in the *second instability* region ($2.2 < V_R < 4.5$) for $K_S < 1.8$. The criterion for end of the motion in the second instability region is given in Figure 9-6.

9.6.3.5 The maximum amplitude of the oscillations relative to the diameter is determined as a function of the stability parameter K_S, see Figure 9-5. In case of varying diameter, the average diameter of the lock-in region may be used.

For more detailed predictions of IL response amplitude, reference is made to DNV-RP-F105 Free spanning pipelines.

9.6.3.6 *Cross flow induced in-line* VIV is relevant for all reduced velocity ranges where cross flow VIV occurs. Cross flow induced in-line VIV can be estimated by:

— The IL mode with its eigen frequency closest to twice the (dominant) CF response frequency is chosen as the candidate for the CF induced IL.
— The amplitude can be taken as 40% of the (dominant) CF amplitude.
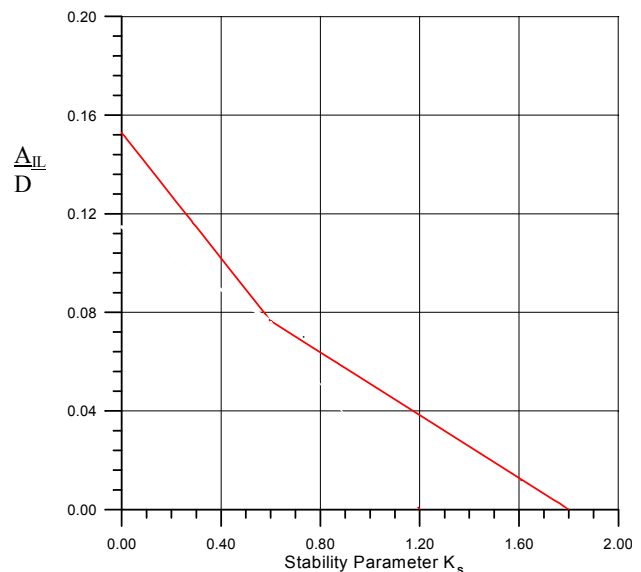
Figure 9-5
Amplitude of in-line motion as a function of K_s (CIRIA, 1977)
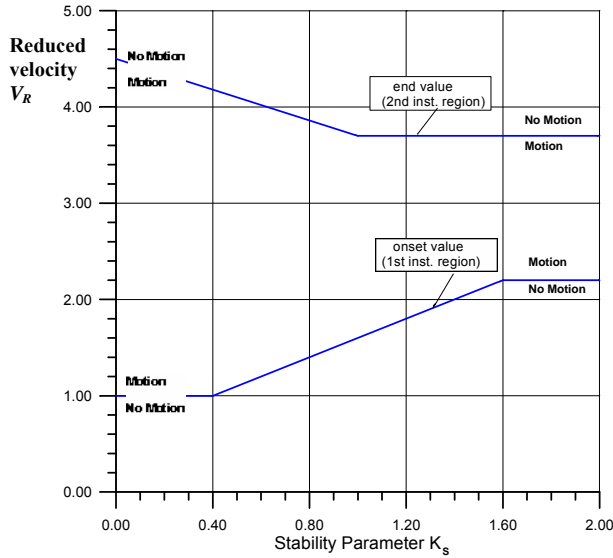
Figure 9-6
Criteria for onset of the motion in the first in-line instability region (1.0 < V_R < 2.2) and end of second instability region

9.6.4 Cross flow VIV response model

9.6.4.1 Cross flow vortex shedding excitation may occur when

$$3 \le V_R \le 16$$

for all Reynolds numbers, and the maximum response is normally found in the range $5 \le V_R \le 9$.

9.6.4.2 The maximum amplitude of the cross flow oscillations relative to the diameter D and the mode shape γ may be determined from Figure 9-4. In case of varying diameter, the average diameter of the lock-in region may be used.

9.6.4.3 A more detailed response model in uniform steady flow is outlined as follows: The amplitude response (*A/D*) as a function of the reduced velocity V_R can be constructed from:

$$V_{R,onset}^{CF} = 3$$

$$V_{R,1}^{CF} = 7 - 3.5 \cdot \left(1.3 - \frac{A_{Z,1}}{D}\right)$$

$$V_{R,2}^{CF} = 16 - \left(\frac{7}{1.3}\right) \cdot \left(\frac{A_{Z,1}}{D}\right)$$

$$V_{R,end}^{CF} = 16$$

$$\left(\frac{A_{Z,1}}{D}\right) = 1.3 \text{ or } 0.9; \text{ see below}$$

$$\left(\frac{A_{Z,2}}{D}\right) = \left(\frac{A_{Z,1}}{D}\right)$$

9.6.4.4 The maximum cross flow response amplitude of 1.3D is only applicable for rigid body modes of flexibly mounted cylinders or the first symmetric bending mode of flexible members, and for single mode response. For all other cases the maximum response amplitude is limited to 0.9D.
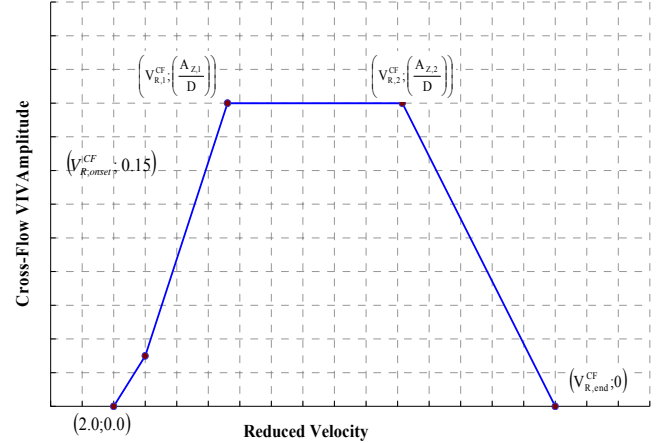
Figure 9-7
Response Model generation principle

9.6.4.5 The characteristic amplitude response for cross flow VIV as given above may be reduced due to the effect of damping.

$$\frac{A_{CF}}{D} = \frac{A_z}{D} R_k$$

where the reduction factor, R_k is given by:

$$R_k = \begin{cases} 1 - 0.15K_s & \text{for } K_s \le 4 \\ 3.2K_s^{-1.5} & \text{for } K_s > 4 \end{cases}$$

The corresponding standard deviation may be obtained as

$$(A/D)/\sqrt{2}$$

9.6.5 Multimode response

9.6.5.1 When the eigen frequencies are relatively close, several modes may potentially be excited at the same inflow velocity. This section provides a simple model for multimode response.

9.6.5.2 The non-dimensional cross flow response amplitude, A_Z/D, for each potentially participating mode is computed based on the response model given in the previous section. It should be noted that the maximum amplitude of a single mode is limited to 0.9 when several modes are excited.

9.6.5.3 The CF mode with the largest A_Z/D value predicted from the response model at the given velocity is the dominant CF mode. The contributing modes are defined as the modes for which the amplitude is at least 10% of the amplitude of the dominant CF mode. The CF modes which are contributing but do not dominate, are referred to as the "weak" CF modes.

9.6.5.4 The dominant CF mode is included by the amplitude value predicted by the response model. The weak CF modes are included by half the amplitude value predicted by the response model.

9.6.5.5 The combined CF induced stress can be calculated as the 'square root of the sum of squares' (SRSS) value. The cycle counting frequency can for simplicity be taken as the Strouhal frequency.

9.7 Wave induced vortex shedding

9.7.1 General

9.7.1.1 The orbital motions in waves may generate vortex shedding on structural members. For certain critical velocities

this may lead to resonant vibrations normal to the member axis or to vibrations parallel with the flow. The alternating type of vortex shedding takes place in that part of the wave motion where the acceleration is small.

9.7.1.2 The current flow velocity ratio is defined as

$$\alpha = \frac{u_C}{u_C + v_m}$$

If $\alpha > 0.8$, the flow is current dominated and the guidance in 9.6 is applicable.

9.7.1.3 The Keulegan-Carpenter number, K_C, is defined as

$$K_C = v_m \frac{T}{D}$$

where

v_m = maximum orbital velocity due to wave motion perpendicular to member axis for stationary cylinder. If the cylinder moves with the waves, it is the maximum relative velocity between the wave motion and the member.

T = wave period

The K_C number is a function of depth. This variation shall be considered in the calculations.

9.7.1.4 In irregular flow the K_C number can be calculated by substituting v_m with the "significant fluid velocity", v_s. Based on sea state parameters, the significant velocity in deep water can be estimated as

$$v_s(z) = \frac{\pi H_S}{T_P} e^{k_P z}$$

where

H_S = significant wave height
T_P = peak wave period
k_P = wave number corresponding to a wave with period T_P
z = vertical coordinate, positive upwards, where mean free surface is at $z = 0$

9.7.1.5 Alternatively, the significant velocity can be calculated as

$$v_s = 2\sqrt{v_{rms}}$$

where v_{rms} is the standard deviation of the orbital velocity due to wave motion perpendicular to member axis for stationary cylinder. If the cylinder moves with the waves it is the relative velocity between the wave motion and the member.

9.7.1.6 The vortex shedding in waves falls into two categories depending on the Keulegan-Carpenter number, K_C:

1) Vortex shedding of the same type as in steady currents. This type exists for $K_C > 40$.

2) Vortex shedding for $6 < K_C < 40$. In this range the vortex shedding frequency will be determined by the type of wave motion. There will be two limiting cases

— the frequency will be a multiple of the wave frequency if the wave motion is regular

— the frequencies will be the same as in steady current if the wave motion is very irregular (i.e. determined by the Strouhal number St).

For narrow band spectra the vortex shedding frequencies will be a combination of the two limiting cases.

9.7.2 Regular and irregular wave motion

9.7.2.1 For *regular wave* motion, a kind of resonance between waves and vortex shedding takes place. The vortex shedding frequency will be a multiple of the wave frequency. The number of vortex shedding oscillations per wave period, *N*, is in regular wave motion given by:

K_C	N
7-15	2
15-24	3
24-32	4
32-40	5

9.7.2.2 The strength of the transverse forces is increased at the resonance conditions. Using the method of analysis defined in 9.6.1. the vortex shedding coefficient C_f shall be modified as shown in Figure 9-10.

9.7.2.3 In *irregular wave* motion, vortex flow regimes undergo substantial changes. The resonance between wave frequency and vortex frequency is not developed. Instead the vortex shedding behaves as for $K_C > 40$.

9.7.2.4 In practice it may be difficult to decide where the transition from irregular to regular waves is present. Therefore the analysis shall be made as for $K_C > 40$ but with the modified vortex shedding coefficient C_f shown in Figure 9-10.

9.7.3 Vortex shedding for $K_C > 40$

9.7.3.1 Vortex shedding for $K_C > 40$ exists only when the orbital velocity component changes less than 100% in a vortex shedding cycle. When the velocity changes quickly in a typical vortex period it can be difficult to distinguish any alternating vortex shedding. A practical criterion for when alternating vortex shedding can be considered present is given below

$$\left| \frac{u^2}{\dot{u}} \right| > \frac{D}{St}$$

where

u = total fluid velocity $u = u_c + u_w$
$\dot{u}$ = fluid orbital acceleration in wave motion

9.7.3.2 In pure wave motion (no current) the criterion above can be written in terms of K_C number defined in 9.7.1,

$$\frac{2\pi}{K_C \cdot St} < \left| \frac{u}{v_m} \right| < 1$$

where v_m is the maximum orbital velocity. In a linear regular wave where $u/v_m = \cos(\omega t)$, this expression defines a time window for alternating vortex shedding. An example is depicted in the middle graph of Figure 9-8.
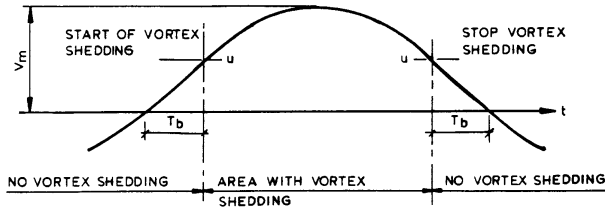
Figure 9-8
Criterion for presence of vortex shedding in waves (the time window for vortex shedding)

9.7.3.3 Resonance vibrations due to vortex shedding (locking-on) may occur as follows for $K_C > 40$:

In-line excitations:

$1 < V_R < 3.5$

$K_S < 1.8$

Cross flow:

$3 < V_R < 9$

$V_R = V_R(x,t)$ and $K_S = K_S(x,t)$ so the parameters will change in the wave period. In wave motion these conditions will only be present temporarily in a time slot.

9.7.4 Response amplitude

9.7.4.1 The maximum possible response which can exist in the time slot where the locking-on criteria are present can be found from Figure 9-4 and Figure 9-5. The time slot with lock-in conditions may, however, be too short for the development to this final value so it will only develop partially, Figure 9-8.
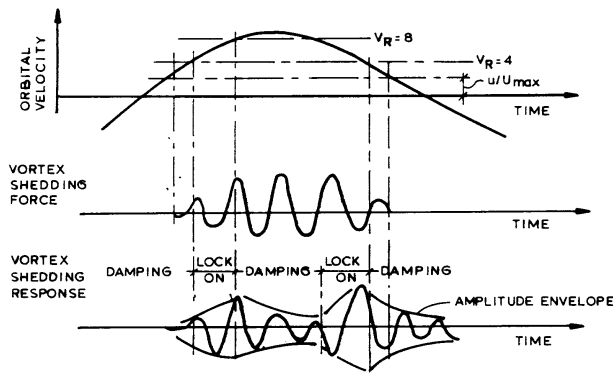
Figure 9-9
Vortex shedding and vortex shedding response cross flow (locking-on) in wave motion

9.7.4.2 The development of response in a lock-in period in unsteady flow is usually so complicated that they must be calculated with mathematical models. As an approximation, the development of the cross-flow response in a locking-on period can be calculated as

$$A_{max} = A_{CF} \sqrt{\frac{l_c(A_{max})}{L}}(1 - \exp(-\delta n_n))$$

where

n_n = the number of load cycles in the locking-on period
A_{CF} = the maximum cross flow amplitude as derived from Figures 9.4 and 9.5

δ = generalised logarithmic decrement as defined in 9.1.8

9.7.4.3 Between the time slots with locking-on conditions the vibration amplitudes are reduced to

$$A = A_{max} \exp(-\delta n_d)$$

where n_d is the number of cycles in the damped region.

9.7.5 Vortex shedding for KC < 40

9.7.5.1 Locking-on conditions for $K_C < 40$:

In-line: $V_R > 1$

Cross flow (with associated in-line motion): $3 < V_R < 9$

$V_R = V_R(x,t)$ in wave motion so the locking-on region may constantly change position.

9.7.5.2 The maximum amplitude response of the cross flow component is around 1.5 diameters or less. The associated in-line amplitude component is less than 0.6 diameter.

9.7.5.3 The lift coefficient C_f from Figure 9-10 shall only be used in areas where the vibration amplitude is smaller than 2 diameters. If the vibration amplitude is greater than 2 diameters the oscillating vortex shedding is destroyed and $C_f = 0$.
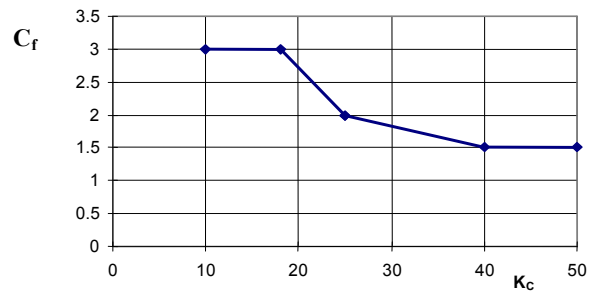
Figure 9-10
Lift coefficient C_f as function of K_C number.

9.8 Methods for reducing VIO

9.8.1 General

There exist two ways for reducing the severity of flow-induced oscillations due to vortex shedding, either a change in the structural properties, or change of shape by addition of aerodynamic devices such as strakes, shrouds or spoiling devices which partly prevent resonant vortex shedding from occurring and partly reduces the strength of the vortex-induced forces.

9.8.1.1 Change of structural properties means changing of natural frequency, mass or damping. An increase in natural frequency will cause an increase in the critical flow speed

$$v_{crit} = k_1 \frac{f_n D}{St}$$

Thus v_{crit} may become greater than the maximum design flow speed, or V_R may come outside the range for onset of resonant vortex shedding. k_1 is a safety factor (typically 0.85).

9.8.1.2 An increase in non-structural mass can be used to increase K_S and hence decrease the amplitude of oscillations. Due attention has however to be paid to the decrease of natural frequency which will follow from an increase of mass.

9.8.2 Spoiling devices

9.8.2.1 Spoiling devices are often used to suppress vortex shedding locking-on. The principle in the spoiling is either a drag reduction by streamlined fins and splitter plates (which break the oscillating pattern) or by making the member irregular such that vortices over different length becomes uneven and irregular. Examples of this may be ropes wrapped around the member, perforated cans, twisted fins, or helical strakes, Figure 9-12.
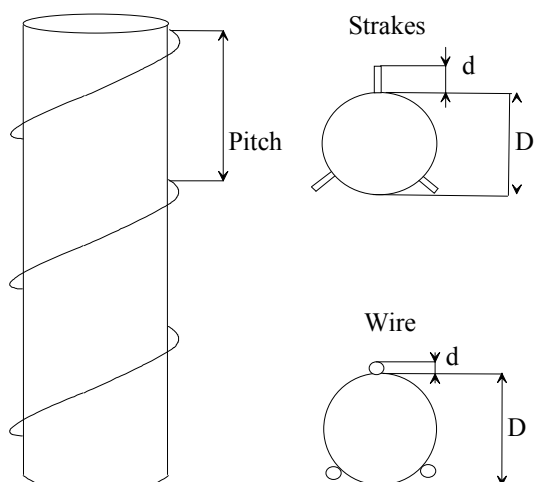
Figure 9-11
Helical strakes and wires
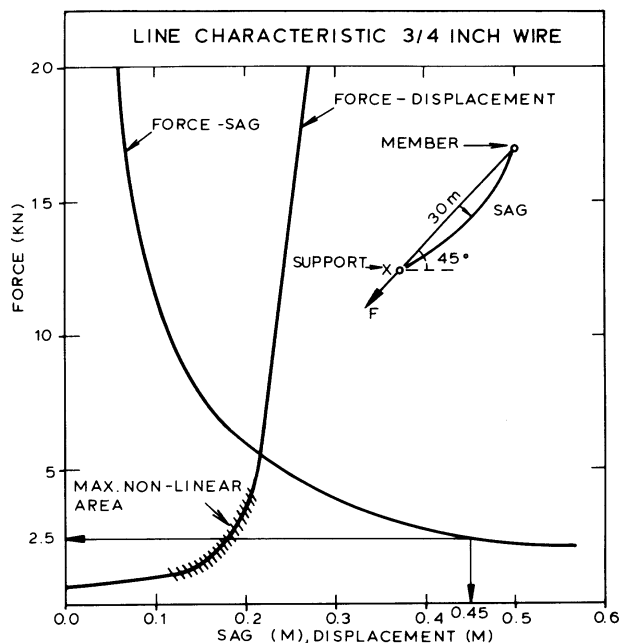
Figure 9-12
Force-deflection curve for 3/4 inch stranded guy-wire with geometrical configuration as shown

9.8.2.2 In order for the spoiling devices to work they shall be placed closer than the correlation length for the vortex shedding.

9.8.2.3 The efficiency of the spoiling device should be determined by testing. The graphs for in-line and cross flow motion can be directly applied for the spoiling system by multiplying with the efficiency factor.

9.8.2.4 Using spoilers the marine growth may blur the shape and may make them less effective. The changed shape shall be taken into account in the analysis.

Typical examples of the efficiency of helical strakes are given in Table 9-3.

Table 9-3 Efficiency of helical strakes and helical wires.					
	No. of windings	*Height of Strakes*	*Pitch*	*Lift Coefficient C_L*	*Drag Coefficient C_D*
Helical Strakes	3 3	0.11 D 0.11 D	4.5 D 15 D	0.238 0.124	1.6 1.7
Helical Wires	3-4 3-4 3-4 3-4	0.118 D 0.118 D 0.238 D 0.238 D	5 D 10 D 5 D 10 D	0.2 0.2 0.2 0.2	1.17 1.38 - -
No spoilers				0.9	0.7

9.8.3 Bumpers

For pipes closely spaced to a wall or to a greater pipe, bumpers may be used to limit the maximum response. Besides reducing the amplitude it will break up the harmonic vibrations.

9.8.4 Guy wires

9.8.4.1 Use of pretension guy wires has proven effective to eliminate resonant vortex shedding. The guy wires should be attached close to the midpoint of the member and pretensioned perpendicularly to prevent cross flow oscillations.

9.8.4.2 The effect of guy wires can be summarized as follows:

— Increase member stiffness and hence natural frequency (small effect)
— Hysteresis damping of wires (large effect)
— Geometrical stiffness and damping of wires (large effect) (due to transverse vibrations of wire)
— Nonlinear stiffness is introduced which again restrains resonance conditions to occur.
— The wires have to be strapped and pretensioned in such a way as to fully benefit from both hysteresis and geometrical damping as well as the non-linear stiffness. The pretension for each guy wire should be chosen within the area indicated on Figure 9-12. Total pretension and number of wires has to be chosen with due consideration to member strength.
— An example is shown in Figure 9-12 where a 3/4 inch wire is used to pretension a member with 30 m between the member and the support point. A tension (force) of 2.5 kN will in this case give maximum non-linear stiffness.
— Instead of monitoring the tension, the wire sagging may be used to visually estimate the tension. In the example shown, a sag of around 0.45 m corresponds to the wanted tension of 2.5 kN.

References

1) ASCE Task Committee on Wind Forces (1961): Wind forces on structures. Trans. ASCE, 126:1124-1198

2) Blevins, R.D. (1990), "Flow-Induced Vibrations". Krieger Publishing Company.

3) Bruschi, R., Montesi, M., Tura, F. and Vitali, L.(1989), "Field tests with pipeline free spans exposed to wave flow and steady current", OTC 1989

4) CIRIA Underwater Engineering Group (1977), Report UR8: "Dynamics of Marine Structures", London, June 1977.

5) DNV RP-F105 "Free spanning pipelines"

6) DNV RP-F203 "Riser interference"

7) DNV RP-F204 "Riser fatigue"

8) Fredsø, J., Sumer, B.M., Andersen, J., Hansen, E.A (1985).: "Transverse Vibrations of a Cylinder very close to a Plane Wall", Proc. Offshore Mechanics and Arctic Engineering Symposium, 1985

9) Gopalkrishnan, R. (1993) "Vortex induced forces on oscillating bluff cylinders". PhD Thesis, Dept. of Ocean Engineering, MIT.

10) Hamil-Derouich, D., Robinson, R. and Stonor, R. (1984), "Assessment of an analysis of an instrumented drilling jack-up conductor", OTC 1994

11) King, R., Prosser, M.J., (1973) "On Vortex Excitation of Model Piles in Water", Journal of Sound and Vibrations, Vol. 29, No. 2, pp. 169_180, 1973

12) Jacobsen, V., Bryndum, M.B., Nielsen, R., Fines, S. (1984), "Vibration of Offshore Pipelines exposed to Current and Wave Action", Proc. Third International Offshore Mechanics and Arctic Engineering Symposium, 1984

13) Jacobsen, V., Ottesen Hansen, N.E. and Petersen, M.J. (1985), "Dynamic response of Mono-tower platform to waves and currents", OTC 1985

14) Kosakiewicz, A., Sumer, B.M. and Fredsøe, J. (1994), "Cross flow vibrations of cylinders in irregular oscillatory flow", ASCE 1994

15) Ottesen Hansen, N.E., Jacobsen, V. and Lundgren, H. (1979), "Hydrodynamic Forces on Composite Risers and Individual Cylinders", OTC-paper 3541, May 1979

16) Ottesen Hansen, N.E. (1984), "Vortex Shedding in Marine Risers and Conductors in Directional Seas", Symposium of Directional Seas in the Oceans, Copenhagen 1984

17) Ottesen Hansen, N.E. (1982) "Vibrations of pipe arrays in waves", BOSS 82

18) Sarpkaya, T. (1979) "Vortex-Induced Oscillations - A selective review", Journal of Applied Mechanics, Vol. 46, pp. 241-258, June 1979

19) Sumer, B.M., Fredsø, J. (1986), "Transverse Vibrations of a Pipeline exposed to Waves", Proc. 5th International Symposium on Offshore Mechanics and Arctic Engineering (OMAE 86), Tokyo, Japan

20) Sumer, B.M. and Kosakiewicz, A.(1995) "Visualization of flow around cylinder in irregular waves", ISOPE 1995

21) Thomsen, J. R., Pedersen, B., Nielsen K.G, and Bryndum, M.B. (1996), "Full-scale field measurements of wave kinematics and vortex shedding induced vibrations in slender structures", ISOPE 1996

22) Vandiver, J.K. (1983) "Drag coefficients of long flexible cylinders", Offshore Technology Conference, OTC 4490, 1983

23) Vandiver, J.K. (1993) " Dimensionless parameters important to the prediction of vortex-induced vibration of long, flexible cylinders in ocean currents" Journal of Fluids and Structures 7, pp. 423-455, 1993

24) Vikestad, K., Vandiver, J.K., Larsen, C.M. (2000) "Added mass and oscillation frequency for a circular cylinder subjected to vortex-induced vibrations and external disturbance". J. Fluid and Struct. 14, 1071-1088.

25) Willden, R.H.J. and Graham, J.M.R. (2000), Vortex induced vibrations of deep water risers, Flow-Induced Vibrations Proc., pp. 29-36.

10. Hydrodynamic Model Testing

10.1 Introduction

10.1.1 General

10.1.1.1 Small scale model testing is a well established tool for the validation of theoretical hydrodynamic and aerodynamic models, estimation of related coefficients, as well as within the design verification of new or modified marine structures. The strong and rapid development of numerical tools, and the broad range of new applications, represents a continuous demand for proper updating of procedures and choices in the planning and execution of such experiments.

10.1.1.2 This chapter gives a general guidance on when to do model tests, and on principles of procedures. The guidance must be seen in light of the previous chapters of this RP. The need for model testing depends on the actual problem and purpose, and must be judged in each given situation.

10.1.1.3 The focus here is on model testing of stationary (moored) and fixed structures in a wave basin or towing tank. The contents are based on Stansberg and Lehn (2007). For additional details and a more comprehensive description on this topic, see e.g. Chakrabarti (1994).

10.1.2 Types and general purpose of model testing

10.1.2.1 Small-scale hydrodynamic model testing can, from a practical point of view, be roughly categorized into the following four general types:

— determine hydrodynamic coefficients for individual structural components
— study of global system behaviour
— validate new numerical models
— examine marine operations and demonstrate functionality or special effects.

10.1.2.2 Actual purposes of the model testing may, in detail, differ between the different types, but there are some overall leads. Thus, in NORSOK N-003, it is recommended that (citation):

"Hydrodynamic model testing should be carried out to:

— confirm that no important hydrodynamic action has been overlooked (for new types of installations, environmental conditions, adjacent structure,---)
— support theoretical calculations when available analytical methods are susceptible to large uncertainties
— verify theoretical methods on a general basis".

There may also be cases where model testing is necessary to demonstrate behaviour or effects that are simply impossible to predict theoretically.

More details on actual topics and cases where testing is relevant are described in the following.

10.1.3 Extreme loads and responses

10.1.3.1 For strongly nonlinear problems, model testing can be used for direct estimation of extreme loads and responses. Such estimation requires a qualified assessment of extremes corresponding to given return periods. For the selection of sea states, one method is to use environmental contours as described in 3.7.2 and identify the most extreme sea states along such contours.

10.1.4 Test methods and procedures

10.1.4.1 In the present RP, the focus is on basic principles for model tests, not on details in the set-up. After an introductory description on when to carry out model tests in 10.2, calibra-

tion of the input environmental conditions is covered in 10.3. Furthermore, simplifications and limitations are addressed in 10.4. Calibration of physical model test set-up is addressed in 10.5. Specific guidance on measurement of various parameters and phenomena is given in 10.6. Nonlinear extremes are covered in 10.7, data acquisition during model tests in 10.8, and scaling effects are addressed in 10.9.

10.1.4.2 It is important to have in mind in what way the results will eventually be used. In the planning of experiments, one should take actions not to exclude the possibility to observe unexpected behaviour.

10.2 When is model testing recommended

10.2.1 General

10.2.1.1 Particular problem areas within marine hydrodynamics that most often need experimental input or validation are listed and briefly commented in the following. The list is general and the need for testing must be judged for each case. The description is focused mainly on loads and responses on fixed and stationary floating marine structures due to environmental conditions (waves, wind and current). The list below summarizes a broad range of items, and in a given model test situation only some of them will be relevant:

— hydrodynamic load characteristics
— global system concept and design verification
— individual structure component testing
— marine operations, demonstration of functionality
— validation of numerical models
— estimation of extreme loads and response.

Each of these items is described in 10.2.2 – 10.2.7.

10.2.1.2 Model tests are important in order to check whether all essential phenomena have been included in the numerical analysis or not. Unknown or unexpected phenomena can often be revealed during model testing.

10.2.2 Hydrodynamic load characteristics

10.2.2.1 Hydrodynamic drag and added mass coefficients: New experimental data are often needed, or need to be verified, for drag and added mass coefficients of a given structural geometry. Hydrodynamic drag is relevant for motion damping and for external current drag forces. Motion decay tests are needed in calm water, and are sometimes run also in current, in waves, and in combined waves with current. Experimental data are particularly needed for perforated (ventilated) objects.

10.2.2.2 Mean and slowly varying wave drift forces: Wave drift forces are commonly calculated from linear potential theory combined with use of Newman's approximation (7.4.3). This is often a robust approach, at least for horizontal motions in deep water. However, experience has shown that there are many cases where adjustments are needed either by more accurate methods, by experiments, or both.

10.2.2.3 Full quadratic transfer functions (QTF's): Newman's approximation means that only the diagonal terms of the QTF matrix are needed, which can be calculated from linear theory. Off-diagonal QTF terms can be important for low-frequency resonant vertical motions. This is partly because the natural frequencies are higher than for horizontal motions, but also due to the characteristics of the excitation QTF itself. They can be relevant also for horizontal motions, especially in shallow water. The full matrix can be computed by fully second-order panel models, but this is not always practically possible, or estimates may be uncertain and should in many cases be checked.

10.2.2.4 Slow-drift damping: This includes wave drift damping from potential theory, hydrodynamic drag on the vessel,

and forces due to drag on the lines/risers. The accurate numerical estimation is uncertain and needs to be validated or determined from experiments.

10.2.2.5 Viscous wave drift forces: These can be significant on column-based floating platforms in severe sea states - in waves only as well as in waves with current. Time-domain prediction methods based on Morison's equation are sometimes used, while they need to be validated or calibrated. Viscous effects on ship roll motion can also influence the wave drift excitation.

10.2.2.6 Higher-order slow-drift effects: Nonlinear water plane stiffness, bow effects etc. can lead to increased drift forces on ship-shaped structures in steep and high waves.

10.2.2.7 Wave-current interaction: The presence of a current can add significantly to the drift forces. This includes potential flow effects ("wave drift damping") as well as viscous effects. Analytical tools that take this into account to some extent have been developed, but they are presently considered to be uncertain and should be validated or calibrated.

10.2.2.8 Confined water volume problems: Special problems that often need to be checked through experiments, or need empirical input, include: Moonpool dynamics, Multi-body hydrodynamic interaction, Loads and motions of fixed and floating bodies in shallow water, and sloshing. Common to these areas is the need to estimate or verify viscous and highly nonlinear effects.

10.2.2.9 Higher-order wave loads: Analysis of higher-order loads on vertical column structures in steep energetic waves, which can lead to resonant dynamical responses known as "ringing", should be validated against model tests, according to NORSOK, N-001 and N-003.

10.2.2.10 Nonlinear coupling and instability effects: For certain floating structure geometries, testing is needed in order to check out uncertainties with respect to possible coupling and instabilities. Two examples are possible heave-pitch coupling of a Spar buoy and special nonlinear water plane geometries.

10.2.2.11 Green water; negative air-gap; run-up: The prediction of water on deck (on ships) and negative air-gap and run-up (on platforms) involves strongly nonlinear problems. Standard analysis tools are semi-empirical based on linear or second-order hydrodynamics, and model testing calibration is needed in the design process. See also NORSOK, N-001, N-003 and N-004.

10.2.2.12 Vortex-induced vibrations (VIV) and rigid motions (VIM): Tools for analysis of VIV and VIM are presently incomplete and / or immature. Data from model testing is critical for the engineering prediction models, and is also necessary for the theoretical modelling with CFD. For very large Reynolds numbers, large scale testing in fjords or lakes should be considered.

10.2.3 Global system concept and design verification

10.2.3.1 For a "complete" structure system, i.e. either a bottom-fixed structure or a moored floater with moorings and risers, model tests are carried out to verify results from global analysis. This is done for final design but is helpful also in concept stages. Parameters to be experimentally verified or checked for various types of structures are given below.

10.2.3.2 Bottom-fixed structures: For slender jacket or jack-up platforms, model tests provide global and local wave deck impact forces. For gravity based structures (GBS), experimental verification of global wave forces and moments (potential and drag) is often desired or required, in particular higher-order wave forces on columns. This is also the case for flexible or compliant bottom-fixed structures. In addition, experimental verification is needed for wave amplification and run-up on columns, wave impact on deck and slamming on components.

10.2.3.3 Stationary floating structures: Parameters to be experimentally verified include: Hydrodynamic excitation, damping and global response in six degrees of freedom, mooring line forces and effects from moorings and risers on vessel motion, riser top-end behaviour and connection forces, dynamic positioning, relative motions and wave impact. Below are listed particular issues for different floater types:

Ship-shaped structures:

— slow-drift horizontal motions
— roll excitation and damping
— fish-tailing
— turret forces (FPSO)
— relative motion
— green water and loads on bow and deck structures.

Semi submersibles:

— slow-drift motions in 5 degrees of freedom (yaw is normally not critical)
— wave amplification; air-gap
— deck impact
— local impact on columns
— vortex induced motions
— dynamic positioning.

Spar platforms

— classical spars and truss spars
— slow-drift excitation and damping in 5 DOF (yaw is normally not critical)
— coupled heave-roll-pitch motions
— heave damping
— moonpool effects
— stiff steel risers with top-end buoyancy cans or top tensioners
— wave amplification and air-gap
— deck impact
— vortex induced motions and effects from strakes
— effects from heave plates (for Truss Spars).

Tension Leg Platforms

— slow-drift horizontal motions
— tether tensions (high vertical stiffness)
— second-order sum-frequency excitation (springing)
— higher-order sum-frequency excitation (ringing)
— wave amplification and air-gap
— deck impact
— vortex induced motion (in some cases).

Buoys

— model tests for *large buoys* may be carried out for slow-drift motions, wave amplification, relative motions, green water and impact on deck structures
— parameters to be tested for small floaters e.g. *calm buoys*, viscous excitation and damping for wave frequency heave/roll/pitch motions and mooring/riser forces on buoy.

10.2.3.4 Multiple body problems: These cases typically include either two floating structures, or one floater and a GBS. If the structures are close to each other, hydrodynamic interaction may be significant. This includes complex potential flow forces, viscous damping of the fluid, and viscous damping of the vessel motions. The complexity increases in shallow water. If the bodies are more distant but connected by lines or hawsers, mechanical interaction is important. In currents and in winds, there may also be complex shadow effects. In all these cases experiments are recommended for verification.

10.2.3.5 Combined wave, current and wind conditions: The global system behaviour in combined environmental conditions, should be experimentally verified. This is to verify the overall behaviour, but also because particular hydrodynamic and mechanical parameters are influenced. Wave-current interactions can be significant for hydrodynamic loads. Wind modelling in wave basins is normally required in global analysis verification studies to simulate realistic conditions, while pure wind coefficients should be determined from wind tunnel tests.

10.2.3.6 Damaged structures: The analysis of non-intact marine structures is more complex than that for intact structures. Therefore, experimental studies are of particular value.

10.2.4 Individual structure component testing

Model tests are often carried out to study details of parts of a structure only. These are typically more basic experiments, with the purpose to obtain general knowledge about parameters as described in 10.2.2.

10.2.5 Marine operations, demonstration of functionality

It is often beneficial to investigate planned operations through model testing. This gives quantitative information, and it demonstrates specific functionality or phenomena. Possible unexpected events can be detected and taken care of. Displaying system behaviour by video recordings is essential. Operations are usually carried out in moderate or good weather, thus extreme environmental conditions etc. are not normally the main focus. Special details can be emphasized, which may set requirements on the minimum scaling possible.

10.2.6 Validation of nonlinear numerical models

10.2.6.1 The development of new nonlinear codes and models requires experimental validation. This is generally true for all types of modelling, while two examples are highlighted below: Computational Fluid Dynamics (CFD) and simulation of nonlinear irregular waves.

10.2.6.2 Validation of fully nonlinear and CFD tools: The strong development of new nonlinear and CFD tools requires parallel significant efforts within experimental validation, together with benchmarking against other theoretical and numerical tools. Careful planning and rational procedures are needed for such experiments.

10.2.6.3 Validation of nonlinear irregular wave models: Theoretical and numerical descriptions of nonlinear steep random waves are not yet complete, especially not in irregular seas and in shallow water. There is a need for continued learning from experiments in this area, and correlate them with more complete input from field data. Particular items include:

— prediction of extreme wave heights and crest heights in irregular sea
— non-gaussian statistics
— splash zone kinematics in steep irregular seas
— shallow water effects
— modifications of wave kinematics due to a mean current .

10.2.7 Extreme loads and responses

To verify design loads, model tests in storm sea states with realistic irregular waves are often needed in order to include all relevant nonlinearities in the waves as well as in the wave-structure interaction. Analysis tools must in various cases be calibrated. This applies to parameters such as extreme slow-drift offset; mooring loads; impact forces in extreme waves (green water / negative air-gap). In NORSOK, N-003, model test verification is described as one method to document non-Gaussian extreme mooring loads.

10.3 Modelling and calibration of the environment

10.3.1 General

10.3.1.1 At the specification stage of model tests, simplifications are made relative to the "real" world. Conditions are described through a limited set of wave, current and wind parameters, which are believed to describe the main characteristics. This is similar for numerical analyses. In addition, there are also laboratory given limitations or chosen simplifications.

10.3.1.2 In order to avoid disturbances from the physical model on the documentation of the actual condition, it is generally recommended to pre-calibrate before the tests, or in some cases, to post-calibrate after the tests. This procedure requires a minimum level of repeatability in the basin, which should be checked.

10.3.1.3 In order to obtain an optimal basis for comparison between model tests and numerical modelling, it is sometimes recommended to use actual measured (calibrated) conditions in the simulations, instead of "targets". This will reduce possible unnecessary uncertainties due to deviations from the target input.

10.3.2 Wave modelling

10.3.2.1 Most often, point measurements of wave elevation time series are made by use of wave probes (staffs) at selected locations in advance of the tests with the model. During calibration, the main probe is located at the reference origin of the model in calm water, and is removed after calibration. A selected number of the other probes are kept in place during the tests.

10.3.2.2 When calibrating *regular waves*, average wave heights and periods in the selected time window are matched against specified targets. While measured regular wave periods are normally within 1% of specified values, the criterion for deviations of wave heights is typically 5%, sometimes lower. Possible variations in time and space should be documented.

10.3.2.3 For calibration of *irregular waves*, matching of given spectral parameters and characteristics is done against specified targets. Tolerance levels of significant wave heights (H_s) and spectral peak periods (T_p) are normally set to e.g. ± 5% relative to targets, sometimes lower. The measuring accuracy of the actual measurements, as they are, should certainly be higher. Measured wave spectra are matched to target spectra.

10.3.2.4 Requirements to observed extreme wave and crest heights are sometimes specified. These are random variables (see below), and one way to obtain the required condition is to re-run the spectra with other random seed numbers (other realizations). For other parameters there are normally no requirements, but documentation of statistics, extremes and grouping should be made. Possible non-Gaussian characteristics can be observed from statistical parameters and from peak distributions. Parameters not specified will be subject to statistical variations.

10.3.2.5 Sample extremes from a random realization are subject to *sampling variability*. This is a basic phenomenon, not a laboratory effect. This also applies to group spectra. It is not obviously correct to match observed sample extreme against a deterministic target. A better and more robust way to match extremes to specified models is to consider extremes estimated from the observed peak distributions, or from the distribution tail. For extensive studies of nonlinear extreme wave and response statistics, a large number of different realizations of the actual spectrum can be run. See also 10.7.

10.3.2.6 Use of so-called *transient waves*, or *single wave groups*, is sometimes referred to. The wave groups can be deterministic events designed for the purpose, or they can be selected as particular events from long-duration random wave

records. The latter may be considered to be more robust if knowledge of the probability of occurrence is important.

10.3.2.7 Model tests are most frequently specified with unidirectional waves or a combination of such, while *multidirectional wave conditions* may also be specified, depending on the facility. A multiflap wavemaker is required for the generation of multidirectional conditions. In the real ocean, waves will be more or less multi-directional. Unidirectional model waves are often considered to be conservative, but this is not always the case. Documentation of actual directional spreading is more laborious than that of scalar spectral properties, and connected with larger uncertainties. There are laboratory-defined limitations on possible wave directions and combinations.

10.3.2.8 Normally, it is assumed that simulated, irregular sea states are stationary in time, over durations of e.g. 3 hours full scale. This is often different in real ocean wave fields. It is in principle possible to generate *non-stationary conditions* in the laboratory, such as squall winds, although it can be a practical challenge, and care should be taken to properly interpret the response statistics from such tests. See also DNV-RP-H103.

10.3.2.9 Waves will change due to refraction when a *current* is added. In collinear conditions, wave heights get slightly reduced and wave lengths increase. The wave periods, remain unaltered. Wave calibration is usually done separately without and with current, to take into account this effect. If current is simulated by towing, the shifting to a moving co-ordinate system means that encounter waves must be considered rather than the stationary observations. Thus the physical wave length in current should be reproduced.

10.3.2.10 Too high *wave basin reflections* lead to partial standing wave patterns and inhomogeneous fields. With good wave absorbers, amplitude reflections lower than 5% is possible (with no model present). This is considered a reasonably good standard for wave basins and tanks. With large models in the tank or basin, re-reflections from side walls and the wavemaker may occur, especially if no absorption is made. A large basin is then preferable to a small basin or tank, due to less blockage effects, a larger length of absorbers and more dissipation over a large area.

10.3.2.11 Active wavemaker control can reduce wavemaker re-reflections. Other non-homogeneities in the wave field can also occur, such as basin diffraction effects in a wide basin, or nonlinear wave transformations and dissipation in a long tank. For the generation of directional waves, there are restrictions in the useful basin area.

10.3.2.12 Generation of waves in a laboratory is normally done by assuming linear theory. In finite and especially in shallow water, this can lead to the generation of freely propagating difference- and sum-frequency waves, which may disturb the wave field. This is relevant for e.g. moored floating structures in shallow water, for which slow-drift forces can be influenced by such *"parasitic" waves*. Procedures exist to reduce this effect through nonlinear adjustments in the wave generation, or to take it into account in the numerical analysis, although it is a complex procedure not implemented in all laboratories.

10.3.3 Current modelling

10.3.3.1 The current is measured at certain points in horizontal and vertical space. Depending on the number of points, the matching to a specified vertical profile can be made. If there are restrictions on the profiles that are possible to generate in the basin, actions must be taken in the specification process such that the resulting conditions for loads and responses will be equivalent to the target conditions.

10.3.3.2 Current is normally specified as constant (although real currents will have some variability). In real basins, current generated by pumps, propellers or nozzles will exhibit a certain degree of *variations*. This may occur if strong shear is modelled, in which turbulence is unavoidable.

10.3.3.3 Current simulation by towing is a reasonable alternative, and gives a constant model current, but there may be questions relating to nonlinear wave-current interactions and their effects on bodies. Also, the rigging will be more complex than for stationary tests, and long-duration sea states including waves can be more complex to carry out. If such tests are carried out in a long tank with waves, care should also be taken to assure a homogenous wave field.

10.3.3.4 Mechanical force (i.e winch force) simplifications can be made if the force is known before the tests. It is most often not preferred since wave-current interactions, and certain current-body interactions (such as vortex induced vibrations) are not included.

10.3.3.5 In a linear model, the presence of waves will not influence the current. To second order, however, there is a small return current under wave groups, which will apparently slightly reduce the observed mean current when measured with waves. This is enhanced in steep waves and in shallow water. For calibration, one normally considers the current as measured without waves.

10.3.3.6 For calibration of mean currents in basins, acoustic and electromagnetic point sensors are frequently in use. They can usually measure in 2 or 3 orthogonal directions. Wave particle velocities can also be measured. Current calibration is normally done without waves, which will add a nonlinear term to the observed current. The sensors should be calibrated through towing.

10.3.4 Wind modelling

10.3.4.1 In model basins, wind is usually calibrated with respect to proper wind forces, not velocities, since the scaling of wind forces does not follow the Froude scaling laws. Wind moments are also important, but due to the scaling effects and simplifications made in the topside modelling, it is quite a challenge to match forces as well as moments at the same time. In practice wind *forces* are calibrated, while *moments* should at least be documented if they cannot be matched accurately.

10.3.4.2 Wind generation by use of fans installed in the basin is generally preferred to winches and to fans on the model, although all types are in use. Care should be taken to assure reasonably homogenous wind fan fields, vertically as well as horizontally. One cannot, however, expect perfect wind tunnel conditions in a typical model basin, and separate wind tunnel tests are recommended for accurate determination of wind and current coefficients. An overview of wind modelling in model basins is given in ITTC (2005).

10.3.5 Combined wave, current and wind conditions

In real conditions, waves, current and wind generally occur from different directions, although there will normally be some correlation between the wind and the waves. In model tests, collinear conditions are often run, partly because these are considered to be conservative, but non-collinear conditions are also frequently modelled. Limitations in the basin outfits may introduce restrictions on the actual directional conditions.

10.3.5.1 Unwanted wave-current interactions can occur through refraction as a result of spatial current variations, especially for short waves in high currents.

10.3.5.2 Influences from fan generated wind models on the waves are normally assumed to be negligible in typical wave basins. The influence from waves on the local wind field near the surface is, however, more uncertain - in model testing as well as in the real field.

10.4 Restrictions and simplifications in physical model

10.4.1 General

10.4.1.1 Given the actual purpose of a model test experiment, one will plan and execute the tests in a way that is optimal for that purpose. One cannot include all possible details from the real world; hence some effects are emphasized while others are paid less attention. Non-significant details are omitted. This is decided from a hydrodynamic force point of view, and in some cases there are additional requirements from a display point of view (video recordings). The emphasis may differ between different types of experiments. There are also basic and practical limitations in small-scale laboratory modeling, which need to be taken into account.

Some particular items are commented below. Scaling problems are discussed in a separate 10.8.

10.4.2 Complete mooring modelling vs. simple springs

10.4.2.1 For the global response verification of floating systems including floater, moorings and risers, the aim is to model individual mooring lines as accurately as possible with respect to hydrodynamic loads, and mechanical couplings between the floater and moorings/risers. For pure studies of hydrodynamic forces and responses on a moored vessel alone, however, tests can be done by modelling a soft horizontal stiffness by simple wires and springs only, in order to neglect effects from lines and risers.

10.4.2.2 Testing of ultra deepwater floating systems in a limited basin, and still reproducing the real mooring forces on the floater, is described separately in 10.4.4.

10.4.3 Equivalent riser models

Riser bundles are often modelled as one equivalent lump riser representing the actual hydrodynamic forces. This can sometimes also be done for anchor lines, but this is less frequently done since the line forces on the vessel are more important, and individual line modelling reduces possible uncertainties.

10.4.4 Truncation of ultra deepwater floating systems in a limited basin

10.4.4.1 Today's test basins are not deep enough to give space for full-length models of systems deeper than about 1000 m, if scaled models shall be kept larger than 1:100 – 1:150 which is a reasonable requirement (see 10.9). In the place of a full depth basin experiment for the verification of a global design analysis, there may in principle be several possible alternatives:

— truncated set-up experiments combined with numerical simulations (off-line hybrid model testing)
— ultra-small scale (physical models smaller than 1:100)
— fjord or lake testing.

None of the alternatives are "perfect", with respect to keeping total verification uncertainties as low as with full modelling, but this is unavoidable.

10.4.4.2 For general use, an off-line hybrid model testing is recommended, and is described in Stansberg et. al. (2002, 2004). The other three alternatives above have clear limitations. Ultra-small scale testing will eventually encounter practical depth or scale limitations, although it may be a realistic alternative in some cases (see Moxnes and Larsen (1998)). Fjord or lake testing may be a valuable alternative for particular research studies ref. Huse et. al. (1998), but is difficult for standard use.

10.4.4.3 An off-line hybrid procedure is described as follows: Experiments are first run with a truncated set-up. Truncations should be made such that the resulting floater motions (that is, the time-varying force vectors on the floater) are similar to those expected for the full-depth case, while dynamic loads on moorings and risers are generally not modelled accurately. The measurements are used to validate or calibrate a numerical model of the actual experiment, for example by coupled analysis. Finally, the calibrated data are applied in full-depth simulations, based on the same numerical modelling, from which final verification results are obtained.

10.4.4.4 Using test results directly from truncated set-ups, without performing complementary numerical modelling, is generally not recommended for line tensions and riser responses, nor for final estimates of floater slow-drift damping due to lines and risers. However, for strongly nonlinear responses such as green water, air-gap etc., for which numerical modelling is presently incomplete, measurements can be used directly if the set-up is properly designed according to the above hybrid procedure.

10.4.5 Thruster modelling / DP

Modelling is often done by simplifying the total set of thrusters to a reduced, equivalent number that generates the proper forces and moments on the vessel. When using such a reduced system, care must be taken with respect to include important thrust losses, such as

— frictional losses between the propeller race and the hull surface;
— deflection of the propeller race around bilges etc.;
— propeller race hitting other thrusters or parts of the construction (neighboring pontoon, truss work etc.);
— heave and roll damping effects of operating thrusters;
— air ventilation (out of water effects).

These effects are normally taken care of by using correct propeller diameter, correct propeller duct clearance to the hull, correct location on the hull and correct propeller race velocity relative to current velocity. A more detailed description is given in Lehn (1992).

10.4.6 Topside model

Topsides are usually not modelled in full detail, as long as the total platform hydrostatic properties including metacentric heights, moments of inertia etc. are properly reproduced. Important topside effects include wind forces and moments, deck slamming, and visual display considerations.

10.4.7 Weight restrictions

Parts of the instrumentation are installed on board the vessel model. With many measuring channels, care must be taken to control the total vessel weight relative to target values. This is in particular important with ultra-small scale models. Weights and moments from hanging cables etc. must also be reduced to a minimum.

10.5 Calibration of physical model set-up

The model and its total set-up should be checked and documented.

10.5.1 Bottom-fixed models

For fixed, stiff models the following items should be calibrated/ checked:

— model characteristics (geometry)
— global stiffness of installed model, in particular when the model has low natural periods
— check of instrumentation; sensor characteristics; accuracy levels.

For elastic or articulated models, the mass distribution and stiffness is also important.

10.5.2 Floating models

For floating models the following items should be calibrated/checked:

— model characteristics (geometry, mass, mass distribution, metacentric heights, waterline)
— restoring force stiffness from moorings and risers
— heeling stiffness, when applicable
— natural periods in actual degrees of freedom (in air; in water)
— check of instrumentation; sensor characteristics; accuracy levels.

10.6 Measurements of physical parameters and phenomena

10.6.1 Global wave forces and moments

Global forces on a fixed model can be measured by a bottom-founded dynamometer. In general, six degrees-of-freedom equipment is used, for measurements of translational as well as rotational excitation. It is important to keep natural frequencies of the set-up away from the actual desired range of the experiment, either through a very light-weighted structure or a very large mass in order to separate frequencies. Wave-induced hydrodynamic pressure underneath the structure should be avoided.

10.6.2 Motion damping and added mass

10.6.2.1 The coefficients are normally estimated from decay tests. Also natural periods are estimated, from which added mass coefficients can be found if the stiffness is known. Test conditions include calm water, and may also include current, waves, and waves + current. Drag and added mass coefficients are generally frequency-dependent. Thus coefficients in steady flow must be generally assumed to differ from those in waves.

10.6.2.2 The decay tests must be performed in such a way that coupling effects are minimized. If coupling can not be avoided, only the first part of the decay should be used, and the test should be repeated at a smaller start amplitude.

10.6.2.3 For linear systems, the relative damping can be found directly from the amplitudes of the decaying motion. For relative damping less than 10%, the relative damping can simply be expresses as $1/2\pi$ multiplied by the natural logarithm of the ratio of two preceding amplitudes. By plotting the relative damping as function of amplitude, both linear and quadratic damping can be determined. If the damping coefficients per unit velocity shall be derived, the stiffness of the system and the total oscillating mass (model mass including added mass) must be known. The total mass is derived from the measured response frequency and the stiffness around the position of equilibrium, if the problem can be considered linear.

10.6.2.4 The damping characteristics in waves can be determined from motion decay tests in waves. If the resonance frequency is far from the wave frequency band, the decaying motion can be separated by filtering methods. In this case one should be aware of eventually difference-frequency excitation. This can be avoided if the waves repeat exactly. First, a test without decay is performed. Then the same wave is run and several decaying motions are excited during the test. By subtraction the two time series, times series of decaying motions are found. Eventually excitation is now removed by the subtraction.

10.6.2.5 If the restoring system is non-linear over the oscillating part, the model will be exposed to the full non-linear stiffness during one oscillation for the largest amplitudes. Thus, special attention must be paid to the method of analysis and the determination of the stiffness around the position of equilibrium for the sake of determination of added mass when calculating the damping coefficient per unit velocity.

10.6.3 Wave-induced motion response characteristics

10.6.3.1 Linear motion transfer functions (RAOs) in the wave-frequency (WF) range are found from tests in regular or in irregular waves. Motions at the water surface are most often made in 6 DOF by absolute optical recordings (in air), related to a defined origin which is normally either COG or at the horizontal COG and still water level. Motions at other locations can be derived. Accuracy levels must be documented. Accelerometers can be used as verification or back-up. Video recording can in principle also be used, while accurate recordings may then be more difficult. For underwater recordings, ultrasonic or video methods have been in use, while new optical methods are now available.

10.6.3.2 The undisturbed input wave elevation is normally used as the reference. For the relative phase, the actual reference point in the basin must be documented. For standard testing situations, use of irregular waves is often the best way to cover a wide frequency range, and to accurately identify natural periods. Especially, broad-banded spectra with low energy are used to study conditions equivalent to linear, while analysis from steeper sea states will give "linear zed" RAOs where nonlinear effects may be included. Sea states of different steepness may be needed to quantify nonlinear effects in the WF range, such as viscous damping of roll etc. Regular waves can be used for check-points, for systematic basic research studies, or to study effects at particular wave frequencies.

10.6.4 Wave-induced slow-drift forces and damping

10.6.4.1 With a floating body in a moored set-up condition, tests in regular waves can be used to estimate mean wave drift excitation coefficients directly, at selected wave frequencies, from the mean offset and a given restoring stiffness and dividing with the square of the calibrated undisturbed wave amplitude. Similarly, from tests in bi-chromatic waves, off-diagonal QTF terms can be estimated. This is a straightforward procedure, while a large number of such tests are needed to obtain a continuous coefficient variation with frequency, especially if a full QTF is desired.

10.6.4.2 By use of tests in irregular waves, wave drift QTFs can be estimated by means of cross-bi-spectral analysis between the actual response signal and the undisturbed wave elevation record. With a moored body, only motions are measured, not forces nor moments, and transformation from motions into excitation must be done by the assumption of a linearized slow-drift oscillation response. This is a complex type of analysis, but it has shown to give reasonable results. Note that QTFs estimated through this procedure include all apparently quadratic contributions to the drift motions, i.e. both the "real" 2nd order, some contributions from 4th, 6th order etc., and viscous drift excitation.

10.6.4.3 With the body kept in a fixed condition, excitation can in principle be found directly, while that is a more complex experiment from a practical point of view. Also, it may be favourable to estimate the excitation from a condition where the body is moving in a realistic manner, since this could influence the net excitation.

10.6.5 Current drag forces

Drag coefficients can be found either by decay tests, by stationary tests in current or by towing tests (e.g. planar motion). The forces are estimated either through offset and a given restoring stiffness, or through direct force measurements on a fixed model. For non-symmetric geometries, testing in different headings is recommended.

10.6.6 Vortex-induced vibrations and motions (VIV; VIM)

10.6.6.1 These tests are normally highly specialized, with particularly careful planning, execution and interpretation. The set-up depends on the actual purpose. Studies of 2D effects are different from those of 3D effects, and need different types of rigging. The scale is important due to the Reynold's number, and large scales are preferred.

10.6.6.2 For studies of current-induced VIV on flexible structures such as risers or cables, the significance of the different natural modes of vibration are of interest. They may be studied through towing tests or rotating rigs. Local displacements and structural dynamics are observed through local accelerations and bending stress, traditionally measured by accelerometers and/or stress-strain sensors. Recently, methods using optical fibres have been established.

10.6.6.3 Natural vibration modes depend on the velocity, and in a sheared current condition this will vary along the length. The problem is quite complex due to the frequency-dependent added mass. Particular analysis methods are required to analyse this. Flow fields can be studied by Particle Imaging Velocimetry (PIV).Visualisations by other special optical methods are also done. Comparison to numerical flow models is essential. For further details on VIV analysis, reference is made to Ch. 9 in this RP document.

10.6.6.4 Studies of vortex-induced motions (VIM) of column-shaped rigid bodies like Semi's and Spars can be done through towing tests or through stationary tests in current. Stationary tests are simpler to carry out in which case the floater is kept in its mooring condition, but since currents always contains a certain level of 2D and 3D fluctuations, towing tests are sometimes preferred. The rigging in the towing tank must then resemble that of the actual mooring condition.

10.6.7 Relative waves; green water; air-gap

10.6.7.1 To record the relative elevation between waves and a deck, wave probes are fixed on the structure (following the possible deck motions in the case of a moving vessel) at selected locations. This will also include possible wave amplification due to the structure. The probes will then follow the possible horizontal vessel motions in the wave field as well. The absolute wave amplification can be estimated, if desired, by subtracting the measured local vertical vessel motion at the actual location.

10.6.7.2 For ship-shaped structures, a selected number of probes are located at the critical locations, which includes the bow region and sometimes the midship and stern regions. For large-volume platforms, critical locations are often considered to be in front of upwave and downwave columns, as well as at the platform front centre and at lifeboat positions. For a more detailed advance evaluation of possible critical locations, it is often recommended to do a numerical analysis first.

10.6.7.3 Green water elevation on a deck is measured by another set of deck-mounted wave probes. Additionally, visual observations from high-resolution close-up video and photo recordings are also very helpful in these problems.

10.6.8 Slamming loads

10.6.8.1 Wave impact loads (typically slamming and sloshing) are high pressures of short duration. A slamming peak is typically 10-100 ms in full scale, while a sloshing pressure is typically 1-5 ms. In model tests, they are normally measured by use of force panels or small pressure cells. The transducer system is a mass-spring-damper system and measures the response to the impact load.

10.6.8.2 Statistical scatter. Slamming loads belongs to responses that are strongly non-linear, with extreme peaks exhibiting a large statistical scatter. If, e.g., one or two slamming events occur during a 3-hour random wave simulation, a representative value can not be assesses based on these two values, only. For that purpose, a long duration is needed, e.g. through running a large number of 3-hour realisations, see 10.7.

10.6.8.3 Force panels and pressure cells. Slamming or high pressure peaks are very local and do not occur simultaneously, even over a limited area. Slamming forces can be measured by pressure cells or by force panels. While a pressure cell is a few millimetres in diameter (model scale), the force panel is typically a few centimetres in diameter. Therefore the scatter from pressure cells is much larger than for force panels, which in fact registers the averaged load, in time and space, of small individual pressure peaks. For structural design of plate fields of, say 2-5 m^2, the overall loading is more important than local loads, and for this purpose it is recommended to use force panels. By using pressure cells it will be necessary to use a kind of averaging method based on several neighbouring cells to get reasonable data. If hydro-elastic effects are expected to occur, this must be treated by special methods.

10.6.8.4 Transducer stiffness and sampling frequency. The transducer with the forces panel is a dynamic system measuring the response to the slamming load. Due to the mass and damping of the system, the response force will not be identical to the slamming load. Depending on the duration of the slam compared to the resonance period of the transducer, the response force can be amplified. The dynamic amplification is dependent on the rise time of the slam. To determine the rise time, the resonance frequency of the transducer should be high enough to oscillate at least 1-2 times during the rise of the slam. However, this requirement may result in an extremely stiff transducer with poor resolution. As a compromise between stiffness and resolution, a resonance frequency in the range 300-1000 Hz is recommended for force panels. For pressure cells, a sampling frequency larger than 20 kHz is recommended.

10.6.8.5 The dynamic amplification can be assessed by use of numerical simulation programs based on mass and damping determined from the measurements of the decaying, resonant motions during the slam. As a rule of thumb, the sampling frequency should therefore be about 10 times the resonance frequency of the transducer.

10.6.9 Particle Imaging Velocimetry (PIV)

10.6.9.1 For the development of improved nonlinear theoretical models, validation of the predicted flow fields in space and time can be very helpful and improve the understanding. For example, the observation of complex 3D flow vector fields in VIV problems is considered to be of great value. Another example is the diffracted wave kinematics around floating structures in steep waves.

10.6.9.2 Use of Particle Imaging Velocimetry (PIV) is one promising tool, from which quantitative measurements of the vector field are obtained. The technique represents high-level technology and is presently a demanding operation requiring well experienced research personnel, but the potential outcome is large, and it is expected to be increasingly used and developed for these purposes. Other photographic methods are also in use.

10.7 Nonlinear extreme loads and responses

10.7.1 Extremes of a random process

Extreme values in a random process are random variables, with a statistical variability. Therefore a sample extreme from e.g. a 3 hours storm simulation must be interpreted as just one sample among many. The distribution for a given response should be determined and an appropriate high fractile chosen for the characteristic long-term response. A fractile in the order

of 85-95% will often be a reasonable choice for use in design.

10.7.2 Extreme estimate from a given realisation

For linear processes, the behaviour of the extremes are reasonably well known based on the standard deviation of the process, while for nonlinear processes it is essential to use and interpret measured extremes in a proper and consistent way. If only one sea state realisation is run, it is better to use extreme estimates based on fitting of the tail of the peak distribution, rather than a single sample extremes.

10.7.3 Multiple realisations

An extensive and accurate way to overcome the statistical variability problem is to run a large number of different realizations of the same spectrum, in order to obtain robust estimates. Strongly nonlinear processes exhibit a larger statistical scatter than weakly nonlinear processes, and the multiple realization approach is then often recommended. Sample extremes from each realization can be fitted to a Gumbel distribution, from which more robust extreme estimates can be estimated. Bow slamming, negative air-gap and deck slamming represent examples on such very nonlinear problems.

10.7.4 Testing in single wave groups

Model testing with a large number of realizations can be time-consuming, especially if sea states are repeated with several headings and load conditions, etc. Methods are being developed to run single wave group events only, selected from a given criterion representing critical conditions for the problem. To relate the events to a statistical probability of occurrence, events from a pre-calibrated full wave recording can be selected and reproduced, rather than use of artificially designed events. Care must be taken to assure that the resulting statistical response effects really represent those from the full records.

10.8 Data acquisition, analysis and interpretation

10.8.1 Data acquisition

10.8.1.1 Digital data sampling rates must be high enough to satisfactorily resolve the interesting frequency range. Keeping the rate about 10 times higher than the interesting upper frequency range is usually acceptable. If for some reason it needs to be lower, one has to check the effect from analogue filters on phases etc.

10.8.1.2 It is recommended to start acquisition together with the start-up of the wavemaker, to keep control of mean values and possible transient effects. This is also favourable when making numerical reproductions using the calibrated wave as input. In the final data analysis, the start-up sequence is omitted.

10.8.2 Regular wave tests

10.8.2.1 In the data analysis, time windows including 10 – 20 cycles selected in the first stable part of the recordings are usually considered satisfactory. It is preferred that no reflections have returned from the basin beach. For certain low-damped slow-drift responses, however, longer durations are required. Possible reflections, which may influence the results from regular wave tests even when they are at relatively small levels, must then be taken into account.

10.8.2.2 Analysis of data typically includes time series plots, simple statistics (average response amplitudes), and harmonic (Fourier) analysis. From the first harmonics, linear transfer functions (RAOs and relative phases) can be found by dividing with the reference complex wave amplitude. Sum-frequency and difference-frequency Quadratic Transfer Functions (QTF's) are found from the second harmonics and the mean value, respectively, by division with the square of the wave amplitude. For the harmonic analysis it is recommended that the time window includes exactly an integer number of wave cycles. The stability of the measured wave and response signals should be checked from the time series.

10.8.3 Irregular wave tests

10.8.3.1 Primary results obtained from test in irregular waves include simple statistics (mean, standard deviation, maximum, minimum, skewness, kurtosis), spectra and spectral parameters. The skewness and kurtosis indicate possible non-Gaussian properties. Also peak distribution plots are helpful, especially if compared to a reference distribution such as the Rayleigh model. Extreme value estimates based on the tail of the distribution are more robust than just the sample extremes. For analysis of nonlinear extremes reference is made to 10.7 above.

10.8.3.2 Linear transfer functions (RAOs and relative phases) are obtained from cross-spectral analysis between responses and the calibrated reference wave. For consistent phase estimation, the signals should be synchronized, e.g. by using the input signal to the wavemaker as a synchronizing signal. (If this is impossible, phases must be estimated using a wave probe used in the actual tests, placed in line with the model).

10.8.3.3 The linear amplitude coherence function indicates the linear correlation between the wave and the response, and in case of low coherence one should be careful in using the estimates. Typically, for a 3-hours record a coherence level lower than 0.6 – 0.7 indicates increased uncertainties. This is also the case for very low reference wave spectrum levels.

10.8.3.4 If RAOs are estimated simply from the square root of the ratio of the spectra, noise introduces a bias error which can lead to significant over-predictions for low signal levels.

10.8.3.5 Quadratic transfer functions (QTFs) can be obtained from cross-bi-spectral analysis. This is a more complex and computer consuming process than the simpler linear cross-spectral analysis above, and must be carried out with care in order to avoid analysis noise. Verification of the procedure against known, numerical cases is recommended. A proper time synchronization between the reference wave and the response signal is even more critical than in the linear case. The procedure is still not in regular use, but if used properly it can add value to the outcome from tests in irregular waves. A basic description is given in Bendat (1990), while an implementation is given in Stansberg (2001). See also 10.6.4.

10.8.4 Accuracy level; repeatability

Uncertainties in the model test results depend on a series of contributions in a long chain. Important sources of inaccuracies can be:

— instrument uncertainties
— uncertainties in the set-up
— uncertainties in test and analysis procedures
— uncertainties in reproduction and imperfect repeatability of the environmental conditions
— deviations from "target" conditions (unless this is taken care of by using documented conditions)
— improper documentation.

Repeatability should be documented.

10.8.5 Photo and video

10.8.5.1 Photographs and continuous video recordings are usually required from all model tests, including design verification, component testing and marine operations. Two or more cameras are often used to cover different views of the model. The high-resolution quality of present available digital equipment makes this a very helpful tool. It serves primarily a visualization purpose, but can in some cases also be used for quantitative information.

10.8.5.2 Underwater video recordings can be used to study riser behaviour and possible interactions with lines and the vessel.

10.9 Scaling effects

10.9.1 General

10.9.1.1 The most common way to scale models is by use of Froude's scaling law (see Table 10.1) based on the effects of gravitational acceleration, and the scaling is defined by the Froude number. It is normally applicable for the main hydrodynamic forces in typical ship and platform problems.

10.9.2 Viscous problems

10.9.2.1 When viscous forces are significant, the Reynolds number is also relevant due to vortex shedding, and corrections to the Froude scaling may be needed. Such corrections are normally referred to as "scaling effects". It is in principle also possible to base the complete scaling on the Reynolds number instead of the Froude number, but that is not commonly done. Effects due to air pockets and phenomena governed by surface tension such as wave breaking, also scale differently from the Froude approach.

Table 10-1 Froude's scaling law			
Parameter	*Scaling factor*	*Model unit (typical)*	*Full scale unit (typical)*
Length	λ	m	m
Velocity	$\lambda^{1/2}$	m/s	m/s
Linear acceleration	λ^0	m/s^2	m/s^2
Angular acceleration	λ^{-1}	deg/s^2	deg/s^2
Angle	$\lambda 0$	degrees	degrees
Force	λ^3 1.026	N	kN
Moment	λ^4 1.026	Nm	kNm
Time	$\lambda^{1/2}$	s	s

10.9.2.2 Viscous scaling effects are normally not significant when the body geometry is defined by surfaces connected by sharp edges, e.g. bilge keels, with radii of curvature (in the model) small relative to the viscous eddy formation. This generates a well defined shedding. For circular cylinders, however, corrections may be needed for smaller diameters, i.e. when the model Reynolds number becomes smaller than 10, in which case the forces are conservative and the set-up should be adjusted by use of smaller model diameters. Scale effects should in some cases also be considered when the full scale Reynolds number is larger than 10^5; this can be relevant for the slow-drift damping of large floating platforms.

10.9.3 Choice of scale

10.9.3.1 The model scale should be sufficiently large in order to ensure that:

— the hydrodynamic forces and phenomena that are important for the test results are correctly simulated,
— scaling of results can be performed based on proven model laws and empirical correlation data,
— the model scale is adequate with respect to the testing tank and test facilities, as well as the capability of generation of the environmental conditions,
— acceptable measuring accuracies can be obtained.

10.9.3.2 It is realized that the choice of scale may be a compromise between the above requirements. The reasons for the proposed scale should be clearly stated.

10.9.3.3 In practice, scales are typically chosen between 1:30 and 1:100, although this is sometimes deviated from. Larger scales are limited by laboratory sizes and practical/ economical considerations, while smaller scales are seldom used - mainly

due to increased uncertainties and less repeatability in the modelling, but also due to scaling effects. Tests on moored floating structures in scales as small as 1:170 have in fact been checked and compared to larger scale experiments in /9/, showing basically reasonable agreement in motions and mooring line forces, but the modelling accuracy required is quite challenging, and repeatability in environmental modelling becomes poorer. Very small scales may also be limited by special details in the model such as thrusters etc.

10.9.4 Scaling of slamming load measurements

10.9.4.1 Slamming and sloshing pressures in water are scaled according to Froude's law of scaling. Scale effects on the pressures are therefore mainly related to air content in the water. Entrained air has been shown to reduce maximum impact pressures and increase rise time ref. Bullock. et. al. (2001) Due to different physical, chemical and biological properties of freshwater and seawater, the bubbles that form in freshwater tend to be larger than those which form in seawater and they coalesce more easily. Consequently, air can escape more quickly from freshwater than from seawater. Thus, scaling by Froude's law overestimates the measured pressure peaks.

10.9.4.2 In cases where air is entrapped, the pressure peak scales with the square root of the scale ratio, while for Froude's scaling, the pressure peak scales with the scale ratio. However, the time also scales differently in such a way that the impulse of the pressure peak becomes equal ref. Graczyk et. al. (2006).

10.9.5 Other scaling effects

10.9.5.1 The fluid free surface tension does not scale according to Froude's law, and must be handled with care if it is important. It defines a fundamental lower scale limit for gravity wave modelling, but does usually not affect scale ratios larger than about 1:200.

10.9.5.2 Structural stress, strain and elasticity of a continuum cannot be directly observed from model tests, and if it shall be included in tests it must be handled by modelling of e.g. discrete intersections where local moments are measured.

References

1) Bendat, J. (1990), *Nonlinear System Analysis and Identification from Random Data*, Wiley-Interscience, New York, N.Y., USA.

2) Bullock, G.N; Crawford, A.R; Hewson, P.J; Walkden, M.J.A; Bird, P.A.D. (2001) "The influence of air and scale on wave impact pressures"; *Coastal Engineering* , Vol. 42.

3) Chakrabarti, S.K. (1994) *Offshore Structure Modelling*, World Scientific, Singapore.

4) DNV-RP-H103 "Modelling and analysis of marine operations".

5) Graczyk, M; Moan, T; Rognebakke, O. (2006) "Probabilistic Analysis of Characteristic Pressure for LNG Tanks."; *Journal of Offshore Mechanics and Artic Engineering;* Vol. 128.

6) Huse, E., Kleiven, G. and Nielsen, F.G. (1998), "Large Scale Model Testing of Deep Sea Risers", *Proc., Paper No. OTC 8701, the 30th OTC Conf.*, Houston, TX, USA, (1998).

7) ITTC, Ocean Engineering Committee Report, *Proceedings, 24th International Towing Tank Conference*, Edinburgh, UK, September 2005.

8) Lehn, E. (1992); "Practical Methods for Estimation of Thrust Losses"; FPS 2000 Mooring and Positioning, Part 1.6 Dynamic Positioning-Thruster Efficiency; MARINTEK Rep. no. 513003.00.06, Trondheim, Norway.

9) Moxnes, S. and Larsen, K. (1998) "Ultra Small Scale

Model Testing of a FPSO Ship", *Proc., Paper No. OMAE98-0381, the 17th OMAE Conf.*, Lisbon, Portugal.

10) NORSOK Standard, N-001, "Structural Design", Rev. 4, Standards Norway, February 2004.

11) NORSOK Standard, N-003 Rev. 4 (2007) "Actions and Action Effects", Norwegian Technology Standards Institution.

12) NORSOK Standard, N-004, "Design of Steel Structures", Rev. 4, Standards Norway, October 2004.

13) Stansberg, C.T. (2001), "Data Interpretation and System Identification in Hydrodynamic Model Testing", *Proc., Vol. III, the 11th ISOPE Conference*, Stavanger, Norway, pp. 363-372.

14) Stansberg, C.T., Ormberg, H. and Oritsland, O. (2002) "Challenges in Deepwater Experiments – Hybrid Approach", *ASME Journal of Offshore Mechanics and Arctic Engineering*, Vol. 124, No. 2, pp. 90-96.

15) Stansberg, C.T., Karlsen, S.I., Ward, E.G., Wichers, J.E.W. and Irani, M. B. (2004) "Model Testing for Ultra-deep Waters", OTC Paper No. 16587, *Proceedings, Offshore Technology Conference (OTC) 2004*, Houston, TX, USA.

16) Stansberg, C.T. and Lehn, E. (2007), "Guidance on hydrodynamic model testing, Phase 1 + 2". Marintek Report No. 580072.00.01, Trondheim, Norway.

APPENDIX A
TORSETHAUGEN TWO-PEAK SPECTRUM

The Torsethaugen spectrum is a double peak spectral model developed based on measured spectra for Norwegian waters (Haltenbanken and Statfjord) (Torsethaugen, 1996; Torsethaugen and Haver, 2004). Each sea system is defined by five parameters H_s, T_p, γ, N and M, which are parameterized in terms of the sea state significant wave height (unit meters) and spectral peak period (unit seconds).

The distinction between wind dominated and swell dominated sea states is defined by the fully developed sea for the location where peak period is given by

$$T_f = a_f H_s^{1/3}$$

Then $T_P < T_f$ is the wind dominated range, and $T_P > T_f$ is the swell dominated range. The factor a_f depend on fetch length, viz. $a_f = 6.6$ (sm$^{-1/3}$) for a fetch length of 370 km, and $a_f = 5.3$ (sm$^{-1/3}$) for fetch length of 100 km.

The spectrum is defined as a sum of wind sea and swell:

$$S(f) = \sum_{j=1}^{2} E_j S_{nj}(f_{nj})$$

$j = 1$ is for the primary sea system, and $j = 2$ for the secondary sea system. Here

$$f_{nj} = f \cdot T_{Pj}$$

$$E_j = \frac{1}{16} H_{Sj}^2 T_{Pj}$$

$$S_{nj}(f) = G_0 A_{\gamma j} \Gamma_{Sj} \gamma_{Fj}$$

A.1 General Form

$$\Gamma_{Sj} = f_{nj}^{-N} \exp\left[-\frac{N}{M} f_{nj}^{-M} \right]$$

$$G_0 = \left[\frac{1}{M} \left(\frac{N}{M} \right)^{-\frac{N-1}{M}} \Gamma\left(\frac{N-1}{M} \right) \right]^{-1}$$

$$\gamma_{F1} = \gamma^{\exp\left[-\frac{1}{2\sigma^2}(f_{n1}-1)^2 \right]}$$

$$\gamma_{F2} = 1$$

$\sigma = 0.07$ for $f_{nj} < 1$ and $\sigma = 0.09$ for $f_{nj} \geq 1$
Regression analysis shows that A_g can be approximated as:

$$A_\gamma \gamma - 1 = 4.1\left(N - 2M^{0.28} + 5.3\right)^{\left(0.96-1.45M^{0.1}\right)} [\ln \gamma]^{f_2}$$

$$f_2 = \left(2.2M^{-3.3} + 0.57\right) N^{0.53-0.58M^{0.37}} + 0.94 - 1.04M^{-1.9}$$

Simplified for $M = 4$ and $\gamma \neq 1$:

$$A_\gamma \gamma - 1 = 4.1\left(N + 2.35\right)^{-0.71} [\ln \gamma]^{0.87+0.59N^{-0.45}}$$

which gives for $N = 4$:

$$A_\gamma \gamma - 1 = 1.1[\ln \gamma]^{1.19}$$

and for $N = 5$:

$$A_\gamma \gamma - 1 = 1.0[\ln \gamma]^{1.16}$$

Common parameters:

$$N = 0.5\sqrt{H_S} + 3.2$$

$$T_f = 6.6H_S^{1/3}$$

(assuming fetch 370 km)

A.1.1 Wind dominated sea ($T_P \leq T_f$)

A.1.1.1 Primary peak

$$H_{S1} = H_{Sw} = r_{pw} H_S$$

$$T_{P1} = T_{Pw} = T_P$$

$$\gamma = 35\left(1 + 3.5\exp(-H_S)\right)\left[\frac{2\pi}{g} \frac{H_{Sw}}{T_P^2} \right]^{0.857}$$

$$M = 4$$

A.1.1.2 Secondary peak

$$H_{S2} = H_{Ssw} = \sqrt{1 - r_{pw}^2}\, H_S$$

$$T_{P2} = T_{Psw} = T_f + 2.0$$

$$\gamma = 1$$

$$M = 4$$

The parameter r_{pw} is defined by:

$$r_{pw} = 0.7 + 0.3\exp\left(-\left(2\frac{T_f - T_P}{T_f - 2\sqrt{H_S}} \right)^2 \right)$$

A.1.2 Swell dominated sea (T$_P$> T$_f$)

A.1.2.1 Primary peak

$$H_{S1} = H_{Ssw} = r_{ps}H_S$$

$$T_{P1} = T_{Psw} = T_P$$

$$\gamma = 35\left(1 + 3.5\exp\left(-H_S\right)\right)\left[\frac{2\pi}{g}\frac{H_S}{T_f^2}\right]^{0.857}\left(1 + 6\frac{T_P - T_f}{25 - T_f}\right)$$

$$M = 4$$

A.1.2.2 Secondary peak

$$H_{S2} = H_{Sw} = \sqrt{1 - r_{ps}^2}\,H_S$$

$$T_{P2} = T_{Pw} = \max\left(2.5\,;\left[\frac{16s_4 \cdot 0.4^N}{G_0 H_{Sw}^2}\right]^{-\frac{1}{N-1}}\right)$$

$$s_4 = \max\left(0.01\;;\;0.08\cdot\left(1 - \exp\left(-\frac{1}{3}H_S\right)\right)\right)$$

$$\gamma = 1$$

$$M = 4\left(1 - 0.7\exp\left(-\frac{1}{3}H_S\right)\right)$$

where:

$$r_{ps} = 0.6 + 0.4\exp\left(-\left(\frac{T_P - T_f}{0.3\left(25 - T_f\right)}\right)^2\right)$$

A.2 Simplified Form

Some of the parameters for the general form have only effect for low sea states and are of marginal importance for design. The exponent of the high frequency tail is $N = 4$ for all sea states. This will be conservative for lightly damped systems. The spectral width parameter $M = 4$ is used for all sea states.

For the simplified version of the spectrum it follows:

$$\Gamma_{Sj} = f_{nj}^{-4}\exp\left[-f_{nj}^{-4}\right]; j = 1.2$$

$$G_0 = 3.26$$

$$\gamma_{F1} = \gamma^{\exp\left[-\frac{1}{2\sigma^2}(f_{n1}-1)^2\right]}$$

$$\gamma_{F2} = 1$$

$$\sigma = 0.07 \text{ for } f_{nj} < 1 \text{ and } \sigma = 0.09 \text{ for } f_{nj} \geq 1$$

$$A_{\gamma 1} = (1 + 1.1\left[\ln(\gamma)\right]^{1.19})/\gamma$$

$$A_{\gamma 2} = 1$$

Common parameter:

$$T_f = 6.6H_S^{1/3}$$

A.2.1 Wind dominated sea (T$_P$≤ T$_f$)

A.2.1.1 Primary peak

$$H_{S1} = H_{Sw} = r_{pw}H_S$$

$$T_{P1} = T_{Pw} = T_P$$

$$\gamma = 35\left[\frac{2\pi}{g}\frac{H_{Sw}}{T_P^2}\right]^{0.857}$$

A.2.1.2 Secondary peak

$$H_{S2} = H_{Ssw} = \sqrt{1 - r_{pw}^2}H_S$$

$$T_{P2} = T_{Psw} = T_f + 2.0$$

$$\gamma = 1$$

The parameter r$_{pw}$ is defined by:

$$r_{pw} = 0.7 + 0.3\exp\left(-\left(2\frac{T_f - T_P}{T_f - 2\sqrt{H_S}}\right)^2\right)$$

A.2.2 Swell dominated sea (T$_P$> T$_f$)

A.2.2.1 Primary peak

$$H_{S1} = H_{Ssw} = r_{ps}H_S$$

$$T_{P1} = T_{Psw} = T_P$$

$$\gamma = 35\left[\frac{2\pi}{g}\frac{H_S}{T_f^2}\right]^{0.857}\left(1 + 6\frac{T_P - T_f}{25 - T_f}\right)$$

A.2.2.2 Secondary peak
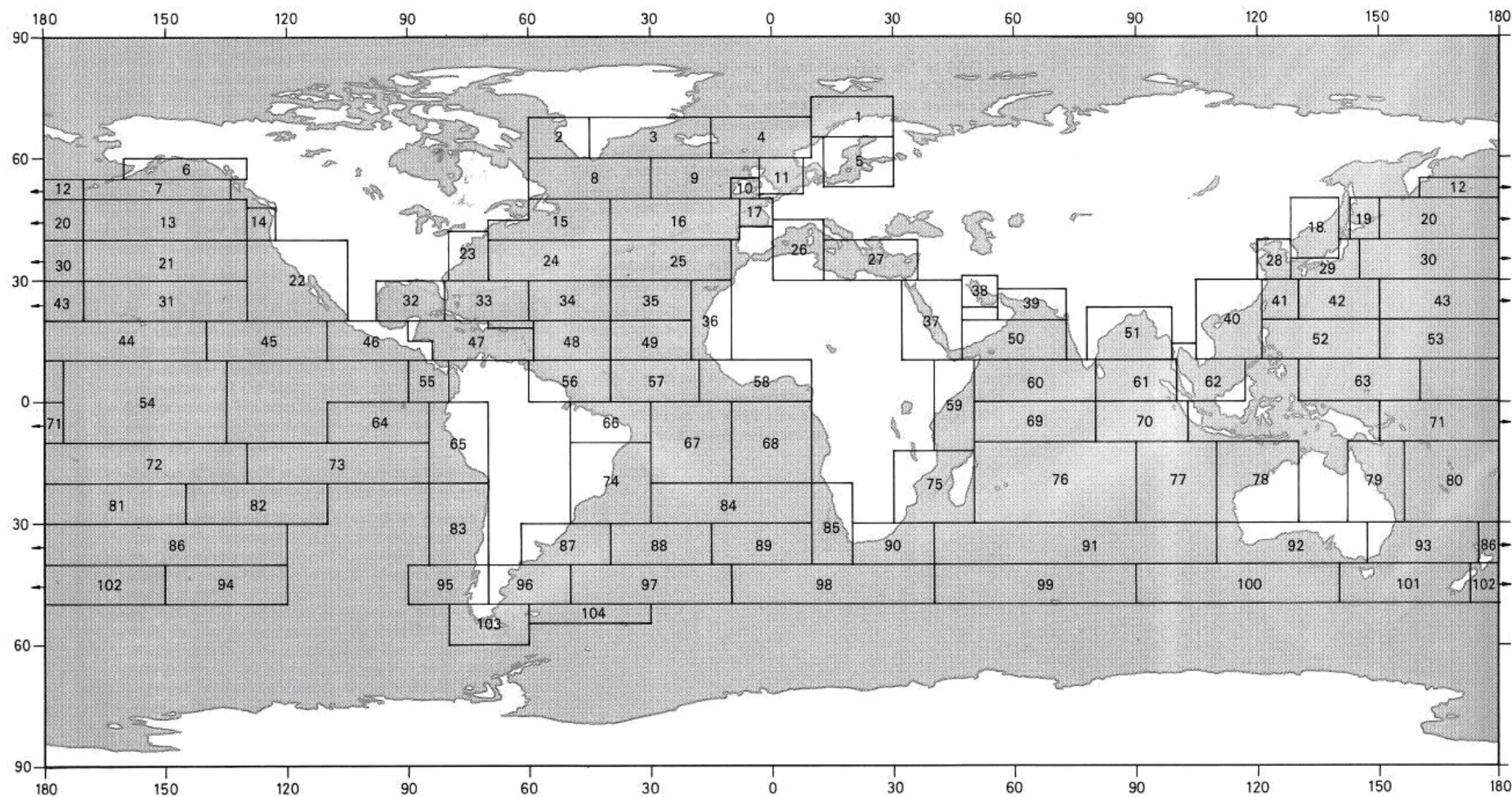
$$H_{S2} = H_{Sw} = \sqrt{1 - r_{ps}^2}\,H_S$$

$$T_{P2} = T_{Pw} = 6.6\,H_{Sw}^{1/3}$$

$$\gamma = 1$$

where:

$$r_{ps} = 0.6 + 0.4\exp\left(-\left(\frac{T_P - T_f}{0.3\left(25 - T_f\right)}\right)^2\right)$$

APPENDIX B
NAUTIC ZONES FOR ESTIMATION
OF LONG-TERM WAVE DISTRIBUTION PARAMETERS

DET NORSKE VERITAS

APPENDIX C
SCATTER DIAGRAMS

Table C-1 2-parameter Weibull parameters and Log-Normal distribution parameters for H_S and T_Z ($\gamma_s = 0$)											
Area	α_s	β_s	a_1	a_2	b_1	b_2	Area	α_s	β_s	a_1	a_2	b_1	b_2
1	2.33	1.33	0.974	0.205	0.1263	-0.0201	53	2.56	1.93	1.188	0.129	0.1041	-0.0091
2	1.96	1.34	0.994	0.175	0.1414	-0.0238	54	2.45	2.19	1.176	0.168	0.1097	-0.0091
3	2.74	1.35	1.127	0.160	0.1255	-0.0912	55	1.83	1.96	1.046	0.143	0.1542	-0.0191
4	2.84	1.53	1.125	0.150	0.0978	-0.0074	56	2.40	2.18	1.157	0.157	0.1067	-0.0169
5	1.76	1.59	0.828	0.167	0.3449	-0.2073	57	2.17	2.19	1.083	0.214	0.1202	-0.0173
6	2.76	1.45	1.128	0.154	0.0964	-0.0066	58	1.85	2.08	1.013	0.165	0.1578	-0.0248
7	3.39	1.75	1.256	0.118	0.0809	-0.0069	59	2.02	1.76	1.025	0.159	0.1432	-0.0254
8	3.47	1.57	1.272	0.114	0.0728	-0.0015	60	1.93	1.39	1.057	0.145	0.1349	-0.0215
9	3.56	1.61	1.260	0.119	0.0755	-0.0054	61	2.10	1.82	1.080	0.132	0.1300	-0.0261
10	2.45	1.37	1.036	0.181	0.1166	-0.0137	62	1.73	1.39	0.871	0.214	0.1941	-0.0266
11	2.19	1.26	0.935	0.222	0.1386	-0.0208	63	1.88	1.70	1.026	0.155	0.1477	-0.0224
12	3.31	1.56	1.150	0.150	0.0934	-0.0409	64	2.34	2.16	1.138	0.186	0.1134	-0.0062
13	3.18	1.64	1.257	0.111	0.0850	-0.0032	65	2.02	1.90	1.132	0.169	0.1187	-0.0125
14	2.62	1.46	1.215	0.115	0.0976	-0.0111	66	2.33	2.15	1.115	0.183	0.1192	-0.0203
15	3.09	1.50	1.207	0.134	0.0855	-0.0124	67	2.43	2.21	1.159	0.155	0.1056	-0.0194
16	3.42	1.56	1.243	0.126	0.0898	-0.0528	68	2.42	2.16	1.121	0.155	0.1243	-0.0151
17	2.77	1.41	1.197	0.135	0.0954	-0.0083	69	2.23	1.89	1.177	0.124	0.1176	-0.0101
18	1.66	1.14	1.310	0.121	0.4006	-0.2123	70	2.32	1.84	1.170	0.167	0.1659	-0.2086
19	2.48	1.35	1.085	0.166	0.1071	-0.0096	71	1.79	1.69	1.005	0.147	0.1602	-0.0309
20	3.15	1.48	1.196	0.139	0.0914	-0.0248	72	2.44	1.93	1.158	0.187	0.1068	-0.011
21	2.97	1.69	1.249	0.111	0.1044	-0.0452	73	2.80	2.26	1.174	0.182	0.1050	-0.0493
22	2.29	1.72	1.139	0.117	0.1160	-0.0177	74	2.23	1.69	1.143	0.148	0.1148	-0.0087
23	2.23	1.39	1.039	0.167	0.1248	-0.0131	75	2.69	1.67	1.216	0.118	0.0991	-0.0103
24	2.95	1.48	1.211	0.131	0.0859	-0.0059	76	2.86	1.77	1.218	0.143	0.1016	-0.0251
25	2.90	1.61	1.268	0.096	0.1055	-0.0521	77	3.04	1.83	1.213	0.152	0.0844	0
26	1.81	1.30	0.858	0.232	0.1955	-0.0497	78	2.60	1.70	1.244	0.073	0.1060	-0.0059
27	1.76	1.30	0.880	0.218	0.1879	-0.0419	79	2.18	1.53	1.069	0.131	0.1286	-0.0173
28	1.81	1.28	0.841	0.241	0.1977	-0.0498	80	2.54	1.70	1.201	0.131	0.1019	-0.0101
29	2.31	1.38	0.976	0.197	0.1288	-0.0184	81	2.83	1.71	1.218	0.144	0.1017	-0.0258
30	3.14	1.56	1.243	0.118	0.0861	-0.0122	82	2.84	1.94	1.209	0.146	0.0911	0
31	2.62	1.79	1.219	0.126	0.1022	-0.0116	83	2.60	1.83	1.214	0.132	0.1076	-0.008
32	1.81	1.47	0.950	0.158	0.1685	-0.0312	84	2.92	2.10	1.190	0.170	0.1018	-0.0972
33	2.17	1.66	1.111	0.135	0.1191	-0.0147	85	3.32	1.94	1.226	0.145	0.0947	-0.0505
34	2.46	1.70	1.189	0.141	0.1059	-0.0055	86	2.91	1.54	1.261	0.111	0.0865	-0.0031
35	2.74	2.05	1.219	0.128	0.1097	-0.0101	87	2.43	1.40	1.203	0.129	0.1009	-0.0072
36	2.32	1.82	1.111	0.143	0.1165	-0.0189	88	3.35	1.75	1.248	0.128	0.0842	-0.0194
37	1.66	1.53	0.815	0.199	0.2754	-0.1051	89	3.02	1.45	1.249	0.124	0.0938	-0.0444
38	1.23	1.24	0.616	0.332	0.3204	-0.0054	90	3.35	1.59	1.266	0.116	0.0766	-0.0051
39	1.74	1.37	0.798	0.239	0.2571	-0.0908	91	3.54	1.68	1.281	0.110	0.0829	-0.04
40	2.36	1.42	0.975	0.195	0.1288	-0.0214	92	3.42	1.71	1.283	0.105	0.0831	-0.023
41	2.47	1.50	1.044	0.161	0.1166	-0.0158	93	2.66	1.45	1.233	0.119	0.1011	-0.0198
42	2.32	1.41	1.121	0.128	0.1159	-0.0118	94	3.89	1.69	1.296	0.112	0.0632	0
43	2.78	1.78	1.222	0.124	0.1029	-0.0078	95	3.71	1.93	1.256	0.131	0.0726	-0.0022
44	2.83	2.17	1.181	0.149	0.1005	-0.0124	96	2.65	1.47	1.200	0.110	0.0986	-0.0103
45	2.60	2.07	1.177	0.173	0.1017	-0.0258	97	3.61	1.63	1.279	0.114	0.0733	-0.0029
46	1.76	1.44	1.070	0.139	0.1365	-0.0306	98	3.53	1.70	1.248	0.135	0.0744	-0.0025
47	2.30	1.78	1.058	0.149	0.1301	-0.025	99	4.07	1.77	1.305	0.106	0.0614	-0.0011
48	2.55	2.20	1.160	0.172	0.1048	-0.0233	100	3.76	1.54	1.279	0.120	0.0636	-0.0006
49	2.50	2.13	1.141	0.149	0.1223	-0.0123	101	3.21	1.57	1.261	0.116	0.0934	-0.0049
50	2.05	1.28	0.879	0.237	0.1651	-0.0344	102	3.08	1.60	1.243	0.130	0.0833	-0.0046
51	1.78	1.44	0.952	0.159	0.1763	-0.0544	103	3.52	1.58	1.253	0.122	0.0758	-0.0056
52	2.14	1.50	1.072	0.133	0.1271	-0.0245	104	2.97	1.57	1.267	0.108	0.0847	-0.0049

Table C-2 Scatter diagram for the North Atlantic																
T_Z (s)	3.5	4.5	5.5	6.5	7.5	8.5	9.5	10.5	11.5	12.5	13.5	14.5	15.5	16.5	17.5	18.5	Sum
H_S (m)																	
0.5	1.3	133.7	865.6	1186.0	634.2	186.3	36.9	5.6	0.7	0.1	0.0	0.0	0.0	0.0	0.0	0.0	3050
1.5	0.0	29.3	986.0	4976.0	7738.0	5569.7	2375.7	703.5	160.7	30.5	5.1	0.8	0.1	0.0	0.0	0.0	22575
2.5	0.0	2.2	197.5	2158.8	6230.0	7449.5	4860.4	2066.0	644.5	160.2	33.7	6.3	1.1	0.2	0.0	0.0	23810
3.5	0.0	0.0	34.9	695.5	3226.5	5675.0	5099.1	2838.0	1114.1	337.7	84.3	18.2	3.5	0.6	0.1	0.0	19128
4.5	0.0	0.0	6.0	196.1	1354.3	3288.5	3857.5	2685.5	1275.2	455.1	130.9	31.9	6.9	1.3	0.2	0.0	13289
5.5	0.0	0.0	1.0	51.0	498.4	1602.9	2372.7	2008.3	1126.0	463.6	150.9	41.0	9.7	2.1	0.4	0.1	8328
6.5	0.0	0.0	0.2	12.6	167.0	690.3	1257.9	1268.6	825.9	386.8	140.8	42.2	10.9	2.5	0.5	0.1	4806
7.5	0.0	0.0	0.0	3.0	52.1	270.1	594.4	703.2	524.9	276.7	111.7	36.7	10.2	2.5	0.6	0.1	2586
8.5	0.0	0.0	0.0	0.7	15.4	97.9	255.9	350.6	296.9	174.6	77.6	27.7	8.4	2.2	0.5	0.1	1309
9.5	0.0	0.0	0.0	0.2	4.3	33.2	101.9	159.9	152.2	99.2	48.3	18.7	6.1	1.7	0.4	0.1	626
10.5	0.0	0.0	0.0	0.0	1.2	10.7	37.9	67.5	71.7	51.5	27.3	11.4	4.0	1.2	0.3	0.1	285
11.5	0.0	0.0	0.0	0.0	0.3	3.3	13.3	26.6	31.4	24.7	14.2	6.4	2.4	0.7	0.2	0.1	124
12.5	0.0	0.0	0.0	0.0	0.1	1.0	4.4	9.9	12.8	11.0	6.8	3.3	1.3	0.4	0.1	0.0	51
13.5	0.0	0.0	0.0	0.0	0.0	0.3	1.4	3.5	5.0	4.6	3.1	1.6	0.7	0.2	0.1	0.0	21
14.5	0.0	0.0	0.0	0.0	0.0	0.1	0.4	1.2	1.8	1.8	1.3	0.7	0.3	0.1	0.0	0.0	8
15.5	0.0	0.0	0.0	0.0	0.0	0.0	0.1	0.4	0.6	0.7	0.5	0.3	0.1	0.1	0.0	0.0	3
16.5	0.0	0.0	0.0	0.0	0.0	0.0	0.0	0.1	0.2	0.2	0.2	0.1	0.1	0.0	0.0	0.0	1
Sum	1	165	2091	9280	19922	24879	20870	12898	6245	2479	837	247	66	16	3	1	100000

The H_s and T_z values are class midpoints.

Table C-3 Scatter diagram for the World Wide trade																
T_Z(s)	3.5	4.5	5.5	6.5	7.5	8.5	9.5	10.5	11.5	12.5	13.5	14.5	15.5	16.5	17.5	Sum
Hs (m)																
1.0	311	2734	6402	7132	5071	2711	1202	470	169	57	19	6	2	1	0	26287
2.0	20	764	4453	8841	9045	6020	3000	1225	435	140	42	12	3	1	0	34001
3.0	0	57	902	3474	5549	4973	3004	1377	518	169	50	14	4	1	0	20092
4.0	0	4	150	1007	2401	2881	2156	1154	485	171	53	15	4	1	0	10482
5.0	0	0	25	258	859	1338	1230	776	372	146	49	15	4	1	0	5073
6.0	0	0	4	63	277	540	597	440	240	105	39	13	4	1	0	2323
7.0	0	0	1	15	84	198	258	219	136	66	27	10	3	1	0	1018
8.0	0	0	0	4	25	69	103	99	69	37	17	6	2	1	0	432
9.0	0	0	0	1	7	23	39	42	32	19	9	4	1	1	0	178
10.0	0	0	0	0	2	7	14	16	14	9	5	2	1	0	0	70
11.0	0	0	0	0	1	2	5	6	6	4	2	1	1	0	0	28
12.0	0	0	0	0	0	1	2	2	2	2	1	1	0	0	0	11
13.0	0	0	0	0	0	0	1	1	1	1	0	0	0	0	0	4
14.0	0	0	0	0	0	0	0	0	1	0	0	0	0	0	0	1
Sum	331	3559	11937	20795	23321	18763	11611	5827	2489	926	313	99	29	9	0	100000

Table C-4 North Atlantic		
α_{Hs}	β_{Hs}	γ_{Hs}
3.041	1.484	0.661
a_0	a_1	a_2
0.70	1.27	0.131
b_0	b_1	b_2
0.1334	0.0264	-0.1906

Table C-5 Average World Wide operation of ships		
α_{Hs}	β_{Hs}	γ_{Hs}
1.798	1.214	0.856
a_0	a_1	a_2
-1.010	2.847	0.075
b_0	b_1	b_2
0.161	0.146	-0.683

APPENDIX D
ADDED MASS COEFFICIENTS

Table D-1 Analytical added mass coefficient for two-dimensional bodies, i.e. long cylinders in infinite fluid (far from boundaries). Added mass (per unit length) is $m_A = \rho C_A A_R$ [kg/m] where A_R [m²] is the reference area.
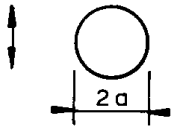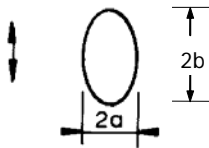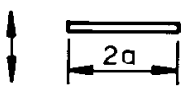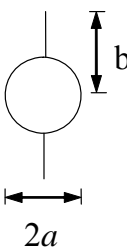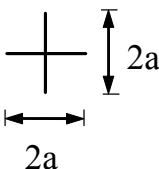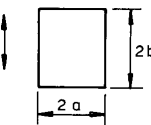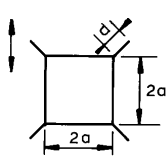
Section through body	Direction of motion	C_A	A_R	Added mass moment of inertia [(kg/m) × m²]
2 a		1.0	$\pi\,a^2$	0
2b, 2a	Vertical	1.0	$\pi\,a^2$	$\rho\dfrac{\pi}{8}(b^2-a^2)^2$
	Horizontal	1.0	$\pi\,b^2$	
2 a	Vertical	1.0	$\pi\,a^2$	$\rho\dfrac{\pi}{8}a^4$
b, 2a, Circular cylinder with two fins	Vertical	1.0	$\pi\,a^2$	$\rho a^4(\csc^4\alpha\,f(\alpha)-\pi^2)/2\pi$ where $f(\alpha)=2\alpha^2-\alpha\sin 4\alpha$ $+\,0.5\sin^2 2\alpha$ and $\sin\alpha=2ab/(a^2+b^2)$ $\pi/2<\alpha<\pi$
	Horizontal	$1-\left(\dfrac{a}{b}\right)^2+\left(\dfrac{a}{b}\right)^4$	$\pi\,b^2$	
2a, 2a	Horizontal or Vertical	1.0	$\pi\,a^2$	$\dfrac{2}{\pi}\rho a^4$

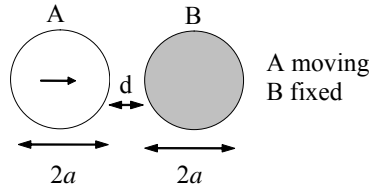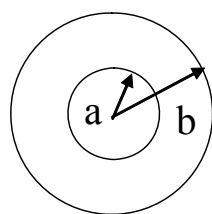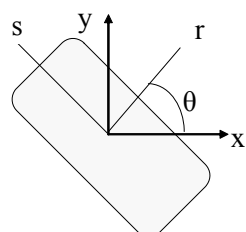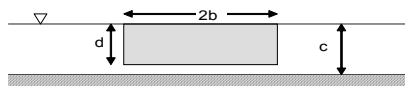| Section through body		Direction of motion	C_A	A_R	Added mass moment of inertia [(kg/m) × m²]		
2b, 2a	$a/b=\infty$ $a/b=10$ $a/b=5$ $a/b=2$ $a/b=1$ $a/b=0.5$ $a/b=0.2$ $a/b=0.1$	Vertical	1.0 1.14 1.21 1.36 1.51 1.70 1.98 2.23	$\pi\,a^2$	$\beta_1\rho\pi a^4$ or $\beta_2\rho\pi b^4$		
					a/b	β_1	β_2
					0.1	-	0.147
					0.2	-	0.15
					0.5	-	0.15
					1.0	0.234	0.234
					2.0	0.15	-
					5.0	0.15	-
					∞	0.125	-
d, 2a, 2a	$d/a=0.05$ $d/a=0.10$ $d/a=0.25$	Vertical	1.61 1.72 2.19	$\pi\,a^2$	$\beta\rho\pi a^4$		
					d/a	β	
					0.05	0.31	
					0.10	0.40	
					0.10	0.69	
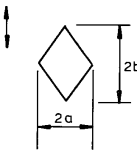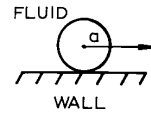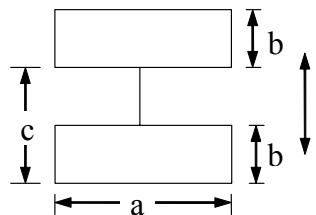
Table D-1 Analytical added mass coefficient for two-dimensional bodies, i.e. long cylinders in infinite fluid (far from boundaries). Added mass (per unit length) is $m_A = \rho C_A A_R$ [kg/m] where A_R [m^2] is the reference area. (Continued)

Section through body	Direction of motion	C_A					A_R	Added mass moment of inertia [(kg/m) × m^2]
	$a/b = 2$ $a/b = 1$ $a/b = 0.5$ $a/b = 0.2$	Vertical		0.85 0.76 0.67 0.61			πa^2	0.059 $\rho \pi a^4$ for $a = b$ only
	All directions	$\dfrac{\pi^2}{3} - 1$					πa^2	

Section through body	Direction of motion	C_A				A_R	Added mass moment of inertia
	Vertical	*c/a*	b/a			2*ab*	

c/a	b/a 0.1	0.2	0.4	1.0
0.5	4.7	2.6	1.3	-
1.0	5.2	3.2	1.7	0.6
1.5	5.8	3.7	2.0	0.7
2.0	6.4	4.0	2.3	0.9
3.0	7.2	4.6	2.5	1.1
4.0	-	4.8	-	-

Section through body	Direction of motion	C_A	A_R	Added mass moment of inertia
A moving B fixed	Horizontal	$d/a = \infty$ 1.000 $d/a = 1.2$ 1.024 $d/a = 0.8$ 1.044 $d/a = 0.4$ 1.096 $d/a = 0.2$ 1.160 $d/a = 0.1$ 1.224	πa^2	
	Cylinder within pipe	$\dfrac{b^2 + a^2}{b^2 - a^2}$	πa^2	
	Cross section is symmetric about r and s axes	$m_{yy}^a = m_{rr}^a \sin^2 \theta + m_{ss}^a \cos^2 \theta$ $m_{xx}^a = m_{rr}^a \cos^2 \theta + m_{ss}^a \sin^2 \theta$ $m_{xy}^a = \dfrac{1}{2}(m_{rr}^a - m_{ss}^a)\sin 2\theta$		
Shallow water 		$\dfrac{b}{c\varepsilon} - \dfrac{2}{\pi}\ln 4\varepsilon + \dfrac{2}{\pi} - \dfrac{2b}{c} + \varepsilon\dfrac{b}{c} + \dfrac{2}{3\pi}\varepsilon^2$ $\dfrac{d}{c} = 1 - \varepsilon$ where $\varepsilon << 1$ Valid for long periods of oscillation	$2\rho c^2$	

Table D-2 Analytical added mass coefficient for three-dimensional bodies in infinite fluid (far from boundaries).
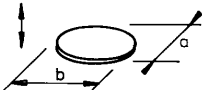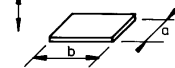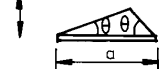Added mass is $m_A = \rho C_A V_R$ [kg] where V_R [m³] is reference volume.
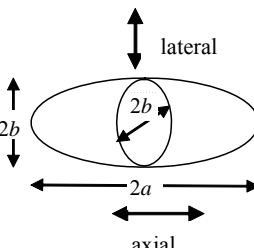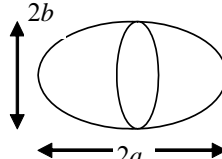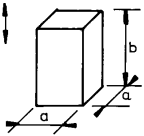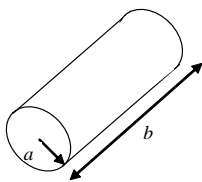
Body shape		Direction of motion	C_A				V_R
Flat plates	Circular disc	Vertical	$2/\pi$				$\frac{4}{3}\pi a^3$

Elliptical disc — Vertical:

b/a	C_A	b/a	C_A
∞	1.000	5.0	0.952
14.3	0.991	4.0	0.933
12.8	0.989	3.0	0.900
10.0	0.984	2.0	0.826
7.0	0.972	1.5	0.758
6.0	0.964	1.0	0.637

$V_R = \frac{\pi}{6}a^2 b$

Rectangular plates — Vertical:

b/a	C_A	b/a	C_A
1.00	0.579	3.17	0.840
1.25	0.642	4.00	0.872
1.50	0.690	5.00	0.897
1.59	0.704	6.25	0.917
2.00	0.757	8.00	0.934
2.50	0.801	10.00	0.947
3.00	0.830	∞	1.000

$V_R = \frac{\pi}{4}a^2 b$

Triangular plates — Vertical: $\frac{1}{\pi}(\tan\theta)^{3/2}$, $V_R = \frac{a^3}{3}$

Spheres — Any direction: $\frac{1}{2}$, $V_R = \frac{4}{3}\pi a^3$

Bodies of revolution — Spheroids — Lateral or axial:

a/b	C_A Axial	C_A Lateral
1.0	0.500	0.500
1.5	0.304	0.622
2.0	0.210	0.704
2.5	0.156	0.762
4.0	0.082	0.860
5.0	0.059	0.894
6.0	0.045	0.917
7.0	0.036	0.933
8.0	0.029	0.945

$V_R = \frac{4}{3}\pi b^2 a$

Ellipsoid — Axis $a > b > c$ — Axial:

$$C_A = \frac{\alpha_0}{2 - \alpha_0}$$

where

$$\alpha_0 = \varepsilon\delta \int_0^\infty (1+u)^{-3/2}(\varepsilon^2 + u)^{-1/2}(\delta^2 + u)^{-1/2}\,du$$

$$\varepsilon = b/a \quad \delta = c/a$$

$V_R = \frac{4}{3}\pi abc$

Table D-2 Analytical added mass coefficient for three-dimensional bodies in infinite fluid (far from boundaries).
Added mass is $m_A = \rho C_A V_R$ [kg] where V_R [m^3] is reference volume. (Continued)

Body shape		Direction of motion	C_A			V_R
Square prisms		Vertical	b/a	C_A		$a^2 b$
			1.0	0.68		
			2.0	0.36		
			3.0	0.24		
			4.0	0.19		
			5.0	0.15		
			6.0	0.13		
			7.0	0.11		
			10.0	0.08		
Right circular cylinder		Vertical	b/2a	C_A		$\pi a^2 b$
			1.2	0.62		
			2.5	0.78		
			5.0	0.90		
			9.0	0.96		
			∞	1.00		

APPENDIX E
DRAG COEFFICIENTS

Table E-1 Drag coefficient on non-circular cross-sections for steady flow C_{DS}. Drag force per unit length of slender element is $f = \frac{1}{2}\rho C_{DS} D u^2$. D = characteristic width [m]. $R_e = uD/\nu$ = Reynolds number. Adopted from Blevins, R.D. (1984) *Applied Fluid Dynamics Handbook*. **Krieger Publishing Co. Ref. is also made to Ch.5 for drag coefficients on I-profiles and to Ch.6 for drag coefficients on circular cylinders.**

Geometry	Drag coefficient, C_D		
1. Wire and chains	Type ($R_e = 10^4 - 10^7$)		C_D
	Wire, six strand Wire, spiral no sheating Wire, spiral with sheating Chain, stud (relative chain diameter) Chain studless (relative chain diameter)		1.5 - 1.8 1.4 - 1.6 1.0 - 1.2 2.2 - 2.6 2.0 - 2.4

2. Rectangle with thin splitter plate

L/D	T/D		
	0	5	10
0.1	1.9	1.4	1.38
0.2	2.1	1.4	1.43
0.4	2.35	1.39	1.46
0.6	1.8	1.38	1.48
0.8	2.3	1.36	1.47
1.0	2.0	1.33	1.45
1.5	1.8	1.30	1.40
2.0	1.6	-	1.33

$$R_e \sim 5 \times 10^4$$

3. Rectangle in a channel

$$C_D = (1-D/H)^{-n} C_D |_{H=\infty} \quad \text{for } 0 < D/H < 0.25$$

L/D	0.1	0.25	0.50	1.0	2.0
n	2.3	2.2	2.1	1.2	0.4

$$R_e > 10^3$$

4. Rectangle with rounded corners

L/D	R/D	C_D	L/D	R/D	C_D
0.5	0	2.5	2.0	0	1.6
	0.021	2.2		0.042	1.4
	0.083	1.9		0.167	0.7
	0.250	1.6		0.50	0.4
1.0	0	2.2	6.0	0	0.89
	0.021	2.0		0.5	0.29
	0.167	1.2			
	0.333	1.0			

$$R_e \sim 10^5$$

5. Inclined square

θ	0	5	10	15	20	25	30	35	40	45
C_D	2.2	2.1	1.8	1.3	1.9	2.1	2.2	2.3	2.4	2.4

$$R_e \sim 4.7 \times 10^4$$

Table E-1 Drag coefficient on non-circular cross-sections for steady flow C_{DS}. Drag force per unit length of slender element is $f = \frac{1}{2}\rho C_{DS} D u^2$. D = characteristic width [m]. $R_e = uD/\nu$ = Reynolds number. Adopted from Blevins, R.D. (1984) *Applied Fluid Dynamics Handbook*. Krieger Publishing Co. Ref. is also made to Ch.5 for drag coefficients on I-profiles and to Ch.6 for drag coefficients on circular cylinders. (Continued)
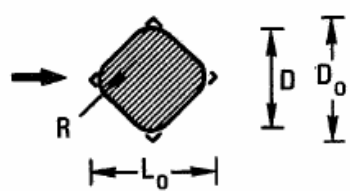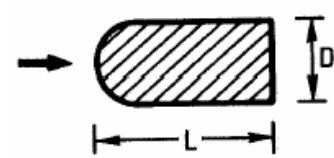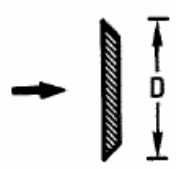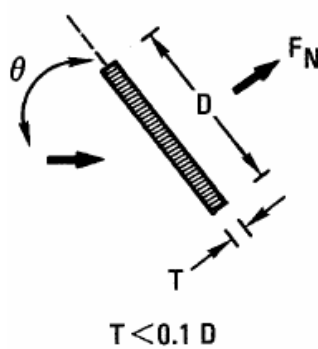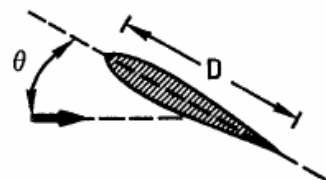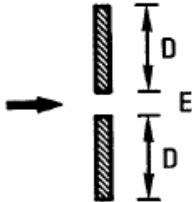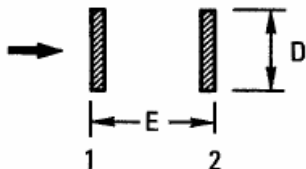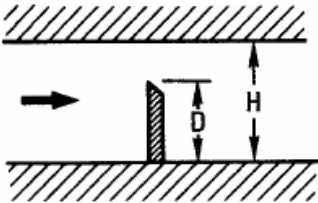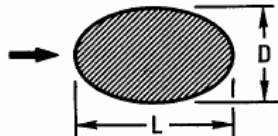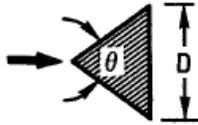
Geometry	Drag coefficient, C_D			
6. Diamond with rounded corners	L_0/D_0	R/D_0	C_D	
	0.5	0.021 0.083 0.167	1.8 1.7 1.7	Fore and aft corners not rounded
	1.0	0.015 0.118 0.235	1.5 1.5 1.5	
	2.0	0.040 0.167 0.335	1.1 1.1 1.1	Lateral corners not rounded
	$R_e \sim 10^5$			

Geometry	Drag coefficient, C_D	
7. Rounded nose section	L/D	C_D
	0.5 1.0 2.0 4.0 6.0	1.16 0.90 0.70 0.68 0.64

Geometry	Drag coefficient, C_D
8. Thin flat plate normal to flow	$C_D = 1.9,\ R_e > 10^4$
9. Thin flat plate inclined to flow	$$C_N = \begin{cases} 2\pi \tan\theta, \theta < 8^o \\ \dfrac{1}{0.222 + 0.283/\sin\theta} \end{cases}, 90^o \geq \theta > 12^o$$ $$C_L = C_N \cos\theta$$ $$C_D = C_N \sin\theta$$
10. Thin lifting foil	$C_D \sim 0.01$ $C_L = 2\pi \sin\theta$ $C_M = (\pi/4)\sin 2\theta$ (moment about leading edge) $C_M = 0$ about point D/4 behind leading edge

Table E-1 Drag coefficient on non-circular cross-sections for steady flow C_{DS}. Drag force per unit length of slender element is $f = \frac{1}{2}\rho C_{DS}Du^2$. D = characteristic width [m]. $R_e = uD/\nu$ = Reynolds number. Adopted from Blevins, R.D. (1984) *Applied Fluid Dynamics Handbook*. Krieger Publishing Co. Ref. is also made to Ch.5 for drag coefficients on I-profiles and to Ch.6 for drag coefficients on circular cylinders. (Continued)

Geometry	Drag coefficient, C_D		
11. Two thin plates side by side	E/D	C_D	multiple values due to jet switch Drag on each plate.
	0.5	1.42 or 2.20	
	1.0	1.52 or 2.13	
	2.0	1.9 or 2.10	
	3.0	2.0	
	5.0	1.96	
	10.0	1.9	
	15.0	1.9	
	$R_e \sim 4 \times 10^3$		
12. Two thin plates in tandem	E/D	C_{D1}	C_{D2}
	2	1.80	0.10
	3	1.70	0.67
	4	1.65	0.76
	6	1.65	0.95
	10	1.9	1.00
	20	1.9	1.15
	30	1.9	1.33
	∞	1.9	1.90
	$R_e \sim 4 \times 10^3$		
13. Thin plate extending part way across a channel	$C_D = \dfrac{1.4}{(1 - D/H)^{2.85}}$ for $0 < D/H < 0.25$ $R_e > 10^3$		
14. Ellipse	D/L	C_D ($R_e \sim 10^5$)	
	0.125	0.22	
	0.25	0.3	
	0.50	0.6	
	1.00	1.0	
	2.0	1.6	
15. Isosceles triangle	θ	C_D ($R_e \sim 10^4$)	
	30	1.1	
	60	1.4	
	90	1.6	
	120	1.75	
16. Isosceles triangle	θ	C_D ($R_e = 10^4$)	
	30	1.9	
	60	2.1	
	90	2.15	
	120	2.05	

APPENDIX F
PHYSICAL CONSTANTS

Table F-1 Density and viscosity of fresh water, sea water and dry air						
Temperature [^oC]	Density, ρ, [kg/m^3]			Kinematic viscosity, ν, [m^2/s]		
	Fresh water	Sea water*	Dry air**	Fresh water	Sea water*	Dry air
0	999.8	1028.0	1.293	1.79×10^{-6}	1.83×10^{-6}	1.32×10^{-5}
5	1000.0	1027.6	1.270	1.52	1.56	1.36
10	999.7	1026.9	1.247	1.31	1.35	1.41
15	999.1	1025.9	1.226	1.14	1.19	1.45
20	998.2	1024.7	1.205	1.00	1.05	1.50
25	997.0	1023.2	1.184	0.89	0.94	1.55
30	995.6	1021.7	1.165	0.80	0.85	1.60

*) Salinity = 35 parts per thousand

**) The air density applies for a pressure of 1.013×10^5 Pa.